UNIVERSITAT DE BARCELONA

Targeting strategies against *Plasmodium* and practical applications: blocking parasite development with heparin derivatives and identifying new aptamers for diagnosis

Elena Lantero Escolar

Doctoral Thesis

Universitat de Barcelona – Facultat de Farmàcia i Ciències de l'Alimentació

Doctorat en Biotecnologia

Title

Targeting strategies against Plasmodium *and practical applications: blocking parasite development with heparin derivatives and identifying new aptamers for diagnosis.*

ELENA LANTERO ESCOLAR

2020

Director: Dr. Xavier Fernàndez-Busquets

Tutor: Dr. Josefa Badía Palacín

Content

Abbreviations

ACT Artemisinin combination therapy

AMA1 Apical membrane protein 1

aPTT Activated partial thromboplastin time

CD36 Cluster of differentiation 36

CelTOS Cell traversal protein of ookinetes and sporozoites

CS Chondroitin sulfate

CSA Chondroitin sulfate A

CSP Circumsporozoite surface protein

CTRP Circumsporozoite- and thrombospondin-related anonymus protein (TRAP)-related protein

DNA Deoxyribonucleic acid

EBA Erythrocyte binding antigen

EBL Erythrocyte binding ligand

EPCR Endothelial protein C receptor

FIND Foundation for Innovative New Diagnostics

GalNAc N-acetyl-D-galactosamine

GAG Glycosaminoglycan

GlcA D-glucoronic acid

GlcNAc N-acetyl-D-glucosamine

GPI Glycosylphosphatidylinositol

HS Heparan sulfate

HRP2 Histidin-rich protein II

IC_{50} Half maximum inhibitory concentration

ICAM1 Intercellular adhesion molecule 1

IdoA Iduronic acid

ITN Insecticide-treated bed nets

Kd Dissociation constant

LAMP Loop-mediated isothermal amplification

LNA Locked nucleic acids

MSP Merozoite surface protein

PCR Polymerase chain reaction

PEG Poly(ethyleneglycol)

NPP New permeation pathways

PfCCp *Plasmodium falciparum* Limulus clotting factor C, Cochlear protein 5b2 and Lung gestation protein 1 domain-containing proteins

PfEMP1 Plasmodium falciparum erythrocyte membrane protein 1

PfRh Plasmodium falciparum rhoptry protein

pLDH Plasmodium lactate dehydrogenase

pRBC Parasitized red blood cell

PS Phosphatidylserine

PSOP25 Putative secreted ookinete protein 25

PV Parasitophorous vacuole

PVM Parasitophorous vacuole membrane

RBC Red blood cell

RDT Rapid diagnostic test

RIFIN Repetitive interspersed family

RNA Ribonucleic acid

RON2 Rhoptry neck protein 2

SELEX Systematic evolution of ligands by exponential enrichment

SERA Serine repeat antigen

SOPT subtilisin-like ookinete protein

SP Sulfadoxine-pyrimethamine

ssDNA Single stranded deoxyribonucleic acid

TBV Transmission blocking vaccine

TRAP Thrombospondin-related anonymus protein

WARP von Willebrand factor A domain protein

WHO World Health Organization

Abstract

Infection by *Plasmodium* spp. is the cause of malaria, a disease transmitted by *Anopheles* mosquito bites. Although it is a treatable and preventable disease, malaria still remains as a major cause of death in children and it is highly transmitted in developing countries. The reasons why malaria has not been yet eradicated are mostly related to: (i) the high number of antimalarial drug resistances; (ii) the lack of diagnostic tools that can be brought to the endemic areas and, at the same time, are sensitive enough to detect early and asymptomatic cases; (iii) low efficacy (about 40%) of the only vaccine being implemented; and (iv) the difficulties and lack of effectiveness in the vector-control measures applied (also due to insecticide resistances), besides other socio-economic reasons.

As a strategy to solve some of these issues, nanotechnology has started to be applied to malaria research to enhance the efficacy of antimalarial drugs, to improve diagnostic devices, to offer new antimalarial or insecticide strategies and as part of vaccine components. However, the mechanisms for direct targeting to the parasite (either for drug delivery or for diagnosis) mostly rely on antibody use or tools that do not generally meet the cost-efficiency requirements to develop new devices or treatments for a tropical disease. New targeting tools against *Plasmodium* could be developed by selecting those surface targets previously described in literature and exploiting their known interactions/inhibitors or by 'blind' selection with whole cells. The main difficulty with both strategies resides in the intracellular nature of the parasite while infecting humans, which limits the number of antigens exposed, and the antigenic variation that has been already described for this organism as a way to avoid the immune system.

In this work, targeting molecules have been studied by two approaches: the exploitation of the already-known sulfated glycosaminoglycan-parasite interactions, both in human and mosquito stages, and the screening of new ligand-target interactions by whole cell selection of aptamer sequences.

The first article here compiled explores heparin application, a sulfated glycosaminoglycan that possesses antimalarial and anticoagulant activities, as it can block the parasite invasion of red blood cells. The objective was to obtain molecules derived from heparin lacking anticoagulant activity, so they could be applied safely for *in vivo* antimalarial treatment.

In addition, other modifications (drug conjugation or covalent linking to liposomes) were tested to enhance the antimalarial effect.

Continuing with the exploration of heparin potential, inhibition of parasite growth in the mosquito stages was also tested. The second article included in this work provides evidence of heparin blocking the formation of *Plasmodium berghei* oocysts when administered together with infected blood in membrane feeding assays to *Anopheles stephensi* mosquitoes.

Finally, the third article of this thesis describes the selection of aptamers against fixed *Plasmodium falciparum* infected red blood cells. Their characterization with flow cytometry and fluorescent microscopy indicated high specificity (>84% of trophozoites and <0.06% of non-parasitized cells were positive for aptamer labeling) and affinity (all aptamers had apparent dissociation constant between low μM and high nM range), although this was only observed in fixed or permeabilized cells, which suggested that the target is intracellular. Further characterization with protein extracts and other *Plasmodium* species was also performed. The results presented the obtained aptamers as suitable diagnostic tools.

Both approaches for the development of targeting tools showed great potential at different levels. Besides, the combination of different targeting tools or the selection of aptamers against specific parasite proteins or stages could be of use in the development of targeted delivery products or new diagnostic devices for malaria.

Resumen

La malaria es una enfermedad infecciosa producida por *Plasmodium*, protozoo transmitido a través de la picadura de mosquitos del género *Anopheles*. Aunque existen tratamientos y medidas de prevención, en los países tropicales sigue teniendo una alta incidencia debido a problemas como la aparición de resistencias (tanto a los fármacos como a los insecticidas), la inexistencia de una vacuna eficaz y la necesidad de herramientas de diagnóstico más baratas y sencillas para llevar a zonas rurales, entre otras cuestiones socioeconómicas.

A nivel de investigación, las herramientas de nanotecnología se exploran para mejorar la eficacia de fármacos, como componentes de vacunas o fabricación de nuevos fármacos o insecticidas. Sin embargo, las herramientas de direccionamiento de los sistemas de tratamiento o las usadas en detección de antígenos para el diagnóstico aún no cumplen los requisitos de relación coste/efectividad para una enfermedad de los países en desarrollo.

Este trabajo se ha enfocado en la exploración de interacciones ligando-diana de los compuestos glicosaminoglicanos sulfatados y el desarrollo de nuevos elementos direccionadores, los aptámeros, como nuevas herramientas con posible aplicación en la eliminación de la malaria. Esta investigación ha quedado compilada en tres artículos. Los dos primeros artículos resumen los resultados de la aplicación de heparina y sus derivados para bloquear el desarrollo del parásito, tanto en las fases de infección de mamíferos como en el mosquito. En el tercer artículo se describe la selección y caracterización de aptámeros con potencial aplicación al diagnóstico de la malaria.

Estas herramientas de direccionamiento hacia el parásito son más baratas que los anticuerpos y se podrían aplicar en sistemas nanotecnológicos de transporte de fármacos, utilizar como adyuvantes de tratamientos o incluir en pruebas de diagnóstico.

Introduction

1. Malaria relevance

Malaria is a tropical disease with 228 million cases and 405 000 deaths worldwide in 2018, according to the World Health Organization (WHO). The incidence rate of malaria has been decreasing globally since 2010 (251 million cases), although between 2014 and 2018 there has been an increase in case incidence (217 million cases in 2014). 93% of malaria cases in 2018 were in the African Region, 3.4% in South-East Asia and 2.1% in Mediterranean Region [1–3].

This disease has accompanied humans through evolution, being referred to in biblical passages and in Hippocrates' writings [4]. Even with the treatments available, it is a major burden for humankind, and many economic, political, research and health-care efforts are spent on its eradication, as WHO publishes every year in its reports [2,3].

Not so long ago, malaria was more widely spread around the world, but due to environmental changes and following elimination campaigns conducted between the 1950s and 1960s, it was eliminated from many regions of Europe and North America [4]. Today's distribution of the disease remains in the tropical regions (Figure 1), with some countries slowly becoming malaria free, for example Paraguay and Uzbekistan since 2018 and Algeria and Argentina since early 2019 [2].

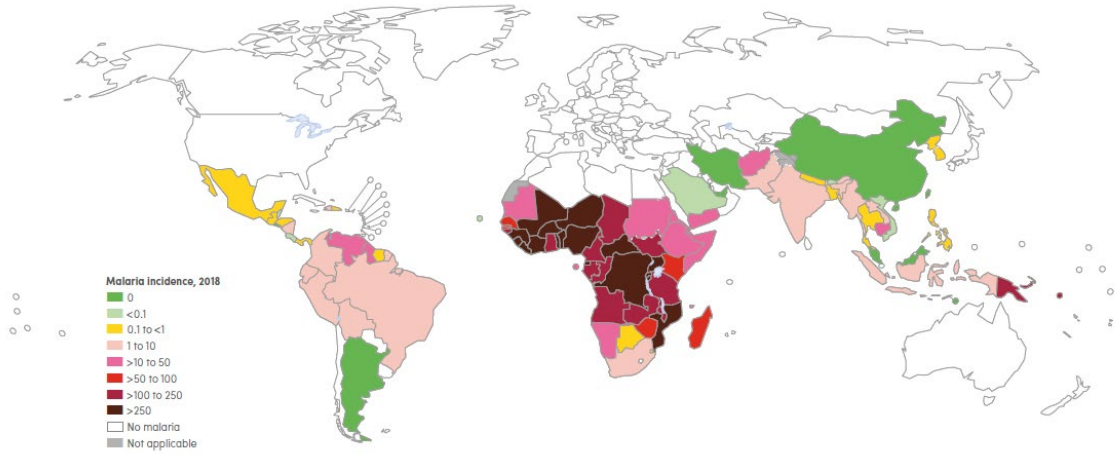

Figure 1: Distribution and disease incidence rate (cases per 1000 people at risk) in current malaria endemic regions. Most of the cases are in African countries. Adapted from [3].

Malaria in humans is caused by six species of protozoa parasites from the genus *Plasmodium*. *Plasmodium falciparum* is the most prevalent species in sub-Saharan Africa (99.7% of the cases), while *Plasmodium vivax* is predominant in America (74.1% of the cases) and represents 37.2% of the cases in South-East Asia and 30.1% in the Eastern Mediterranean [2] (Figure 2). The other species are *Plasmodium malariae*, *Plasmodium ovale curtisi, Plasmodium ovale wallikeri* and *Plasmodium knowlesi*, being the three first human malaria species, and the last one, monkey malaria transmitted zoonotically [5].

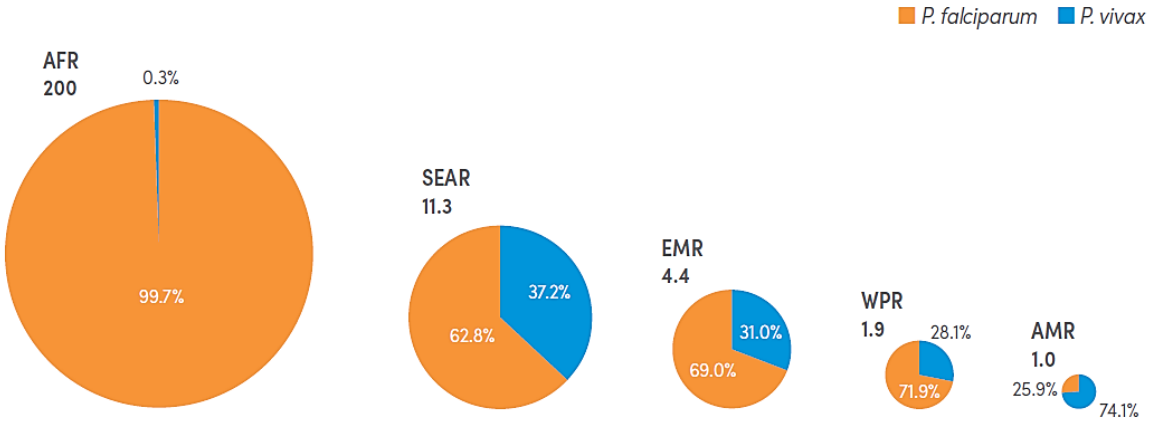

Figure 2: Estimated number of cases (millions) in each region in 2016. The areas of the charts are proportional to the number of cases, and proportions of the two main species of malaria causing parasites are represented in different colors. AFR, WHO African Region; AMR, WHO Region of the Americas; EMR, WHO Eastern Mediterranean Region; SEAR, WHO South-East Asia Region; WPR, WHO Western Pacific Region. Adapted from [2].

Malaria transmission occurs mainly via bites of female mosquito from the genus *Anopheles*, of which about 30 species are important vectors [5]. It can also be transmitted by inoculation of infected blood and congenitally [4]. The symptoms of the illness at initial stages include fever, headache, chills, and weakness, and can be difficult to recognize as malaria. These symptoms appear 10-15 days after the infective mosquito bite, and, if not treated promptly, when produced by *P. falciparum*, they can progress to severe illness, with an abnormal level of consciousness, severe anemia, hypoglycemia, renal failure, and multisystem failure, often leading to death. Children, elderly, pregnant women, and people with underlying chronic illness are at higher risk of developing severe malaria. In endemic regions, people may develop partial immunity, thus having asymptomatic infections that become a parasite reservoir for transmission [4,5].

Even though *P. vivax* has a wider distribution, as it can develop in the mosquito vector at lower temperatures, and has a relapse mechanism thanks to its dormant stages that can

activate months after the infection [3], the deadliest of malaria causing parasites is *P. falciparum*. It is also the parasite responsible for the highest number of cases. Therefore, and with no intention to minimize the concern that other species can arise too, this work has focused mainly on *P. falciparum*.

1.1. Parasite biology

Plasmodium spp. Is classified as protozoan within the *Apicomplexa* phylum, *Aconoidasida* class, *Haemosporida* order and *Plasmodiidae* family. They are unicellular and have multiple characteristics that make them different from mammalian cells, which are exploited for the treatment of their infections.

P. falciparum is classified in the Laverania subgenus, and differs from other *Plasmodium* spp. that cause human infections [6]. This organism seems to have been originated from a western gorilla parasite, possibly after an event of host transfer [7]. The most closely related parasite is *P. praefalciparum* [8]. Its genetic diversity seems to follow the human migration along the globe, exposing the parasite to bottlenecks when a small population of humans traveled to other regions [9].

In the next subsections, some other important characteristics of *Plasmodium* spp. are described to highlight those that allowed the development of treatment or targeting tools.

1.1.1. Life cycle

Plasmodium parasites are beings with a complex life-cycle, which live inside two different hosts: a vertebrate, host of the asexual forms, and a mosquito, inside which the sexual reproduction occurs. As *P. falciparum* life-cycle is the one of relevance for this text, it is its life cycle the one described below. Other species have similar life cycles with different timings and/or morphologies of their stages.

The cycle inside the human host (Figure 3) starts with an infected mosquito bite, which inoculates sporozoites: parasite forms that travel within the blood and accumulate in the liver, where they infect the hepatocytes. The parasite develops intracellularly, becoming a multinucleate liver-schizont, until it bursts, liberating thousands of merozoites: free parasite forms that enter the blood circulation until they reach an erythrocyte, the next cell host

for this parasite. Inside the red blood cells (RBC) is where the intraerythrocytic cycle occurs: the parasite feeds and grows inside its RBC, forming what is known as ring stage, which grows into a trophozoite, and finally starts to divide asexually, forming the schizont. Mature schizonts release new merozoite forms into the blood stream, which invade new erythrocytes. These cycles of division are related with the periodical cycles of fever in malaria patients, one of the main symptoms that allow malaria diagnosis, and, depending on the *Plasmodium* species, these cycles last differently [4]. In *P. falciparum*, maturation of intraerythrocytic forms takes 48 hours, and fever periodicity follows such pattern [10].

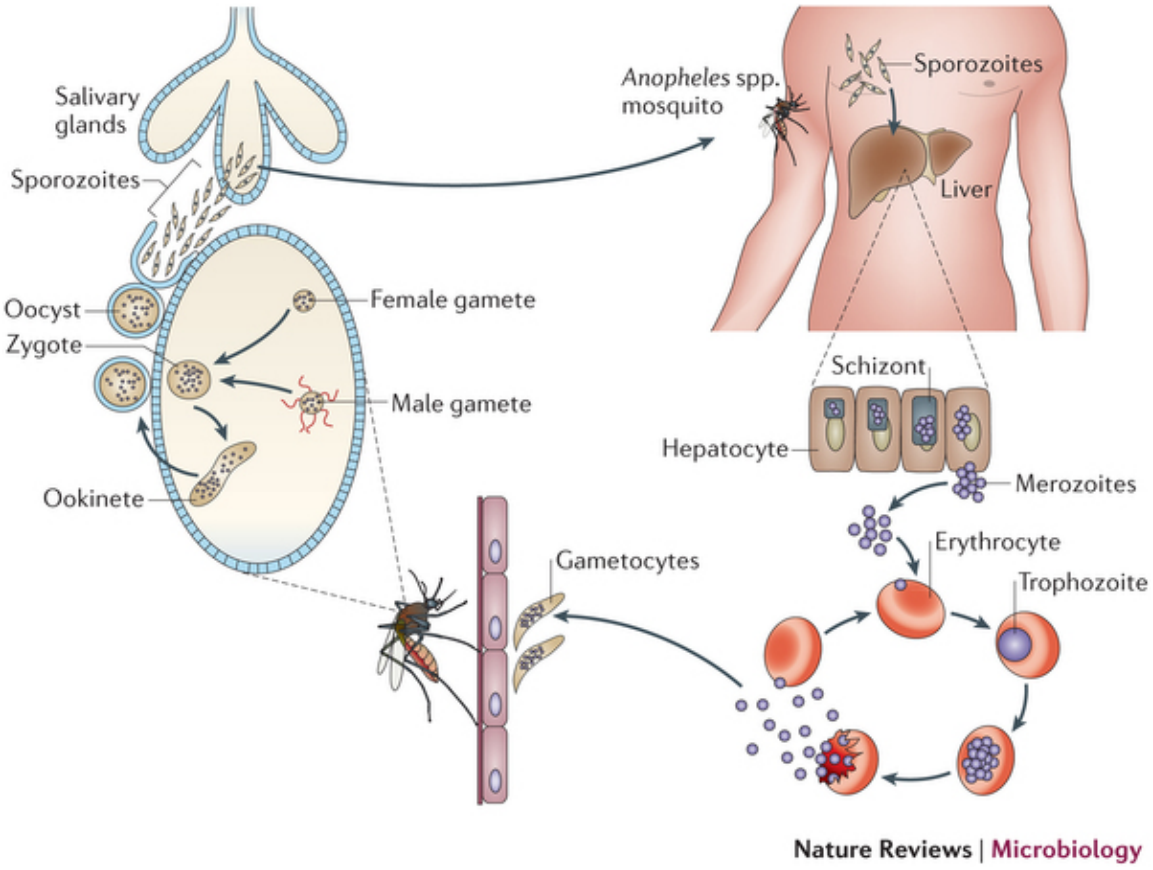

Figure 3: Scheme of the *Plasmodium* life cycle. It involves two hosts: human, in which the parasite reproduces asexually, and mosquito, in which the parasite does sexual reproduction. After an infected mosquito bites a human, the parasite travels to the liver, where it divides intracelullarly, before being released into the blood. Is during the intraerythrocytic cycle when the malaria symptoms occur. Within the blood, precursors of the sexual stages will be taken up by the mosquito, inside which the fertilization occurs. The parasite divides in a sporogonic manner inside the mosquito, and, then, it reaches the salivary glands to invade the next host. Schemme from [11].

Within the intraerythrocytic cycle, some of the ring forms differentiate into gametocytes, the precursors of the sexual forms (the mechanisms that produce this differentiation are reviewed in [12]). These remain sequestered in the bone marrow during their maturation,

and are released into the blood when their deformability changes as they are fully mature [13–15]. In *P. falciparum*, gametocytes mature in 10-12 days, while other species like *P. vivax* have these stages fully mature in 2 days. Parasites used in animal models such as *P. berghei* and *P. yoelii* have mature gametocytes 30 hours after RBC invasion [12].

The sexual part of the cycle starts when a mosquito bites an infected human that has gametocytes circulating. Such forms enter into the mosquito when it is feeding, and inside the digestive system of the insect, they develop into gaemetes, by emerging from the RBC, in a process called egress. When a female gamete, or macrogamete, and a male gamete, or microgamete, encounter inside the mosquito, they fuse, forming the zygote, which undergoes meiosis and genetic recombination shortly after. Within the next 24 hours, the zygote becomes an ookinete form, enlongated and motile, which attaches and crosses the mosquito midgut epithelium. Over the external surface of the midgut, ookinetes become oocyst forms, which undergo numerous asexual divisions for the next 10-12 days, forming sporozoites inside the cell. Sporozoites egress from mature oocysts and get into the insect hemolymph, reaching the salivary glands, where they accumulate until the mosquito bites its next human host [16].

The intraerythrocytic cycle of the parasite is responsible for the clinical outcome observed in human patients: the merozoite release and reinvasion is related with fever episodes and the mechanisms evolved by *P. falciparum* to evade the immune system result in pasasite cytoadhesion, producing tissue sequestration and rosetting, which may arise the symptoms charactersitic of severe malaria [17–22]. The molecular mechanisms of cytoadhesion will be described in detail later on, as many of them can be of use for targeting the parasite.

1.1.2. Cell morphology

As this unicellular parasite goes from one host to another, through changing environments and very different stages, either free forms or intracellular phases, its morphology and cellular components are constantly changing. There are, of course, many shared elements too, and an overview of them is presented in this section, with especial emphasis on those useful for targeting and treatment.

Free parasitic forms that are invasive have some common structures: they are polarized towards an **apical** side, in which several secretory organelles accumulate that have im-

portant functions in the invasion process. This is so for **merozoites**, **ookinetes** and **sporozoites** (Figure 4), existing some differences between them depending on their respective invasive behaviors. These organelles have differential release according to their function: (i) the egress from the previous cellular form is mediated by exonemes –which are present in the merozoite, and the proteolytic activity needed for sporozoite egress indicates that they might be present in this stage too–; (ii) the motility and invasion relies on micronemes; (iii) the function of the rhoptries is focused on cell infection and **parasitophorous vacuole (PV)** formation –they are not present in ookinetes, because they just traverse the cells of the mosquito midgut endothelium and do not establish inside–; and (iv) the dense granules are released to form the PV and start remodelling the host cell. In addition, all these stages have glycosylphosphatidylinositol (GPI) anchored proteins covering the cell surface, among other shared molecular characteristics. These shared features are common for more parasites of the phylum, as *Toxoplasma gondii* has also many of these structures in its invasive form, though the contents of the organelles are different [23].

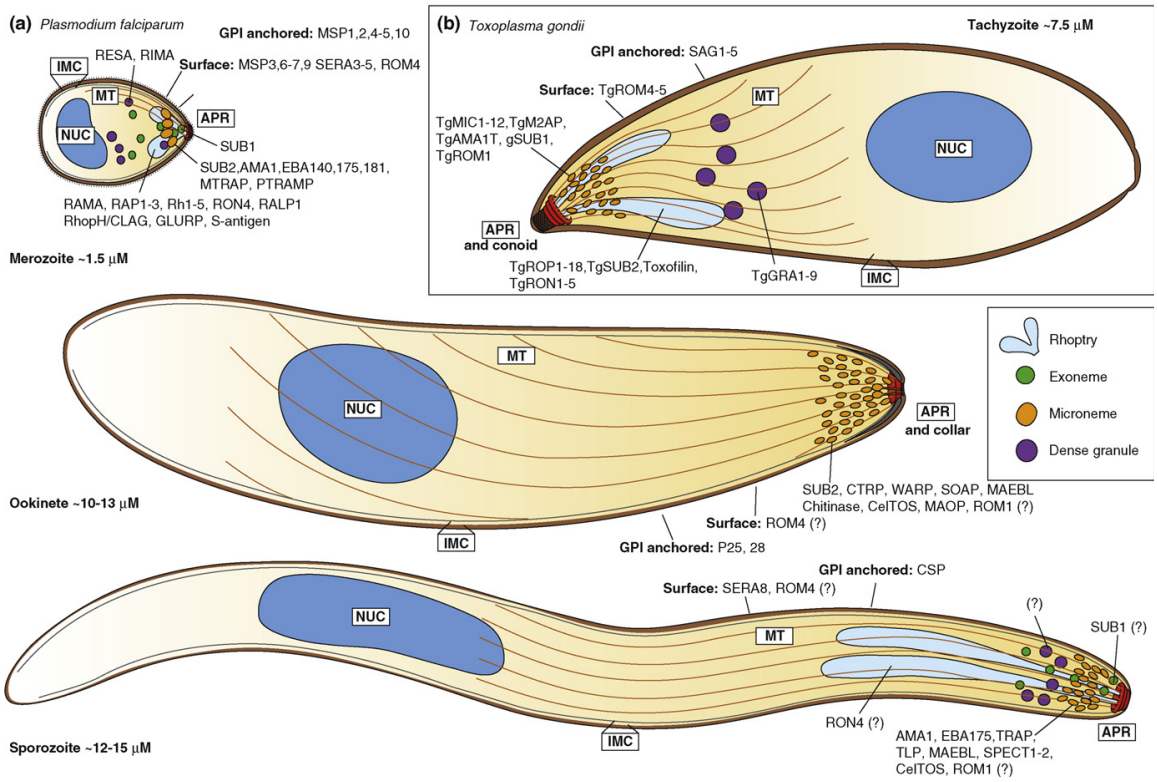

Figure 4: Main shared structures between free invasive forms of the Apicomplexa parasites. Most of the proteins required for invasion are indicated in the organelle or structure where they are accumulated. A scheme of the invasive form of *Toxoplasma gondi* can be seen in panel **b** for comparison. Image from [23].

Targeting the invasion process is one of the exploited strategies for vaccine and treatment development [24–27], and it is related with the objectives of this work.

Another common element in most species of the *Apicomplexa* phylum is the presence of the **apicoplast**, a remnant plastid originated from the assimilation of a red algal organism. It is essential for *Plasmodium* survival, has its own 35 Kb circular genome and expresses a small number of genes, even though most of its proteins are encoded in the nucleus. Apicoplasts are not photosynthetic and their main functions are related to fatty acid, isoprenoid and heme synthesis; their pathways in these functions are typically prokaryotic, which have been exploited as drug targets for antibiotics. Research focused on this organelle aims at finding new antimalarial drugs [28,29]. This plastid is always near the mitochondrion in the intraerythrocytic stages (Figure 5), and comes to contact with the food vacuole as the parasite grows, as well as its complexity increases. In schizont stages, during merozoite formation, both apicoplast and mitochondrion replicate several times, so that there will be one of each in every merozoite [30].

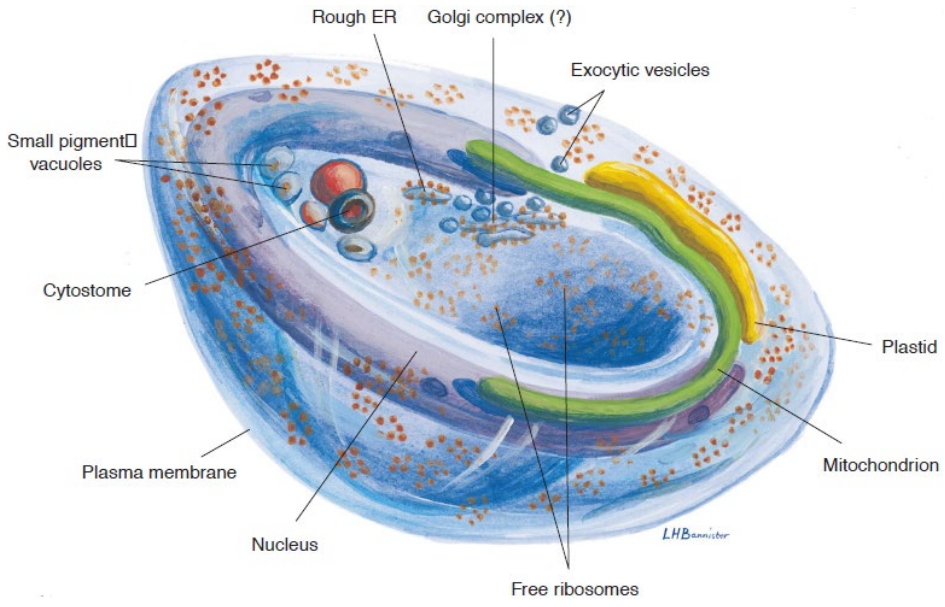

Figure 5: Morphology interpretation of a cup-shaped ring stage. Just the parasite is represented, without the host cell or PV. All organelles are depicted: plastid, mitochondrion, ribosomes, nucleus with elongated shape, and even small pigment vacuoles that later on will fuse forming just one large food pigmented vacuole. Image from [30].

In addition to these traits, it is also common in intracellular parasites to be inside a PV, formed by invagination of the host cell membrane. In *Plasmodium*, this happens in liver and intraerythrocytic stages. The **PV membrane (PVM)** has many alterations in its

components compared to the host membrane due to the export of lipids and proteins from the rhoptries during invasion. Many proteins from the parasite, which may form pores for nutrient intake or are part of the protein exporting machinery, are located in the PVM and are placed there either by the rhoptry discharge or through exportation by the parasite once it is inside the host (reviewed in [31]).

For protein export, special organelles called **Maurer's Clefts** seem to have an outstanding role. These organelles were discovered by Maurer in 1902 [32], who described them as small spots appearing during parasite growth, thanks to alkaline methylene blue staining. With the use of electron microscopy, Maurer's clefts could be observed in detail: narrow clefts, like vacuoles or sack-like structures, in the cytosol of the infected red blood cell bordered by a single membrane. They start forming early after invasion, possibly originating from the PVM and acquiring a flattened structure in later stages. There is a complex net of connection between individual Maurer's clefts, the PVM and the erythrocyte membrane (reviewed in [33]). So far research has pointed out their function as 'sorting stations', and only a few proteins are transported through the erythrocyte cytosol without passing through them. Many parasite proteins find their final destination in the Maurer's clefts, to form part of the export machinery. Since about 10% of parasite proteins are exported, this process has interest for the discovery of new drug targets (reviewed in [34]).

After passing through the Maurer's clefts, many parasite proteins are exported to the host cell membrane, where they mainly accumulate in the **knobs**: firstly described as *electron-dense infected erythrocyte protrusions*, these areas concentrate many strain-specific proteins that interact with the host, predominantly in cytoadhesion. Depending on the type of molecules displayed, parasites can form rosettes (aggregates formed when a parasitized cell attaches to healthy RBCs) or can be sequestered in the capillar endothelium of certain tissues, which are some of the traits that can arise symptoms of acute complicated malaria [35,36].

Finally, *P. falciparum* has a large **food vacuole**, formed through the fusion of smaller ones in early stages. Because the food vacuole is not present in merozoites, it forms part of the cell debris left after egress and starts forming from scratch once the invasion of a new host cell is completed. The food vacuole is acidic (pH 5.0 – 5.4) and has hemoglobinase and ATPase activity (reviewed in [37]). Here is where **hemozoin**, a characteristic crystalline pigment that grows as the parasite develops, is located.

The formation of hemozoin is very relevant for parasite survival and treatment development. Its discovery roots in microscopic observations of a golden-brown to black pigment within the infected erythrocyte that was promptly associated with malaria [38]. In 1891, Carbone suggested that such pigmented granule contained metalloporphyrin hematin [39]. Presence of hematin was confirmed in 1911 [40], and later investigations described it as 16% of hemozoin composition. The rest of components were of protein (65%) and carbohydrate (6%) nature, with trace amounts of lipids an nucleic acids [41].

Hemozoin derives from hemoglobin digestion. This protein is the main source of amino acids for intraerythrocytic malaria parasites, as its content in erythrocytes decreases during the parasite growth inside those [42]; the free amino acid concentration inside non-infected cells is lower and, when hemoglobin is labeled, such label appears in parasite proteins (reviewed in [43]). Hemoglobin is taken up by trophozoites and early schizonts when they ingest cytoplasm in cytosomes, which are transported to the food vacuole [44]. When hemoglobin is proteolyzed, α-hematin (also known as ferriprotoporphyrin IX) is released. This compound is a pro-oxidant, and can produce reactive oxygen species, becoming toxic for the cell. In addition, hematin can disrupt cell membranes, adding another toxic effect as it could lysate the erythrocyte [45]. To avoid this toxicity, parasites produce hemozoin by crystallization, forming insoluble and inert β-hematin crystals in a process in which pH, lipid interactions and/or enzymes could be involved [46,47]. Among the proteins that have a role in the process, Heme Detoxification Protein is secreted in the infected RBC cytosol and accompanies hemoglobin in its incorporation into the food vacuole, where hemozoin forms [48].

Hematin toxicity and hemozoin synthesis blocking is one of the exploited mechanisms in antimalarial treatment. Quinolines, such as quinine and chloroquine, interact with the hematin found in hemozoin [49,50], and artemisinin activity also involves interactions with heme groups [51].

Not only hemozoin formation is an important target for drug treatment, but also its physicochemical characteristics provide mechanisms for isolation of parasites through magnetic interactions [52]. Besides, its crystalline structure can help to identify parasite stages through light depolarization [53] and both magnetic and optical characteristics were studied for developing malaria diagnostic tools [54,55]. New research approaches study its influence on parasite growth under magnetic rotating fields [56].

1.1.3. Interactions with the human host, parasite evasion and immune responses

The interactions between *Plasmodium* and its human host are very complex. During its intraerythrocytic strages, the parasite can be subject of spleen sequestration, as this organ naturally filters defective RBCs mechanically. The increased stiffness of the parasitized RBCs (pRBCs), specially at their late stages, retains them in this organ, and can produce splenomegaly or enlargement of the spleen, which has been associated with anemia (the spleen role in malaria infection has been reviewed in [57]). To avoid clearance from the circulation system, there is another type of sequestering induced by the parasite: adherence to endothelium of capillaries, which is characteristic of *P. falciparum*. This occurs mainly in trophozoite and schizont stages, when the parasite exposes proteins that interact with the endothelium ligands, and has enough rigidity to be cleared up by the spleen. Besides, clonal switching in the parasite can tune the adhesion to melanoma cells [58]. There are several proteins (that will be described in section 1.1.4) involved in endothelium sequestration that are subjects of antigenic variation: the protein variants are expressed differently in different parasite clones, and are subject of selection by antibody recognition, when the immune system raise a response against a specific clone of the parasite, other different clones can escape from it. The switching has epigenetic nature, and each new generation of parasites randomly expresses different alleles of these proteins (antigenic variation and influence in the disease has been reviewed in [59,60]).

Both cytoadhesion of the parasite and the antibody response of the host relate with the clinical outcome in humans. Severe malaria mostly appears in non-exposed individuals when they first encounter the parasite, either children or naïve adults from non-endemic regions. With exposure, humans can have almost complete protection against the death from malaria, although they will still carry the parasite and mild illness or an asymptomatic version of the disease develops [61]. Complete sterile immunity does not seem to be achieved through parasite exposition, though this partial immunity can limit parasite density and symptoms [62]. In addition, it seems that for maintaining this level of immunity, frequent exposure to *P. falciparum* is needed. Parasite derived material or the infected erythrocytes can interfere with the generation of memory T cells and antibodies, leading to this partial immunity [63]. The complex relationship of the parasite with the immune system is impairing so far the development of an effective vaccine.

As a result of selection pressure along human biological evolution, some traits have been maintained within the population like sickle cell disease, hemoglobinopathies, cytokine mutation and enzyme deficiencies that confer some resistance to *Plasmodium* infection [64,65].

1.1.4. Natural exposed parasite targets

In several sections of this work, surface targeting of the parasite will be discussed as vaccination, drug delivery, treatment or diagnostic approaches in malaria research. In this section, different molecular features that have potential for targeting *Plasmodium* are described, with focus on what the parasite exports to the membrane of the RBC and the parasite forms that are not intracellular.

Adhesive proteins exposed in the erythrocytic cycle

Several surface characteristics distinguish a healthy cell from a *Plasmodium*-infected one. Among these features in the parasitized cells, the knobs that have already been described display many of the parasite proteins present on the surface of the pRBC, and they are related to cell adhesion.

First in line, ***P. falciparum* erythrocyte membrane protein 1 (PfEMP1)** is a protein exposed in the erythrocyte surface involved in **adhesion and sequestration processes**. It is encoded by var genes, of which there are more than 60 allelic variants, subject to the antigenic variation mechanism and are expressed in a mutually exclusive manner [60]. There are 3 main subgroups of *var* genes (known as A, B and C), 2 intermediate subgroups (with shared characteristics between B/A and B/C) and 2 gene subfamilies that do not fit within any of the groups (*var1* and *var2*) [66]. This classification correlates with the types of adhesion domains present in the protein, and, therefore with the parasite cytoadhesion tropism [67].

PfEMP1 is displayed on the knobs, and the variant expressed can influence knob density and distribution [68]. Some reviews [22,69,70] have already covered the characteristics and importance of this protein in the sequestration process and the interaction with the immune system during infection. Only some highlights related to the binding interactions are described here: those important in the clinical outcome and those generally more represented.

Among the **endothelial receptors** that PfEMP1 binds to, cluster of differentiation 36 (CD36) is the most common (Figure 6). Evidence suggest that their interaction is not implicated in severe malaria, but in mild forms of the disease [71,72]. Subgroups B and C of the parasite protein mostly bind CD36, with the binding site in the cysteine-rich-interdomain-region 1 alpha. These subgroups are formed by a wide variety of different sequences that conserve adherence but elicit antibodies that are not cross-reactive between the variants [73], producing the immune system evasion-effect when the parasite switch the allele.

Some other variants from PfEMP1 subgroups B and C recognize intercellular adhesion molecule 1 (ICAM1) [69]. This interaction has been related with cerebral malaria [71]. Antibodies against these variants are also selective for specific parasite isolates [74]. Several parasite

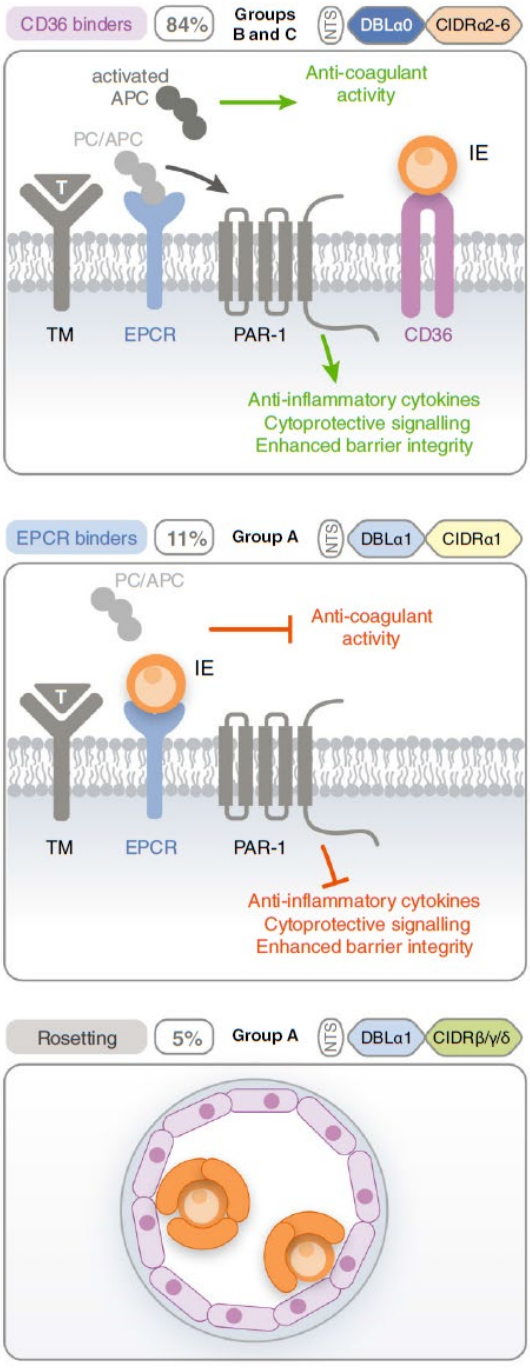

Figure 6: Depiction of the main subgroups of PfEMP1, their most common head structure and the outcome when binding their receptors. The most common adhesion is with CD36, associated with mild malaria. EPCR binding and rosetting is linked to subgroup A of PfEMP1, and is associated with severe malaria. When parasite (IE) sequesters, interferes in the signaling cascade of which EPCR is effector: protein C (PC) binding of EPCR is activated by the thrombin (T)/thrombomodulin (TM) complex; activated protein C (APC) is released and mediates anticoagulant activity while interactions with EPCR activate the protease activated receptor 1 (PAR-1) and mediates intracellular signaling with its effects. Figure from [70].

lines have synergetic interaction between both CD36 and ICAM1 [75].

However, the variants that are more related to severe malaria are within the subgroup A of *var* genes, as those that bind the endothelial protein C receptor (EPCR). The binding blocks the signaling pathway of which EPCR is responsible, having implications in coagulation and cytoprotection, and might contribute to the neurological damage and mortality produced in cerebral malaria [76,77] (Figure 6). In addition, synergetic interactions have also been observed for ICAM1 and EPCR, and are associated with increased risk of developing cerebral malaria [78].

Besides, some other variants of PfEMP1 from the subgroup A mediate **rosetting**. These are rarely expressed *in vitro* and require selection for maintaining them [72]. This phenomenon is dependent on the ABO blood-group antigens [79]. Several publications point to heparan sulfate proteoglycans as ligand for rosette formation, which can be disrupted by heparin or related molecules [80–82]. This topic will be discussed in section 3.

Among the variants related to severe disease outcomes, and belonging to its own family of *var* genes (*var2*), **VAR2CSA** is a specific variant of PfEMP1 responsible for *P. falciparum*-infected RBC **sequestration in the placenta**. Such accumulation of parasites is the cause of placental malaria, a severe syndrome that occurs when pregnant women, especially primigravidas, are infected with *P. falciparum*. The main symptoms are anemia and low birth weight infants, occurring due to alterations in the inflammation responses and structure of the placenta, which can subsequently provoke placental insufficiency and intrauterine growth retardation [83–85]. The ligand associated with the sequestration is chondroitin sulfate A (CSA), present in the intervillous spaces of the placenta in the form of chondroitin sulfate proteoglycans.

Upregulation of the *var2csa* gene in parasite isolates selected for CSA adhesion *in vitro*, and in placental isolates relative to those from peripheral blood in children, demonstrated the role of this variant in placental malaria [86]. The protein was found in CSA-selected pRBCs, and, when anti-VAR2CSA IgG levels were high in pregnant woman, the risk of low birth weight was reduced [21]. In addition, disruption of the *var2csa* gene abolishes parasite binding to CSA [87], proving that this gene provides the capacity of adhesion to CSA in this parasite. The recombinant protein could bind directly to immobilized CSA [88].

The VAR2CSA subfamily is defined by its ability to bind CSA and by their unusual structure: these proteins have seven domains, three N-terminal DBLx (also named DBL_{PAM}), then three DBLε domains and one single $CIDR_{PAM}$ domain placed between DBLx2 and DBLx3 [69]. Research towards finding the binding site of CSA highlights the importance of the DBL regions, though there is no consensus on which would have the main role: some evidence points to DBLx2 [89,90] or DBLx3 [91] regions or the combination of binding sites in neighbor regions between DBLx1-DBLx3 [92,93]. Some other publications differ from this interpretation, attributing the binding site to other regions [94] or arguing that the greatest affinity is only obtained with the full-length protein [95,96].

It should be pointed out that the affinity and strength of the binding between VAR2CSA and CSA depends on the allelic differences of this protein. *P. falciparum* isolates expressing different variants of *var2csa* had different preferred structural motifs for adhesion, correlating with the polymorphisms found on the proteins [88]. Such polymorphisms have been related with different signatures and parasitemia rates in the placenta, and it is suggested that a higher parasitemia in these cases could be related with a higher affinity for CSA [97]. Allelic-variant presence makes it harder to obtain a cross-reactive antibody for placental malaria prevention.

Other non-PfEMP1 proteins are also being studied with the objective of broadening the knowledge of all *Plasmodium* cytoadhesive processes. Repetitive interspersed family (**RIFIN**) proteins and subtelomeric variable open reading frame (**STEVOR**) proteins are also localized and exposed on the erythrocyte surface [98]. STEVOR recognizes Glycophorin C on the RBC surface and it is involved in rosette formation independently from PfEMP1 [99,100]. Both RIFIN and surface-associated interspersed gene family (**SURFIN**) proteins elicit antibodies in the human host and might have a role in rosetting [101]. Although these proteins are less studied than PfEMP1 so far, they also have potential for developing targeting tools towards the parasite due to their exposure.

New permeation pathways in the erythrocytic cycle

Other important exposed pRBC features are all the proteins that form channels for nutrient uptake by the cell. Known as **new permeation pathways (NPP)**, their function is maintaining nutrient uptake and ion pumping for the parasite. It has been suggested that

there are several of these channels [102], and they could be either expressed by the parasite itself or by upregulation of host channels [103].

Most of the evidence about parasite expressed channels resides in the studies about the plasmodial surface anion channel (PSAC), which has been related to *clag3* genes, and contributes in nutrient acquisition for the intracellular parasites [104]. *clag3* genes have allelic variants that are generally mutually exclusive expressed (though it is not impossible that the variants are expressed at the same time, this is not the usual situation) [105] and recent evidence points to dimeric organization of clag3 proteins to form the PSAC channel, together with two other proteins whose exact function is still not known [106].

PSAC has been studied for developing new antimalarial strategies [107], although its expression can alter susceptibility of the parasite to certain growth inhibitors, in addition to affecting nutrient uptake [108,109].

Lipid composition changes in the pRBC

Not only exported proteins from the parasite make the difference in the pRBC surface, lipid composition can also vary compared to the healthy RBC [110,111].

In addition, the RBC has an asymmetry of lipid composition between the two leaflets of the plasma membrane, phosphatidylserine (PS), for instance, is not usually exposed in the outer leaflet. When it is exposed, PS becomes a marker of RBC aging, and the cell is removed from circulation [112]. PS exposure in most mammalian cells is an apoptotic signal and macrophages phagocytose the cell or cell components exposing PS [113].

In some pRBCs, it has been observed that PS becomes exposed in the cell surface [114]; its exposure increases with parasite maturation and is higher in febrile conditions [115]. PS could increase phagocytosis of pRBCs by spleen macrophages [116] and antibodies against PS have been found in malaria patients infected by *P. falciparum* and *P. vivax*, which could contribute to the removal from circulation of these cells [117–119]. However, the presence of *Plasmodium* seems to accelerate senescence of non-parasitized RBCs and PS exposure on them too [115]. All these mechanisms increase anemia in patients whereas removal of healthy RBCs might limit removal of pRBC [116,119].

Additionally, PS could have a role in pRBC sequestration [120,121], since its exposure increases cytoadhesion of already adhesive phenotypes [122] and it has been suggested that this phenomenon is responsible for *P. vivax* sequestration [123].

Merozoite reinvasion and involved interactions

The process of merozoite invasion of a new RBC is subject for targeting discovery and therapy development, as the parasite is in a free form for a short time, and if the mechanism can be inhibited, it would prevent the next cycle of the parasite's development.

Erythrocyte invasion is a multi-step process (reviewed in [124–126]) composed of the following mechanisms: initial contact, reorientation, commitment to invasion, tight-junction formation and invasion (Figure 7). A summary of these processes will be presented here, but special emphasis will be placed on the initial steps, which are those studied for a targeting approach in the experimental work.

Thanks to the study of blockage of receptor-ligand interactions, it has been proposed the following sequence of events [126,127]:

- First, when the merozoite contacts with the RBC, due to certain interactions between the merozoite surface protein 1 (MSP1) complex and the cell surface, the plasma membrane of the RBC is weakly distorted.
- Shortly after, the erythrocyte binding antigen (EBA) and *P. falciparum* reticulocyte-binding protein homolog (PfRh) ligands allow a stronger binding through alternative pathways, helping in the deformation of the cell and the reorientation of the merozoite.
- Other PfRh ligands, such as PfRh5 –which binds the host receptor basingin-, trigger the process known as rhoptry release, consisting in a calcium influx at the contact point.
- The rhoptry release continues with the translocation of rhoptry neck protein 2 (RON2) into the RBC membrane.
- The binding of RON2 and apical membrane protein 1 (AMA1) forms a tight junction, allowing penetration of the merozoite while forming the parasitophorous vacuole.

- While penetrating, many proteins of the merozoite surface are cleaved, shed and released in the plasma. Examples of these proteins are MSP1, MSP3, MSP7, serine repeat antigen 4 (SERA4), and SERA5 [128].

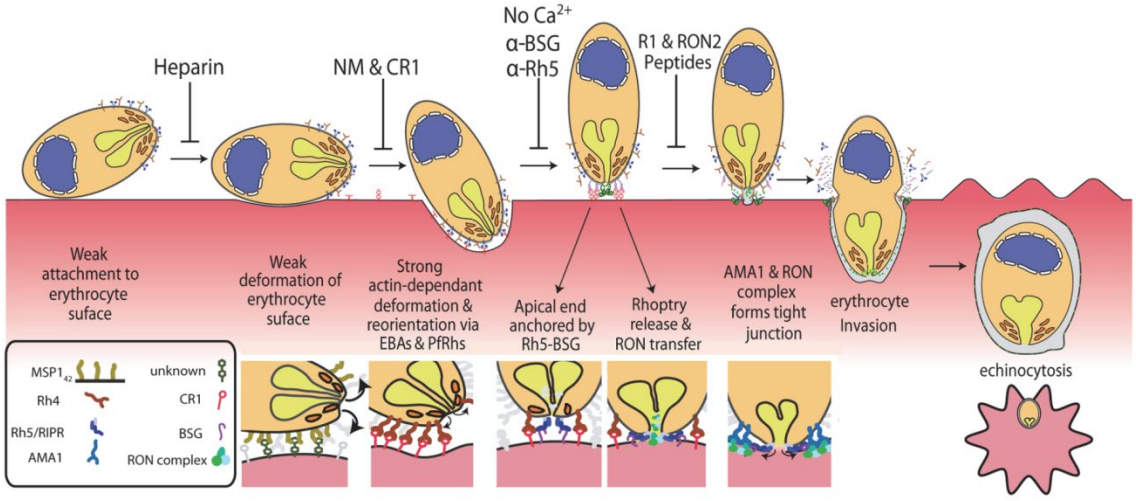

Figure 7: Scheme of the steps and interactions during merozoite invasion. The attachment to the erythrocyte surface involves mainly electrostatic interactions, and a tighter interaction that leads to the deformation of erythrocyte surface can be inhibited by heparin, stopping the process[127,129]. While erythrocyte invasion happens, there is a shedding of surface proteins that are released in the plasma. Adapted from [30].

There are still many unknown ligands and receptors involved in this process, but it has been possible to identify some of them and other molecules that inhibit such binding, and, therefore, the merozoite invasion (Table 1).

Table 1: Main ligand-receptor interactions involved in the RBC invasion and inhibitors of them. As described in [127] with small additions.

Step	Parasite ligand	RBC receptor	Inhibitor
Initial contact	MSP1 complex	Glycophorin A [130] and/or proteoglycan with heparan sulfate chains	Heparin
Reorientation	EBA175	Glycophorin A	Cleavage of sialic acids by neuraminidase
	EBA140	Glycophorin C, heparan sulfate [131]	
	EBL1*	Glycophorin B	
	EBA181	Receptor W (non-identified)	-
	PfRh1	Receptor Y (non-identified)	-
	PfRh2a	Unknown	-
	PfRh2b	Receptor Z (non-identified)	-
	PfRh4	CR1	CR1 protein subunits
	PfRh5	Basingin	Antibodies anti-PfRh5 or anti-basingin
Tight junction	AMA1	RON2 (exported by the parasite)	R1 and RON2 peptides Compounds described in [132]

*EBL stands for erythrocyte binding ligand.

Ca^{2+} is required for invasion, and inhibition of the actin-miosin motor by cytochalasin D stopped the process after the formation of the tight junction, indicating that it is necessary to complete invasion [127]. It has also been hypothesized that STEVOR could have a role in this process, as antibodies against it block merozoite invasion and the protein interacts with glycophorin C [99].

In the initial steps of erythrocyte adhesion, MSP1 is the best studied in terms of functionality. As even in presence of heparin, merozoites are still adhered to RBC, it has been suggested that some other ligand-receptor interaction might be involved in this binding process [126,127]. Until more proteins and their roles are reported, MSP1 remains the most interesting target within this step of invasion. MSP1 is the largest protein of its family –a dimer of more than 500 KDa- and it has the highest copy number. All MSP are GPI-anchored proteins, which have fluid movement in membranes. They could accumulate in the interface were both cells are adhered, and, by joining their ligands, such cumulate interactions could originate the indentation of the RBC membrane [127]. The whole MSP1 complex includes four pre-processed MSP1 fragments that can bind to $MSP7_{22}$, $MSP6_{36}$, MSPDBL1 and MSPDBL2. The precleavage MSP1-42 C-terminal domain is being used for vaccine development [25,26] and antibodies against this protein or its fragment that remains in the merozoite during invasion (MSP1-19) inhibit parasite invasion of RBCs [24]. Antibodies against other members of the complex can also block invasion and confer some protection against malaria [133].

Transmission and mosquito *Plasmodium* stages surface

Even though transmission and mosquito stages of *P. falciparum* do not represent a clinical concern *per se*, as they do not induce any symptom in patients, their elimination is key for eradicating the disease. The number of parasites present in these stages is very attractive in terms of treatment application or blocking strategies development, they are considered parasite 'bottle-necks' [134]. Some specific targets known from these stages are here described.

Although they are still inside a RBC, **gametocytes** are of interest for transmission blocking strategies. These cells are retained in the bone marrow during their maturation, and fully mature gametocytes are released into the blood [13]. How they extravasate and remain out of circulation is a broad topic of discussion. It seems that this 'sequestration' profile might not be driven by adhesive proteins, as gametocytes from stages I-IV do not produce antibodies in

natural infections [135], and there is evidence of enhanced gametocyte formation in red blood cell precursors [136]. The two main proposed mechanisms are (i) after extravasation of young gametocytes, and either they adhere or their stiffness increase and remain in the bone marrow until maturation, or (ii) the asexual pRBCs extravasate, and when in the bone marrow they mature and burst and the newly invaded cells in the erythroblastic islands form mostly gametocytes [137].

Stage V mature gametocytes do produce antibody response [135], but this mainly comes from intracellular targets, thus it is hypothesized that those proteins are exposed when gametocytes die in circulation [138].

After **gametes** egress from the RBC, many proteins that were hidden become fully exposed to the environment. This occurs inside the mosquito midgut, but still antibodies and human complement remain within the blood meal, making feasible to block parasite fertilization. Among the proteins exposed, those that had been arousing more interest are:

- **Pfs48/45:** it is a GPI-anchored surface protein expressed in gametes with a prominent role in male fertility (disruption of the gene does not impair female gamete fertility in the orthologous gene of *P. berghei*) [139]. Antibodies against this protein block fertilization and parasite development in the mosquito [140].
- **Pfs230:** forms a complex with the previous protein and antibodies against it also block transmission [141]. It is suspected to have a role in fertility [142].
- **Pfs25:** is another GPI-anchored protein, but only present in the female gamete surface, also conserved after fertilization and ookinete development, which elicits transmission blocking antibodies [143]. In ookinetes, as it seems to interact with laminin, it might have a role in parasite-host interaction [144].

Many of these are considered adhesive proteins, and seem to form large complexes between them and with other proteins. Evidence suggests that the complex with Pfs48/45 and Pfs230 interact with six proteins of the family of LCCL (Limulus clotting factor C, Cochlear protein 5b2 and Lung gestation protein 1) domain-containing proteins, known as PfCCp, possibly already inside the PV in the gametocytes, and Pfs25 might come in contact with the complex when gametes have egressed (see Figure 8) [145]. Some of the PfCCp proteins are essential for fertilization, and they can also be promising candidates for transmission-blocking [146].

With this evidence, it is highlighted that the complexity of interactions and the high number of proteins present on the gamete surface could allow many approaches for interventions in transmission blocking strategies. However, because this stage is not present in humans, interventions on it do not have an effect on disease development, and, on the other hand, interventions at molecular level are difficult to assess in mosquito populations.

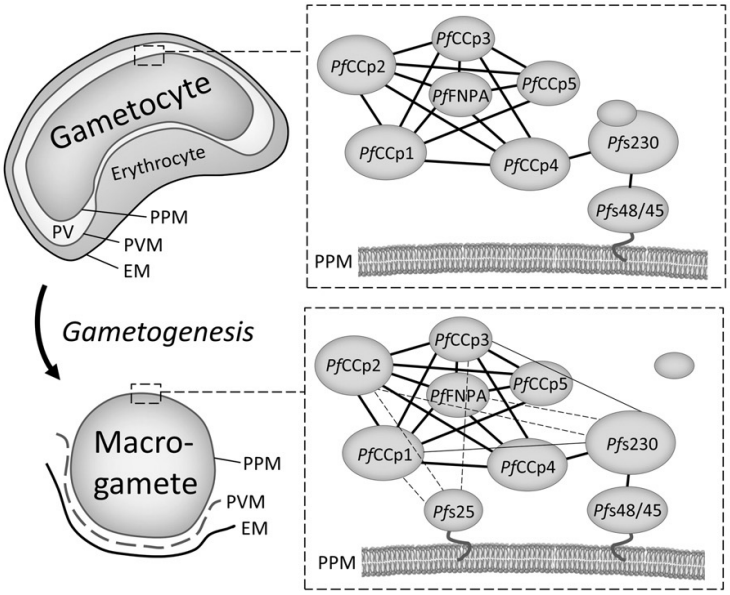

Figure 8: Proteic multicomplexes described in gametocytes and macrogametes. Interactions of the proteins in the parasitophorous vacuole of gametocytes associated to the parasite plasma membrane are represented with thick lines. Thin lines represent additional interactions after gamete egress. Dashed lines indicate protein complex affiliation without the evidence of direct protein interaction. Pfs230 is processed during gametogenesis, as represented by the release of a fragment. EM, erythrocyte membrane; PPM, parasite plasma membrane; PV, parasitophorous vacuole; PVM, parasitophorous vacuole membrane. Adapted from [145].

When fertilization occurs, the **zygote** and its mature form, the **ookinete**, can also be subjects of targeted intervention by blocking the interactions with the mosquito midgut epithelium, necessary for traversing the midgut and allowing oocyst development. Besides the proteins already highlighted that are inherited from macrogametes, the gliding (motility) machinery proteins also have interest for targeted strategies. Of this protein complex, circumsporozoite- and thrombospondin-related anonymus protein (TRAP)-related protein (**CTRP**) is realeased from micronemes [147], and stays exposed on the ookinete surface. Disrupting the gene that encodes this protein produces parasites with reduced motility that fail invading the midgut [148]. It contains six von Willebrand factor A-like (A) domains, which are essential for gliding [149].

Additionally, on the ookinete surface, putative secreted ookinete protein 25 (**PSOP25**) is also a highly conserved protein that, when knocked out, affects the formation of oocysts and antibodies against it can reduce oocyst density [150]. Similarly, subtilisin-like ookinete protein (**SOPT**) is also present on the cell surface and, when deficient, less oocysts develop for these parasites [151].

Among the mosquito stages, the **oocyst** is possibly the most difficult to reach in terms of targeting. Placed between the migdut epithelium and the basal lamina, it is rather protected from agents coming from mosquito feeding. However, these sessile forms do arise mosquito immunity responses (reviewed in [152]), and therefore development of targeting molecules helping in this process might be of interest.

In contrast with other less studied mosquito stages, **sporozoites** bear much interest because they are the transmission forms between mosquito and human. Their potential targets for vaccine and treatment development are:

- **Thrombospondin-related anonymous protein (TRAP)**, is stored in micronemes and released when the sporozoite contacts with a host cell, allowing its penetration, as it links the actin-myosin motor and binds the hepatocyte with its extracellular part [153]. It is a transmembrane protein with a thrombospondin type 1 repeat (TSR) domain and an A domain, both related with heparin-like proteoglycans binding in a cooperative way [154].
- **Circumsporozoite surface protein (CSP)**: this protein is uniformly distributed over the surface of sporozoites [155]. Even though different parasite isolates can present differences in their CSPs (such as apparent molecular weight), cross reactivity with antibodies is possible, indicating that they share certain epitopes [156].
- **AMA1**: this micronemal protein is also present in sporozoites (not only in merozoites) and in this stage it is also related with the cell-invasion process [157].
- **Cell traversal protein of ookinetes and sporozoites (CelTOS)**: is a micronemal secreted protein in both sporozoite and ookinete stages, its function is related with the passage from blood to hepatocytes in sporozoites and midgut endothelium transcellular crossing in ookinetes [158].

Both approaches, using individual proteins and whole attenuated sporozoites, have been researched to block parasite transmission by vaccine development.

1.2. Treatment

The first known effective therapy against malaria in the form of an isolated compound was quinine, obtained from Cinchona bark since 1820 [159]. The quinine mechanism of action seems to be related with heme processing in the food vacuole of the parasite [160]. As this compound had important adverse effects, when a new well tolerated and inexpensive antimalarial appeared, it rapidly became the first line treatment for malaria. This drug was chloroquine, synthesized in Germany in the mid-1930s and widely applied after World War II [159]. Its use, together with vector-elimination measures, were the two main reasons for the success of the malaria elimination campaing in all the endemic non-tropical regions during the 1950-1960's [4]. However, due to the emergence of resistances to chloroquine, application of other antimalarials was required [161].

Current antimalarial therapies relay on the artemisinin combination therapy or ACT. The Chinese Youyou Tu, who was researching for new antimalarial therapies by checking ancient Chinese farmacopeia, discovered artemisinin in the 70's. It is extracted from *Artemisia annua*, and many derivatives have been developed to improve its characteristics for antimalarial treatment. The mechanism of action of these compounds is not well defined yet, but it is related with hemoglobin digestion and formation of oxidizing species [162]. More recently, it has been reported that artemisinin has influence on parasite proteostasis, influencing its protein expression, degradation and folding [163].

ACTs are based on the use of artemisinin or one of its derived molecules together with another partner drug. Artemisinin derivatives have a very fast parasite clearance action, but also a very short circulation time, and thus the strategy is to combine them with a longer-acting partner drug that also has slower elimination. This measure can prevent evolution of resistances against artemisinin-derived compounds and it is suggested that it could serve as post-treatment prophylaxis [164]. However, the fact that only one drug is present for long periods of time could also arise some resistances against it, and thus this kind of treatment is not exempt of controversy [165].

WHO guidelines about malaria treatment specify that **uncomplicated malaria** (except for pregnant women in their first trimester) should be treated with one of the following oral ACTs formulations [164]:

- **Artemether + lumefantrine**. Artemeter is a water-insoluble, lipid-soluble compound, it is metabolized into dihydroartemisinin, which bears the antimalarial activity, and it is eliminated 7 hours after administration, with a circulation half-life ($t_{1/2}$) of 2-3 hours. Lumefantrine is also lipophilic and is recommended to be administered together with fatty foods or milk for better absorption. Lumefantrine has a $t_{1/2}$ of ~3 days, and it has never been used as monotherapy, which reduces the risk of resistance evolution.
- **Artesunate + amodiaquine**. Artesunate is water-soluble and it is metabolized into dihydroartemisinin. Amodiaquine is similar in structure and mechanism of action to chloroquine. Its active metabolite is desethylamodiaquine which has a $t_{1/2}$ of 4-10 days. There are not pediatric formulations for this ACT.
- **Artesunate + mefloquine**. Mefloquine is structurally related to quinine and it is thought to have a similar mechanism of action. It has an elimination $t_{1/2}$ longer than 3 weeks.
- **Dihydroartemisinin + piperaquine.** Dihydroartemisinin has poor solubility in water, but it is well absorbed in the digestive track. Piperaquine is from the family of compounds related to chloroquine, and it is thought to act similarly to it. It has a $t_{1/2}$ of 2-4 weeks.
- **Artesunate + sulfadoxine-pyrimethamine (SP)**. Sulfadoxine and pyrimethamine inhibit the synthesis of folic acid in protozoa acting on different enzymes of the metabolic route. Their $t_{1/2}$ is 4-11 days and 3-19 days respectively. There are not pediatric formulations available for this ACT.

Special treatment guidelines are applied for pregnant women in their first trimester (quinine combined with clindamycin is used in this case) and for Human Immunodeficiency Virus (HIV) co-infection (were artesunate + SP and artesunate + amodiaquine can have undesired effects when administered with some retroviral treatments).

The guidelines for severe malaria are different, as the patients might not be able to take oral treatment. In these cases, parenteral or intramuscular administration of artesunate is recommended until the patients can tolerate oral ACTs [164].

Despite how potent most antimalarials available are, there are several flaws that can limit their use: the widespread emergence of resistances, their toxicity, their pharmacokinetics, and few others that will be described in the following pages.

Resistances

Most of the antimalarials available have some resistance in the field (figure 9).

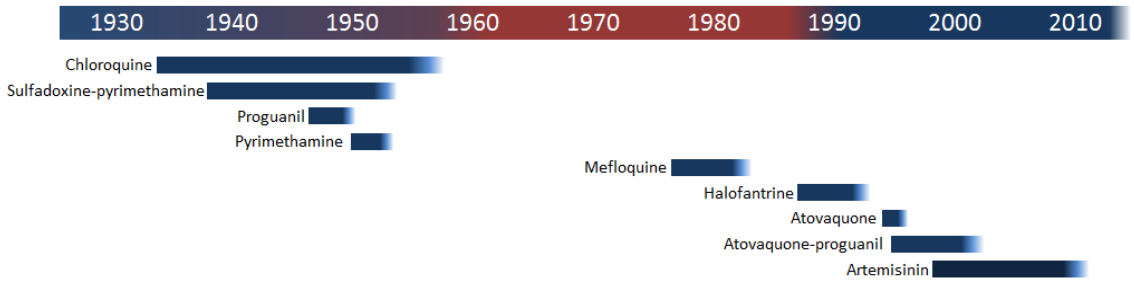

Figure 9: Resistance timeline to antimalarial drugs. Approximate periods from drug discovery or application to identification of resistances. Adapted from http://www.multimension.com/project/visualizing-global-health-challenge-malaria/.

First observations of antimalarial treatment failure dates from the late 1950s, in Southeast Asia and Latin America, and during the 1980s chloroquine resistance spread across Africa [166]. The main mechanism for chloroquine resistance is to increase its efflux from the digestive vacuole [167], where it blocks the heme detoxification pathway [168]. Mutations in transporter proteins can produce resistance to quinolines, as happens with the *P. falciparum* chloroquine resistance transporter [167], and *P. falciparum* Na+/H+ exchanger 1 that is related to quinine resistance [169]. Similarly, other protein transporter gene, *P. falciparum multidrug resistant gene 1* (*pfmrg1*), produces resistance to mefloquine when present in high copy number [170], while, with low gene copy number, the parasite's drug susceptibility is increased for mefloquine, lumefantrine, halofantrine, quinine and artemisinin [171].

Artemisinin resistance was first reported in 2009, associated to slow parasite clearance with artesunate-mefloquine [172]. Most cases of reduced artemisinin susceptibility relate to mutations in the *pfk13* gene [173,174], though additional mechanisms not associated with this gene could also induce artemisinin resistance [175,176].

In addition, specific biological conditions have been observed to reduce parasite susceptibility to drugs, such as metabolic changes of the parasite [177] or sequestration in the spleen [178].

In order to cope with antimalarial resistance evolution, new strategies are being proposed and tested, including: (i) changing the ACT combination used in the region where treatment failure increases [164], (ii) preparing new combinations with other antimalarials [179], (iii) administrating triple drug combinations [180], (iv) researching new antimalarial compounds [181–183], and (v) developing new formulations for increasing antimalarial efficacy, which will be discussed in section 2 of this work.

Toxicity and side effects

Many antimalarials produce important adverse effects or have some toxicity in certain patients:

- Quinine has common adverse effects like headache, tinnitus, deafness, dysphoria, all together known as cinchonism [159].
- Other antimalarials like proguanil or amodiaquine can have higher toxicity in patients with polymorphisms in drug-metabolizing enzymes or transport proteins [184].
- A similar situation occurs with primaquine, where patients with deficiency of glucose-6-phosphate dehydrogenase can have hemolysis when this drug is administered [185].
- Mefloquine can produce important neuropsychiatric adverse effects and, more commonly, gastrointestinal adverse effects [164].
- Piperaquine can have cardiovascular adverse effects if ingested with high-fat meals [164].

These adverse and toxic effects can limit the dosing window at which antimalarials are efficient and do not produce toxicity. In addition, patient's adherence to treatment is highly influenced by these effects.

Pharmacokinetics of antimalarials

In general, artemisinin derivatives have short half-lives [186,187], so, to ensure parasire clearance and to reduce the likelihood of artemisinin resistance selection, the accompanying drug is usually long-lived ($t_{1/2}$ of >4 days). However, as discussed before, this approach could enhance resistance selection because of the relative long time time when only one of the drugs

is circulating in the patient [165]. In contrast with other antimalarials, chloroquine has an excellent absorption and circulation time profile [188], but it is not longer recommended due to the emergence of resistance [161]. It is still recommended in areas where resistances are not described yet, but only for treatment of non-*P. falciparum* species [164].

Some other concerns in antimalarial therapy

The routes of administration of antimalarials are mainly parenteral for severe malaria and oral for uncomplicated malaria. In the second scenario, antimalarial compounds must be absorbed in the digestive track and incorporated in the circulation to have any effect, and this is determined by their bioavailabiliy. Some drugs like amodiaquine [189] and all artemisinin derivatives except artesunate [190] have **poor bioavailability**, not reaching 35% in most of them, thus requiring high dosage in patients that could derive in toxic effects.

Besides this, antimalarials have to reach and **penetrate the pRBC**. Artemisinin and derivatives, for example, tend to accumulate in other non-target tissues [190] and interact with plasma proteins [186], both promoting removal of the drug from circulation. Additionally, active compounds must cross at least 3 membranes to reach their molecular targets (the erythrocyte membrane, the PV and the parasite membrane) [191], and some of them even have their target inside organelles. There are two main mechanisms to traverse such membranes: either lipid diffusion or channel transport. Lipophilic drugs with good oral absorption are predicted to be able to cross such lipid bilayers [191]. For other drugs, NPPs are usually the entering gates into the pRBC, and thus variations in expression of these channels can produce either susceptibilities or resistances to drugs, due to facilitation or inhibition of their transport [108,192,193].

Once inside the erythrocyte, further penetration into the PVM or the parasite do not pose much difficulty, as both are permeable for many solutes, [191] possibly to facilitate penetration of nutrients into the pathogen. Penetration into the target organelles when needed and residence inside them for long enough is also important for a good antimalarial activity. As it has been discussed when talking about resistances, chloroquine, quinine and other antimalarials rely on **permanence in the digestive vacuole** for their mechanism of action [169,194,195].

Pharmacodynamics is also a relevant issue in malaria treatment: the possible presence of two or more different metabolites for a drug provides variability in their activities, as

is the case of piperaquine, which has two main metabolites that do not have the same antimalarial activity and neither half-life [165]. Selecting the best antimalarials by paying attention to these details is a concern, as reflected when comparing the combination dihydroartemisinin-piperaquine and artesunate-amodiaquine: the former has better antimalarial activity, but the second combination has improved pharmacodynamics, determined by *ex vivo* plasma treatment of parasite cultures [196]. However, knowing the key antimalarial metabolites requires extensive research, although it could diminish side effects from the treatments, as formation of toxic metabolites derived from the original compound [197,198] could be avoided.

Competition or interaction of antimalarials with other drugs is also an issue to deal with when selecting an appropriate treatment. Aspirin competes with artemisinin and its derivatives for lipid binding, altering their penetration into the cell when administered together [199]. Antibiotics like rifampicin have been associated with quinine treatment failure and reduced levels of mefloquine, artemether, dihydroartemisinin and lumefantrine [164].

1.3. Malaria prevention

The main pillars of malaria prevention research are the avoidance of the transmission and the development of a vaccine that confers immunity.

1.3.1. Preventive and transmission-blocking chemotherapy

Chemoprophylaxis is a strategy for malaria prevention that consist in providing treatment when there is risk of infection, recommended for those travelers that go to malaria endemic countries; in some locations, it is being applied for children [200] and pregnant women [201], following WHO recommendations.

As for the **transmission-blocking approach through chemotherapy**, WHO recommends a single dose of primaquine in addition to ACTs in malaria patients, in order to clear gametocytes that could still be transmitted during the treatment course [202].

1.3.2. Vector control

Vector presence is a key factor in malaria transmission, since it is through an infected mosquito bite how humans become infected. Many campaigns towards malaria elimination focus on eliminating or reducing the numbers of *Anopheles* mosquitoes or preventing their bites [4]. There are approximately 430 *Anopheles* species, and around 40 are responsible of transmitting human malaria in nature (distributed worldwide, as shown in Figure 10), while the rest either bite humans infrequently or cannot sustain development of human malaria parasites [203]. Those mosquito species that are malaria vectors can have biological differences in tropism (both animal preferences when biting and/or behavior differences) and breeding sites [204,205]. Their seasonal development, dependent in many regions of rainy seasons, can drive levels of transmission. Even human activity in endemic areas, like slash-and-burn agriculture or cattle raising, can affect the mosquitoes surrounding and, therefore, the transmission of malaria [206,207].

General approaches that are taken as vector-control measures are insecticide spraying, larvicide application in potential breeding sites and the use of insecticide-treated bed nets (ITN). However, insecticide resistance is an important concern in endemic regions (several insecticides have widespread resistances in mosquitoes) [1], and ITNs are only useful in well-

preserved conditions and if people at risk are under them, thus both ITN distribution [208] and the behavior of mosquito species in the region are important factors for having ITN efficacy in controlling the transmission of the parasite.

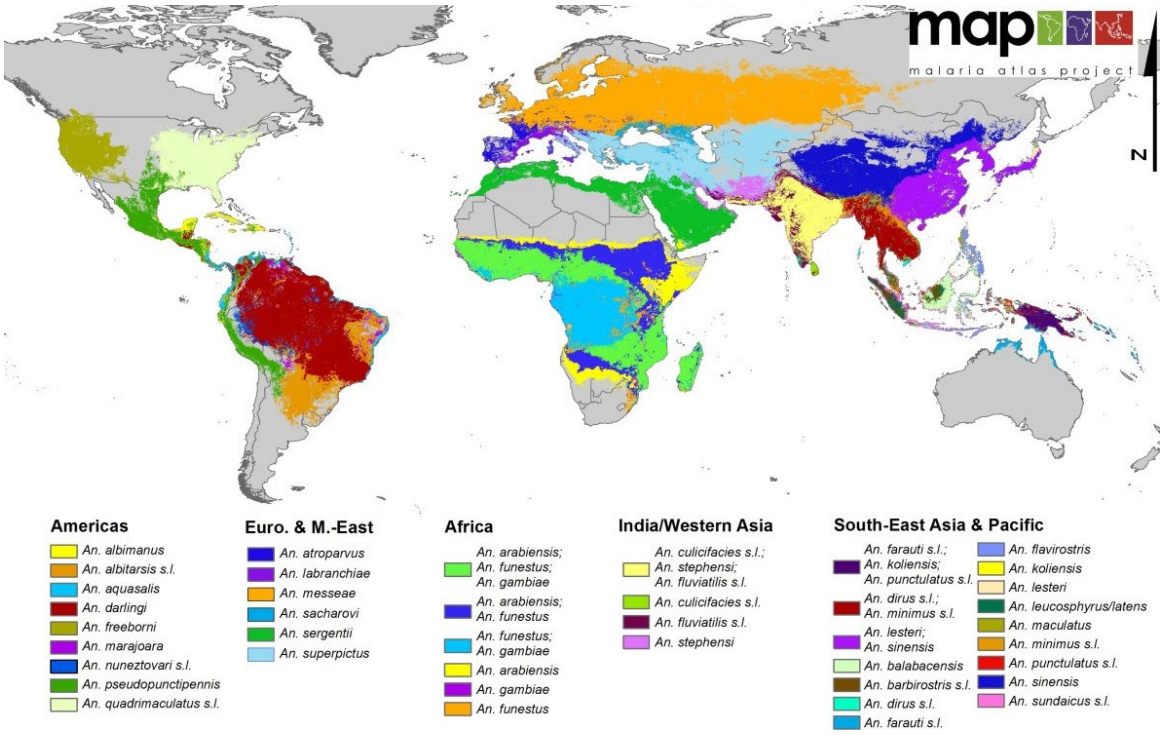

Figure 10: Distribution of the 34 dominant *Anopheles* species that can be *Plasmodium* vectors. These are or have been responsible for most of the parasite transmission to humans, but there are other species considered secondary transmitters that coexist with these. Image from [209].

On the other hand, some other vector-control approaches are being investigated:

- Research of new pesticides, of course, is one of the main pillars in this field. Sought-after approaches are those environmental-friendly, like larvicides from natural sources [210]. Nowadays, there is much interest in an administrable insecticide that is taken together with the blood meal, ivermectin, which has been proven effective and safe for humans [211].
- Limiting the mosquito ability to reproduce: sterilizing measures are being explored as possible ways to control the mosquito population, by physical means like exposition to X-rays [212], chemical exposure [213], or gene modification [214,215].
- Transgenic mosquitoes that block parasite transmission/development: parasites inside the mosquito could be 'attacked' with several approaches, for example, by engineering transgenic mosquitoes producing anti-CSP single chain antibodies in their

salivary glands, which impaired parasite transmission [216], or by suppressing specific mosquito genes essential for parasite development in this host [217].

- Studying other mosquito parasites or symbiotic organisms that can compete with *Plasmodium* might offer means of blocking parasite transmission [218–221].
- Application of antimalarials in the mosquito: recently, it was shown that mosquitoes can absorb the lipophilic antimalarial atovaquone when it is spread over surfaces, in the same way that insecticides over surfaces can penetrate mosquitoes, and arrest parasite development in infected insects [222].

1.3.3. Vaccine development

Vaccines that are being developed for malaria prevention can be classified according to the stages they target to: pre-erythrocytic, erythrocytic and transmission-blocking vaccines.

Pre-erythrocytic

These vaccines are aimed at developing antibodies against sporozoites, for blocking their invasion of hepatocytes, and prevent that malaria disease is developed at all. For now, the vaccine for malaria that has started to be applied belongs to this type: known as RTS,S/AS01 or Mosquirix™, is virus like-particle-based, and contains regions of the *P. falciparum* CSP known to induce humoral (R region) and cellular immune (T region) responses, which are covalently bound to the hepatitis B surface antigen (S), all combined with the adjuvant AS01[223]. It has passed phase 3 clinical trials, and has been able to prevent many malaria cases, but unfortunately its efficacy was near 30-45% (age-dependent) and the immune responses decreased with time [224,225], thus it does not confer high level of protection. Nevertheless, RTS,S received a positive regulatory assessment by the European Medicines Agency (EMA) in July 2015 [226], and WHO has recommended pilot implementation [223].

There are some other proposals, though not so advanced, using recombinant proteins, mostly based in CSP. Shiratsuchi *et al*. have included the same fragments of CSP already mentioned into the capsid protein of an adenovirus [227]. A new strategy tried to improve the immunogenicity of RTS,S by using its same antigens but delimitating more the antigen fragment from hepatitis B virus, a vaccine candidate named R21 [228]. Alternatively, whole CSP immunization has also been tested in preclinical assays [229].

Among other suggested approaches, direct immunization using sporozoite inoculation is being researched. Radiation-attenuated cryopreserved sporozoites were tested for inoculation and proven to be safe [230], though the transport in liquid nitrogen may arise concerns of the costs. Immunization by infection with live sporozoites followed by chloroquine treatment has been studied in murine [231] and non-human primate [232] malaria models. Another strategy is *Pb*Vac, a genetically modified strain of the murine parasite *P. berghei* expressing CSP from *P. falciparum*, to elicit immune response against this last one [233]. Most of these vaccine approaches are between phase I and IIa of clinical trials.

Erythrocytic

In contrast to the previous, immunization against erythrocytic stages does not prevent contracting the parasite, as hepatocyte could still be invaded by sporozoites, but it can block disease development by elimination of merozoites or other parasitic stages or, at least, some of the severe outcomes of the disease by inhibiting parasite sequestration or adhesion.

- Merozoite targeting by vaccination. Antibodies raised against surface merozoite antigens can already block parasite invasion of the RBC, regardless of their function. MSP1 immunogenic characteristics have been explored in several approaches, both for *P. falciparum* [24] and *P. vivax* [234,235] (figure 11), however, due to differences in epitope responses [25] and to the results obtained from phase I trials, which indicated low immunogenicity [26], some other options should be taken in consideration. Other proteins related to invasion machinery are being explored too, such as PfRH5 [236] or AMA1 [237], both already being tested on animals.
- Other parasite stages. Immunization to proteins that are exposed in the surface of trophozoites and schizonts is also being studied, mostly through the schizont egress antigen-1, as antibodies against it can block parasite egress [238], and the glutamic-acid-rich protein, which is expressed in trophozoite stages and antibody binding to this protein seem to activate an apoptosis signaling pathway in the parasite [239]. A recombinant hybrid protein of glutamic-acid-rich protein and MSP3, from merozoite surface, has been formulated as vaccine candidate GMZ2, and has already been tested in early clinical trials [240].
- Placental malaria vaccine. The receptor responsible for placental sequestration, VAR2CSA, has received attention as possible vaccine formulation. Women that had

had at least 1-2 pregnancies develop antibodies that prevent placental malaria in the next pregnancies [241], and a vaccine based on VAR2CSA is expected to do the same, though the heterologous interactions of this protein with CSA is making the advance slower, as the specific antigen or antigens that are best for the approach are difficult to identify [242]. In spite of this challenge, some approaches are reaching clinical trials [243,244].

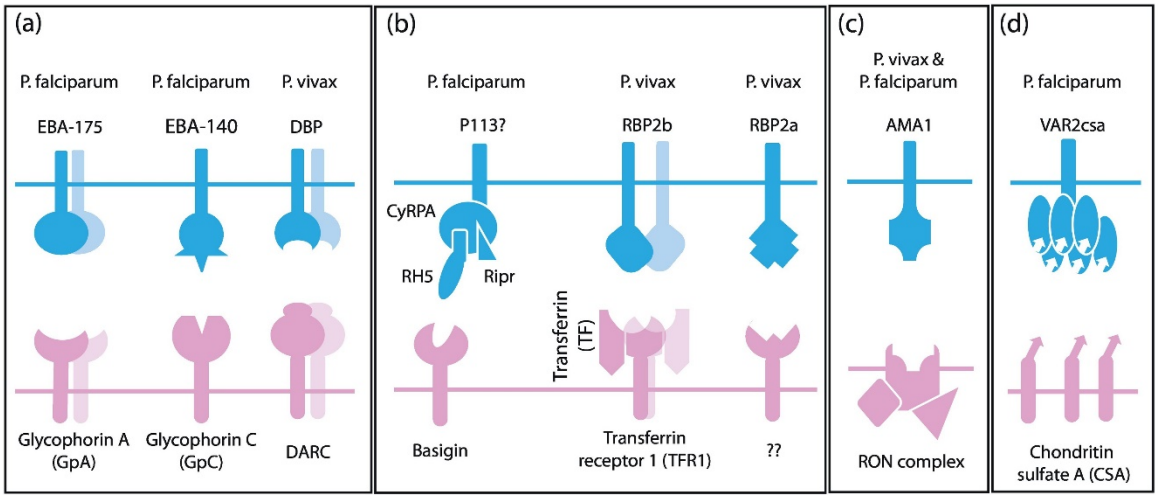

Figure 11: Malaria parasite ligands studied for vaccine development against erythrocytic stages and their red blood cell receptors. Parasite RBC invasion process is driven by reorientation and formation of tight junction, made by (a) EBL and (b) RBL families of parasite proteins. They have redundant pathways through different parasite ligand/RBC receptors pairs. (c) AMA1/RON2 complex produce the active invasion by allowing the movement of the junction. (d) Parasite sequestration mechanisms are susceptible for vaccine development, as immunity against it can prevent disease symptoms, and the most studied for this purpose is VAR2csa protein, responsible for placental sequestration. Figure from [245].

Transmission Blocking

This type of vaccine would not have any direct impact in contracting the infection or the disease symptoms for the individuals, thus it might not be easy to implement, however, it would be desirable as part of the malaria control and elimination program, as it could diminish the number of cases. A transmission blocking vaccine (TBV) could be a key asset for public health even if it is not specifically beneficial for the individual persons to which TBV is administered.

TBV formulations explored are mostly based in recombinant proteins, such as Pfs25, which is in phase 1 clinical study [246], Pfs48/45 [247] and Pfs230 [248]. The two first are being tested

also in form of deoxyribonucleic acid (DNA) vaccines [249]. Not so advanced in its implementation, but also studied as candidate, CelTOS protein seems to have potential for this purpose [250].

1.4. Diagnosis of Malaria

Malaria diagnosis based on clinical symptoms can be tricky, as the main symptoms of uncomplicated malaria (fever, headache, chills, fatigue, etc.) are not limited to it. Periodicity in fever episodes and enlargement of spleen (this organ filtrates most of the debris from the malaria parasite [57,251]) may help in the identification of the disease, but the most reliable way to diagnose malaria is to actually detect the parasite.

That is why the most used diagnostic technique is microscopy detection of *Plasmodium* in peripheral blood. Thin and thick blood smears are stained with Giemsa to observe the presence of parasite. Thin smears are used too to determine the species causing the infection. Though this practice is quite cheap and reliable, it requires some equipment and, importantly, trained personnel to detect visually the parasites, process that is also time-consuming and user-dependent [252]. The limit of detection is around 40 parasites/μL, but it is highly dependent on the expertise of the microscopist [253]. A simpler, cheaper, faster and more reliable method that could be implemented in rural areas or broad scale campaigns with lack of trained personnel would be desirable.

Some other diagnostic methods rely on the polymerase chain reaction (PCR), which can reach a limit of detection of 1-5 parasites/mL of blood [254], and can differentiate between parasite species [255]. The PCR technique is very useful as surveillance tool for resistance spreading, as it can be used to detect the mutations that confer the resistance [256]. However, it is mainly implemented in research and epidemiologic studies, and not that commonly for primary care diagnosis in endemic countries, because PCR is expensive compared to microscopical examination of smears and requires sophisticated equipment and well-trained staff.

Among other methods developed, quantitative buffy coat (QBC®, commercialized by Becton Dickinson) has sensitivity similar to that of microscopy. It consists on concentrating the blood by centrifugation inside capillary tubes which already contain acridine orange for sample staining, which is then examined with by fluorescence microscopy. Baird *et al*. reported more difficulties when applying this technique in the field than when using Giemsa-stained smears [257]. The cost is higher than conventional microscopy, both for the equipment and the reagents, and the technique cannot asses *Plasmodium* species.

Detecting host antibodies against the parasite has also been suggested as tool for diagnostic purposes [258,259], but it has the same disadvantages as the PCR: the need of trained personnel and costs of the reagents. For now, these assays are mainly applied in research.

Additionally, new diagnostic tools have been already assessed by the WHO, and the performance of cost-effective, quick and reliable techniques, such as **Rapid Diagnostic Tests (RDT)** [260] and **Loop-Mediated Isothermal Amplification (LAMP)**, are under evaluation.

LAMP is a technique of DNA amplification developed under isothermal conditions. It is specific, efficient and rapid, and requires a DNA polymerase and a very specific design of primers. There are four different primers that recognize six sequences on the target DNA, in sense and antisense recognition, which in the amplification produce several stem-loop DNA structures [261]. Though it is more expensive than microscopy, it could be more cost-effective in the detection of malaria infections, especially in regions with high prevalence of infection, as the outcome of false-negatives is lower [262]. It is not as expensive as regular PCR, but still requires specific equipment and trained staff.

On the other hand, **RDT** use is equally under evaluation [263], applied for the latest surveillance studies [264,265] and actually used for case-diagnosis in the field [266], thanks to its simplicity and low cost. These tests are devices for antigen detection by a simple immunochromatographic assay, in the presence of monoclonal antibodies impregnated on a test strip. One or more colored test lines indicate the result in only 5-20 minutes. It is a quick and simple technique and very easy to interpret. When used for malaria detection, RDTs require only 5-15 μL of blood [267]. In addition, the tests are commercially available with different combinations of antibodies for detecting different species of *Plasmodium* (usually *P. vivax*, *P. falciparum,* a common pan-malaria antigen or a combination of them) [268]. The WHO, in collaboration with the Foundation for Innovative New Diagnostics (FIND, Switzerland) and the Centers for Disease Control and Prevention (CDC, USA) are joining efforts to test and evaluate their performance [263].

The antigens used in RDTs are mainly *Plasmodium* lactate dehydrogenase (pLDH), histidine-rich Protein II (HRP2) and/or a genus-specific aldolase enzyme:

- pLDH is an enzyme that catalyzes conversion of lactate into pyruvate and back. Different antibodies against pLDH can provide diagnosis of *P. falciparum*, *P. vivax*

or *Plasmodium spp*. (known as pan-malaria diagnosis). The tests based on this antigen can remain positive for several days after treatment, because gametocytes also express this protein and might remain circulating [269].

- HRP2 is only used for *P. falciparum* infection detection, not for other species [1]. It is a small protein expressed during ring stage in the intraerythrocytic cycle (Figure 12) [270]. RDTs based on this antigen remain positive for weeks after treatment because the antigen remains in circulation, especially after artemisinin-related treatment [271]. Deletions of the *hrp2* gene, which produce a false-negative for malaria infection in these tests, have been reported [272,273]. Beside deletions, HRP2-based tests also provide false negatives when there is an excess of antigen, which prevents the movement of the detection antibodies (a phenomenon known as prozone) [274], or when there is presence of HRP2 antibodies in the human host that block the binding [275].
- The detection of aldolase (which participates in glycolysis) is usually combined with HRP2 for reporting either *P. falciparum* infections or non-*falciparum* ones [263].

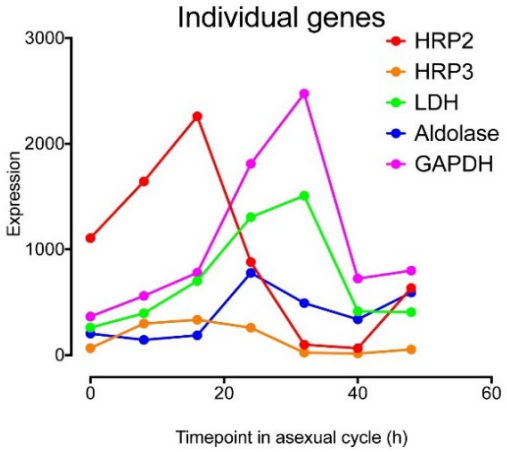

Figure 12: Levels of gene expression of the antigens used in malaria RDT detection. HRP2 is highly expressed when the parasite is at ring stage, and the expression diminishes as it develops into trophozoites. So does HRP3 but with lower levels of expression. In contrast, LDH, aldolase and *Plasmodium* glyceraldehyde-3-phosphate dehydrogenase (GAPDH) expression increases in trophozoite stage. HRP3 contributes to the signal of HRP2 detection, although it is less abundant [270]. GAPDH has been pointed out as interesting target for diagnosis [544], though right now there are not commercial RDTs based on it under evaluation. Adapted from [270].

In general, sensitivity against non-*falciparum* infections is lower using RDTs [268]. Moreover, they do not reach the sensitivity of molecular methods as standard PCR or LAMP [276]. Another flaw of RDTs resides in their poor stability under the temperature and humidity conditions usually present in the endemic countries [277], although WHO is already assessing this issue in their selection for testing [278]. And yet, at the moment RDTs are considered cost-effective for case-diagnosis [279]. Other cheap and easy to use but more sensitive methods are required for closer surveillance of asymptomatic cases with low parasitemia.

2. Nanotechnology

Within this context of drug discovery, diagnostic tool development and target screening, the evolving field of nanotechnology becomes a valuable ally for researchers and medical workers. Nanostructured materials and technologies are increasingly present in our everyday lives: cosmetics, sunscreens [280,281], many kinds of personal care products, and many others used in clothes, sport, filtration, gardening, automotive, electronics, etc., have incorporated such components. The Project on Emerging Nanotechnology, created for providing an inventory of those products, had a list of more than 1800 by 2014 [282].

The Greek word nanos –from which comes the prefix 'nano'– means dwarf. In science, 'nano' is used to indicate a factor of 10^{-9} or one billionth. Despite the existence of different definitions of nanomaterials, according to the European Commission of Enviroment, these objects have at least one dimension between 1 and 100 nanometers long [283]. The, so termed, 'nanomaterials' can be natural, manufactured or by products of human activity depending on their origin but nanotechnology mostly focuses on synthetic materials, which can be produced by physical methods [284], chemically [285] or even by biological means [286].

This field of research and production is interdisciplinar as it develops from the conjugation of many different sciences and their techniques (from chemistry, materials science and physics to pharmacology, genetic engineering and so on) when they are focused on downsizing for controlling processes and products in the nanoscale. Due to their size, nanomaterials present novel physical, chemical and biological properties, which make them suitable for a wide range of applications [287].

In the life sciences, nanotechnology has been a platform for the development of new delivery strategies (e.g. drugs or genes) [288–291], imaging tools [292,293], approaches for measuring and obtaining data from single-molecule interactions [294], sensing devices [295] and so on. These can be used in, among many other applications, cancer research, diagnosis and therapy [296] (and combinations of both of them), reproductive medicine [297], and, of course, infectious diseases [298].

The different nature of nanomaterials developed is as wide as the applications they have [287]. Nanoparticles have high surface to volume ratios, different optical properties from those of bulk materials, tunable shapes and/or facility for surface modification, being very

suitable for controllable transport of drug cargo *in vivo* [299]. Thanks to those surface modifications, these materials have an amazing versatility: many different moieties can be added to them to increase their biocompatibility [300,301], reactivity [302,303], targeting capacity [304,305], and many other properties.

As well as in many other fields, nanotechnology is explored in malaria research to obtain improvements in the current therapeutic, vaccination, vector control and diagnostic tools, and to develop brand new strategies for these purposes.

2.1. Nanotechnology applied to malaria therapy

In terms of drug delivery, nanostructured capsules and similar technologies are able to provide a platform for lowering overall drug dosage, while obtaining therapeutic concentrations at the tissue or cells where they are needed. The goal of these strategies is precisely to improve the therapeutic efficiency of drugs that have poor pharmacokinetic profiles, low stability or solubility or to improve the dose-limiting toxicity [299]. This can have the double advantage of **reducing side effects** while being more effective at killing the parasite, potentially **reducing the emergence of resistances** [306]. Besides, many nanodelivery tools can have sustained release over time and a prolonged circulation time compared to the free drug, which would allow **longer therapeutic levels** without increasing the number of administrations [307]. Controlling the size, shape, chemical composition and surface of nanocarriers, it is possible to tune their extravasation from the circulatory system or their interaction with specifics organs/cells [299]. Many different materials can be used to build these nanodelivery tools (Figure 13). The different formulations described here are classified according to their form of application and the drug drawbacks that they aim to tackle.

2.1.1. Simple drug encapsulation

Although the strategy might be simple, these forms of drug administration can increase circulation time or provide a sustained release, both improving the therapeutic life of the compound. Longer blood circulation times and reduced organ extravasation can be beneficial for treating the erythrocytic cycle of the malaria parasite. Materials that can be used to encapsulating antimalarials are:

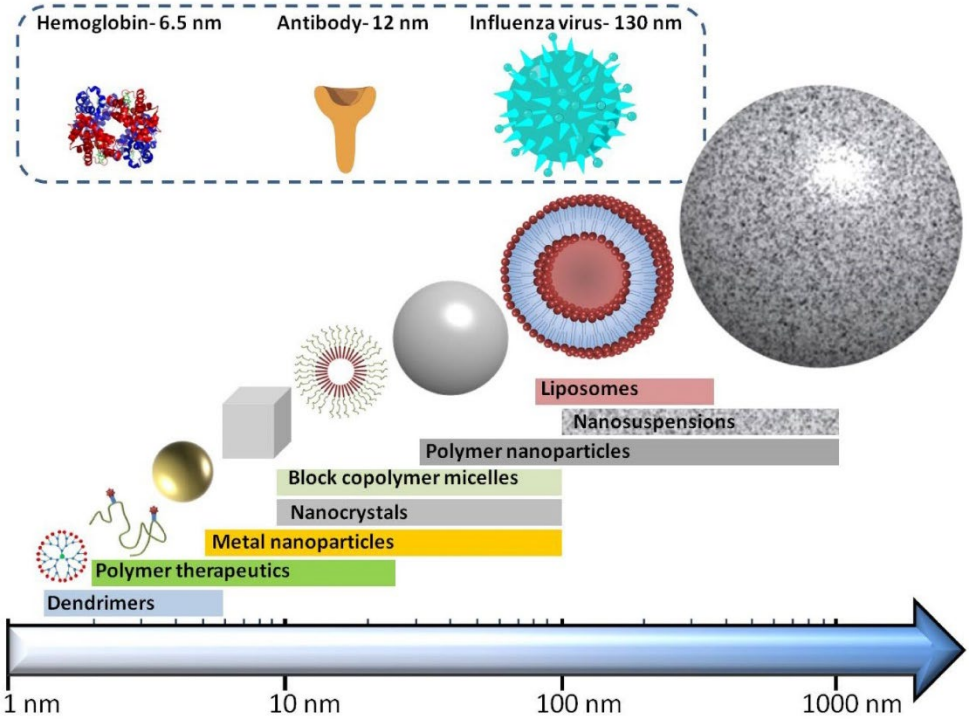

Figure 13: Different nanomaterials and the usual range of size that they present. Nanomaterials usually have sizes ranging from protein to organelle sizes. Adapted from [308].

Liposomes

These are artificial bilayered lipid vesicles, which represent one of the first strategies developed for drug delivery at the nanoscale. Liposomes have an aqueous lumen where hydrophilic drugs can be loaded, whereas their lipid membrane allows loading of lipophilic agents. The phospholipids that constitute the liposomes self-assemble in aqueous media and usually are highly biocompatible. It is possible to modify them to confer them different useful properties [309,310]. Liposomal formulations can passively encapsulate the drugs, but their physical properties can be tuned to have specific pH gradients and permeability coefficients for active loading of compounds [311], which can help to stabilize the encapsulated drugs and reduce their leaking out of target, thus minimizing the risk of toxic side effects.

For malaria therapy, liposomes have been applied as strategy for providing sustained and controlled release *in vivo* of artemisinin [312], doxycycline [313], modified di-artesunate [314], and even some newly explored antimalarials, such as maduramicin [315] or artelinic acid [316]. In

addition, poly(ethyleneglycol) (PEG) coated liposomes can increase circulation times for encapsulated artemisinin [312] and monesin [317]. The main disadvantage of liposomal formulations is that they are relatively expensive as antimalarial treatment and their production can be difficult to scale up [318], although new scalable systems of production by means of microfluidics are being assessed [318].

Other lipid-based formulations

Other lipid-based **nanostructured lipid carriers** (NLC) have been investigated for antimalarial drug delivery. NLCs are microemulsions composed by solid and liquid lipids, forming a matrix where the drugs are solved. They have been applied *in vivo* in murine models, for the intravenous administration of artemether [307] and primaquine [319].

Polymers

Polymers have also been widely researched for drug delivery strategies in malaria. Polymeric formulations consist of multiple repetitions of covalently bond units (monomers). This is a largely heterogeneous group of molecules, which can have a wide variety of lengths, can be linear or branched, and the drug encapsulation mechanism varies depending on the nature of the monomers and/or the modifications used to obtain reactive groups along the chains. This heterogeneity allows polymers to be made biodegradable and adaptable to many different applications.

- **Polyamidoamines** are a type of polymers whose monomers are a combination of amide and amine groups. They have been used for applications in malaria research since 1999, in an approach for gene transfection into *P. falciparum* by branched polyamidoamines [320]. Linear structures of this type of molecules have been tested as drug carriers for chloroquine [321], ferrocene derivatives and neridronate [322,323].
- **Dendrimers** are branched macromolecules of a very precise structure, designed and grown by controlled chemical reactions. Peptide-based dendrimers with galactose moiety ends tested for chloroquine encapsulation could reduce hemolytic activity of the drug, as well as macrophage uptake [324], reducing toxic effects. Sim-

ilarly designed poly-lisine peptides with a CSA coating were also used to encapsulate chloroquine, decreasing hemolysis and macrophage while obtaining a longer sustained release of the drug *in vitro* [325]. pRBC-binding dendrimers composed of 2,2-bis(hydroxymethyl)propionic acid (bis-MPA) and Pluronic® polymers, were applied for encapsulating chloroquine and primaquine and tested *in vitro* and *in vivo* [326]. Another dendronized hyperbranched polymer from the same family (polyester skeleton derived from 2,2′-bis(hydroxymethyl)propionic acid with amino ends) showed preferential uptake by trophozoites and schizonts [327], possibly due to NPP facilitated transport.

- **Copolymers** are polymers with different characteristics bound together to form a single macromolecule. These structures can have amphiphilic properties or benefit from different structural and functional groups plazed on different sites of the structure. Copolymers can easily self-assemble, forming micelles or polymerosomes, thus facilitating drug cargo incorporation.

  Copolymers made of methoxy-PEG and dendritic poly-lysine could increase artemether solubility in water by forming micelles [328]. Artesunate has been encapsulated in micelles made of the triblock copolymer poly(ε-caprolactone)–(PEG)–Poly(ε-caprolactone), increasing its circulation time and antimalarial efficacy [329].

  In the work by Martí Coma-Cros *et al*., the synthesis of an hybrid dendritic-linear-dendritic block copolymer based on Pluronic® F127 and amino terminated 2,2′-bis(glycyloxymethyl)propionic acid dendrons with a poly(ester amide) skeleton is described. Such polymer could self-assemble into micelles, suitable for drug encapsulation, and was able to interact with both healthy and parasitized RBCs [327].

Polymers are also commonly applied in combination with other materials. Such different combinations of molecules in the same nanostructure can exploit their different characteristics; for example, the already mentioned PEG polymers are extensively used as surface moiety for stabilizing nanostructures and prevent their aggregation [330], and increase their circulation time *in vivo* [331].

Saccharide-based formulations

Chitosan is obtained from chitin, a natural polysaccharide present in arthropods. Its lack of toxicity and high biocompatibility, together with its weak basic nature (it gets protonated at pH < 6.5) have made it very suitable for preparing nanoparticles based on polyelectrolyte interactions for biomedical purposes. Addition of polyanions such as sodium triphosphate pentabasic [332] or heparin [333] into solutions of chitosan under stiring easily form nanoparticles, in a process known as ionotropic gelation. Chitosan–triphosphate nanoparticles have been shown to encapsulate chloroquine [334].

Clyclodextrins are cyclic oligosaccharides made of glucose subunits forming a macrocyclic ring. These molecules are suitable for drug delivery, and colloidal systems made of these and artemisinin had good profiling of drug release and antimalarial activity *in vitro* [335].

Another saccharide-based nanoformulation tested for antimalarial delivery was composed of **dextran** and carried chloroquine. Dextran is a polysaccharide with glucose units, and which was suggested that could be deposited into the food vacuole of the parasite, since the half maximum inhibitory concentration (IC_{50}) was lower for the nanoformulation than for chloroquine alone for both susceptible and resistant strains [336].

2.1.2. Coencapsulation of different drugs

Nowadays, most antimalarial treatments use combination therapy to limit the advance of resistances. Formulations combining two different drugs are more convenient than separated formulations, as they can help in patient compilance, especially when the individual formulations have different prescribed posologies.

In addition, research interest is becoming increasingly focused in drug synergies: phenomenon that can provide a better drug efficacy than that resulting from the simple addition of individual drug efficacies. Coformulation of drugs with synergistic effects can give rise to highly efficacious treatments using lower doses, thus reducing even more the possible side effects [337].

In the case of **liposomes**, the presence of two different environments (aqueous lumen and hydrophobic membrane) allows for the coencapsulation of compounds of very different nature, opening the perspective for combination therapy at the level of the nanoscale. For

example, monesin combined with different antimalarials (chloroquine, piperaquine and FR900098) have been encapsulated in a liposomal formulation and tested both *in vitro* and *in vivo* [338]. Just tested *in vitro*, but with promising prospects for transmission blocking treatment, Biosca *et al*. combined atovaquone with pyronaridine into liposomal formulations [339].

NLCs with glyceryl-dilaurate have also tested for the delivery of combinations artemether/clindamycin and artemether/lumefantrine, with promising results for intravenous administration in murine models [340]. Another NLC formulation containing artemether/lumefantrine showed sustained drug release and high efficacy in a cerebral malaria murine model [341].

Polymeric formulations are also researched for combination therapy strategies. Polyphosphazenes [342] and poly(organophosphacenes) [343], which contain hydrophilic and hydrophobic side groups, have been explored as nanocarriers for primaquine and dihydroartemisinin coencapsulation.

Though these strategies can improve bioavailability and/or drug kinetics, and provide a base for combination therapy in a single formulation, those described above are not suitable for oral administration, and, therefore, difficult to be widely applied in malaria endemic countries. Some authors suggest that they still have potential for intravenous administration in severe cases when oral administration is not feasible [341].

2.1.3. Nanoformulations for improving oral delivery

A liposomal formulation has been proposed that destabilizes in gastric and intestinal fluids, and releases mefloquine, providing higher bioavailability for this drug that is poorly soluble in digestive fluids, also masking the bitter taste of mefloquine, which could increase treatment adherence [344].

However, oral administration of liposomes is not usual due to their instability in gastric conditions [345], which might led to drug loss. Certain surface modifications, however, allow the oral delivery of liposomes. **Coating liposomes with polymers** resistant to the gastric environment has made them suitable for this kind of administration. Either natural (chitosan or its derivatives [345]) or synthetic polymers (for example, Eudragit® [346]) can be used for this purpose. In malaria research, this approach has been applied to improve the administration

curcumin, an hydrophobic natural compound with antimalarial activity [347] but poor bioavailability, by combining phospholipids with hyaluronan and Eudragit®, with Nutriose [348] or with Nutriose and Eudragit® [349]. Coating with Eudragit® a coprecipitate of zinc salts and artesunate also enhanced the bioavailability of the drug [350].

With a focus towards cheap and easy to produce formulations, **oil nanoemulsions** have been explored as a platform to enhance bioavailability of hydrophobic antimalarials. They are based on the emulsion into nanostructures of vegetable oils together with the drugs. Coformulation of artemether and lumefantrine nanoemulsions had more effect in a mouse *in vivo* model at lower doses than currently used formulations [351]. Other nanoemulsion of just arthemeter was tested for oral administration and exhibited improved bioavailability and antimalarial activity *in vivo* [352]. Other self-emulsifying lipid-based formulation was tested for curcumin and artemether oral codelivery [353]. This approximation is cheap and simple and enhances the bioavailability of the tested antimalarials. Their lipidic nature helps solubilizing lipophilic drugs that are not easily solubilized in the digestive juices, thus easing their absorption.

Other lipidic formulations known as **solid lipid nanoparticles** have also been explored for oral antimalarial therapy. Dihydroartemisinin encapsulation was very stable in them and the drug release was sustained for 20 hours, leading to an increased *in vivo* antimalarial activity [354]. Similaly, **NLCs**, were used to encapsulate the combination artemether-lumefantrine in an industrially feasible technique, which enhanced the oral efficacy of the drugs [355].

The main potential of polymers for oral administration resides in that their exposed groups can be designed for maximal stability in the digestive track and interaction with the intestinal mucosa, allowing efficient drug delivery. Cationic polymers have these characteristics and are being explored for oral administration [356]. **Polyamidoamines** can be administered orally, and have been tested for chloroquine encapsulation [357]. **Poly(D,L-lactic-co-glycolic acid)** polymers were used for making biodegradable nanoparticles encapsulating curcumin [358] and a curcumin-artesunate combination [359], and were also tested for oral delivery, providing increased cellular uptake, and improved bioactivity *in vitro* and higher bioavailability *in vivo*. **Chitosan** can also be used for oral administration, and, when encapsulating curcumin, the chitosan nanoparticles increased its chemical stability and and bioavailability when fed to mice [360,361].

2.1.4. Direct antiplasmodial action of the nanostructure

Some metallic or metal-oxide nanoparticles have been tested for *Plasmodium* toxicity, since their sizes are usually small enough to enter the parasite and their synthesis is simple and easy to scale up. Silver-made nanoparticles were proven to be toxic for *P. falciparum* [362]. Titanium oxide nanoparticles, synthesized with *Momordica charantia* leaf aqueous extract, had some degree of antimalarial activity, though not much higher than the leaf extract alone [363]. Biologically produced magnetic nanoparticles (by *Magnetospirillum gryphiswaldense*) had moderate antimalarial activity, but their unspecific cytotoxicity was too high to consider them as suitable candidates for antimalarial therapy [364]. In an interesting approach, where magnetic nanoparticles were coated with pheophorbide A, the nanoparticle size allowed them to enter pRBCs through the NPPs, and the shell molecule, a photosensitizer, formed reactive oxygen species (ROS) under irradiation. These nanoparticles had *in vitro* antimalarial activity, although their development is still in a very early stage [365].

2.1.5. Targeted drug delivery

This strategy allows direct action of the drugs over the diseased cells thanks to targeting-ligand interactions exploited when designing the nanocapsule containing the treatment. Targeting the liver for malaria treatment of intrahepatocytic parasites is feasible through different approaches:

- Targeting the asialoglycoprotein receptor in the hepatocytes. This receptor recognizes glycosaccharide residues, and has been targeted using dendrimers with galactose functional ends [366], using pullulan, a polysaccharide formed by maltotriose units, in dextran sulfate nanoparticles [367], and also using poly-γ-glutamic acid modified with a synthetic trivalent glyco-ligand [368]. All these formulations showed enhanced accumulation in the liver *in vivo*, and contained primaquine as antimalarial with action against infected hepatocytes.
- Using a CSP peptide that targets the liver heparan sulfate, which has a higher sulfation degree than in other cells [369]. The specific targeting of peptide-functionalized liposomes could be confirmed [370] and refined by optimization of component

ratio [371], with good targeting *in vivo*. These nanostructures were applied for doxorubicin (antitumoral treatment) delivery in 2009 [372]. However, these formulations have not been tested as antimalarial treatment, and recent publications using them have not been found.

Transferrin has been used to target brain tissue for the specific treatment of cerebral malaria with quinine encapsulated in NLCs, although so far only pharmacokinetic *in vivo* assays have been performed [373].

For erythrocytic stages, when nanoparticles were not designed in size for passive targeting (by entering through NPPs [326] or by the pores formed before schizonts burst [374]), active targeting strategies have been implemented mostly by using antibodies. These approaches targeted either pRBCs [375] (with very good results due to the presence of proteins exported by the parasite to the RBC membrane [376]), or all the RBCs, using antibodies against glycophorin A [377] or equivalent molecules for their application in animal models [378]. These approaches improve circulation time and distribution of the drugs loaded in the liposomes, slowing down their removal from blood.

However, antibody targeting is an expensive tool for malaria treatments, and difficult to scale up in production. Besides, these explored formulations still require intravenous administration, which would only be applied in severe malaria cases.

Taking advantage of known traits of parasite biology can be key to obtain cheaper formulations and easier to scale up targeting strategies. For instance, as pRBCs have higher glucose uptake than healthy RBCs, corn starch-based nanoparticles have been used to target the parasite through glucose residues, using quinine as antimalarial [379]. This approach has only been tested *in vitro* so far.

Some other non-expensive targeting molecules have been explored too, e.g. heparin [380]. Heparin targeting is one of the main topics of this thesis work, thus will be discussed more in detail in Section 3.

2.2. Nanotechnology in vaccine development

Vaccine formulation is a key point for obtaining good immune responses, and certain adjuvants based on nanostructures have been tested for the developing of malaria vaccines. Liposomal formulations have aroused interest in malaria vaccine applications [381]. The very same RTS,S/AS01 or Mosquirix™ contains liposome-based adjuvants [223]. The liposomal composition helps to decrease hemolytic activity of the immunogenic compound QS-21, a natural saponin extracted from the *Quillaja saponaria* tree, thus, making the vaccine composition safer [382].

Liposomes can be part of the adjuvant composition or even part of the delivery system: by embedding the antigens in them and functionalizing their surface with mannose, Ssemaganda and coworkers aimed to target the liposomes to antigen-presenting cells, to obtain immunity against erythrocytic stages of the parasite [383]. TBV candidates using liposomal formulations have been explored too, using polyhistidine tagged Pfs25and liposomes containing cobalt porphyrin–phospholipid, so that the protein could bind spontaneously to the nanostructures [384].

As another nanotechnology-based approach, gold nanoparticles have been tested as adjuvants for a TBV candidate based on Pfs25 too, and they seemed to improve immunogenicity of this antigen [385].

Lastly, FMP014 is a vaccine candidate composed by self-assembling protein nanoparticles as antigen delivery system, which were designed to contain in each monomer different CSP epitopes. As adjuvant composition, it contains army liposomal formulation, and therefore this vaccine candidate makes use of nanotechnology for both antigen bearing and adjuvant components [386].

2.3. Nanotechnology applied to vector control measures

There is a whole trend of investigating environmentally-friendly synthesis of **metallic nanoparticles** that could be applied as insecticides or larvicides. Made of silver [387–390], zinc oxide [391] or gold [392] by using metallic salts and plant, algae or lichen extracts, all of them proved that could be toxic to *Anopheles stephensi* mosquitoes, either at larva, pupa or adult stages. Even at non killing concentrations, some of these publications showed that nanoparticle exposure could have certain degree of toxicity, making the larva or pupa more susceptible to predation [388,391]. Additionally, silver nanoparticles were proven non-toxic for non-target arthropod organisms [389,390].

These approaches are very promising but should be further tested before application: though their production is environmental friendly, and the non-target insect assays and *in vitro* unspecific toxicity test indicate that they are safe to use, evaluation on the impact in trophic chains would be crucial, to assure that no other fauna is affected by the nanoparticles.

Nanotechnology can also be indirectly applied in vector control research, by means of gene modification, for example, as nanotechnological tools can be used for DNA or RNA delivery. **Polyamidoamines** might have application in vector delivery approaches, as it seems that they can reach several insect organs when mosquitoes are fed with them [357].

2.4. Diagnostic applications of nanotechnology

Since RDTs are usually based on the use of gold nanoparticles coated with the detection antibody, nanotechnology is already part of current malaria diagnostic systems. The accumulation of the gold nanoparticles, either the antigen retention strip or the control strip of the chromatographic paper is what generates a colored band that can be read as a result (Figure 14).

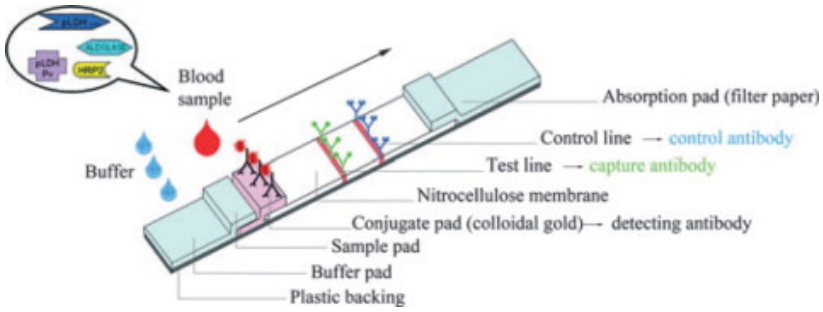

Figure 14: Schematic representation of RDT components. The RDT consist on a nitrocellulose membrane, which is the chromatographic support, and detecting antibodies conjugated to gold nanoparticles (also known as colloidal gold), are prepared to move with the sample flow. Two striped lines, one with the capture antibody and the other one with the control antibody, will retain the conjugated detecting antibodies and provide the result. Figure from [393].

A new prototype for malaria diagnosis is being developed using also gold nanoparticles, for detecting MSP10 DNA from *P. vivax* in urine. The gold nanoparticles are coated with oligonucleotides containing the two terminal sequences of MSP10, being the N-terminal more sensitive (84%), and both equally specific (97%). These tests require pretreatment of the urine, but the whole procedure lasts only 45 minutes, and cost of the raw materials per test is estimated to be 0.2 USD [394]. It is a promising approach that however requires additional studies for confirmation of its sensitivity.

Nanotechnology-based diagnostic tools are being researched to obtain imporved reading and antigen capture devices. There are some examples of those tools being developed for malaria application.

The so-called particle-based DNA amplification has been applied to diagnostic development in malaria: detection of *Pfg377* gene was mediated by grafting DNA primers into magnetic latex particles, providing support for PCR amplification, and quantum dots encapsulated into polymeric particles were used for signalling [395]. Althought highly sensitive and specific, this approach does not differ much from a typical PCR in terms of technical requirements, time and cost.

A promising tool is DiscoGnosis, a 'lab on a chip' (described even better as a 'lab on a disc') device based in microfluidics, for which only 50 µL of blood should be enough for diagnosing several infectious tropical diseases, malaria included. According to the information shared in the webpage of the project [396], this device includes a spinning disc with several small chambers containing magnetic beads that allow separation of the specific pathogen DNA/RNA. The beads distribute through the connected chambers that contain reagents for LAMP amplification, which allows identification through fluorescent probes. Cost estimation is around 10 USD per disc, much lower than all the individual diagnostic reactions for the pathogens that it could detect [397]. However, the last updates from this product development date from 2016, possibly indicating discontinuation of the project.

The main drawback of these last described approaches is that they require sophisticated capturing or reading platforms that can increase the price of the test and/or pose more difficulties for application in malaria endemic point of care sites.

2.5. Insights into targeting strategies towards *Plasmodium*-infected cells

As it has been discussed in the previous sections, nanostructured material delivery to *Plasmodium* can be achieved through antibody targeting of specific pRBC-exposed proteins [376] (or of the host RBC membrane proteins [377]), taking advantage of differences in transporter expression [379], or through harnessing the parasite adhesion mechanisms to host molecules [380], which have already been described.

Many of these formulations have been tested *in vivo*, exhibiting different ranges of efficacy. To the best of our knowledge, there are no published reports of these formulations advancing into clinical trials, possibly due to difficulties in production scaling up, or lack of interest by pharmaceutical companies, as cost/benefit ratio might not be good enough for embarking into a long and costly chain of clinical trials for nanoformulation and/or targeted delivery of antimalarials.

A key asset to improve current targeting strategies for *Plasmodium* drug-delivery or diagnosis would be to obtain a cost-effective production of the molecule to be used, while maintaining a high affinity and specificity of binding, which will keep low the cross-reactivity with other non-target cells. This variety of options that already exists reflects how parasite research can be approached at many levels to develop new targeting tools. In the following sections, two main strategies explored in this thesis are detailed.

3. Heparin and sulfated glycosaminoglycans as natural ligands

Glycosaminoclycans (GAGs) are long linear polysaccharides produced in virtually all types of animal cells. They are usually found forming part of proteoglycans (a core protein to which one or more GAG chains are attached covalently) exposed on the cell surface, embedded in extracellular matrices or placed in secretory granules. They have a wide variety of functions, including, among others, cell signaling, cell adhesion, cell-cell communication and structural roles [398]. They can be used by infectious organisms as ligands for recognition, attachment, movement and invasion [399,400].

In the following sections, the structure and relevant interactions of GAGs with the malaria parasites will be described, with special focus on perspectives towards treatment or targeting tool development.

3.1. Structure of sulfated glycosaminoglycans

GAGs are formed by the repetition of disaccharides consisting of an amino sugar, which is usually *N*-acetyl-D-glucosamine (GlcNAc) or *N*-acetyl-D-galactosamine (GalNAc), and an uronic acid, either D-glucuronic acid (GlcA) or iduronic acid (IdoA) (Figure 15). Here will be further described two main groups of GAGs that are important for the host-parasite interaction of *Plasmodium*: **chondroitin sulfate (CS) and heparan sulfate (HS)**. Heparin is considered to be within the group of HS [401].

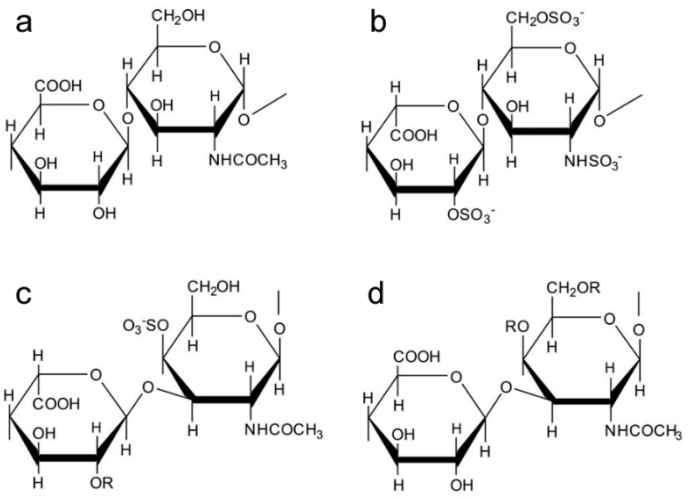

Figure 15: Most relevant disaccharide structures of the GAGs described. (a) heparan sulfate**, (b)** heparin, **(c)** dermatan sulfate and **(d)** chondroitin sulfate. R: H or SO_3^-. Adapted from [401]**.**

Both types of GAGs are linked to serine residues in the proteins by way of xylose [398]. The repeating units that form **CS** are mainly GalNAc-GlcA disaccharides making a polymeric chain with average sizes around 20KDa (approximately 40 disaccharides per chain), then 4-O and 6-O-sulfation can be present in GalNAc residues. In dextran sulfate (DS), the starting chain would be basically the same, and then epimerization of GlcA into IdoA occasionally occurs, also adding sulfation in 2C of this sugar. CS chain formation depends on the type of cell expressing the proteoglycan.

Heparin and HS structure is based on the dissacharides GlcNAcα1-4GlcAβ1-4. *N*-deacetylation and *N*-sulfation in GlcNAc is typically present in clusters along the chain, forming $GlcNSO_3$ and occasionally just deacetylated GlcN. Epimerization occurs in the GlcA residues immediately adjacent to such $GlcNSO_3$, and the IdoA generated is further 2-O-sulfated. Finally, 6-O-sulfate groups are added to the GlcN residues adjacent to the uronic acid. Certain arrangements of sulfated residues can be additionally 3-O-sulfated. The clustering pattern of these modifications provides regions lacking sulfate within the modified parts of the chains, and not all the modifications are present in all the regions, providing large chemical heterogeneity. This diversity results in specific ligand recognition of HS or heparin by the appropriate receptors.

Heparin is distinguished within this group as it is produced only by mast cells (while HS can be produced in any cell), and has more extensive sulfation and uronic acid epimerization. Tipically, more than 85% of GlcN are N-sulfated and more than 70% of the uronic acid is in form of IdoA. It has pharmaceutical interest, as it has high anticoagulant activity [398].

HS forms part of cell surface and extracellular matrix proteoglycans, and it is involved in embryonic development, inflammation and immune defense processes and cell growth [402]. Heparin can interfere in some of these processes possibly due to a mimicking action thanks to its similarity to HS. This widens the potential therapeutic uses of heparin or GAG mimicking compounds [403].

3.2. Role of sulfated glycosaminoglycans in liver invasion

Following an infected mosquito bite, sporozoites travel from the mosquito salivary glands and, soon after, invade hepatocytes. The presence of the CSP in this process has been introduced **in section 1.1.4**.

In the liver, HS is present on the surface of hepatocytes [404] and in the extracellular matrix in the space of Disse (region between hepatocytes and endothelial cells) [405], and it was shown to mediate in the interaction with *Plasmodium* sporozoites, as it is described below.

After observing the homology in sequence with other proteins such as antistasin [406] and properdin [407], which had affinity for sulfated glycoconjugates, it was suggested that CSP could also bind to such molecules in a specific manner [404]. The amino acid sequence Cys-Ser-Val-Thr-Cys-Gly-x-Gly-x-x-x-Arg-x-Arg/Lys was present in all CSPs reported at that time, and it was shown to bind heparin, fucoidan, and dextran sulfate. Further experiments were performed where it was shown that sporozoite infectivity was inhibited in the presence of these three molecules. Infectivity in mice was also inhibited by dextran sulfate and fucoidan, pointing to the conclusion that sporozoites may interact with this type of compounds when pursuing invasion of host hepatocytes [404].

A more recent study demonstrated the preferential binding of two conserved CSP regions to highly sulfated oligosaccharides in HS. These oligosaccharides were heparin-like in sulfation pattern. Peptides of such regions (I and II-plus) could inhibit binding of recombinant CSP to HepG2 cells in a concentration-dependent manner. Furthermore, presence of heparin was able to inhibit the action of endoproteinase Arg-C, which cleaves recombinant CSP mainly at the conserved region I. Guided by these results, it was suggested that the high sulfation of liver HS would explain the selectivity of CSP targeting the liver cells [408].

Additionally, experiments of interaction in real time using surface plasmon resonance and isothermal titration calorimetry showed that, among a number of glycosaminoglycans tested, heparin had the strongest binding towards CSP. The corresponding affinity was in the nanomolar range, and a particular decasaccharide sequence was defined as the minimum-sized binding sequence. It could block CSP interaction with HepG2 cells and its sequence was shown to bind apolipoprotein E, pointing to a common mechanism involved in invasion of hepatocytes by *Plasmodium spp.* and in the liver uptake of lipoproteins from the blood.[409]

In another study, the motif defined as region I-plus, containing basic residues, had high affinity towards heparin and HS. It had a binding constant K_d = 5.0 μM and a stoichiometry of n = 7.8 binding sites per heparin chain. The binding sites with higher binding efficiency on HS were rich in sulfate groups and iduronic acid, similarly to the corresponding heparin pattern. Such components are unusually abundant in the liver extracellular matrix in contrast to other organs, supporting their role in sporozoite targeting [410].

In order to take advantage of this known interaction, liposomes have been designed containing a peptide derived from CSP, which efficiently targeted the liver *in vivo* [370].

3.3. Role of sulfated glycosaminoglycans in blood stages

3.3.1. pRBC adhesiveness

Rosettes

Presence of rosettes –a pRBC adhered to a number of RBCs- is a common phenotype related with severe malaria[17,18]. Certain sulfated glycosaminoglycans, such as heparin and HS, had the capability of disrupting those rosettes in a strain- specific manner, whereas pretreatment of erythrocytes with heparinase III could avoid rosette formation *in vitro*.[411] In addition, heparan sulfate was found to be present on the RBC surface, confirming its role as ligand for rosette formation. [412]

Some research groups have focused in the receptor for this GAG interaction with pRBCs: as discussed in section 2.2.1, PfEMP1 is the main effector of cytoadhesion and rosetting, and was observed to bind HS through its DBL1α domain [413]. *E. coli* expression of recombinant of the N-terminal segment of DBL1α was used to screen a variety of GAGs and calculate their affinity by surface plasmon resonance, proving that heparin, fucoidan and dextran sulfate can interact with this domain [80]. Later on, by using a set of recombinant mutated proteins expressed in *E. coli*, it was proposed that the binding site resides in a particular sequence of basic amino acid residues of the subdomains 1 and 2 of DBL1α [82].

Other works have studied the different modifications that can be applied to common GAGs as heparin to obtain molecules with antirosetting effect but without anticoagulant activity. For example, periodate-depolymerized heparin was capable of disrupting rosettes *in vitro* and its use in *in vivo* models (rats and the non-human primate *Macaca fascicularis*) releases sequestered parasites [414]. Curdlan sulfate, a semisynthetic sulfated glycoconjugate, could reduce rosette formation in a wide range of *P. falciparum* laboratory strains and clinical isolates *in vitro* [415]. Further experiments with other modifications of heparin studied the activity of sevuparin and DFX232, derivatives of heparin without anticoagulant activity due to splitting of C2-C3 bonds of non-sulfated hexuronic acid residues and cleavage of heparin chain at these sites. Both compounds could disrupt rosettes in a large number of fresh parasite isolates, an effect which was more pronounced in isolates from complicated malaria cases than in those from mild cases [416]. As sevuparin has progressed into clinical trials as adjuvant therapy for malaria [417], it has been tested again with another large batch of fresh parasite isolates to characterize its effect in rosetting and cytoadhesion [418].

Cytoadhesion in capillary endothelium

Sulfated GAGs (sGAGs) not only were likely to have a role in rosetting, but also in sequestration within tissues. Several sulfated GAGs were able to suppress cytoadherence of *P. falciparum* HB3EC-6 to C32 melanoma cells, of which dextran sulfate (500 KDa) had the highest effect [419]. In addition, pRBCs of the parasite strain FCR3S1.2 and wild type clinical isolates were able to adhere to HS present on different types of endothelial cells. Such adhesion could be suppressed by enzymatic removal of HS, and DBL1α was identified as the HS-binding region of the cytoadhesive protein PfEMP1 [413].

Some strains of *Plasmodium* parasites can be selected to have binding towards GAGs. One publication, in which *P. falciparum* 3D7 was selected for binding CSA, describes how this *in vitro* model could be used to test a panel of sulfated GAG mimetics in terms of binding inhibition [420].

In addition to compound screening for rosetting disruption, pRBC cytoadherence inhibition was tested in the same works or in other ones close in time. Fucosylated chondroitin sulfate (FucCS), a GAG obtained from sea cucumber, was capable of *in vitro* inhibition of pRBC cytoadhesion to human lung endothelial cells and placenta cryosections, being the sulfated fucose branches essential in this action [421]. Different semisynthetic glycans (obtained from natural sources and chemically sulfated) were also tested for cytoadhesion inhibition [422]. Not surprisingly, sevuparin has also been tested in this type of assays, and was able to inhibit cytoadherence in concentrations of ≥ 100 μg/mL [418]. Along phase I/II clinical assays with malaria patients, mature parasites appear transiently in the circulation, possibly indicating that sevuparin is releasing sequestered parasites [417].

Cytoadhesion in placental malaria

The relevance of placental malaria, which can cause anemia and low birth weight infants, and the wide number of publications on this topic, allow discussing in more profound details about the interactions involved.

The *Plasmodium* receptor (VAR2CSA) involved in placental malaria has been dealt with in section 1.1.4, and the following paragraphs will cover a deeper description of the ligand (CSA) and the nature of the interaction between them.

It is not discarded that some other receptors could be involved in parasite sequestration in placenta [423], although most of the evidence points to VAR2CSA and CSA as the main effectors of this sequestration type [424], and in consequence they are the most studied.

CSA is present in the intervillous spaces of the placenta in the form of CS proteoglycans. These placental GAGs have a unique and distinct pattern: they have low sulfation (2-8% of the disaccharide repeats are 4-sulfated) [425] distributed in specific domains (clustered in the chain forming regions of 6-14 repeating disaccharide units with 20-28% 4-sulfate, while other regions have few or no sulfate groups) [426] which make them very different from CSA present in other tissues. Six or more disaccharide repeats were required for blocking the cytoadhesion of pRBCs, and were more active when having just 2-3 sulfate groups per molecule [427].

The low sulfation of this placental CSA hindered its proper characterization and was misidentified as hyaluronic acid (HA) [425,428], which is actually in lower proportion in placental tissue [425]. A study even reports that "Commercial preparations of HA have been contaminated by CSA (…)" [429] , which suggests that the role of hyaluronic acid in placental malaria might be smaller than expected.

The CS proteoglycan to which pRBCs bind is of fetal origin, and its levels of expression are increased when the infected cells are present [428]. Among other GAGs present in the placenta (DS in the fibrous tissue, two types of CS proteoglycans associated to cells, and low sulfated and extracellular CS proteoglycan in the intervillous space), the CS present in the intervillous space was responsible for sequestration [425]. Interestingly, these observations also apply to *P. vivax* placental sequestration [430], and the binding is sustained along most of the pregnancy period [431].

Structura screenings assays showed that there are isolate-specific differences in the affinity for structural motifs in CSA, which correlated with polymorphisms in the parasite receptor protein [88]. The interaction between VAR2CSA and CS is likely a cooperative interaction dependent on CS density [432], and the protein might have multiple binding sites for CS, thus providing an allosteric effect [433].

3.3.2. Merozoite invasion

sGAGs have been found to inhibit merozoite invasion *in vitro*. This inhibition was dually proven together with cell adhesion inhibition for the parasite line HB3EC-6 with a variety of GAGs, such as dextran sulfate, sulfatides, fucoidan and heparin. Non-sulfated molecules with similar structure did not block invasion or cytoadherence, proving that sulfated polyanions interfere with the ligand-receptor interaction needed for these processes [419]. In a more recent study, it was proven that modification of heparin length and sulfation could neutralize this antimalarial effect and that uptake is not necessary for its activity, strengthening its role as invasion inhibitor [434]. Heparin was found to bind EBA140, being capable of inhibiting its interactions with erythrocytes [131], and seems to exclusively bind the apical tip of the merozoite surface (Figure 16); it is then expected to interact with a protein localized in the apical region [435]. This is in agreement with what is experimentally observed when recording the steps of invasion with real-time microscopy in the presence of heparin: merozoites still can adhere to the erythrocyte surface, but do not reorient [129]. However, data collected from experiments with protein extracts suggested that the target of this activity could be the MSP1 protein, more specifically the $MSP1_{42}$ processed fraction –in the fragment that later on during invasion is shed in the form of $MSP1_{33}$ [129]. In addition, heparin is capable of blocking the initial RBC deformation that occurs immediately after the merozoite makes contact, and inhibits the invasion from this point [127,129], a mechanism in which MSP1 is the most probable effector. One plausible explanation is that besides MSP1, heparin would be interacting with some other proteins in the apical part, which therefore would not be reaching their ligands on the erythrocyte surface to start the merozoite reorientation. As the structure of heparin is prone to interact with many proteins [436], it could be interacting synergistically with more than one, and the combination of these diverse binders would be mostly present in the apical part of the cell. Besides interactions with MSP1 and EBA140, heparin can interact with some of the proteins present in the rhoptries (such as PfRh2 or RON3), and SERA5, a protease involved in the merozoite egress process [437].

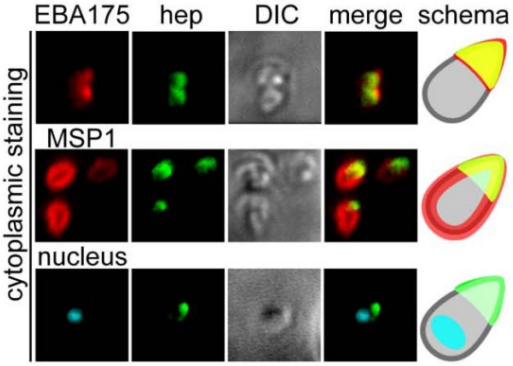

Figure 16: Colocalization studies between heparin and merozoite proteins. The staining observed for heparin in these images colocalizes with the staining obtained with an antibody against EBA175, a protein present in the apical part of the merozoite. This suggests that heparin might not be binding MSP1, which is distributed all over the merozoite surface, but maybe some other protein present in the apical part of the merozoite. Adapted from [435].

Blocking the invasion of a new RBC might not be the only mechanism through which heparin blocks parasite development: it can enter into the perforated membrane of schizonts about to burst and retain the merozoites inside, inhibiting the egress process, possibly acting as anchor between inner erythrocyte membrane molecules and the surface merozoite proteins [374]. The observed interaction between SERA5 and heparin [437], provides more evidence sustaining the feasibility of this way of blocking.

Regardless of the mechanism, sulfation of GAGs is a key requirement for their invasion inhibiting activity [419]: the higher the sulfation degree, the greater the activity, for which sulfation of GlcNAc and 6-*O* sulfation of hexuronic acid residues are essential [129]. The length of the GAG chain also plays a role in the interaction, as low molecular weight fractions of heparin have higher IC_{50} than high molecular weight fractions [438], and a minimum length of six monosaccharide units is required for substantial activity [129].

Both for defining the appropriate sGAG structure required in the the parasite invasion arrest and for exploring new approaches of treatment, several works have been using heparin modifications [129], related glycans [439] or sGAG mimicking molecules [414,420] for *in vitro P. falciparum* growth inhibition. The most extensive work in this field tested a large panel of different polymeric molecules (not only of polysaccharide nature) modified with sulfate groups [440].

So far, very few *in vivo* assays have been performed with this kind of molecules with the purpose of inhibiting merozoite invasion. Almost 25 years ago, long chains of 500-KDa dextran sulfate, chosen for their observed *in vitro* growth inhibition and cytoadherence blocking, were used in a mouse model of cerebral malaria (*P. berghei* ANKA); although some statistically significant differences were observed, the results were not very promising in terms of survival of the animals [419]. More recently, in our group, several sulfated polysaccharides from marine organisms exhibited antimalarial activity *in vitro*, and, as they had much lower anticoagulant activity than heparin, were tested *in vivo* in a *P. yoelii* XL mouse model. The survival trends were very similar to the untreated control, except for animals treated with fucan from the sea cucumber *Isostichopus badionotus* [439].

These *in vivo* results indicate that the translation from promising *in vitro* results into successful preclinical assays is not an easy step, and a deeper characterization of the samples in terms of pharmacokinetics and pharmacodynamics would be helpful in the development of these types of compounds as treatment.

In contrast, promising results seem to derive from the phase I/II clinical study of sevuparin as adjuvant in antimalarial treatment: parasite numbers at ring stage seemed to be reduced in the patients that were treated with sevuparin, compared with the control group. Still, both groups were administered atovaquone/proguanil as antimalarial treatment. Additionally, there was a large variability of ring percentages between individuals of the same group [417], additional studies will be required to confirm that servuparin reduces merozoite invasion in patients.

3.4. Role of sulfated glycosaminoglycans in mosquito stages

Not only mammalian tissues have sGAGs. Most of the research about GAG presence in arthropods is based on *Drosophila melanogaster*, where HS and CS were found [441]. Although *D. melanogaster* is an excellent model for research, the observations made for in organism might not be applicable to all arthropods; in the next sections, specific results in *Anopheline* research and the corresponding implications in parasite development are highlighted.

3.4.1. Midgut invasion

Midgut microvilli of *Anopheles gambiae* contains CS chains, specifically CSA and CSE [442,443]. Interaction of such chains with *P. falciparum* ookinetes has been demonstrated by fluorescent labeling *in vitro* (Figure 17), and suppression of the biosynthesis of CS by iRNA significantly impaired the development of the parasite in the mosquito [442]. A polysulfated polymer mimicking CS (vinyl sulfonic acid, VS1) could also diminish *P. berghei* oocyst numbers in *A. stephensi* mosquitoes following blood feeding to VS1-administrated and infected mice, and in *A. gambiae* mosquitoes, to which gametocytes of *P. falciparum* grown *in vitro* were fed [443]. In experiments of ookinete midgut invasion, addition of wheat germ agglutinin, which binds to carbohydrates such as GlcNAc, blocked ookinete interaction with the midgut [444], confirming the importance of the availability of midgut endothelium GAGs for parasite development.

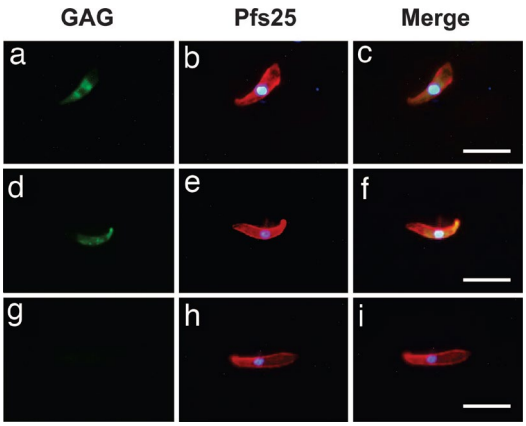

Figure 17: *P. falciparum* ookinetes bind to specific CS GAGs. CSA (a–c) and CSE (d–f) bind to mature ookinetes, whereas HA (g–i) do not. CSC, CSD, and DS produced similar results to HA. For detection, GAGs were biotinylated and streptavidin conjugated to Alexa 488 provides the green signal. An antibody against Pfs25 was used to identify mature ookinetes (red). DAPI was used to stain parasite nuclei (blue). Scale bars are ~10 μm. From [442].

Staining with ruthenium red also demonstrated the presence of GAGs in the midgut epithelium of *A. aquasalis* [445], a malaria vector in the American continent, suggesting that the invasion mechanism in this species could also involve GAG interactions.

The receptors responsible for the ookinete-midgut interaction seem to be CTRP and the von Willebrand Factor A domain protein (WARP), both recombinant *P. falciparum* WARP and *P. gallinaceum* first vWA (von Willebrand adhesive) domain of CTRP bind heparin *in vitro*

[147]. Homologous recombinant *P. vivax* proteins were able to bind VS1, a previously mentionend CS-mimetic, suggesting that the interaction that produces the blocking in development is likely the same [443]. CTRP contains seven of such vWA domains (also known as A domains), which have been identified as heparin-binding domains [446].

Previous work in our group has also pointed out that fluorescently labeled heparin can bind to *P. berghei* ookinetes [447] (Figure 18). Thus, heparin or other sulfated related molecules are interesting targeting molecules for this parasite stage, and that is why we selected them for our experiments.

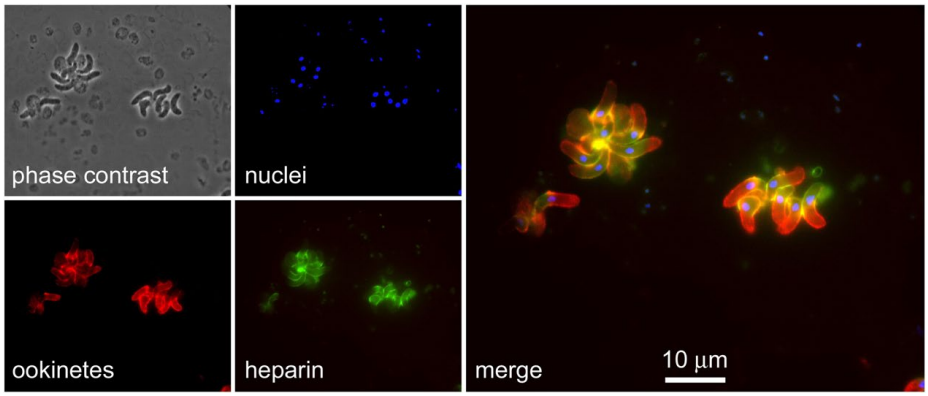

Figure 18: Confocal image of heparin binding ookinetes. *P. berghei* ookinetes expressing mCherry and stained with DAPI, show also the fluorescence of heparin-FITC, interacting at their surface. The labeling seems to be polarized preferentially towards the ookinete apical side. From [447].

Besides, other protozoan parasites such as *Leishmania braziliensis* [448] and *Trypanosoma cruzi* [449,450] also use sulfated GAGs as ligands when invading their insect vector, possibly indicating that a common mechanism of interaction could have evolved convergently.

3.4.2. Salivary gland invasion by sporozoites

A couple of publications explored if GAGs could have a role in the salivary gland invasion inside the mosquito. The presence in the salivary glands of the mosquito *A. stephensi* of HS with a pattern of sulfation similar to that of the liver, offered a promising candidate as ligand for mosquito salivary gland invasion by the sporozoites [451]. HS was also identified in the salivary gland basal lamina of *A. gambiae*. However, knocking down the biosynthesis of HS in the mosquito did not impair sporozoite invasion, and thus it is likely that some other ligands facilitate the entrance of the parasite [452].

3.5. Use of heparin in nanoformulations against malaria

Some previous publications have already explored the strategy of binding heparin to nanostructures to be used as antimalarial treatment. Such strategies would benefit from the nanostructured properties, while gaining a mimicking-like activity, as heparin will be arranged in the surface exposing chains as HS does over the RBC.

formulation that reduced its anticoagulant activity, and was applied as drug delivery approach, using primaquine as liposome content. Heparin was expected to act as targeting molecule against the mature pRBC surface, and the *in vitro* antimalarial results seemed indeed promising [380]. The presence of heparin in solid lipid nanoparticles encapsulating chloroquine also seemed to increase its effect *in vitro* [453]. Heparin has even been used as the nanomaterial itself: covalently bound to artesunate, the modified molecule could self-assemble into micelle-like structures and prolong artesunate circulation time *in vivo* [454].

A second explored approach is using heparin to mimic the surface structure of a RBC. Polymersomes [455] and giant polymersomes [456] benefited from surface-attached heparin to gain antimalarial activity *in vitro*, and merozoites were observed to bind these structures (Figure 19). Further characterization of these nanomimic structures showed that they have antimalarial activity with different heparin proportions and even with depolymerized chains [457].

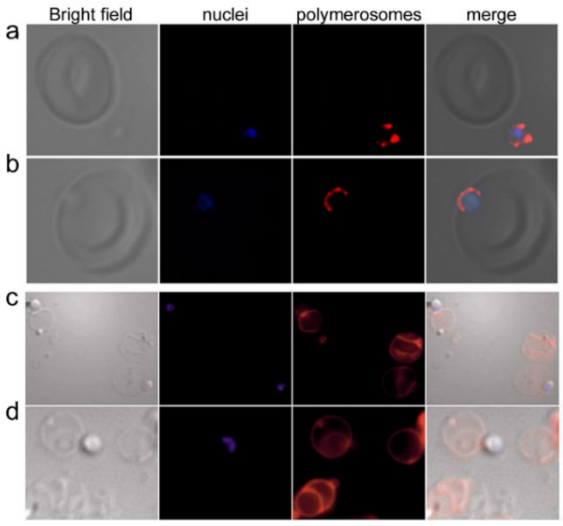

Figure 19: Polymersomes coated with heparin targeting the merozoites. (a & b) small size po-lymerosomes can bind the merozoite surface and block the invasion (adapted from [455]). (c & d) giant polymerosomes covered with heparin mimicking RBCs can also bind the merozoites (adapted from [456]).

In two of these publications [380,456], it has been suggested that attachment of merozoites to these nanostructures could prolong the time that these cells are exposed in the blood stream, which might help the immune system in antigen recognition from the parasite.

4. Development of new targeting tools: Aptamers

New cost-effective and specific targeting tools are necessary for advancing the targeted drug delivery field for malaria. In this regard, binding specificities and affinities comparable to those of monoclonal antibodies can be obtained with **aptamers**, much faster and less expensive to produce [458].

Aptamers are short single-stranded oligonucleotide chains used for specific ligand recognition. They are generally single-stranded DNA (ssDNA) or ssRNA, and, in both cases, the 3D structure formed by their self-folding produces some structural features that can bind to other molecules (figure 20). For *in vivo* applications, aptamers can be chemically modified to confer them resistance against nucleases or they can be tagged with fluorescence reporters or nanoparticles for localization or pull-down experiments of target proteins.

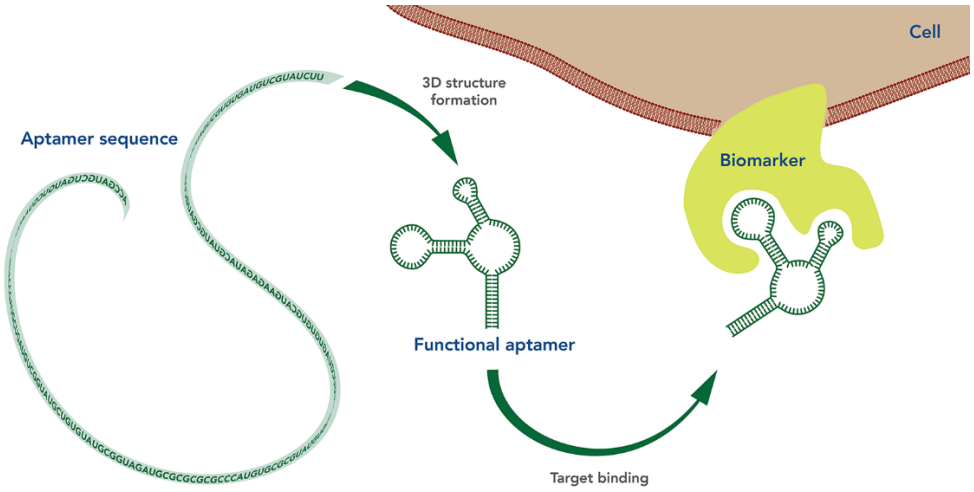

Figure 20: Depiction of the interaction aptamer-target. Aptamers are single stranded oligonucleotides that fold in a 3D conformation capable to interact with other molecules, for example proteins, by 'induced fit', structure compatibility, electrostatic interactions or hydrogen bonds. Image from: https://www.idtdna.com/pages/education/decoded/article/planning-to-work-with-aptamers.

These molecules offer a good alternative to antibodies, as they do not require immunogenic and nontoxic targets, because aptamers do not relay on laboratory animals for their production, since all the selection process can be carried out *in vitro*. Their nucleic acid nature is an advantage for production (they can be chemically synthesized at low cost), stability (their denaturalization and renaturalization does not affect function) and easy modification and they are generally non-immunogenic [459]. Additionally, their small size and all the knowledge available about base pairing and nucleic acid interactions with other molecules makes them more suitable for computational analysis and *in silico* selection [460].

4.1. The aptamer selection process

To select aptamers for the recognition of ligands, a library of different random sequences is used. The usual method of selection is the **systematic evolution of ligands by exponential enrichment (SELEX)**, but aptamers can also be selected on a chip. SELEX was firstly described in the 1990s [461,462]. The selection method starts by mixing the target of interest with an oligonucleotide library, which allows interactions between them, and, then, those oligonucleotides that have interacted with the target are isolated and non-interacting ones are discarded. Those selected oligonucleotides are amplified by PCR, the single strands are generated, and they are incubated again with the target, repeating the cycle for as long as it takes to obtain few sequences with high specificity. It is an iterative process that takes at least 6-12 cycles [463].

The starting library of oligonucleotides can be either ssRNA or ssDNA, and is designed to have fixed regions on each end and a random central sequence of about 30-60 nucleotides. The library should be as large as possible to obtain a maximally randomized sequence, but in most cases there are about 10^{15} different sequences. This can be sufficient to obtain highly specific aptamers, but it can lead to sequence bias, as the starting pool covers only about 0.01% of the possible sequences for a 30-nucleotide oligomer [464]. Thus, the starting pool highly influences which aptamers are selected.

Conviniently, the SELEX method has been tuned and adapted to the different targets used. Effective separation of the non-binding sequences is key to enhance enrichment of the selected ones, and incrementing the stringency of binding along the selection cycles or opting for active selection can accelerate the process and reduce the number of cycles. Here are compiled several strategies for a good target-library interaction:

- **Using a purified and/or recombinant protein as target**: this is the most common target, especially for biomedical applications. The different methods applied solve the problem of separation of selected sequences in diverse ways:
    - Filter separation: proteins coated with binding sequences are separated by filtration through a nitrocellulose filter, while free sequences are washed out [465]. This technique can only be used with target proteins that can be retained in the filter, and the efficiency of capture depends on the protein. Aptamers that bind the filter can be enriched easily [459].

- Usually, the protein is retained on a solid support that allows separation of selected and not selected sequences. This support can be different types of beads/resins, for example, if the recombinant protein has tags like polyhistidine, gluthatione S-transferase or maltose binding protein, the beads or resins will have matrixes for affinity separation, as nickel, glutathione or amylose respectively. Then, the non-binding sequences can be separated by pull-down or column washes. If the beads are magnetic, they can be separated using a magnetic field, (FluMag-SELEX) [466]. After washing away the non-binding oligonucleotides, selected molecules are eluted alone or with the protein.
    - Combining bead retention and flow cytometry for active selection of binding sequences allows obtaining high affinity sequences in less cycles of selection: a fluorescent tag indicates level of binding with the target, and only those with high level of fluorescence are selected for the next PCR. This method is called Particle Display [467].
    - Microfluidics has also been applied in combination with beads as support, whereby the number of cycles can be reduced too, thanks to continuous washings. In addition, the reagents and volumes are decreased thanks to miniaturization [468].
- Simple protein adsorption can provide separation, for example, into 96-well plate wells. In this protocol, non-binding sequences are removed by gently washing and binding ones are eluted by heat [469].
- Electrophoresis-based SELEX: it takes advantage of the differences in electrophoretic mobility of free sequences vs. protein-bound sequences, which are slowed down. The generally applied methods are capillary electrophoresis (CE-SELEX) [470] and micro free-flow electrophoresis [471]. This type of selection avoid the recovery of sequences that bind the immobilization support.

- **Using small molecules**: in contrast to antibodies, aptamers can be raised against non-immunogenic molecules, such as small chemicals. Applying the previously described selection methods to small molecules is possible, but it usually depends on the molecule nature and if this can be immobilized or not. When immobilization of the target is not feasible, the main techniques applied are:

- The already mentioned CE-SELEX [472].
- Capture-SELEX, a method based in the capture of non-binding sequences by complementary oligonucleotides attached to beads. The sequences that bind the target are not captured by the beads, and can be amplified [473].

- **Using whole cells**: very complex substrates as the cell surface can be used too as target for the SELEX technique. Usually what is implemented is the **cell-SELEX** technique (Figure 22), in which the cells and bound aptamers are separated from non-selected sequences just by centrifugation pull-down, but some other variants apply other separation techniques, like microfluidic strategies [474]. The main advantages of this technique are its suitability for the discovery of new biomarkers, while, in addition, prior knowledge of the target is not required [475]. However, it is a complex and time consuming technique compared with other means of aptamer development: the challenge of having a good cell culture that remains as unchanged as possible along the selection cycles, the difficulties in target identification (not many research groups achieve this) and the numerous technical problems that can appear along the process hamper a wider application of this methodology [476].

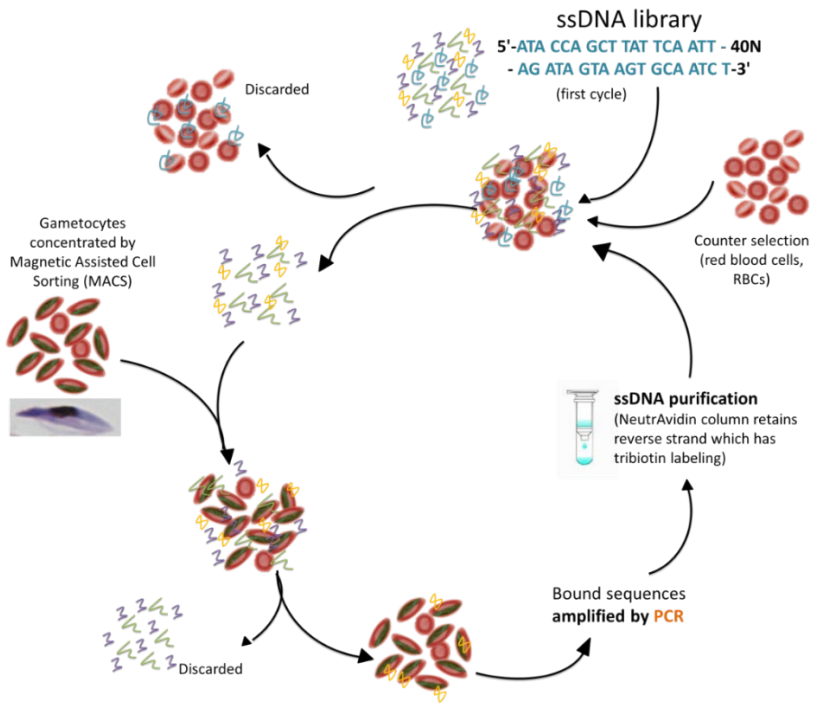

Figure 21: Depiction of the cell-SELEX process, exemplified using an oligonucleotide pool of ssDNA, *P. falciparum* gametocytes as cell targets and RBCs as counter selection. The cells were drawn by Javier Lantero Escolar.

Counter-selection is needed in many cases to increase specificity, either for washing away sequences that bind to the immobilization substrate or for selecting aptamers that can distinguish very similar molecules [464]. For cell-SELEX and biomarker identification is crucial to perform a counter-selection, which usually relies on incubation of the sequences with a 'healthy' cell of the same type as the selected target cell [475].

The remaining process is fairly similar independently of the target: either reverse transcription-PCR for RNA aptamers or simple PCR for DNA aptamers. This step can be problematic for two reasons: undesired by-products of the amplification are common when the same pool is used in many cycles of PCR [477] and the amplification can have bias towards certain nucleotides [478]. After amplification, the sequences are either transcribed to ssRNA or the ssDNA is separated, which can be made using biotinylated primers (obtaining one strand of the amplified pool with the biotin) and streptavidin-bead retention, with elution by alkaline denaturation, the ssDNA can be released [475]. Asymmetric PCR and/or exonuclease digestion can also yield ssDNA [479].

Although it is not exempt of bias and selection issues, the SELEX troubleshooting has been assessed by several research groups [475,477,479], representing a faster and technically easier process than the establishment of a monoclonal antibody production chain.

4.2. Post-selection modification of aptamers and their potential applications

After selecting aptamers against a given target, it is often necessary to proceed with some chemical modifications, to provide more stability or specific functionalities, so the molecule can be functional for the final application.

In addition, aptamers can be truncated or their bases modified one by one to screen for sequences with even higher affinity.

4.2.1. Modifications of aptamers for increased stability

Because aptamers can be targets of nuclease activity, modifications that confer resistance to nucleases are highly recommended for almost any application. The most usual modifications target the sugar ring, the bases or the oligonucleotide ends.

The 2' position of the **sugar ring** can be modified with 2'-NH_2, 2'-F, and 2'-O-CH_3 groups, which confer nuclease resistance [480–482]. Alternatively, locked nucleic acids (LNA) can be used: LNA are bases with an extra bridge connecting their 2' oxygen and 4' carbon, which have high stability against ribozymes, low toxicity and outstanding thermal stability [483].

The **nucleotide bases** can also be modified to confer nuclease resistance to the molecule, being most common the modifications in the fifth position of the pyrimidine with iodide, bromide, chloride, amino or azide [484]. Besides, some chemical modifications can add extra affinity for the selected targets by imparting a more hydrophobic, hydrophilic, or charged character to the oligonucleotide. As an example, 5-(N- benzylcarboxyamide)-dUTP modification of an aptamer raised against nucleolin protein expressed in cancer cells increased its affinity to target cells by 2.5-fold [485]. Chemical modification of some nucleotides incorporating in them 2'-deoxyinosine increased their anti-proliferative activity [486].

Other common modifications are related to y 3' or 5' **capping**. Due to their small molecular weight, aptamers can be easily excreted by the kidneys, and therefore, when designed for *in vivo* applications, like therapy, imaging and others, modifications oriented to elongate the circulation time of the aptamers are highly desirable. In this regard, 3′ or 5′ capping can provide longer circulation times and even protection to nucleases. 3' capping can be done with 2'-4'-bridged nucleotides [487], streptavidin-biotin [488] or inverted thymidine, while 5' caps include amine or phosphate groups, PEG, cholesterol, fatty acids and peptides or proteins.

PEG or other polymers attached to the oligonucleotides can prolong their residence time in the body, by reducing extravasation and kidney filtration [489].

The first approved therapy based on aptamers, Macugen, consists on a truncated 28 nucleotide aptamer that has been raised against the vascular entothelial growth factor isoform 165 from a 2'-F pyrimidine library and modified with several 2'-O-methyl purines. This modification already conferred nuclease resistance, and, in addition, its residence time was elongated by 5' PEGylation [490]. Its application in clinical trials was successful for the treatment of neovascular age-related macular degeneration [491].

Attaching the aptamers to **nanoparticles** can also help increasing their circulation time due to the size increase of the conjugated structure. It can also have other advantages too: due to the binding to gold nanoparticles, certain ligand-aptamers could not escape from lysosomes in targeted cells, where the protein ligand was degraded, thus activating apoptosis and contributing to death of the targeted cancer cells [492]

4.2.2. Function-oriented modification of aptamers

Many aptamers have been developed towards sensor applications, for example, aptamers raised against antibiotics, with the objective of developing sensors for controlling and evaluating antibiotic residues and avoid resistance emergence. The sensors developed are usually electrochemical, to have an easy-to-use but sensitive measurement platform, and the aptamers are grafted into the surface of the electrodes, either directly or using a linking molecule [493].

Sometimes aptamers just bear certain labels, like fluorescent molecules or radioisotopes, to help identifying the specific target that they bind to. For example, for diagnostic purposes, fluorescence anisotropy of the aptamer can detect biomarkers in nanomolar concentrations [494]. These modifications can also be used for labeling and separation of target cells by fluorescence-activated cell sorting [495].

Of course, one of the main topics toward which aptamers are focused is targeted drug delivery. There is a review covering precisely this topic [496], which mentions the diversity of molecules/nanostructures that can be linked to aptamers: drugs, nanoparticles formed by liposomes, polymers or others bearing the drug cargo, metallic nanoparticles with the activity

of interest, recombinant streptavidin-protein of interest to be carried inside the cell, chimeric aptamers fused to micro RNAs or small interference RNAs as therapeutic agents, and so on.

Among other applications, aptamers can be a mechanism of gene expression when used as riboswitches or in similar approaches. The sequence of an aptamer, which recognizes a small molecule that can diffuse into cells, is fused to the gene of interest, usually at the 5' end to be transcribed into RNA. The presence of the molecule that the aptamer sequence recognizes can make the mRNA adopt a 3D structure that does not allow access to the ribosome and therefore cannot be translated. Without the molecule that the aptamer recognizes, the mRNA can be translated [497]. The other way around is possible too: the aptamer sequence forms a hairpin with the mRNA sequence, and this conformation opens when the aptamer-binding molecule is present, allowing the ribosome to access the mRNA start codon [498]. When fusing into the gene the aptamer and a ribozyme-encoding sequence that would usually degrade the mRNA, when the aptamer ligand is present the mRNA is stabilized and can be translated [499]. Such riboswitches can also occur naturally [500], and studying them in organisms can be a source of new aptamer sequences. These systems can be applied for basic research purposes or as chemical sensors [498].

Several aptamers have been patented for clinical purposes [490], and also two patent applications have been filed for use in personal care products [501,502]. Many companies (Aptus Biotech, Aptamer Group, Aptagen, Oak Biosciences, Novaptech, NeoVentures Biotechnology, SomaLogics, Noxxon Pharma AG, Gilead, and more) are already commercializing and developing aptamers and platforms for their application. Among their services, they offer aptamer identification, optimization, and assay development.

4.3. Applications of aptamers in malaria

4.3.1. Aptamers for malaria diagnosis

Some aptamers have already been developed for the recognition of *Plasmodium* proteins. Most of them are focused on diagnostic applications, and many have been raised against *Plasmodium* lactate dehydrogenase (pLDH), because it is a well-characterized biomarker of infection (as mentioned in section 1.4) and its translation into diagnostic devices can be relatively simple. With this focus, Lee *et al*. described the selection of aptamers using recombinant pLDH from both *P. falciparum* (*Pf*LDH) and *P. vivax* (*Pv*LDH) with the FluMag technique. The obtained aptamer, pL1, could detect both protein variants (with K_d = 16.8-49.6 nM) by immobilizing it into an electrode and measuring impedance changes [503]. pL1 was also tested in colorimetric biosensors, based on aggregation of gold nanoparticles in the presence of the protein to be detected, obtaining high sensitivity for biomarker detection in human serum and being capable to correlate the sensing to parasites/µL measurements [504,505].

In parallel, Tanner et al. were also developing an aptamer against *Pf*LDH, called 2008s, with K_d = 42 nM, and tested its performance in a similar gold nanoparticle-based colorimetric sensor [506]. The main difference with pL1 is that 2008s is species-specific. Interestingly, the research group further developed a colorimetric biosensor prototype based on *Pf*LDH activity. L-lactate was added to PfLDH immobilized through binding to 2008s, and the substrate was metabolized into the products pyruvate and NADH; in the presence of nitrotetrazolium blue chloride, which is subsequently reduced by NADH into a diformazan dye product, the enzymatic activity could be measured colorimetrically [507]. This type of biosensor was called aptamer-tethered enzyme capture (APTEC), and was tested in clinical samples to validate its potential [508]. A prototype platform has been proposed that approaches its application to the field using microfluidics and this APTEC sensing (Figure 22) [509]. The aptamer 2008s was also tested in other sensing platforms: (i) one based on luminescence of silver nanoclusters [510], (ii) as part of a DNA origami assembly [511] that can change shape in presence of the biomarker [512], and (iii) as a combination of the DNA origami assembly, by making DNA polyhedrons that can hold more aptamer molecules, and using the APTEC strategy as detection method [513].

A third group led by Goswami has developed an aptamer (P38) against *Pf*LDH with K_d of 0.35 µM. They tested the quantitative detection also with a gold nanoparticle aggregation system [514] and by immobilization in graphene oxide, over an electrode, generating a very sensitive biosensor that could detect up to 0.5 fM of protein [515].

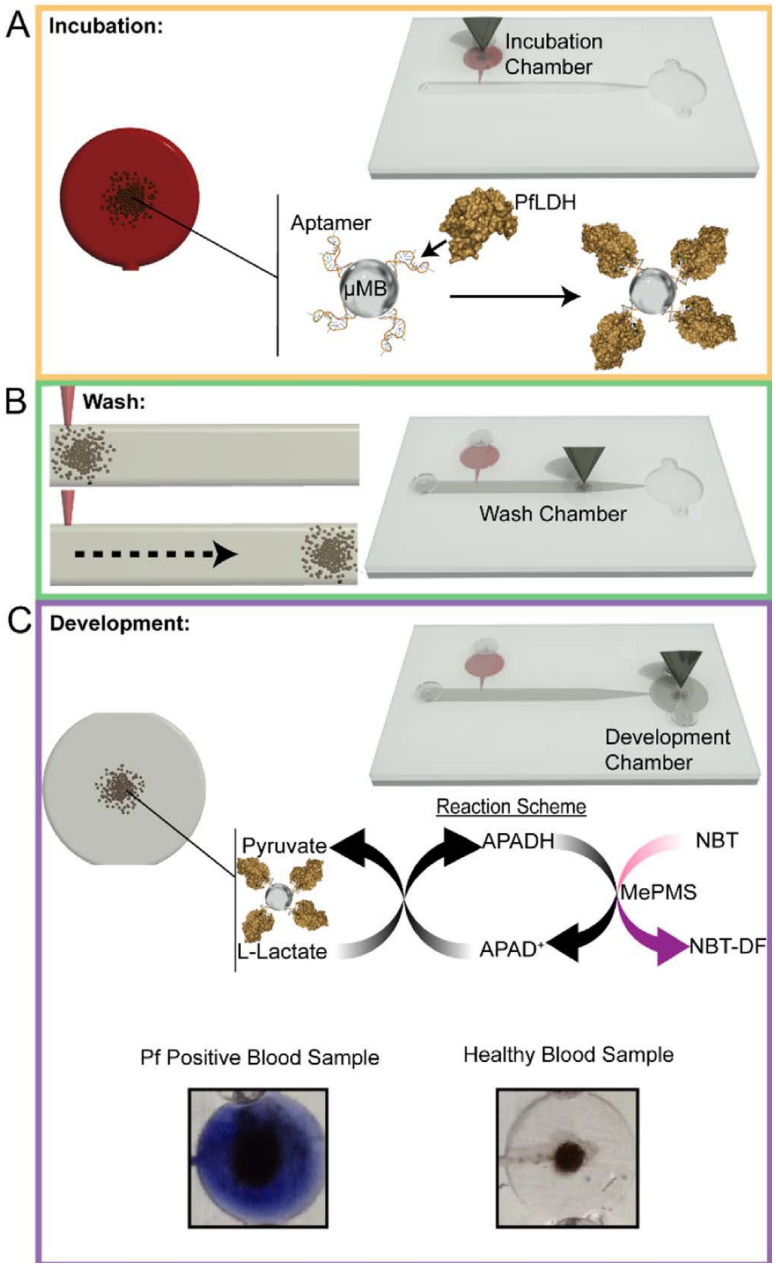

Figure 22: APTEC-based microfluidic device for malaria diagnosis. The detection is performed in 3 steps: (A) micro magnetic beads (µMB) containing the aptamers are incubated with the blood sample, if PfLDH is present, it will be bound; (B) the beads are then washed and separated by magnetic attraction, and (C) accumulated in the development chamber, where there is already the development solution, which changes color in presence of PfLDH due to the reaction shown in the scheme. Figure from [509].

Recently, more aptamers against PfLDH were raised using the whole recombinant protein and also testing specific epitopes that would allow species-specific recognition, separating the positive binding-sequences by nitrocellulose filtration of the target-oligonucleotide complex. The authors suggested that working directly with known epitopes can help to advance faster in aptamer discovery [465].

Although generally aptamers are oligonucleotides, there is potential for peptides as 'aptameric' tools too. In this context, thanks to *in silico* modeling predictions, one peptidic aptamer against *Plasmodium* lactate dehydrogenase was developed, and the preliminary assays indicate that it has a good diagnostic performance [516].

pLDH is not the only parasite protein being explored for diagnostic purposes: Goswami's group has also developed aptamers against *Plasmodium* glutamate dehydrogenase, described in a couple of publications, which also bear potential for developing diagnostic tools [517,518].

One last approach explored in aptamer discovery for diagnosis was using the high mobility group box 1 protein of *P. falciparum*, chosen due to its conservation and high levels of expression along all blood stages. The aptamers selected had dissociation constants between nano and micromolar ranges, and still had some unspecific binding towards the human homolog protein depending on pH [519].

4.3.2. Aptamers for therapy

Aptamers can also be a tool for therapeutic interventions, e.g. aptamers raised against an enzyme can block its activity [520]. There is one attempt reported at developing aptamers as malaria therapy, where the authors describe inhibition of *P. falciparum* growth using DNA aptamers that could bind the heme group, suppressing its detoxification pathway in the parasite [521].

4.3.3. Aptamers against the pRBC surface

It has been suggested that aptamers against proteins or features of the pRBC could be used as adjuvant therapy in malaria, preventing cytoadhesion or rosetting as some antibodies do [522].

Using a recombinant DBL1α domain from PfEMP1, RNA aptamers capable of rosette disruption have been generated [523]. Additionally, using a whole cell-SELEX approach combined with microfluidic separation of non-bound sequences, aptamers were raised against the *P. falciparum* CS2 strain, which expresses the var2CSA variant of PfEMP1. The sequences

selected could recognize epitopes in this protein and potentially some other membrane features, as one of the sequences could still bind trypsin-treated CS2 parasites [474].

A slightly different approach with the same objective is to target the receptors to which the parasites bind: RNA aptamers have recently been raised against CD36 with the perspective of applying them for malaria therapy [524].

However, obtaining aptamers against surface targets of the pRBCs is quite challenging. Alhough adhesive proteins are exported to the infected cell surface [525], they can be lost in the process of establishing a *P. falciparum* line for cell culture, as cell adhesion and other features are lost in a short time without selective pressure; major changes in transcription and translation can be observed depending on culture conditions [526]. Moreover, the exposed domains in these proteins are highly variable, due to allelic variation, and thus the aptamers raised might not be useful for all parasite strains.

Objectives

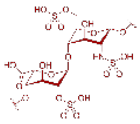

To explore the potential application of **heparin and heparin-derived** molecules as antimalarial compounds against different parasite stages

To develop **DNA aptamers** with specific binding to *Plasmodium falciparum* infected red blood cells, of potential use in therapeutic and/or diagnostic approaches.

Article 1: Repurposing Heparin as Antimalarial: Evaluation of Multiple Modifications Toward *In Vivo* Application

Authors: Elena Lantero, Carlos Raúl Aláez-Versón, Pilar Romero, Teresa Sierra and Xavier Fernàndez-Busquets

Journal: *Pharmaceutics*

Volume: 12

Issue: 9

Article number: 825

Published: 29th August 2020

DOI: 10.3390/pharmaceutics12090825

Journal Impact Factor: 4.421

Categories: Pharmaceutical Science (Q1)

Abstract:

Heparin is a promising antimalarial drug due to its activity in inhibiting Plasmodium invasion of red blood cells and to the lack of resistance evolution by the parasite against it, but its potent anticoagulant activity is preventing the advance of heparin along the clinical pipeline. We have determined, in in vitro Plasmodium falciparum cultures, the antimalarial activity of heparin-derived structures of different origins and sizes, to obtain formulations having a good balance of in vitro safety (neither cytotoxic nor hemolytic), low anticoagulant activity (≤23 IU/mL according to activated partial thromboplastin time assays), and not too low antimalarial activity (IC_{50} at least around 100 μg/mL). This led to the selection of five chemically modified heparins according to the parameters explored, i.e., chain length, sulfation degree and position, and glycol-split, and whose in vivo toxicity indicated their safety for mice up to an intravenous dose of 320 mg/kg. The in vivo antimalarial activity of the selected formulations was poor as a consequence of their short blood half-life. The covalent crosslinking of heparin onto the surface of polyethylene glycol-containing liposomes did not affect its antimalarial activity in vitro and provided higher initial plasma concentrations, although it did not increase mean circulation time. Finding a suitable nanocarrier to impart long blood residence times to the modified heparins described here will be the next step toward new heparin-based antimalarial strategies.

pharmaceutics

MDPI

Article

Repurposing Heparin as Antimalarial: Evaluation of Multiple Modifications Toward In Vivo Application

Elena Lantero [1,2], Carlos Raúl Aláez-Versón [3], Pilar Romero [4], Teresa Sierra [4] and Xavier Fernàndez-Busquets [1,2,5,*]

1 Barcelona Institute for Global Health (ISGlobal, Hospital Clínic-Universitat de Barcelona), Rosselló 149-153, ES-08036 Barcelona, Spain; elantero@ibecbarcelona.eu
2 Nanomalaria Group, Institute for Bioengineering of Catalonia (IBEC), The Barcelona Institute of Science and Technology, Baldiri Reixac 10-12, ES-08028 Barcelona, Spain
3 BIOIBERICA S.A.U., Polígon Industrial "Mas Puigvert", Ctra. N-II, km. 680.6, ES-08389 Palafolls, Spain; cralaez@bioiberica.com
4 Instituto de Nanociencia y Materiales de Aragón (INMA), University of Zaragoza-CSIC, Pedro Cerbuna 12, ES-50009 Zaragoza, Spain; promero@unizar.es (P.R.); tsierra@unizar.es (T.S.)
5 Nanoscience and Nanotechnology Institute (IN2UB), University of Barcelona, Martí i Franquès 1, ES-08028 Barcelona, Spain
* Correspondence: xfernandez_busquets@ub.edu; Tel.: +34-93-227-5400 (ext. 4581)

Received: 30 June 2020; Accepted: 7 August 2020; Published: 29 August 2020

Abstract: Heparin is a promising antimalarial drug due to its activity in inhibiting *Plasmodium* invasion of red blood cells and to the lack of resistance evolution by the parasite against it, but its potent anticoagulant activity is preventing the advance of heparin along the clinical pipeline. We have determined, in in vitro *Plasmodium falciparum* cultures, the antimalarial activity of heparin-derived structures of different origins and sizes, to obtain formulations having a good balance of in vitro safety (neither cytotoxic nor hemolytic), low anticoagulant activity (≤23 IU/mL according to activated partial thromboplastin time assays), and not too low antimalarial activity (IC50 at least around 100 µg/mL). This led to the selection of five chemically modified heparins according to the parameters explored, i.e., chain length, sulfation degree and position, and glycol-split, and whose in vivo toxicity indicated their safety for mice up to an intravenous dose of 320 mg/kg. The in vivo antimalarial activity of the selected formulations was poor as a consequence of their short blood half-life. The covalent crosslinking of heparin onto the surface of polyethylene glycol-containing liposomes did not affect its antimalarial activity in vitro and provided higher initial plasma concentrations, although it did not increase mean circulation time. Finding a suitable nanocarrier to impart long blood residence times to the modified heparins described here will be the next step toward new heparin-based antimalarial strategies.

Keywords: malaria; heparin; *Plasmodium falciparum*

1. Introduction

Despite being preventable and treatable, malaria continues to have a devastating impact on people's health and livelihoods around the world. According to the last World Malaria Report [1], around 228 million cases of malaria occurred globally in 2018 (up from 216 million in 2016), and the disease led to an estimated 405,000 deaths, mostly children under five years of age in sub-Saharan Africa. Although there were an estimated 11 million fewer malaria cases in 2018 than in 2010, data for the period 2015–2018 highlight that no significant progress in reducing global malaria incidence was made in this timeframe. In the Greater Mekong subregion, there is now *Plasmodium falciparum* resistance to artemisinin and other drugs, which is leading to treatment failure. Resistance to antimalarial drugs has

had a significant impact on the cost of global malaria control, as new drugs have had to be developed to replace those that have become ineffective. In this context, the application of the 3 Rs of drug development (rescue, repurpose, reposition) to previously discarded compounds is an interesting strategy to return value to potential treatments in decline or on hold.

Red blood cells (RBCs) infected with mature stages of the malaria parasite bind to the endothelial cells in the capillaries of tissues in a phenomenon known as sequestration, which allows *Plasmodium* to replicate while evading splenic clearance [2]. *Plasmodium*-infected RBCs (pRBCs) can also adhere to non-infected erythrocytes giving rise to rosettes, and they can form clumps through platelet-mediated binding to other pRBCs [3]. These events, which may lead to occlusion of the microvasculature, are thought to play a major role in the fatal outcome of severe malaria. Because the blood-stage infection is responsible for all symptoms and pathologies of malaria, pRBCs have traditionally been a main chemotherapeutic target [4]. One of the main pRBC-binding molecules are glycosaminoglycans (GAGs), a family of ubiquitous polysaccharides, some of whose members count among the most negatively charged natural polymers. Binding to the GAG chondroitin 4-sulfate (CSA) is thought to cause pRBC sequestration in the placenta, which has been linked to the severe disease outcome of pregnancy-associated malaria [5]. Heparan sulfate (HS), or a HS-like molecule exposed on RBCs, is the ligand responsible for rosetting [6], and is also targeted by the circumsporozoite protein in the sporozoite attachment to hepatocytes during the primary stage of malaria infection in the liver [7,8]. GAG-based therapies against malaria have been proposed in the wake of the results from different assays showing that soluble CSA, heparin, HS, heparin/HS derivatives, and other sulfated glycoconjugates can inhibit pRBC sequestration, disrupt rosettes, and block sporozoite adhesion to hepatocytes [9–11]. Heparin had actually been used in the treatment of severe malaria [12], but it was abandoned because of its strong anticoagulant action, with side effects such as intracranial bleeding. However, depolymerized heparin lacking anticoagulant activity has been found to disrupt rosette formation and pRBC cytoadherence in vitro and in vivo in animal models and in fresh parasite isolates [13].

Heparin has also a direct antimalarial activity on the pathogen, which operates through the inhibition of parasite invasion of RBCs [14], mainly by interaction with the merozoite surface protein 1 (MSP1) [15] involved in the initial contact and reorientation of the *Plasmodium* cell pursuing invasion [16]. Single-molecule force spectroscopy data have revealed a complete specificity of adhesion of heparin to late form pRBCs (schizonts) vs. RBCs, with a binding strength matching that of antibody-antigen interactions [17]. Confocal fluorescence analysis showed that when added to living pRBC cultures fluorescein-labeled heparin enters late schizonts about to burst and in only 15 min colocalizes with the intracellular parasites [18]. In agreement with this binding to the intraerythrocytic late stage pathogen, heparin has been described to inhibit the egress of merozoites from the parasitized RBC following its binding to MSP1 and to proteins found in the inner part of the RBC membrane [19]. Commercial heparin with a nominal mean molecular weight of 13,000 Da inhibits the in vitro growth of *P. falciparum* with an IC50 around 10 μg/mL (roughly 1 μM). Because heparin is eventually found in the blood, *Plasmodium* must have been exposed to it during its long coevolutionary history with humans and yet parasite resistance has not been described so far [15]. Several heparin modifications with reduced anticoagulant activity but maintaining significant antimalarial activity in vitro have been identified to have potential for novel drug development [20]. Of importance for an optimal inhibitory activity are the presence of *N*- and *O*-sulfate residues and of ≥2 sulfate units per disaccharide, specific spatial arrangements of sulfation requiring sulfate groups positioned together on a single saccharide unit, and a minimum chain length of six monosaccharide residues [15]. Overall, longer-chain heparin molecules of molecular weight >3 to 25 kDa showed a trend toward having higher inhibitory activity than shorter-chain forms <3 kDa [20]. Periodate oxidation of non-sulfated uronic acid residues, which has been reported to abolish anticoagulation [21], increased the activity of some compounds [20].

Here we have explored different combinations of heparin modifications such as chain length, sulfation degree and position, and glycol-split, with the objective of identifying heparin-derived structures having a reduced anticoagulant activity, but maintaining a significant antimalarial potency.

2. Materials and Methods

Except where otherwise indicated, reagents were purchased from Sigma-Aldrich Corporation (St. Louis, MO, USA), and reactions were performed at room temperature (22 to 24 °C). The lipids (all ≥99% purity according to thin layer chromatography analysis) 1,2-dioleoyl-*sn*-glycero -3-phosphocholine (DOPC), 1,2-dioleoyl-*sn*-glycero-3-phosphoethanolamine (DOPE), 1,2-dioleoyl-3 -trimethylammonium-propane (DOTAP), 1,2-distearoyl-*sn*-glycero-3-phosphoethanolamine-*N* -[methoxy(polyethylene glycol)-2000] (DSPE-PEG), 1,2-dioleoyl-*sn*-glycero-3-phosphoethanolamine-*N* -(lissamine rhodamine B sulfonyl) (DOPE-Rho), and cholesterol were purchased from Avanti Polar Lipids Inc. (Alabaster, AL, USA) and stored at −20 °C.

2.1. Heparin Modification and Characterization

Heparin and dermatan sulfate were obtained from animal mucosae and chondroitin sulfate from animal cartilage following standard industrial manufacturing procedures. Unfractionated heparin (UH, >12 kDa) was modified by depolymerization, desulfation, oversulfation, conjugation to primaquine (PQ), and glycol-split, and for the molecules with more than one modification, those were applied in this order. All modifications were performed as described elsewhere [22], and are succinctly described below.

For the depolymerization by nitrous acid [23,24], 4 g of heparin were dissolved in 65 mL of H_2O and cooled to 4 °C. After adding 75 mg of $NaNO_2$, the pH was adjusted to 2 with 0.1 M HCl. The solution was stirred at 4 °C for 20 min, and then the pH was brought to 7.0 by addition of 0.1 M NaOH. 1 g of $NaBH_4$ was added in several portions under stirring. After 2–3 h, the pH was adjusted to 4 with 0.1 M HCl, and 15 min later the solution was neutralized with 0.1 M NaOH. The products, medium molecular weight heparin (MMWH, 8 to 12 kDa), low molecular weight heparin (LMWH, 4–8 kDa), and ultralow molecular weight heparin (ULMWH, ≤4 Kda) were precipitated with three volumes of ethanol, then dissolved in water and recovered by freeze-drying.

For 2-*O*-desulfation [22], 500 mg of heparin were dissolved in 10 mL of 1 M NaOH and then heated at 85 °C for 1 h. After cooling below 30 °C, the solution was brought to pH 7 with 0.1 M HCl and heated at 70 °C for 48 h. Then, the samples were cooled, dialyzed against H_2O (cellulose acetate membranes, 1000-Da cut-off), and recovered by freeze-drying.

For 6-*O*-desulfation [25], 200 mg of sodium heparin salt was passed through a column of Amberlite IR-120, neutralized with pyridine, and lyophilized to obtain pyridinium heparin salt, which was solubilized in 20 mL of dry pryridine, to which 4 mL of *N*,*O*-bis(trimethylsilyl)acetamide were added. The mixture was incubated 2 h at 60 °C until a clear solution was obtained. The reaction was terminated by adding 20 mL of water and the sample was dialyzed against H_2O, its pH adjusted above 7 with NaOH, and dialyzed again immediately. The product was recovered by freeze-drying.

For *N*-desulfation and *N*-acetylation [22], pyridinium heparin salt, as previously obtained [25], was stirred at 20–25 °C in Me_2SO:water (9:1) for 120 min to obtain molecules with *N*-desulfation. For obtaining *N*-acetylation, the previous compounds were incubated with acetic anhydride in alkaline aqueous medium ($NaHCO_3$, 4 °C, 2 h). At the point of *N*-desulfation or *N*-acetylation, products were dialyzed against H_2O and recovered by freeze-drying.

For oversulfation, to obtain a highly sulfated heparin, the procedure described by Maruyama et al. [26] was applied. Briefly, 100 mg of sodium heparin salt were subjected to cation-exchange chromatography to obtain tributylamine salt, lyophilized, and dissolved in 0.8 mL of *N*,*N*-dimethylformamide, which contained an excess of pyridine-sulfur trioxide. After 1 h at 40 °C, 1.6 mL of water were added, and the product was precipitated with three volumes of cold ethanol saturated with anhydrous sodium acetate and collected by centrifugation. The product was dissolved

in water, dialyzed and recovered by freeze-drying. The resulting SO_3^-/COO^- (i.e., SO_3^-/disaccharide) ratio (see below for its determination) of oversulfated heparin was 3.0 (as compared to 1.9–2.0 for native UH).

Glycol-split was done by exhaustive periodate oxidation and borohydride reduction of UH or of a previously depolymerized and/or 2-*O*-desulfated sample [27]. In the first protocol, 250-mg samples were dissolved in 6 mL of H_2O, and 6 mL of 0.1 M $NaIO_4$ were added. After stirring the solution at 4 °C for 16 h in the dark, 1 mL of ethylene glycol was added to stop the reaction, and the solutions were dialyzed against H_2O for 16 h. Solid sodium borohydride (60 mg) was added to the retentate solutions in several portions under stirring. After 2–3 h, the pH was adjusted to 4 with 0.1 M HCl, and after stirring for 15 min, the solutions were neutralized with 0.1 M NaOH. After desalting and a second dialysis against H_2O, the final products were recovered by freeze-drying. In the second protocol, 250-mg samples were dissolved in 5 mL of 1 M NaOH and then heated at 60 °C for 30 min. After cooling below 30 °C, the solutions were brought to pH 7 with 0.1 M HCl and heated at 70 °C for 48 h to induce the partial conversion of iduronic acid $(IdoA)_2SO_3$ to galacturonic acid. After cooling and dialyzing against H_2O, the product was recovered by freeze-drying.

PQ conjugation to MMWH: 2.0 g of MMWH were dissolved in 50 mL of deionized water and the pH of the solution was adjusted to 7.0. 1.35 g of PQ phosphate and 0.075 g of sodium cyanoborohydride were added and the reaction was stirred for 15 min at room temperature. pH was adjusted to 7.0 and stirring was continued for 24 h. Then, an additional 0.075 g of sodium cyanoborohydride were added and the reaction continued for another 24 h. The crude product was centrifuged at 5000 rpm for 15 min, and the supernatant was dialyzed against water until the permeate was colorless. 50 g of VOPC1074 resin were added to the retentate and the solution was stirred for 15 min. Supernatant was discarded and the resin was washed with 400 mL of deionized water for 1.5 h. The resin was filtered and treated with 250 mL of 15% (*w*/*v*) NaCl. The mixture was further stirred for 12 h at room temperature and then vacuum filtered. The filtrate was dialyzed again as before until chloride anions were not detected in the permeate. The product was recovered by freeze-drying.

The molecular weight of most samples was determined by high-performance size exclusion chromatography combined with triple detector array (HP-SEC/TDA) [28]; samples were dissolved at 20 mg/mL in 0.1 M $NaNO_3$, and 100 µL were injected in the SEC/TDA equipment (Viscotek GPCmax with Viscotek module 305 TDA (Malvern Instruments Ltd., Malvern, UK). SO_3^-/COO^- ratio [29], anti-Xa factor [30], and activated partial thromboplastin time (aPTT) activity on dry basis [18] were determined according to established protocols.

2.2. NMR Experimental Procedure

NMR analysis was performed on a Bruker AVANCE 500 spectrometer operating at a frequency of 500.13 MHz for ^1H and 125.75 MHz for ^{13}C equipped with a 5 mm TBO probe. Spectra were processed with Bruker Topspin software version 3.6.2. Around 30–40 mg of heparin samples were dissolved in 0.4 mL of D_2O and the samples were held at a temperature of 298 K during data acquisition. Samples were analyzed by 1D and 2D NMR spectroscopy. Heteronuclear single-quantum coherence (HSQC), proton–proton correlation spectroscopy (^1H-^1H COSY) and total correlation spectroscopy (^1H-^1H TOCSY) were used to characterize their structures. Chemical shift values were measured downfield from trimethylsilylpropionate sodium salt (TSP) as standard. The ^1H-^1H TOCSY spectra were run using 32 scans per t1 increment (400 points) and a mixing time of 80 ms. ^1H-^{13}C HSQC spectra were recorded with carbon decoupling during acquisition with 512 increments of 32 scans for each experiment. Two-dimensional diffusion ordered spectroscopy (DOSY) experiments were performed using stimulated echo sequence with bipolar gradient pulses [31]. Diffusion time (Δ) was set within the interval 220–320 ms. The pulsed gradients were incremented from 2% to 95% of the maximum strength in 16 spaced steps with a duration (δ) of 4–8 ms. (For the internal reference TPS these values were Δ = 140 ms and δ = 2.8 ms). The 2D plots show diffusion coefficient values D in [m^2/s]. The NMR spectra of the heparin formulations selected for in vivo assays are presented in the Supplementary Materials.

2.3. *P. falciparum* Culture and Growth Inhibition Assays

P. falciparum 3D7 parasites were cultured at 4% parasitemia and 3% hematocrit in a hypoxia incubator (cell culture CO_2 incubator, ESCO, Singapore) with a 92.5% N_2, 5.5% CO_2, and 2% O_2 gas mixture, using complete Roswell Park Memorial Institute (RPMI) 1640 medium (supplemented with 2 mM L-glutamine, 50 µM hypoxanthine, 5 g/L Albumax II, 25 mM HEPES, pH 7.2). A modification of this culture medium substituting Albumax II by 10% human inactivated plasma was also used when indicated. Serial dilutions in complete RPMI of each compound tested were incubated with *P. falciparum* 3D7 cells at 1% pRBC and 3% hematocrit in a final volume of 200 µL in 96-well plates (SPL Life Sciences Co., Ltd., Gyeonggi-do, Korea). Every dilution was prepared in triplicate, and the parasites were incubated under hypoxia for 44 h, when parasitemia was determined by flow cytometry, using either FACSCalibur or LSRFortesa (4 laser) cytometers (both from BD Biosciences, San Jose, CA, USA). For each cytometer, cell culture from each sample was diluted at either 0.024% or 0.03% hematocrit in phosphate buffered saline, pH 7.4 (PBS), containing 0.5 nM or 0.25 nM SYTO 11, respectively. Parasitemia percentage was recorded with BD FACSDiva (BD Biosciences) software and further analyzed with GraphPad Prism 6 software (GraphPad Software, San Diego, CA, USA). The experiments with the samples of interest for in vivo assays were repeated three times, twice with the parasites synchronized at ring stage through a 5% (*w*/*v*) sorbitol treatment [32], and once with the parasites synchronized at trophozoite stage through a 70% Percoll treatment [33]. The rest of samples were tested in ring stage synchronized cultures.

2.4. *In Vitro Cytotoxicity Assays*

Human umbilical vein endothelial cells (HUVECs) were cultured in a CO_2 incubator using Medium 199 (M199, LabClinics, Barcelona, Spain) supplemented with penicillin-streptomycin (100 units and 0.1 mg/mL, respectively) and 10% fetal bovine serum (complete M199) in T-25 flasks (SPL Life Sciences Co., Ltd.), allowed to grow up to 70–80% convergence and replated by trypsin treatment. Unspecific toxicity of the samples was tested with the WST-1 cell viability assay (Roche Applied Science, Penzberg, Germany), following the manufacturer's recommendations. Briefly, HUVECs were seeded in 96-well plates at a density of 5000 cells per well in 100 µL of complete M199. After a 24-h incubation at 37 °C, the medium was removed, and 90 µL of fresh M199 were added together with 10 µL of the sample of interest in PBS. HUVECs were placed back in the incubator for 24 h or 48 h. At the moment of reading, 10 µL of WST-1 reagent was added to each well, and, after an incubation of 3–4 h, absorbance at 440 nm was measured with an Epoch™ microplate spectrophotometer (BioTek Instruments Inc., Winooski, VT, USA). For each sample, three different concentrations were tested in triplicates, and each plate contained three seeded wells with 1% bleach (0% viability control) and three wells with 10 µL PBS (100% viability control) as controls.

2.5. *Hemolysis Assays*

In a 96-well plate, 2 µL of sample were added to 200 µL of a 3% hematocrit RBC suspension in RPMI complete medium. After incubating for 3 h at 37 °C, samples were centrifuged at 1000× *g* for 5 min and 150 µL of supernatant from each sample was transferred to a new plate where absorbance was measured at 541 nm in an Epoch™ microplate spectrophotometer (BioTek Instruments Inc.). Assays were done in triplicates, including positive (Triton X-100) and negative (PBS) controls. Data analysis was done with Excel and GraphPad Prism 6 software.

2.6. *In Vivo Toxicity Assays*

Seven-week-old BALB/c female mice (18–20 g, Janvier Laboratories, Le Genest-Saint-Isle, France) were maintained with ad libitum access to food and water under standard environmental conditions (20–24 °C and 12 h/12 h light/dark cycle). The animals were anesthetized with isoflurane (4% for induction and 2.5% for maintenance) in an oxygen stream to ensure administration and minimize

injection stress, while delivery of a 200 µL bolus was done intravenously. An adaptation of OECD 425 Test Guideline, which consisted of a single ordered dose progression, was followed in order to reduce the number of animals used. The first mouse received a dose one order of magnitude lower than the concentration proven safe in vitro, and the dose for the next animal was either decreased or increased by a factor of 3.2 depending on the observation or not, respectively, of acute effects on the first animal. After administration, each mouse was monitored for at least 48 h before the next animal was treated. In addition, other toxicity signs were evaluated maintaining all animals under observation for 14 days after dose injection. Following this protocol, different GAG concentrations (31.5, 100, 320, and 750 mg/kg) were tested, prepared in PBS from a 50 mg/mL stock solution of the compound in sterile PBS. When any toxic effects were observed, including, among others, >20% reduction in weight, aggressive and unexpected behavior or the presence of blood in faeces, animals were immediately anesthetized using a 100 mg/kg Ketolar plus 5 mg/kg Midazolan mixture and sacrificed by cervical dislocation. The highest dosage exhibiting absence of toxicity signs was considered the compound maximum tolerated dose. The animal care and use protocols followed adhered to the specific national and international guidelines specified in the Spanish Royal Decree 53/2013, which is based on the European regulation 2010/63/UE. The corresponding protocols were reviewed and approved by the Ethical Committee on Clinical Research from the Hospital Clínic de Barcelona (Reg. HCB/2018/1223, 23 January 2019).

2.7. Antimalarial Activity in Mice

A four-day suppressive test in BALB/c female mice was performed following pre-established protocols [34]. Briefly, animals were infected with 2×10^7 pRBCs from a *Plasmodium yoelii yoelii* 17XL–infected mouse (20–30% parasitemia). Between 3 h and 4 h later, mice were treated intravenously with 100 µL of the test samples; an infection control group treated with PBS only and a treatment control group dosed with 5 mg/kg chloroquine were also included. For the next three days animals were treated following the same procedure at the same times. From day 2 post-infection, blood samples were collected by tail punction, and pRBC percentage was determined by either flow cytometry or blood smear preparation stained with Giemsa followed by optical microscope analysis.

2.8. Preparation of Heparin-Coated Liposomes

The lipid formulation DOPC:DOPE:cholesterol:DOTAP:DSPE-PEG:DOPE-Rho 46.5:30:20:2:2:0.5 was obtained by mixing stock solutions of lipids in chloroform in a round bottom flask. The solvent was evaporated by N_2 flow and the lipid film was further dried under vacuum for 1 h. Then, lipids were hydrated in 1 mL of PBS and vortexed for 3 min, to achieve a final total lipid concentration of 20 mM. To obtain unilamelar liposomes of regular size, the suspension was extruded through 200 nm polycarbonate membranes (Avanti Polar Lipids, Inc.) using a mini extruder device (Avanti Polar Lipids, Inc.). UH at 20 mg/mL was activated for 30 min in 25 mM 2-(*N*-morpholino)ethanesulfonic acid, pH 5, with 39 mM 1-ethyl-3-(3-dimethylaminopropyl)carbodiimide (BioRad) and 55 mM *N*-hydroxysulfosuccinimide. Then, 500 µL of activated UH were added to a liposome suspension containing 0.67 mM total lipid in 3 mL of PBS and incubated under stirring for 2 h. To remove unbound heparin, the sample was centrifuged in a 100 kDa cut-off Amicon® Ultra centrifugal filter and PBS was added to recover the initial volume; this process was repeated five times, until heparin was not detected in the recovered washes according to Alcian Blue quantification [35]. Heparin concentration in the final UH-coated liposome sample was 1.7 mg/mL, corresponding to a ca. 1:15 UH:total lipid molar ratio. Liposomes were detected in plasma by rhodamine fluorescence detection in an Infinite® M Nano microplate reader spectrofluorometer (Tecan, Männedorf, Switzerland) at 553 nm excitation and 586 nm emission.

2.9. Plasma Half-Life Determination

BALB/c mice were inoculated intravenously with 18 mg/kg of the compounds to be tested (UH, 2-*O*-desulfated glycol-split MMWH, or UH-coated liposomes). Blood was collected at different times after administration via facial vein or cava vein extraction under isoflurane anesthesia. Collected blood was mixed with 1/10 volume of 3.2% sodium citrate, and plasma was separated by centrifugation (500× *g*) and frozen until quantification with the Heparin Red® method (Redprobes UG, Münster, Germany), following published protocols [36]. In brief, 20 µL of non-treated mouse plasma containing different heparin concentrations (30, 20, 15, 10, 7.5, 5, 2, 1, and 0 µg/mL) and of the collected plasma from treated mice were placed in duplicates per mouse and time point in a 96-well plate. Enhancer solution, 1 M $MgCl_2$ and Heparin Red® were mixed (85.5:4.5:1 for UH samples and 171:9:1 for 2-*O*-desulfated glycol-split MMWH), 80 µL of the mixture was added to each well, the plate was shaken for 3 min, and fluorescence was recorded at 590 nm excitation and 645 nm emission, using a Synergy microplate reader (BioTek Instruments Inc.).

2.10. Ethics Statement

The human blood and plasma used for *P. falciparum* in vitro cultures were commercially obtained from the *Banc de Sang i Teixits* (www.bancsang.net). Purchased units had been discarded for transfusion, mostly due to an excess of blood relative to anticoagulant solution. Prior to use, blood and plasma units underwent the analytical checks specified in the current legislation. Before being delivered, to guarantee the non-identification of the blood donor, unit data were anonymized and irreversibly dissociated, and any identification tag or label was removed. No blood data were or will be supplied, and the studies reported here were performed in accordance with the current Spanish *Ley Orgánica de Protección de Datos* and *Ley de Investigación Biomédica* and under protocols reviewed and approved by the Ethical Committee on Clinical Research from the *Hospital Clínic de Barcelona* (Reg. HCB/2018/1223, 23 January 2019).

3. Results

3.1. Antimalarial Activity Determination of Different Natural GAGs

Preliminary in vitro antimalarial activity assays of different GAG types (Figure 1a–c) were consistent with previously published data [20] indicating that a >30-fold higher amount of dermatan or chondroitin sulfate than that of heparin was required to obtain similar parasite growth inhibitions (Figure 1d–f). A higher sulfate content in heparin (1.9–2.0 sulfate groups/disaccharide) correlated with its higher antimalarial activity. The source from which heparin was obtained did not have a significant influence on its capacity to inhibit *P. falciparum* growth in vitro.

3.2. Effect on Antimalarial Activity of Heparin Molecular Weight

Because higher molecular weights of heparin are usually related with undesired secondary effects, such as induced thrombocytopenia or hemorrhage [37], in vitro parasite growth inhibition was determined for unfractionated heparin from pig lung and for different fractions obtained from this molecule as precursor. In agreement with previous reports [15], both the curves of percentage of growth inhibition and the derived IC50 values showed that shorter heparin chain lengths had a reduced antimalarial activity, especially for ULMWH (Figure 2). Decreasing the number of disaccharide units below nine significantly lowered the antiplasmodial activity of heparin in vitro.

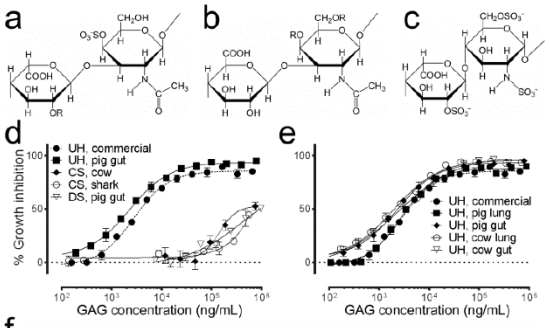

Type of GAG	Source	IC50 (μg/mL)*	SO_3^-/ disaccharide
UH	Pig gut	2.0 - 2.6	1.9 - 2.0
CS	Cow	66.1 - 309.4	1.0
CS	Shark	ud.	1.0
DS	Pig gut	ud.	1.2 - 1.8
UH	Cow lung	1.5 - 2.5	n.d.
UH	Cow gut	1.7 - 3.6	n.d.
UH	Pig lung	2.5 - 3.4	n.d.
UH, commercial	Pig gut	2.4 - 3.3	1.9 - 2.0

Figure 1. In vitro antimalarial activity of glycosaminoglycans (GAGs) from different origin. (**a–c**) Structures of the most represented disaccharide units in (**a**) dermatan sulfate, (**b**) chondroitin sulfate and (**c**) heparin. R: H or SO_3^-. (**d**,**e**) Graphs comparing the in vitro *Plasmodium falciparum* growth inhibition activity of different GAGs. (**f**) Description of the GAGs tested in panels (**d**,**e**). UH: unfractionated heparin, CS: chondroitin sulfate, DS: dermatan sulfate. ud.: undetected, n.d.: not determined. Commercial UH was purchased from Sigma Aldrich (Cat. No. H-4784). * IC50 has been calculated by non-linear regression of the percentage of growth inhibition against molecule concentration. IC50 range represents 95% confidence interval of one experiment.

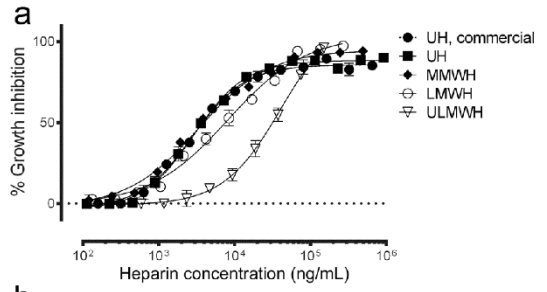

b

Type of molecule	Molecular weight (Da)	Number of disaccharide units*	IC50 (μg/mL)
UH	18440	31	2.5 - 3.4
MMWH	9850	17	2.6 - 4.4
LMWH	5400	9	5.9 - 11.3
ULMWH	3000	5	35.9 - 48.0
UH, commercial	13000	22	2.4 - 3.3

Figure 2. In vitro antimalarial activity of heparins with different molecular weight. (**a**) In vitro *P. falciparum* growth inhibition activity assay of heparin fractions of decreasing chain lengths. (**b**) Description of the heparin samples tested in panel (**a**). MMWH: medium molecular weight heparin, LMWH: low molecular weight heparin, ULMWH: ultralow molecular weight heparin. * The approximate number of disaccharide units was calculated considering the molecular weight of the trisulfated disaccharide unit as 590.9 g/mol. IC50 range represents 95% confidence interval of one experiment.

3.3. *Effect of Sulfate Group Removal on the Antimalarial Activity of Heparin*

Because there is a direct correlation between the number and position of sulfate groups and the anticoagulant activity of heparin [38], the antimalarial capacity of different desulfated heparin structures was analyzed (Figure 3). 2-*O* desulfation of IdoA together with glucosamine *N*-desulfation completely suppressed antimalarial activity, whereas 6-*O*-desulfation and *N*-desulfation significantly increased the IC50 of the resulting structures to >300 µg/mL (Table 1).

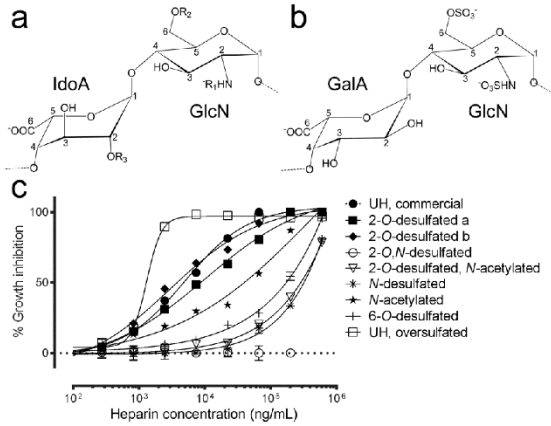

Figure 3. In vitro antimalarial activity of heparins with different sulfation patterns. (**a**,**b**) Structures obtained after desulfation (see Table 1 for the definition of chemical groups R_1, R_2, and R_3). IdoA: iduronic acid, GlcN: glucosamine, GalA: galacturonic acid. (**c**) In vitro *P. falciparum* growth inhibition activity assay of heparin fractions with different sulfation patterns.

Table 1. Description of the heparin samples tested in Figure 3.

Sample	Molecule of Origin	Structure	Molecular Weight (Da)	aPTT (IU/mg)	IC50 (µg/mL)
2-*O*-desulfated structure a	UH	R_1,R_2: SO_3^-; R_3: H	10,721	34	7.6–13.5
2-*O*-desulfated structure b	UH	b	14,023	63	2.2–4.1
2-*O*-desulfated, *N*-desulfated	2-*O*-desulfated a	R_1,R_3: H; R_2: SO_3^-	13,459	20	ud.
2-*O*-desulfated, *N*-acetylated	2-*O*-desulfated a	R_1: Ac; R_2: SO_3^-; R_3: H	10,868	24	>1000
N-desulfated	UH	R_2,R_3: SO_3^-; R_1: H	15,771	42	>1000
N-acetylated	*N*-desulfated	R_2,R_3: SO_3^-; R_1: Ac	15,963	91	>300
6-*O*-desulfated	UH	R_1,R_3: SO_3^-; R_2: H	14,521	45	>1000
UH	-	R_1,R_2,R_3: SO_3	15,792	203	2.0–2.6
UH, oversulfated	UH	R_1,R_2,R_3: SO_3^-	19,990	94	1.2–1.4
UH, commercial	-	R_1,R_2,R_3: SO_3^-	13,000	n.d.	4.1–6.0

ud.: undetected, n.d.: not determined.

2-*O*-desulfation of IdoA significantly reduced the anticoagulant activity of heparin according to aPTT values. This modification had only a moderate effect on antimalarial activity, except when the glucosamine *N*-sulfate was also removed or substituted by an acetyl group, which completely abolished the antiplasmodial action of heparin. The affinity for antithrombin of the two 2-*O*-desulfated samples maintaining a good inhibition of *Plasmodium* growth is likely suppressed, since anti-Xa activity was very low (3 IU/mg and 9 IU/mg for 2-*O*-desulfated structures in Figure 3 panels a and b, respectively) when compared to that of UH (192 IU/mg). The galacturonic acid (stereoisomer of IdoA) modification, shown in panel b in Figure 3, had an in vitro antimalarial activity that improved that of commercial UH. This inversion increases the chain rigidity [38], and it has been suggested that an increment in such rigidity of heparin-like molecules can produce an increase of antimalarial activity [15].

Oversulfated heparin exhibited an increased antimalarial activity relative to unfractionated heparin, although this positive result was not accompanied by a dramatic decrease in anticoagulant activity (94 IU/mg vs. 203 IU/mg, respectively).

3.4. *Effect of Glycol-Split on the Antimalarial and Anticoagulant Activities of Heparin*

Whereas a moderate degree of glycol-split (Figure 4a) slightly reduced the antimalarial activity of heparin (Figure 4b), it dramatically lowered its anticoagulation action according to the aPTT assay (72 IU/mg vs. 203 IU/mg relative to unfractionated heparin; Figure 4c). When glycol-split was applied to the 2-*O*-desulfated structure having the best balance between antimalarial and anticoagulant activities (Figure 3b), aPTT was further decreased (44 IU/mg), although this was accompanied by a decrease in the capacity to inhibit *Plasmodium* growth in vitro. This sample was derived from the 2-*O*-desulfated structure shown in Figure 3b, which had a higher degree of oxidation leading to increased glycol-split, and therefore to more open rings and flexibility than the sample derived from unfractionated heparin. Glycol-split treatment of heparin chains has been described to increase chain flexibility and to decrease interactions with coagulation factors [39], as evidenced by the dramatic decrease in antithrombin binding of glycol-split heparins (Figure 4c).

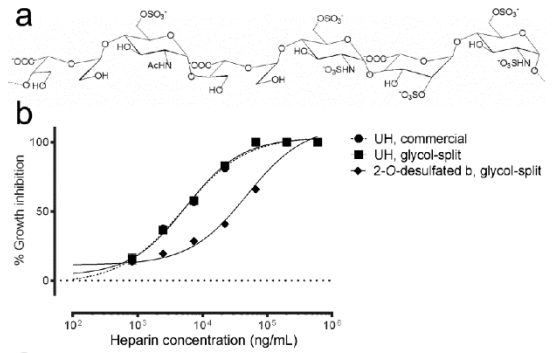

c

Sample	Molecule of origin	Molecular weight (Da)	Anti Xa (IU/mg)	aPTT (IU/mg)	IC50 (µg/mL)
UH, glycol-split	UH	13059	3	72	4.7 - 6.6
2-*O*-desulfated b, glycol-split	2-*O*-desulfated b	14380	2	44	35.4 - 66.2
UH	-	15792	192	203	2.0 - 2.6
UH, commercial	-	13000	n.d.	n.d.	4.1 - 6.0

Figure 4. Effect of glycol-split on the in vitro antimalarial activity of heparin. (**a**) Structure of the heparin chain after glycol-split treatment. (**b**) In vitro *P. falciparum* growth inhibition activity assay of heparin fractions with and without glycol-split. (**c**) Description of the heparin samples tested in panel (**b**). n.d.: not determined.

3.5. *Selection of Heparin Forms Having Reduced Anticoagulant Activity but Maintaining Significant Plasmodium Growth Inhibition*

To advance toward the use of heparin as a clinically useful antimalarial drug, keeping a low anticoagulant activity will be as important as maintaining its capacity to inhibit the growth of the parasite, and therefore a delicate balance has to be met between these two indicators. Several structures having less anticoagulant activity than unfractionated heparin were obtained when applying different combinations of the parameters explored above, i.e., chain length, sulfation degree and position, and glycol-split (Table 2). None of the resulting preparations exhibited significant hemolysis or unspecific toxicity in HUVEC cultures. Since heparins with reduced anticoagulant activity could be used in vivo in larger amounts, a sufficient antimalarial activity could be in principle obtained with them, even if they have a relatively low antiplasmodial potency.

Table 2. Characterization of heparin samples that combine different chemical modifications. Shadowed in gray are the formulations selected for in vivo assays.

Sample	Mw (Da)	SO_3^-/Disaccharide	IC50 (μg/mL ± SD)	IC90 (μg/mL ± SD)	aPTT (IU/mg)	In Vitro Toxicity [1] (% ± SD)	Hemolysis [1] (% ± SD)
MMWH_1	10,497	n.d.	22.7 ± 2.4	178.1 ± 28.4	110	1.1 ± 3.4	0.1 ± 0.2
MMWH_2	11,000	1.9	33.7 ± 21.8	374.8 ± 189.3	130	0.0 ± 6.0	0.5 ± 0.2
2-O-desulfated MMWH_1	8771	1.6	80.7 ± 5.0	270.3 ± 42.5	38	10.0 ± 3.0	0.3 ± 0.4
2-O-desulfated MMWH_2	8776	1.5	91.9 ± 9.0	351.9 ± 43.4	23	0.0 ± 2.3	2.0 ± 2.0
2-O-desulfated MMWH_3	10,198	1.5	59.1 ± 16.3	487.9 ± 161.3	53	17.9 ± 2.1	0.5 ± 0.2
2-O-desulfated MMWH_4	11,190	1.4	68.0 ± 14.3	404.8 ± 119.4	33	7.5 ± 1.8	0.0 ± 0.0
2-O-desulfated glycol-split MMWH_1	7388	1.8	79.6 ± 5.4	893.1 ± 321.0	6	7.3 ± 4.5	0.4 ± 0.1
2-O-desulfated glycol-split MMWH_2	7037	1.5	84.2 ± 13.4	303.4 ± 46.2	5	3.6 ± 5.4	0.0 ± 0.0
ULMWH	4270	2.2	49.3 ± 6.0	236.3 ± 54.9	6	6.8 ± 9.2	0.2 ± 0.1
2-O-desulfated ULMWH_1	4150	1.6	140.9 ± 15.9	322.5 ± 27.5	ud.	20.0 ± 16.7	0.0 ± 0.0
2-O-desulfated ULMWH_2	4450	1.4	129.2 ± 13.1	262.5 ± 16.1	ud.	37.0 ± 9.9	0.2 ± 0.0
2-O-desulfated glycol-split ULMWH_1	4024	1.7	104.4 ± 6.0	192.4 ± 16.2	ud.	2.5 ± 2.3	0.0 ± 0.2
2-O-desulfated glycol-split ULMWH_2	3800	1.6	130.3 ± 15.5	200.5 ± 111.6	ud.	11.5 ± 8.0	0.0 ± 0.1
UH, commercial	13,000	1.9–2.0	9.4 ± 4.4	135.5 ± 12.8	197	0.0 ± 6.0	0.0 ± 0.0

[1] Reported in vitro toxicity in human umbilical vein endothelial cell (HUVEC) culture (% of cell death) and hemolysis data (% of lysed RBCs) have been calculated with 2 mg heparin/mL. The numbers after two compounds with the same name indicate that those samples are replicates, made in order to check the reproducibility of the procedure and tested separately to corroborate if there were any differences in antimalarial or anticoagulant activity. n.d.: not determined, ud.: undetected.

3.6. Conjugation of Heparin with PQ

To explore alternative strategies that could compensate for the loss in antimalarial activity of modified heparins, the antimalarial drug PQ was conjugated to the reducing end of MMWH (Figure 5). The combination of both molecules resulted in an antimalarial potency that significantly improved that of MMWH alone (Table 3). This result could be interpreted as a targeting effect of heparin, whose known affinity for pRBCs [17,18] might contribute to a more efficient delivery of PQ to target cells. This approach offers a potential solution to recover part of the antimalarial activity of heparin, which is lost with the chemical modifications that confer it a reduced anticoagulant action.

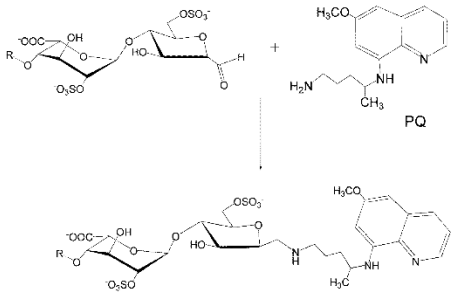

Figure 5. Reaction between the reducing end of heparin and primaquine (PQ), and the resulting molecular structure.

Table 3. In vitro *P. falciparum* growth inhibition activity assay of the heparin-PQ conjugate.

Sample	Mw (Da)	IC50 (μM) ± SD
MMWH-PQ	13,945	1.16 ± 0.40
MMWH_1	11,000	3.1 ± 2.0 [1]
PQ	259	5.20 ± 1.33

[1] The molar concentration of MMWH was calculated considering a molecular weight of 11,000 kDa.

3.7. Antimalarial Activity In Vivo of Heparin-derived Structures

For antimalarial in vivo assays were selected those heparin-derived structures that exhibited a good balance of in vitro safety (neither cytotoxicity nor hemolysis observed), low anticoagulant activity (≤23 IU/mL in aPTT assays) and not too low antimalarial activity (IC50 at least around 100 μg/mL). This led to the selection of the five heparins shadowed in grey in Table 2, whose in vivo toxicity was determined as an additional preliminary check. All five samples were not toxic when administered intravenously at 320 mg/kg (Table 4). Full characterization by NMR (Figures S1–S8) was performed to confirm presence of the expected modifications.

When the five selected heparin formulations were tested in vivo in the *P. yoelii yoelii* 17XL rodent malaria model by intravenous administration in a 4-day suppressive test, neither animal survival nor parasitemia load were significantly improved relative to the control PBS-treated group (Figure 6). Although a tendency was observed toward increased survival time of heparin-treated mice, this result could be due to small differences in parasite inoculation among different animals.

Table 4. Compilation of relevant data for heparin samples to be used in vivo.

Sample	IC50 (μg/mL ± SD)	aPTT (IU/mg)	In Vitro Toxicity [1] (% ± SD)	Hemolysis [1] (% ± SD)	In Vitro Toxicity [2]
2-*O*-desulfated MMWH_2	91.95 ± 8.97	23	0.00 ± 2.34	1.99 ± 2.05	>320 mg/kg
ULMWH	49.31 ± 5.97	6	6.83 ± 9.18	0.21 ± 0.13	>320 mg/kg
2-*O*-desulfated glycol-split MMWH_1	79.60 ± 5.38	6	7.26 ± 4.55	0.36 ± 0.09	>750 mg/kg
2-*O*-desulfated glycol-split MMWH_2	84.20 ± 13.45	5	3.61 ± 5.42	0.00 ± 0.03	>750 mg/kg
2-*O*-desulfated glycol-split ULMWH_1	104.40 ± 6.03	0	2.49 ± 2.35	0.00 ± 0.22	>750 mg/kg

[1] Reported in vitro toxicity in HUVEC culture (% of cell death) and hemolysis data (% of lysed red blood cells) have been calculated with 2 mg heparin/mL. [2] In vivo toxicity refers to the highest concentration tested that did not induce for 15 days after administration any acute or chronic effect in mice.

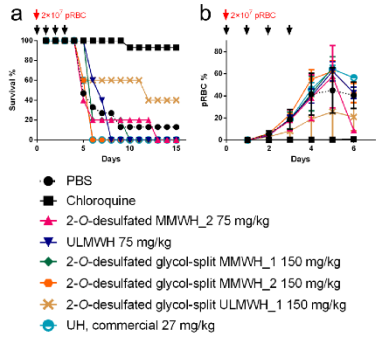

Figure 6. Antimalarial activity in vivo of heparin-derived structures. Mice survival curves (**a**) and parasitemia percentage (**b**) following treatment with the tested compounds at the concentrations indicated. The black arrows indicate the times of test sample administration. $n = 5$ in each group, except PBS- ($n = 15$) and chloroquine-treated mice ($n = 14$).

3.8. Determination of the Circulation Time of Intravenously Administered Heparin

The poor efficiency of the selected formulations for the treatment of in vivo infections could be due, among other reasons, to a rapid elimination from the blood circulation. Because the antimalarial activity of heparin resides in its inhibition of the red blood cell invasion by the merozoite form of the parasite, a phase that lasts only a few minutes within the *P. falciparum* 48-h intraerythrocytic life cycle, a rapid elimination from the blood circulation would significantly reduce the chances of being present when invasion takes place. Commercial UH and 2-*O*-desulfated glycol-split MMWH_2 had similar plasma half-lives (25.7 and 29.1 min, respectively; Figure 7) and became undetectable about 3 h after intravenous administration to mice, suggesting a fast clearance possibly due to interactions with plasma components. In addition, the in vitro activity of these two heparins became reduced when tested in growth medium supplemented with 10% human plasma (Figure 8), indicating that such plasma interactions might compete with the binding to merozoites of heparin, thus decreasing its antimalarial activity.

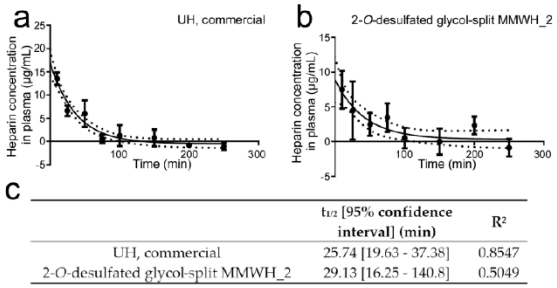

c

	$t_{1/2}$ [95% confidence interval] (min)	R^2
UH, commercial	25.74 [19.63 - 37.38]	0.8547
2-*O*-desulfated glycol-split MMWH_2	29.13 [16.25 - 140.8]	0.5049

Figure 7. Determination of blood circulation time for unfractionated heparin (UH) and 2-*O*-desulfated glycol-split MMWH_2. (**a**,**b**) Concentration of both heparins in mouse plasma along time following intravenous administration to three male and three female mice for each time point. (**c**) Blood half-life values ($t_{1/2}$) for both samples and R^2 of the plotted curves.

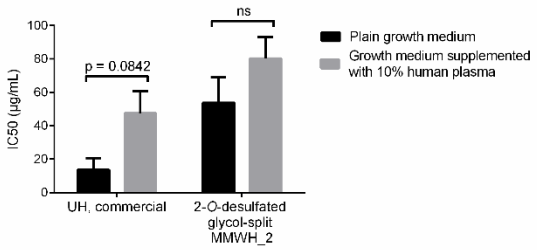

Figure 8. IC50 of the two samples from Figure 7 in *P. falciparum* in vitro cultures grown in either plain growth medium or in growth medium supplemented with 10% human plasma. ns: not significant.

To prevent the absorption of serum proteins, the surface of liposomes can be decorated by hydrophilic and bio-compatible polyethylene glycol (PEG) polymers, which can significantly extend blood circulation times [40]. We explored whether the covalent link of heparin to the surface of PEGylated liposomes increased its blood half-life and affected its antimalarial activity in vitro. The circulation half-life of UH-coated liposomes was 22.4 min (18.4–28.6 min with 95% confidence; Figure 9a), but they could be detected up to 4 h after administration (data not shown). The initial UH concentration 10 min after administration was ca. 40 µg/mL for UH-coated liposomes (as compared to ca. 17 µg/mL for free UH; Figure 7a), whereas the antimalarial activity in vitro of UH-covered liposomes had roughly the same IC50 as UH alone (Figure 9b). Although the liposomal formulation did not significantly extend the half-life of heparin in circulation, it did increase the time that the

molecule was found in plasma at a higher concentration than its in vitro IC50 (21 min for free UH and 49 min for UH-coated liposomes).

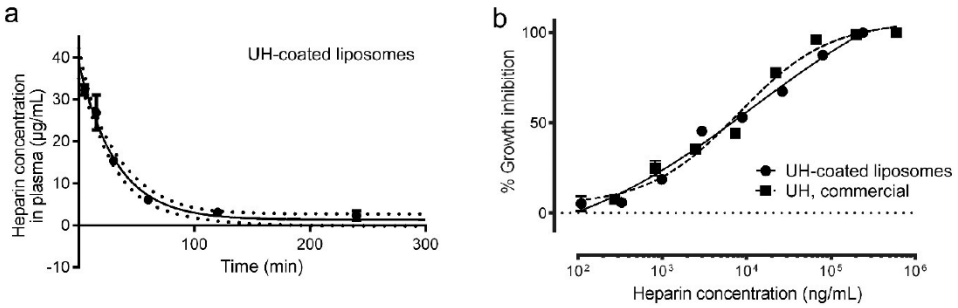

Figure 9. Characterization of circulation time and antimalarial activity of UH-coated liposomes. (**a**) Concentration of liposome-bound UH in mouse plasma along time following intravenous administration to 2 female mice for each time point. (**b**) *P. falciparum* growth inhibition activity assay of UH-coated liposomes and free UH.

4. Discussion

Previous works with sulfated GAGs, heparin modifications, and other sulfated compounds that could act as antimalarials [15,20,41] had placed this type of molecules as good candidates for the development of new drugs. Our data indicate that chemical modification of heparin might not be the only path to a GAG that could offer good perspectives of entering the clinical pipeline. Chondroitin sulfate has in vitro antimalarial activity comparable to those of the chemically desulfated structures prepared in this work, to which has to be added the benefit of a low anticoagulant activity [41]. Other sources of sulfated polysaccharides exhibiting antimalarial activity and inhibition of RBC invasion by *Plasmodium* at low anticoagulant concentrations are certain marine organisms such as algae, sea cucumbers and sponges [41]. Dermatan sulfate has also been explored to control *Plasmodium berghei* infections in mice, but although it could reduce parasitemia in the treated groups, there was no significant effect on animal survival [14]. These and other natural polysaccharides could be modified to improve their antimalarial capacity in a similar way as it was done with sevuparin, a heparin derivative that has reached phase I/II of clinical trials for malaria treatment as adjuvant therapy [42].

Besides their potential applications as antimalarial therapy through their blocking activity of RBC invasion by *Plasmodium* merozoites, the heparin modifications explored here could be of use for other pathological features of the disease. In severe malaria, pRBCs can adhere to naïve RBCs to form cell clumps termed rosettes, which can reduce the blood circulation in capillaries leading to life-threatening conditions [13]. Because heparin and other GAGs can disrupt rosettes, their administration as adjuvant therapy could reduce their formation. As previous research in this field has proven, the molecular structure of the GAG chains that interact with rosette forming pRBCs is variable and highly dependent on the particular *Plasmodium* strain [13]. In this regard, the implementation of a chemical modification toolbox including reactions like those presented in this work will be highly instrumental in the adaptation of these polysaccharides to their target cell types.

Of the different heparin modifications assayed in this work, a combination of reduction in size (MMWH), 2-*O*-desulfation of IdoA, and glycol-split has offered the best balance toward a structure having low anticoagulant activity but maintaining a still acceptable in vitro antimalarial action in *P. falciparum* cultures while showing low hemolysis and in vitro and in vivo toxicities. However, one of the main obstacles that we have identified on the way to a potential clinical application as a treatment for malaria is the fast clearance of heparin from the circulation. The blood half-life of exogenously administered heparin is dependent on the dose, and it can be cleared slowly through the renal system

or through a fast but saturable mechanism that involves binding to cell receptors and macrophages [37]. Depolymerization of the heparin chain has been described to increase circulation time because it reduces some of the undesired interactions with cell surfaces [43]. Conjugation to nanocarriers also has the potential to impart longer blood residence times [44], and there is evidence of loss of the anticoagulant activity of heparin when covalently immobilized on a substrate [45]. Several types of nanostructures have been used as such substrates, e.g., liposomes [18], polymersomes [46], and giant unilamellar vesicles [47]. Heparin has been shown to work as pRBC targeting element of liposomes loaded with antimalarial drugs, which added to its invasion blocking activity in a peculiar type of combination therapy [18]. Heparin itself has been directly conjugated to the highly hydrophobic antimalarial drug artesunate to form micellar nanostructures with improved pharmacokinetic profile [48].

Heparin has an affordable production cost and its purification from animal tissues does not need complicated protocols or costly equipment. The endogenous nature of heparin makes it highly biocompatible and biosafe, especially in the case of low molecular weight heparin, whose chemical preparation is simple and inexpensive. Among the various materials available to form nanocarriers, natural polymers such as glycosaminoglycans are an ideal candidate due to their often endogenous, non-immunogenic nature, ease of availability in relatively large amounts at a comparatively low cost, and presence in their structures of adequate chemical groups for the use of straightforward crosslinking reactions into nanoparticulate structures. Chitosan, a positively charged glycosaminoglycan, is being extensively employed as drug carrier in many clinical applications already and therefore its adaptation to the transport of antimalarial drugs would be immediate. Heparin, a glycosaminoglycan whose antimalarial activity is well known, could be easily incorporated into chitosan nanocarriers, since its high negative charge will provide a strong interaction with chitosan, which if required can be strengthened through a simple chemical reaction by covalent bonds between the abundant amino and carboxyl groups present in chitosan and heparin, respectively. Heparin has been described to have binding affinity for several *Plasmodium* stages, in both human and mosquito hosts, thus being an interesting targeting element of therapeutic nanovessels. In addition to the antiparasitic and targeting activities of heparin, such hybrid glycosaminoglycan nanovectors can be loaded with drugs, sky-rocketing their potential activity against the pathogen. As an added bonus of using chitosan nanoparticles is that they are inexpensive and easy to produce, and are apt to be used in oral therapy [49,50].

Supplementary Materials: The following are available online at http://www.mdpi.com/1999-4923/12/9/825/s1, Figure S1: Partial ^{1}H NMR spectra of heparin and its modifications; Figure S2: Partial ^{13}C NMR spectra of heparin and its modifications; Figure S3: Partial ^{13}C NMR, HSQC, and TOCSY spectra of 2-*O*-desulfated MMWH; Figure S4: Partial HSQC and TOCSY spectra of 2-*O*-desulfated glycol-split MMWH_1; Figure S5: Partial HSQC and TOCSY spectra of 2-*O*-desulfated glycol-split MMWH_2; Figure S6: Partial HSQC and TOCSY spectra of 2-*O*-desulfated glycol-split ULMWH_1; Figure S7: Partial HSQC spectra of ULMWH; Figure S8: ^{1}H DOSY spectra of UH, MMWH, MMWH_1/2, ULMWH, and ULMWH_1.

Author Contributions: Conceptualization, X.F.-B.; methodology, E.L., C.R.A.-V., P.R., T.S. and X.F.-B.; investigation, E.L., C.R.A.-V. and P.R.; formal analysis, E.L.; visualization, E.L. and P.R.; writing—original draft preparation, X.F.-B. and E.L., writing—review and editing, X.F.-B. and E.L.; supervision, X.F.-B.; funding acquisition, X.F.-B, P.R. and T.S. All authors have read and agreed to the published version of the manuscript.

Funding: X.F.-B. received funding support from (i) the Spanish Ministry of Science, Innovation and Universities (http://www.ciencia.gob.es/), grant numbers BIO2014-52872-R and RTI2018-094579-B-I00 (which included FEDER funds), and (ii) BIOIBERICA. P.R. and T.S. received funding support from (i) the Spanish Ministry of Science, Innovation and Universities, grant number PGC2018-097583-B-I00 (which included FEDER funds), and (ii) Gobierno de Aragón-FEDER E47-20R. The authors would like to acknowledge the use of the *Unidad de Apoyo a la Investigación del CEQMA*, CSIC-Universidad de Zaragoza.

Acknowledgments: The authors would like to thank Miriam Ramírez for technical support, Lucía Román for assistance in liposomal preparation, and Fernando J. Pérez Asensio and the technical staff from the Animal Facility Service at the Barcelona Science Park for administrative and technical help. ISGlobal and IBEC are members of the CERCA Programme, *Generalitat de Catalunya*. We acknowledge support from the Spanish Ministry of Science, Innovation and Universities through the *"Centro de Excelencia Severo Ochoa 2019–2023"* Program (CEX2018-000806-S). This research is part of ISGlobal's Program on the Molecular Mechanisms of Malaria, which is partially supported by the *Fundación Ramón Areces*.

Conflicts of Interest: X.F.-B. has received funding from BIOIBERICA, and C.R.A.-V. is employed by BIOIBERICA. The funders had no role in the design of the study; in the collection, analyses, or interpretation of data; in the writing of the manuscript, or in the decision to publish the results.

References

1. World Health Organization. *World Malaria Report 2019*; World Health Organization: Geneva, Switzerland, 2019.
2. Miller, L.H.; Baruch, D.I.; Marsh, K.; Doumbo, O.K. The pathogenic basis of malaria. *Nature* **2002**, *415*, 673–679. [CrossRef]
3. Carlson, J.; Wahlgren, M. *Plasmodium falciparum* erythrocyte rosetting is mediated by promiscuous lectin-like interactions. *J. Exp. Med.* **1992**, *176*, 1311–1317. [CrossRef] [PubMed]
4. Griffith, K.S.; Lewis, L.S.; Mali, S.; Parise, M.E. Treatment of malaria in the United States: A systematic review. *JAMA* **2007**, *297*, 2264–2277. [CrossRef] [PubMed]
5. Beeson, J.G.; Andrews, K.T.; Boyle, M.; Duffy, M.F.; Choong, E.K.; Byrne, T.J.; Chesson, J.M.; Lawson, A.M.; Chai, W. Structural basis for binding of *Plasmodium falciparum* erythrocyte membrane protein 1 to chondroitin sulfate and placental tissue and the influence of protein polymorphisms on binding specificity. *J. Biol. Chem.* **2007**, *282*, 22426–22436. [CrossRef]
6. Juillerat, A.; Igonet, S.; Vigan-Womas, I.; Guillotte, M.; Gangnard, S.; Faure, G.; Baron, B.; Raynal, B.; Mercereau-Puijalon, O.; Bentley, G.A. Biochemical and biophysical characterisation of DBL1a$_1$-varO, the rosetting domain of PfEMP1 from the VarO line of *Plasmodium falciparum*. *Mol. Biochem. Parasitol.* **2010**, *170*, 84–92. [CrossRef] [PubMed]
7. Pradel, G.; Garapaty, S.; Frevert, U. Proteoglycans mediate malaria sporozoite targeting to the liver. *Mol. Microbiol.* **2002**, *45*, 637–651. [CrossRef]
8. Coppi, A.; Tewari, R.; Bishop, J.R.; Bennett, B.L.; Lawrence, R.; Esko, J.D.; Billker, O.; Sinnis, P. Heparan sulfate proteoglycans provide a signal to *Plasmodium* sporozoites to stop migrating and productively invade host cells. *Cell Host Microbe* **2007**, *2*, 316–327. [CrossRef] [PubMed]
9. Rogerson, S.J.; Reeder, J.C.; Al-Yaman, F.; Brown, G.V. Sulfated glycoconjugates as disrupters of *Plasmodium falciparum* erythrocyte rosettes. *Am. J. Trop. Med. Hyg.* **1994**, *51*, 198–203. [CrossRef]
10. Angeletti, D.; Sandalova, T.; Wahlgren, M.; Achour, A. Binding of subdomains 1/2 of PfEMP1-DBL1a to heparan sulfate or heparin mediates *Plasmodium falciparum* rosetting. *PLoS ONE* **2015**, *10*, e0118898. [CrossRef]
11. Vogt, A.M.; Pettersson, F.; Moll, K.; Jonsson, C.; Normark, J.; Ribacke, U.; Egwang, T.G.; Ekre, H.P.; Spillmann, D.; Chen, Q.; et al. Release of sequestered malaria parasites upon injection of a glycosaminoglycan. *PLoS Pathog.* **2006**, *2*, e100. [CrossRef]
12. Sheehy, T.W.; Reba, R.C. Complications of falciparum malaria and their treatment. *Ann. Intern. Med.* **1967**, *66*, 807–809. [CrossRef]
13. Leitgeb, A.M.; Blomqvist, K.; Cho-Ngwa, F.; Samje, M.; Nde, P.; Titanji, V.; Wahlgren, M. Low anticoagulant heparin disrupts *Plasmodium falciparum* rosettes in fresh clinical isolates. *Am. J. Trop. Med. Hyg.* **2011**, *84*, 390–396. [CrossRef]
14. Xiao, L.; Yang, C.; Patterson, P.S.; Udhayakumar, V.; Lal, A.A. Sulfated polyanions inhibit invasion of erythrocytes by plasmodial merozoites and cytoadherence of endothelial cells to parasitized erythrocytes. *Infect. Immun.* **1996**, *64*, 1373–1378. [CrossRef] [PubMed]
15. Boyle, M.J.; Richards, J.S.; Gilson, P.R.; Chai, W.; Beeson, J.G. Interactions with heparin-like molecules during erythrocyte invasion by *Plasmodium falciparum* merozoites. *Blood* **2010**, *115*, 4559–4568. [CrossRef] [PubMed]
16. Beeson, J.G.; Drew, D.R.; Boyle, M.J.; Feng, G.; Fowkes, F.J.I.; Richards, J.S. Merozoite surface proteins in red blood cell invasion, immunity and vaccines against malaria. *FEMS Microbiol. Rev.* **2016**, *40*, 343–372. [CrossRef] [PubMed]
17. Valle-Delgado, J.J.; Urbán, P.; Fernàndez-Busquets, X. Demonstration of specific binding of heparin to *Plasmodium falciparum*-infected vs. non-infected red blood cells by single-molecule force spectroscopy. *Nanoscale* **2013**, *5*, 3673–3680. [CrossRef] [PubMed]
18. Marques, J.; Moles, E.; Urbán, P.; Prohens, R.; Busquets, M.A.; Sevrin, C.; Grandfils, C.; Fernàndez-Busquets, X. Application of heparin as a dual agent with antimalarial and liposome targeting activities towards *Plasmodium*-infected red blood cells. *Nanomed. NBM* **2014**, *10*, 1719–1728. [CrossRef]

19. Glushakova, S.; Busse, B.L.; Garten, M.; Beck, J.R.; Fairhurst, R.M.; Goldberg, D.E.; Zimmerberg, J. Exploitation of a newly-identified entry pathway into the malaria parasite-infected erythrocyte to inhibit parasite egress. *Sci. Rep.* **2017**, *7*, 12250. [CrossRef]
20. Boyle, M.J.; Skidmore, M.; Dickerman, B.; Cooper, L.; Devlin, A.; Yates, E.; Horrocks, P.; Freeman, C.; Chai, W.; Beeson, J.G. Identification of heparin modifications and polysaccharide inhibitors of *Plasmodium falciparum* merozoite invasion that have potential for novel drug development. *Antimicrob. Agents Chemother.* **2017**, *61*, e00709–e00717. [CrossRef] [PubMed]
21. Pisano, C.; Aulicino, C.; Vesci, L.; Casu, B.; Naggi, A.; Torri, G.; Ribatti, D.; Belleri, M.; Rusnati, M.; Presta, M. Undersulfated, low-molecular-weight glycol-split heparin as an antiangiogenic VEGF antagonist. *Glycobiology* **2005**, *15*, 1C–6C. [CrossRef]
22. Naggi, A.; Casu, B.; Perez, M.; Torri, G.; Cassinelli, G.; Penco, S.; Pisano, C.; Giannini, G.; Ishai-Michaeli, R.; Vlodavsky, I. Modulation of the heparanase-inhibiting activity of heparin through selective desulfation, graded *N*-acetylation, and glycol splitting. *J. Biol. Chem.* **2005**, *280*, 12103–12113. [CrossRef] [PubMed]
23. Shively, J.E.; Conrad, H.E. Formation of anhydrosugars in the chemical depolymerization of heparin. *Biochemistry* **1976**, *15*, 3932–3942. [CrossRef] [PubMed]
24. Cifonelli, J.A. Reaction of heparitin sulfate with nitrous acid. *Carbohydr. Res.* **1968**, *8*, 233–242. [CrossRef]
25. Matsuo, M.; Takano, R.; Kamei-Hayashi, K.; Hara, S. A novel regioselective desulfation of polysaccharide sulfates: Specific 6-*O*-desulfation with *N*,*O*-bis(trimethylsilyl)acetamide. *Carbohydr. Res.* **1993**, *241*, 209–215. [CrossRef]
26. Maruyama, T.; Toida, T.; Imanari, T.; Yu, G.; Linhardt, R.J. Conformational changes and anticoagulant activity of chondroitin sulfate following its *O*-sulfonation. *Carbohydr. Res.* **1998**, *306*, 35–43. [CrossRef]
27. Casu, B.; Guerrini, M.; Naggi, A.; Perez, M.; Torri, G.; Ribatti, D.; Carminati, P.; Giannini, G.; Penco, S.; Pisano, C.; et al. Short heparin sequences spaced by glycol-split uronate residues are antagonists of fibroblast growth factor 2 and angiogenesis inhibitors. *Biochemistry* **2002**, *41*, 10519–10528. [CrossRef]
28. Bertini, S.; Bisio, A.; Torri, G.; Bensi, D.; Terbojevich, M. Molecular weight determination of heparin and dermatan sulfate by size exclusion chromatography with a triple detector array. *Biomacromolecules* **2005**, *6*, 168–173. [CrossRef]
29. Casu, B.; Gennaro, U. A conductimetric method for the determination of sulphate and carboxyl groups in heparin and other mucopolysaccharides. *Carbohydr. Res.* **1975**, *39*, 168–176. [CrossRef]
30. Gerotziafas, G.T.; Petropoulou, A.D.; Verdy, E.; Samama, M.M.; Elalamy, I. Effect of the anti-factor Xa and anti-factor IIa activities of low-molecular-weight heparins upon the phases of thrombin generation. *J. Thromb. Haemost.* **2007**, *5*, 955–962. [CrossRef]
31. Monakhova, Y.B.; Diehl, B.W.K.; Do, T.X.; Schulze, M.; Witzleben, S. Novel method for the determination of average molecular weight of natural polymers based on 2D DOSY NMR and chemometrics: Example of heparin. *J. Pharm. Biomed. Anal.* **2018**, *149*, 128–132. [CrossRef]
32. Lambros, C.; Vanderberg, J.P. Synchronization of *Plasmodium falciparum* erythrocytic stages in culture. *J. Parasitol.* **1979**, *65*, 418–420. [CrossRef]
33. Dluzewski, A.R.; Ling, I.T.; Rangachari, K.; Bates, P.A.; Wilson, R.J. A simple method for isolating viable mature parasites of *Plasmodium falciparum* from cultures. *Trans. R. Soc. Trop. Med. Hyg.* **1984**, *78*, 622–624. [CrossRef]
34. Fidock, D.A.; Rosenthal, P.J.; Croft, S.L.; Brun, R.; Nwaka, S. Antimalarial drug discovery: Efficacy models for compound screening. *Nat. Rev. Drug Discov.* **2004**, *3*, 509–520. [CrossRef] [PubMed]
35. Frazier, S.B.; Roodhouse, K.A.; Hourcade, D.E.; Zhang, L. The quantification of glycosaminoglycans: A comparison of HPLC, carbazole, and Alcian Blue methods. *Open Glycosci.* **2008**, *1*, 31–39. [CrossRef] [PubMed]
36. Warttinger, U.; Giese, C.; Harenberg, J.; Holmer, E.; Krämer, R. A fluorescent probe assay (Heparin Red) for direct detection of heparins in human plasma. *Anal. Bioanal. Chem.* **2016**, *408*, 8241–8251. [CrossRef] [PubMed]
37. Hirsh, J.; Fuster, V. Guide to anticoagulant therapy. Part 1: Heparin. *Circulation* **1994**, *89*, 1449–1468. [CrossRef] [PubMed]

38. Esko, J.D.; Prestegard, H.; Linhardt, R.J. Proteins that bind sulfated glycosaminoglycans. In *Essentials of Glycobiology*, 3rd ed.; Varki, A., Cummings, R.D., Esko, J.D., Stanley, P., Hart, G.W., Aebi, M., Darvill, A.G., Kinoshita, T., Packer, N.H., Prestegard, J.H., et al., Eds.; Cold Spring Harbor Laboratory Press: Cold Spring Harbor, NY, USA, 2017; pp. 493–502.
39. Naggi, A. Glycol-splitting as a device for modulating inhibition of growth factors and heparanase by heparin and heparin derivatives. In *Chemistry and Biology of Heparin and Heparan Sulfate*; Garg, H.G., Linhardt, R.J., Hales, C.A., Eds.; Elsevier Science: Amsterdam, The Netherlands, 2005; pp. 461–481.
40. Allen, T.M.; Cullis, P.R. Liposomal drug delivery systems: From concept to clinical applications. *Adv. Drug Deliv. Rev.* **2013**, *65*, 36–48. [CrossRef]
41. Marques, J.; Vilanova, E.; Mourão, P.A.S.; Fernàndez-Busquets, X. Marine organism sulfated polysaccharides exhibiting significant antimalarial activity and inhibition of red blood cell invasion by *Plasmodium*. *Sci. Rep.* **2016**, *6*, 24368. [CrossRef]
42. Leitgeb, A.M.; Charunwatthana, P.; Rueangveerayut, R.; Uthaisin, C.; Silamut, K.; Chotivanich, K.; Sila, P.; Moll, K.; Lee, S.J.; Lindgren, M.; et al. Inhibition of merozoite invasion and transient de-sequestration by sevuparin in humans with *Plasmodium falciparum* malaria. *PLoS ONE* **2017**, *12*, e0188754. [CrossRef]
43. Hirsh, J.; Warkentin, T.E.; Shaughnessy, S.G.; Anand, S.S.; Halperin, J.L.; Raschke, R.; Granger, C.; Ohman, E.M.; Dalen, J.E. Heparin and low-molecular-weight heparin: Mechanisms of action, pharmacokinetics, dosing, monitoring, efficacy, and safety. *Chest* **2001**, *119*, 64S–94S. [CrossRef]
44. Mosqueira, V.C.F.; Loiseau, P.M.; Bories, C.; Legrand, P.; Devissaguet, J.P.; Barratt, G. Efficacy and pharmacokinetics of intravenous nanocapsule formulations of halofantrine in *Plasmodium berghei*-infected mice. *Antimicrob. Agents Chemother.* **2004**, *48*, 1222–1228. [CrossRef] [PubMed]
45. Miura, Y.; Aoyagi, S.; Kusada, Y.; Miyamoto, K. The characteristics of anticoagulation by covalently immobilized heparin. *J. Biomed. Mater. Res.* **1980**, *14*, 619–630. [CrossRef] [PubMed]
46. Najer, A.; Wu, D.; Bieri, A.; Brand, F.; Palivan, C.G.; Beck, H.P.; Meier, W. Nanomimics of host cell membranes block invasion and expose invasive malaria parasites. *ACS Nano* **2014**, *8*, 12560–12571. [CrossRef] [PubMed]
47. Najer, A.; Thamboo, S.; Palivan, C.G.; Beck, H.P.; Meier, W. Giant host red blood cell membrane mimicking polymersomes bind parasite proteins and malaria parasites. *Chimia* **2016**, *70*, 288–291. [CrossRef] [PubMed]
48. Ismail, M.; Du, Y.; Ling, L.; Li, X. Artesunate-heparin conjugate based nanocapsules with improved pharmacokinetics to combat malaria. *Int. J. Pharm.* **2019**, *562*, 162–171. [CrossRef]
49. Schulz, J.D.; Gauthier, M.A.; Leroux, J.C. Improving oral drug bioavailability with polycations? *Eur. J. Pharm. Biopharm.* **2015**, *97*, 427–437. [CrossRef]
50. Shukla, S.K.; Mishra, A.K.; Arotiba, O.A.; Mamba, B.B. Chitosan-based nanomaterials: A state-of-the-art review. *Int. J. Biol. Macromol.* **2013**, *59*, 46–58. [CrossRef]

pharmaceutics

Supplementary Materials: Repurposing Heparin as Antimalarial: Evaluation of Multiple Modifications Toward In Vivo Application

Elena Lantero , Carlos Raúl Aláez-Versón , Pilar Romero , Teresa Sierra, and Xavier Fernàndez-Busquets

NMR characterization

When heparin is selectively *O*-desulfated at the C(2), the conversion of the IdoA2S residue into GalA or IdoA may occur [1]. The signals for H(1) and C(1) at 5.20 ppm and 102.2 ppm, respectively, characteristic of the IdoA2S residue disappear (black arrows in Figure S1 and S2). The formation of GalA is clearly observed in the HSQC spectrum of 2-*O*-desulfated MMWH, as indicated in Figure S3(b). For 2-*O*-desulfated glycol-split MMWH_1 (Figure S4), 2-*O*-desulfated glycol-split MMWH_2 (Figure S5) and 2-*O*-desulfated glycol-split ULMWH_1 (Figure S6), which have undergone subsequent glycol-splitting (see below), the IdoA2S residue is not observed.

Signals corresponding to the glycol-split in the GalA residue can be recognized in 2-*O*-desulfated glycol-split MMWH_1, 2-*O*-desulfated glycol-split MMWH_2 and 2-*O*-desulfated glycol-split ULMWH_1. The set of signals (^{1}H at 3.91 and ^{13}C at 62.9 ppm) which correlates with two protons in the TOCSY spectra at 4.25 and 4.64 ppm (red circles in Figures S4 and S5), is the signal pattern expected for a glycol-split uronic acid residue, with C(1) and C(4) bearing CH_2OH substituents, as previously reported in the literature [2].

For ULMWH, prepared by depolymerization by nitrous acid, the signal patterns observed in its ^{13}C and HSQC spectra (Figure S2 and S7) are consistent with the structure of dalteparin [3,4].

Finally, the application of DOSY NMR experiments has recently been proposed as a quick method for the determination of average molecular weight of heparins [5]. Here we have used this technique as a qualitative method to check the molecular weight of the samples (Figure S8). It is observed that the increase of the diffusion coefficient (D) corresponds to a decrease of molecular weight as expected according to the modifications carried out on UH.

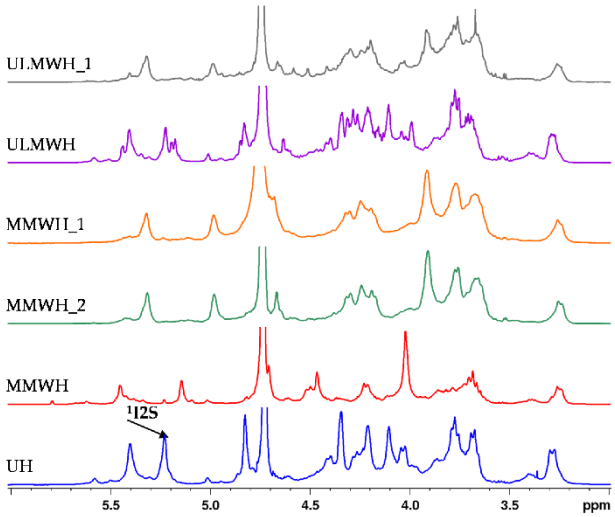

Figure S1. Partial ^{1}H NMR spectra of heparin and its modifications.

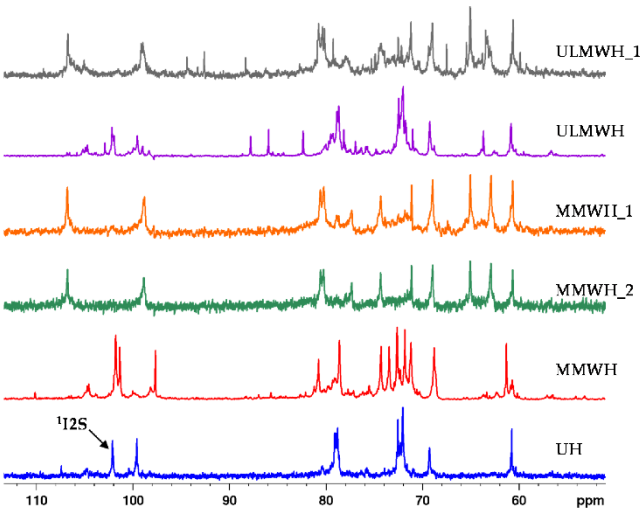

Figure S2. Partial ^{13}C NMR spectra of heparin and its modifications.

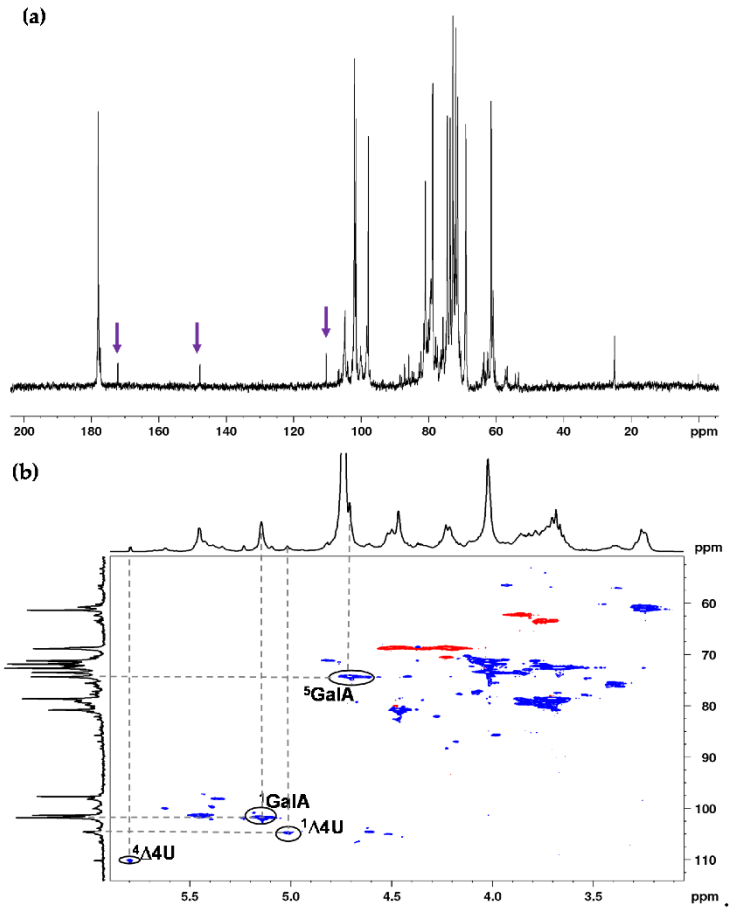

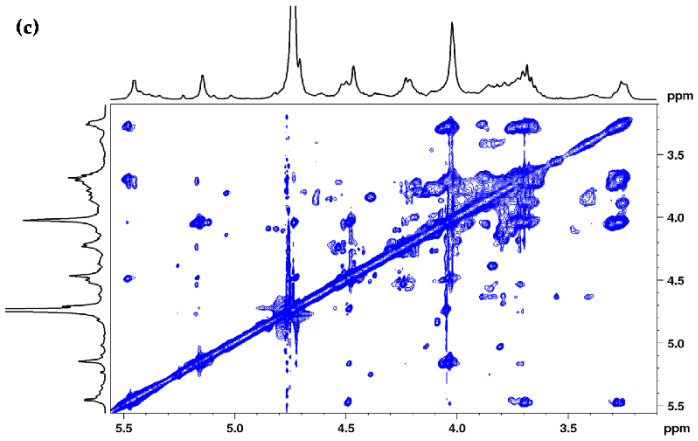

Figure S3. (**a**) Partial ^{13}C NMR spectrum between 200 and 10 ppm of 2-*O*-desulfated MMWH. There is some epoxide signal at 53-54 ppm and signals that correspond to β-elimination of uronic acid 2,5-insaturated ($^{4}\Delta U$) at 172, 147.7 and 110 ppm (purple arrows) (**b**) partial HSQC and (**c**) partial TOCSY spectra of 2-*O*-desulfated MMWH.

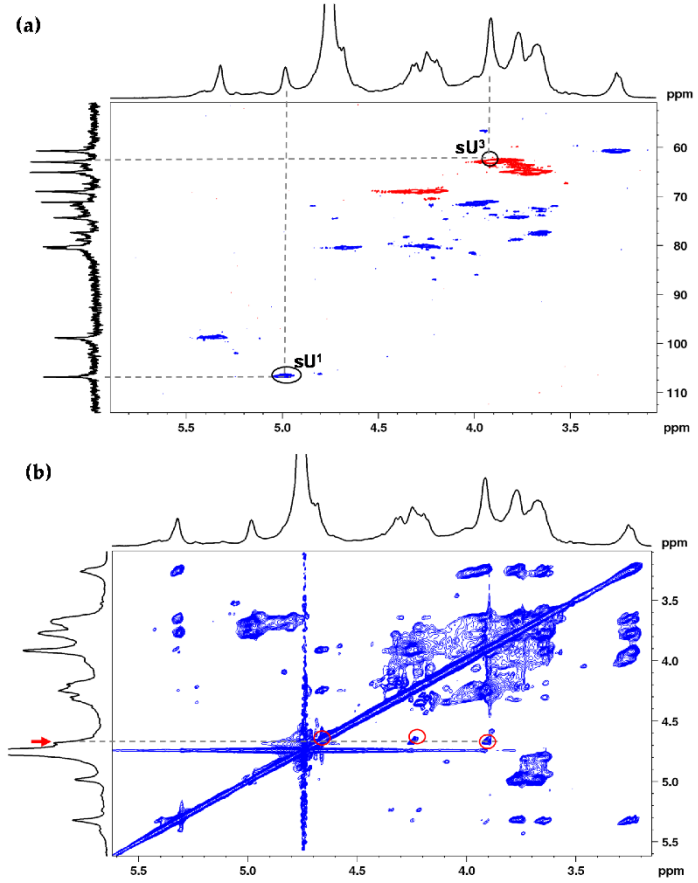

Figure S4. (**a**) Partial HSQC and (**b**) partial TOCSY spectra of 2-*O*-desulfated glycol-split MMWH_1.

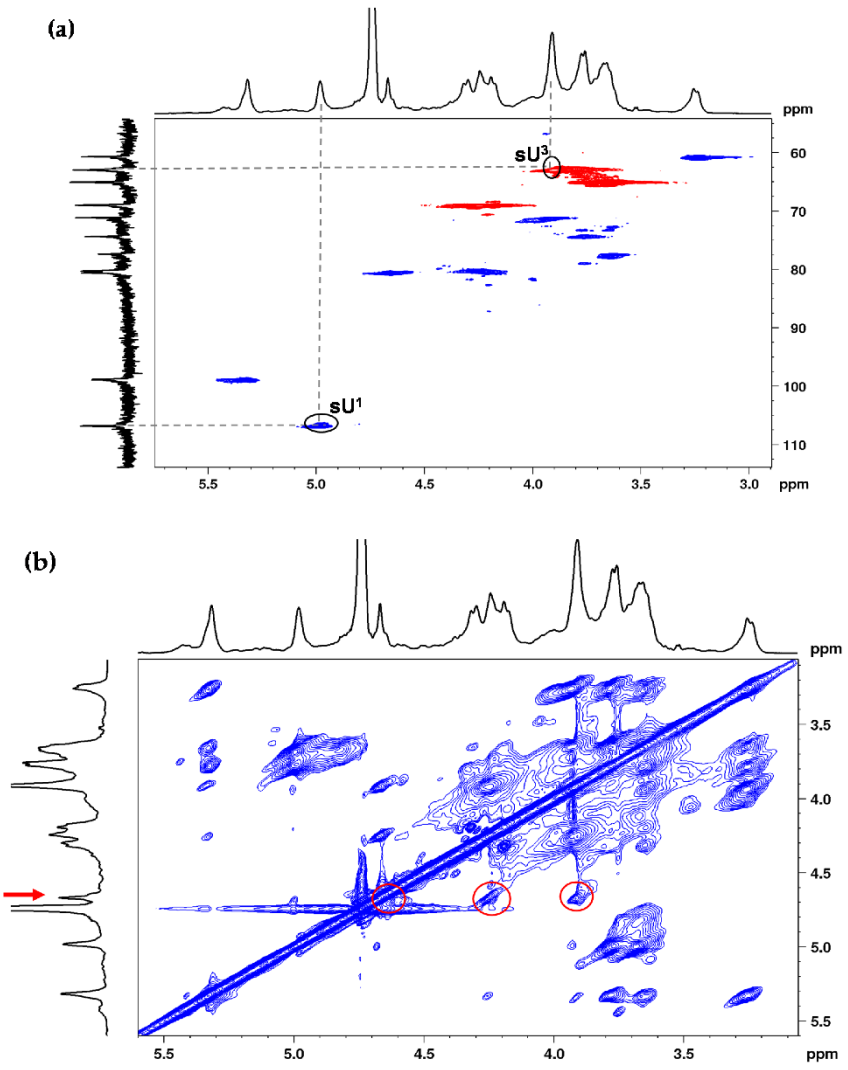

Figure S5. (**a**) Partial HSQC and (**b**) partial TOCSY spectra of 2-*O*-desulfated glycol-split MMWH_2.

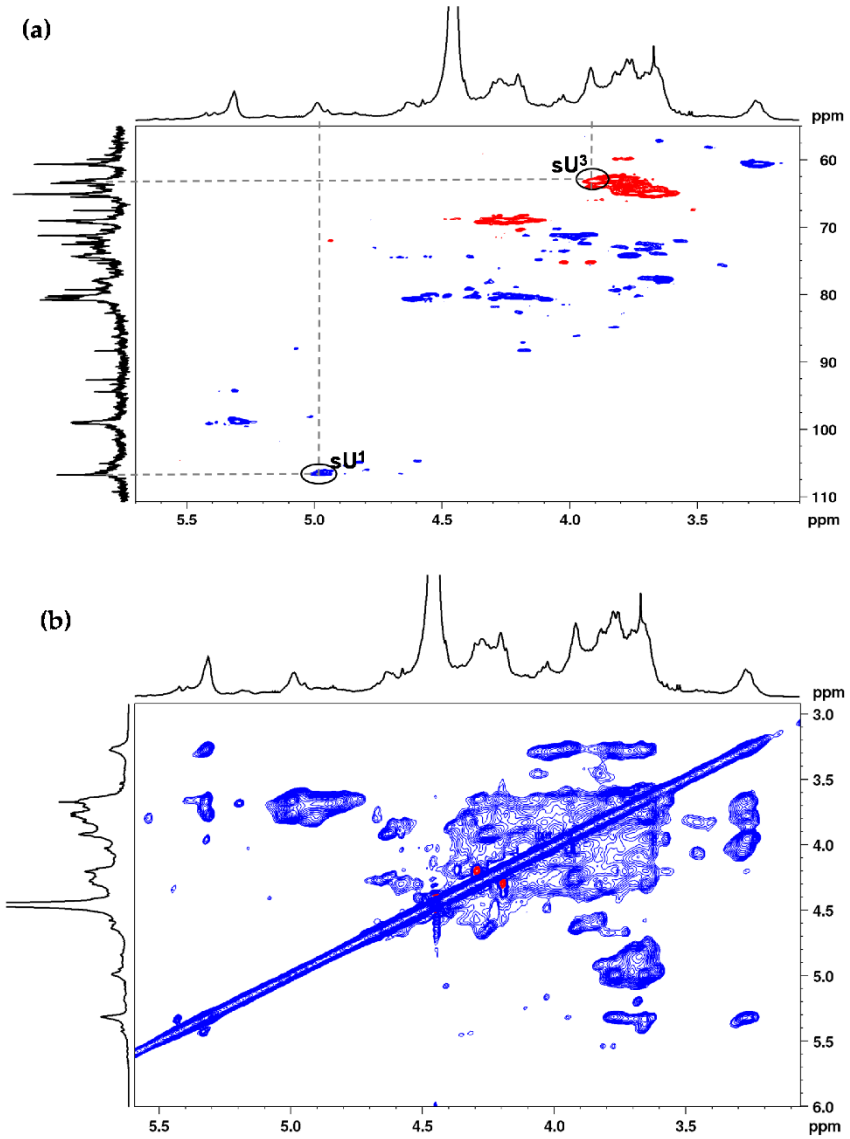

Figure S6. (**a**) Partial HSQC and (**b**) partial TOCSY spectra of 2-*O*-desulfated glycol-split ULMWH_1.

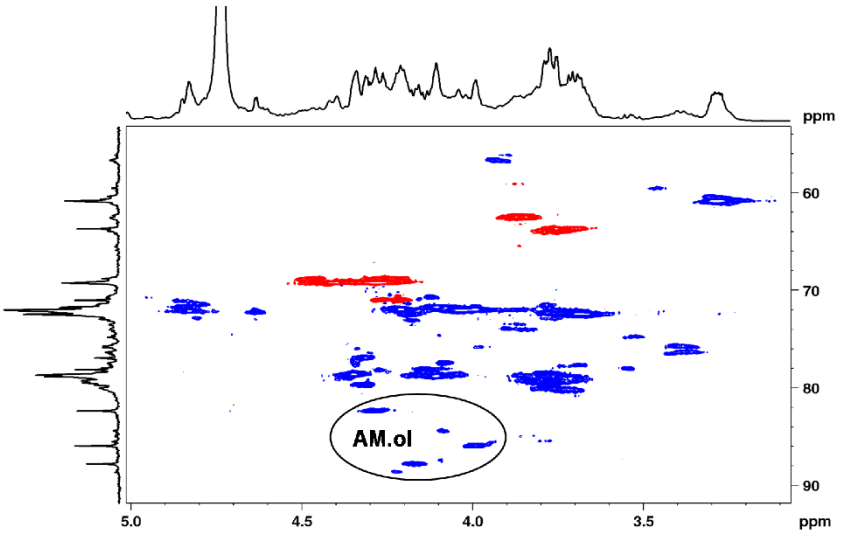

Figure S7. Partial HSQC spectra of ULMWH. Spectra in Figures S1 and S2 indicate that this molecule does not have 2-*O*-desulfation, and it relates with low molecular weight derivatives of heparin as dalteparin: 82.3, 85.9 y 87.8 ppm in ^{13}C correspond to C4, C2 and C5 of the 2,5-anhydro-D-mannitol residue (AM.ol), as observed in previous publications [3,4].

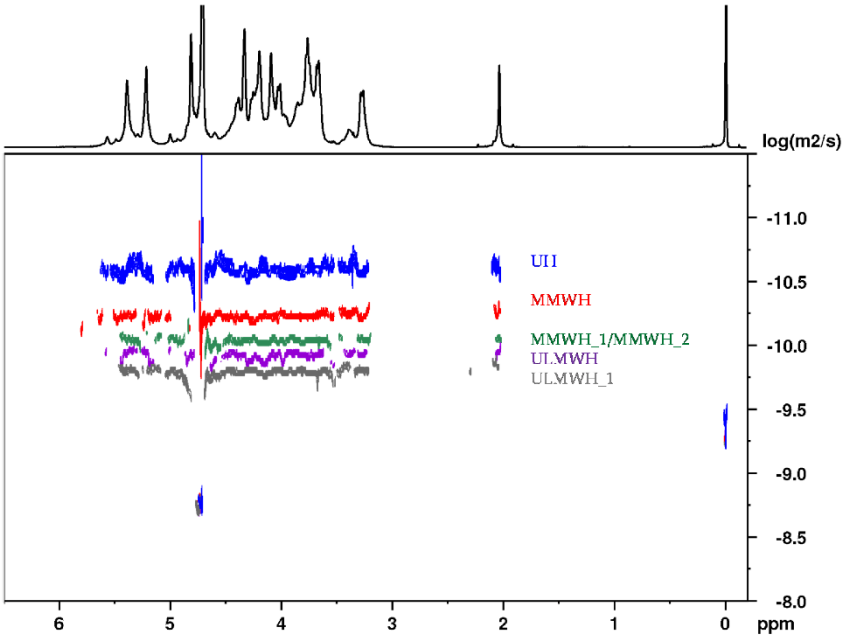

Figure S8. ^{1}H DOSY spectra of UH, MMWH, MMWH_1/2, ULMWH and ULMWH_1. The diffusion coefficients had been obtained relative to an internal standard (TPS) and their mobilities are inversely proportional to the molecular mass. The projection corresponds to UH.

References

1. Naggi, A.; Casu, B.; Perez, M.; Torri, G.; Cassinelli, G.; Penco, S.; Pisano, C.; Giannini, G.; Ishai-Michaeli, R.; Vlodavsky, I. Modulation of the heparanase-inhibiting activity of heparin through selective desulfation, graded *N*-acetylation, and glycol splitting. *J. Biol. Chem.* **2005,** *280* (13), 12103–12113.
2. Casu, B.; Guerrini, M.; Naggi, A.; Perez, M.; Torri, G.; Ribatti, D.; Carminati, P.; Giannini, G.; Penco, S.; Pisano, C.; Belleri, M.; Rusnati, M.; Presta, M. Short heparin sequences spaced by glycol-split uronate residues are antagonists of fibroblast growth factor 2 and angiogenesis inhibitors. *Biochemistry* **2002,** *41* (33), 10519–10528.
3. Guerrini, M.; Guglieri, S.; Naggi, A.; Sasisekharan, R.; Torri, G. Low molecular weight heparins: structural differentiation by bidimensional nuclear magnetic resonance spectroscopy. *Semin. Thromb. Hemost.* **2007,** *33* (5), 478–487.
4. Mauri, L.; Boccardi, G.; Torri, G.; Karfunkle, M.; Macchi, E.; Muzi, L.; Keire, D.; Guerrini, M. Qualification of HSQC methods for quantitative composition of heparin and low molecular weight heparins. *J. Pharm. Biomed. Anal.* **2017,** *136*, 92–105.
5. Monakhova, Y. B.; Diehl, B. W. K.; Do, T. X.; Schulze, M.; Witzleben, S. Novel method for the determination of average molecular weight of natural polymers based on 2D DOSY NMR and chemometrics: example of heparin. *J. Pharm. Biomed. Anal.* **2018,** *149*, 128–132.

Article 2: Heparin administered to *Anopheles* in membrane feeding assays blocks *Plasmodium* development in the mosquito

Authors: Elena Lantero, Jessica Fernandes, Carlos Raúl Aláez-Versón, Joana Gomes, Henrique Silveira, Fatima Nogueira and Xavier Fernàndez-Busquets

Journal: *Biomolecules*

Volume: 10

Issue: 8

Article number: 1136

Published: 1st August 2020

DOI: 10.3390/biom10081136

Journal Impact Factor: 4.082

Categories: Biochemistry (Q1), Molecular Biology (Q2)

Abstract:

Innovative antimalarial strategies are urgently needed given the alarming evolution of resistance to every single drug developed against Plasmodium parasites. The sulfated glycosaminoglycan heparin has been delivered in membrane feeding assays together with Plasmodium berghei-infected blood to Anopheles stephensi mosquitoes. The transition between ookinete and oocyst pathogen stages in the mosquito has been studied in vivo through oocyst counting in dissected insect midguts, whereas ookinete interactions with heparin have been followed ex vivo by flow cytometry. Heparin interferes with the parasite's ookinete–oocyst transition by binding ookinetes, but it does not affect fertilization. Hypersulfated heparin is a more efficient blocker of ookinete development than native heparin, significantly reducing the number of oocysts per midgut when offered to mosquitoes at 5 μg/mL in membrane feeding assays. Direct delivery of heparin to mosquitoes might represent a new antimalarial strategy of rapid implementation, since it would not require clinical trials for its immediate deployment.

biomolecules

MDPI

Communication

Heparin Administered to *Anopheles* in Membrane Feeding Assays Blocks *Plasmodium* Development in the Mosquito

Elena Lantero [1,2], Jessica Fernandes [3], Carlos Raúl Aláez-Versón [4], Joana Gomes [3], Henrique Silveira [3], Fatima Nogueira [3] and Xavier Fernàndez-Busquets [1,2,5,*]

1 Institute for Bioengineering of Catalonia (IBEC), The Barcelona Institute of Science and Technology, Baldiri Reixac 10–12, ES-08028 Barcelona, Spain; clantero@ibecbarcelona.eu
2 Barcelona Institute for Global Health (ISGlobal, Hospital Clínic-Universitat de Barcelona), Rosselló 149-153, ES-08036 Barcelona, Spain
3 Global Health and Tropical Medicine, Instituto de Higiene e Medicina Tropical, Universidade Nova de Lisboa (IHMT-NOVA), Rua da Junqueira 100, 1349-008 Lisbon, Portugal; jessica.j.fernandes94@gmail.com (J.F.); joana.matias.gomes@gmail.com (J.G.); hsilveira@ihmt.unl.pt (H.S.); fnogueira@ihmt.unl.pt (F.N.)
4 BIOIBERICA S.A.U., Polígon Industrial "Mas Puigvert", Ctra. N-II, km. 680.6, ES-08389 Palafolls, Spain; cralaez@bioiberica.com
5 Nanoscience and Nanotechnology Institute (IN2UB, Universitat de Barcelona), Martí i Franquès 1, ES-08028 Barcelona, Spain
* Correspondence: xfernandez_busquets@ub.edu

Received: 2 June 2020; Accepted: 29 July 2020; Published: 1 August 2020

Abstract: Innovative antimalarial strategies are urgently needed given the alarming evolution of resistance to every single drug developed against *Plasmodium* parasites. The sulfated glycosaminoglycan heparin has been delivered in membrane feeding assays together with *Plasmodium berghei*-infected blood to *Anopheles stephensi* mosquitoes. The transition between ookinete and oocyst pathogen stages in the mosquito has been studied in vivo through oocyst counting in dissected insect midguts, whereas ookinete interactions with heparin have been followed ex vivo by flow cytometry. Heparin interferes with the parasite's ookinete–oocyst transition by binding ookinetes, but it does not affect fertilization. Hypersulfated heparin is a more efficient blocker of ookinete development than native heparin, significantly reducing the number of oocysts per midgut when offered to mosquitoes at 5 µg/mL in membrane feeding assays. Direct delivery of heparin to mosquitoes might represent a new antimalarial strategy of rapid implementation, since it would not require clinical trials for its immediate deployment.

Keywords: malaria; heparin; mosquito; *Plasmodium*; *Anopheles*; ookinete; transmission blocking; antimalarial drugs

1. Introduction

The emergence and spread of *Plasmodium falciparum* resistance to most of the existing antimalarial drugs is a key factor that contributes to the global reappearance of malaria [1]. This threat of treatment failure is prompting research oriented to targeting the transmission stages of the pathogen between humans and mosquitoes [2], represented by smaller populations less likely to contain resistant individuals that would benefit from the removal of susceptible parasites [3]. Transmission-blocking vaccines (TBV) aim at stimulating in the human the production of antibodies to actively target and block the parasite development once it is in the mosquito [4]. Among the candidate antigens for TBV

strategies are proteins on the surface of the ookinete [5,6], the motile *Plasmodium* stage that forms in the blood bolus and has to traverse the midgut endothelium to progress to the next stage of the parasite, the oocyst.

Among other transmission-blocking strategies that can be envisaged is the interference with parasite–midgut interaction through the inhibitory action of the sulfated glycosaminoglycan (sGAG) heparin and related molecules, which have already shown antimalarial activity against several *Plasmodium* stages in humans. During initial malaria infection in the liver, heparin and heparan sulfate are hepatocyte receptors for sporozoite attachment [7]. In blood stages, heparin antimalarial activity, against which no resistances have been reported so far, unfolds by inhibition of merozoite invasion of the erythrocyte [8]. Chondroitin sulfate proteoglycans in the mosquito midgut and a synthetic polysulfonated polymer that mimics the structure of sGAGs present in the midgut epithelium have been described to bind *Plasmodium* ookinetes during host epithelial cell invasion [9,10], whereas ookinetes and ookinete-secreted proteins possess significant binding to heparin [11,12]. Here, we have explored the potential of heparin against ookinete development.

2. Materials and Methods

All reagents were purchased from Sigma-Aldrich Corporation (St. Louis, MO, USA) unless otherwise specified. Heparin from pig intestinal mucosa was provided by BIOIBERICA (Palafolls, Spain). Oversulfation to generate hypersulfated heparin was done as previously described [13], obtaining a preparation with three sulfate groups/disaccharide (as compared to 1.9–2.0 in native heparin). Briefly, 100 mg of sodium heparin salt were subjected to cation-exchange chromatography to obtain tributylamine salt, lyophilized, and dissolved in 0.8 mL of *N*,*N*-dimethylformamide, which contained an excess of pyridine-sulfur trioxide. After 1 h at 40 °C, 1.6 mL of water were added, and the product was precipitated with three volumes of cold ethanol saturated with anhydrous sodium acetate and collected by centrifugation. The product was dissolved in water, extensively dialyzed, and recovered by freeze-drying.

2.1. Animals

Female CD1 mice (*Mus musculus*) from the Instituto de Higiene e Medicina Tropical animal house were used to obtain blood for membrane feeding assays (MFAs) and mosquito infections, with the corresponding license (009511 from 21 April 2019) approved by the Portuguese National Authority Health (DGAV). For ex vivo production of ookinetes, female BALB/c mice (Janvier Labs, Le Genest-Saint-Isle, France) were used, following the protocols reviewed and approved by the Ethical Committee on Clinical Research from the *Hospital Clínic de Barcelona* (Reg. 10100/P2, approved on January 2018). In all cases, for the experimental procedure, mice were anesthetized using 100 mg/kg ketamine (Ketolar) mixed with 10 mg/kg xylazine (Rompun) intraperitoneally (i.p.) administered, and regularly monitored. *Anopheles stephensi* mosquitoes were maintained under standard insectary conditions (26 ± 1 °C, 75% humidity and a 12/12 h light/dark cycle). Adult mosquitoes were fed on 10% glucose solution ad libitum until the day before feeding trials.

2.2. Sugar Feed

Heparin directly dissolved at 5 mg/mL or 50 mg/mL in 10% glucose in H_2O, or 10% glucose in H_2O for the control group, were administered to mosquitoes twice (once each 24 h) in a cotton pad on the top of a net-capped paper cup containing 40–50 *A. stephensi* females. Mosquitoes were allowed to feed for 48 h, and then infected by direct feeding on a CD1 mouse parasitized with *Plasmodium berghei* ANKA-GFP (259cl1; MRA-865 [14]) for 10 min. Non-fed mosquitoes were removed, and fed mosquitoes were placed in the insectary at 21 °C and 75% humidity to allow parasite development. After eight days, mosquitoes were dissected, and the number of GFP-expressing oocysts per midgut was counted manually using an Axioskop fluorescence microscope (Zeiss, Oberkochen, Germany).

The total number of mosquitoes analyzed was 61 in the control group, 63 treated with 5 mg/mL heparin, and 46 treated with 50 mg/mL heparin, distributed in three independent experiments.

2.3. Membrane Blood Feeding Assay

Blood obtained from an intracardiac puncture of a CD1 mouse infected with *P. berghei* ANKA-GFP (259cl1; MRA-865) was treated with 1/10 volume of 3.2% *w/v* sodium citrate to prevent coagulation. 6.25 µL of a solution prepared by dissolving heparin at 40 mg/mL or 0.4 mg/mL in phosphate buffered saline (PBS) was added to 494 µL of blood:citrate (to obtain final heparin concentrations of 500 and 5 µg/mL, respectively), which was then placed in feeders prepared with two-sided stretched Parafilm® connected to two plastic tubes for water inlet and outlet. The same volumes of PBS and blood:citrate were used for heparin-free controls. Temperature within the multiple cylindrical water-jacked glass was kept at 37 °C by a constant water flow supply. Each feeder was placed on top of a net-covered paper cup containing 40–50 *A. stephensi* females. Mosquitoes were allowed to feed for one hour. Non-fed mosquitoes were removed, and the rest were treated as above. The final number of mosquitoes analyzed for the non-modified heparin assay was 127 in the control group, 106 treated with 5 µg/mL heparin, and 149 treated with 500 µg/mL heparin, distributed in three independent experiments. The final number of mosquitoes analyzed for the hypersulfated heparin assay was 62 in the control group, 91 treated with 5 µg/mL hypersulfated heparin, and 102 treated with 500 µg/mL hypersulfated heparin, distributed in two independent experiments.

2.4. Detection of Heparin-Cy5 in Mosquitoes

Thirty female *A. stephensi* mosquitoes per cage were allowed to feed on 400 µg/mL heparin-Cy5 (Nanocs Inc., New York, NY, USA) on either sugar for 6 h or MFA for 1 h. Some mosquitoes were taken from the cages at 6, 24, 48, and 72 h post-feeding to check Cy5 fluorescence ($\lambda_{ex}/\lambda_{em}$: 650/670 nm) with an Eclipse 80i microscope (Nikon, Tokyo, Japan). Mosquitoes with fluorescent signal were dissected, and their organs were individually observed.

2.5. Ex Vivo Production of Ookinetes and Flow Cytometry Analysis

Eight days before ookinete production, 200 µL of *P. berghei* CTRP-GFP (kindly provided by Dr. Inga Siden-Kiamos [15]) in cryopreservation solution (RBC pellet:Roswell Park Memorial Institute medium (RPMI, Gibco, Dublin, Ireland):30% glycerol in water, 1:1:2) was administered i.p. to a BALB/c mouse. Four days later, this mouse was the donor to infect i.p. with 5×10^7 parasitized red blood cells in 200 µL of PBS a second mouse that one hour before the infection had been pretreated i.p. with phenylhydrazine (120 µL of a 10 mg/mL solution in PBS). For ookinete production, up to 1 mL of blood carrying gametocytes was collected by intracardiac puncture and diluted in 30 mL of ookinete medium: 10.4 g/L of RPMI supplemented with 2% *w/v* $NaHCO_3$, 0.05% *w/v* hypoxanthine, 0.02% *w/v* xanthurenic acid, 50 U/mL penicillin and 50 µg/mL streptomycin, 20% heat-inactivated fetal bovine serum (FBS, Invitrogen, Carlsbad, CA, USA), 25 mM HEPES, pH 7.4. The culture was incubated for 24 h at 21 °C with orbital shaking at 50 rpm (modified from [16]).

To check heparin influence on fertilization, to 487.5 µL of culture in a well of 24-well plates was added 12.5 µL of PBS containing heparin at 20 or 0.2 mg/mL, to provide final heparin concentrations of 500 µg/mL and 5 µg/mL. Samples were taken at two different time points (just after extraction and after 1 h incubation), including a control consisting of PBS only, in three independent experimental replicates. Twenty-four hours later, samples were diluted 1:100 in PBS and analyzed in a LSRFortessa™ flow cytometer (BD Biosciences, San Jose, CA, USA) set up with the five lasers, 20 parameters standard configuration. The GFP positive ookinete population was selected and counted using 488 nm laser excitation and a 525/40 nm emission collection filter. BD FACSDiva software version 6.1.3 (BD Biosciences) was used in data collection, and Flowing Software 2.5.1 (Turku Centre for Biotechnology, Turku, Finland) was used for analysis.

For targeting assays, mature ookinetes were washed twice with PBS and incubated with heparin-Cy5 at 400 µg/mL in ookinete medium without FBS for 1 h. The sample was finally diluted 1:100 in the same medium containing 0.2 µg/mL Hoechst 33342 and events recorded with an Amnis® ImageStream®X Mk II cytometer (Luminex Corporation, Austin, TX, USA) using 375 nm, 488 nm, and 642 nm excitation lasers for Hoechst 33342, GFP and Cy5 signals respectively. Data were analyzed with IDEAS® 6.3 software (Luminex Corporation).

2.6. Statistical Analysis

Oocysts/midgut counts from three independent experiments were plotted and analyzed in GraphPad Prism 6 using an unpaired Mann–Whitney test to determine significant differences. *t*-Tests with Welch's correction were applied for determining significance in ex vivo ookinete maturation and targeting assays, and degrees of freedom were automatically defined by the software, according to n. In both cases, tests were two-sided.

3. Results

3.1. Characterization of Heparin-Cy5 Binding to Ookinetes

Flow cytometry analysis showed binding of heparin-Cy5 to ookinetes obtained ex vivo from mouse blood infected with the *P. berghei* CTRP-GFP transgenic line (Figure 1a,b), which expresses GFP when reaching ookinete stage. Fluorescence images indicated the binding of heparin-Cy5 to discrete areas on the ookinete (Figure 1c), which suggests clustering of heparin receptors.

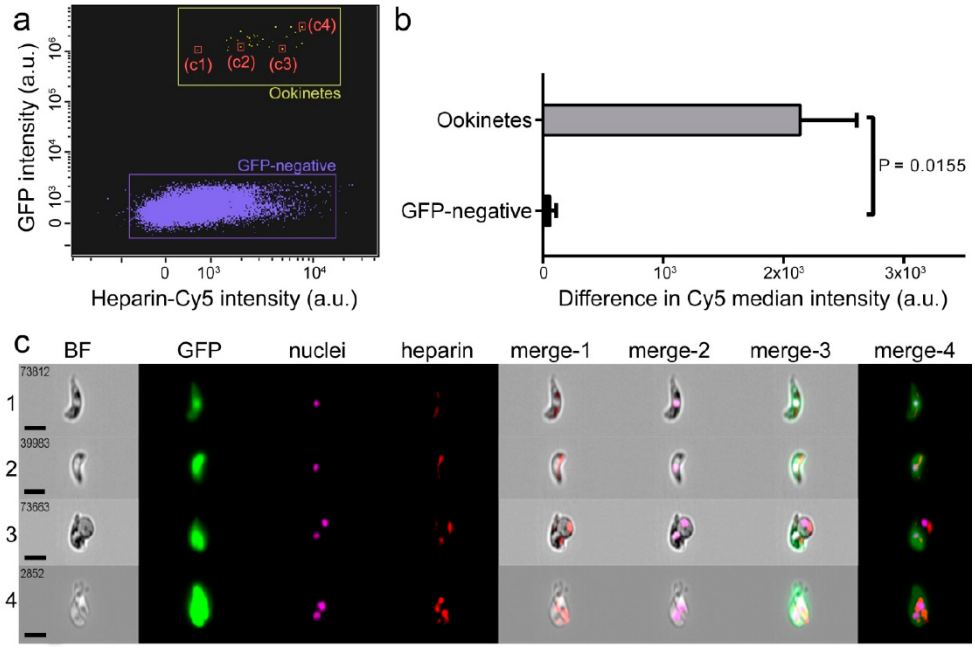

Figure 1. Heparin-Cy5 binding to ookinetes. (**a**) Flow cytometry plot showing heparin-Cy5 signal in green fluorescent protein (GFP)-expressing *P. berghei* ookinetes. GFP-negative events correspond mostly to red blood cells (see Figure S1 for gating strategy). c1 to c4 refer to the individual events reported in panel **c**. (**b**) Difference in Cy5 median intensity between GFP-expressing ookinetes and GFP-negative cells. (**c**) Fluorescence images of the flow cytometry events indicated in panel **a**. The merges of the bright field (BF) image with the fluorescence of heparin, nuclei, GFP, and all three of them, are indicated as merge-1 to merge-4, respectively. Size bars represent 7 µm.

3.2. Effect on Oocyst Development of Heparin Administered to Mosquitoes by Sugar Meal

Heparin-Cy5 fed in the sugar meal to female *A. stephensi* mosquitoes was detected in the midgut of the insects for up to 72 h after administration (Figure 2a–d and Figure S2). Heparin effect on ookinete to oocyst transition was then assessed in live mosquitoes, by offering them heparin by sugar feed during 48 h before infecting them by direct bite to a *P. berghei* ANKA-GFP-parasitized mouse (Figure 2e). Unfed mosquitoes were removed, and eight days later, mosquitoes were dissected, and GFP-expressing oocysts were counted. The prevalence of infection (PI, percentage of mosquitoes with ≥1 oocyst) and the infection intensity (II, number of oocysts per midgut) were not significantly affected when compared to untreated controls up to heparin concentrations in the sugar feed of 50 mg/mL (Figure 2f). It is likely that most of the sugar feed might be pushed out by the blood meal, in which case heparin would not interact with ookinetes. This result led us to explore new strategies to ensure the presence of heparin at the moment of ookinete development in the mosquito midgut by including heparin in a *Plasmodium*-infected blood meal.

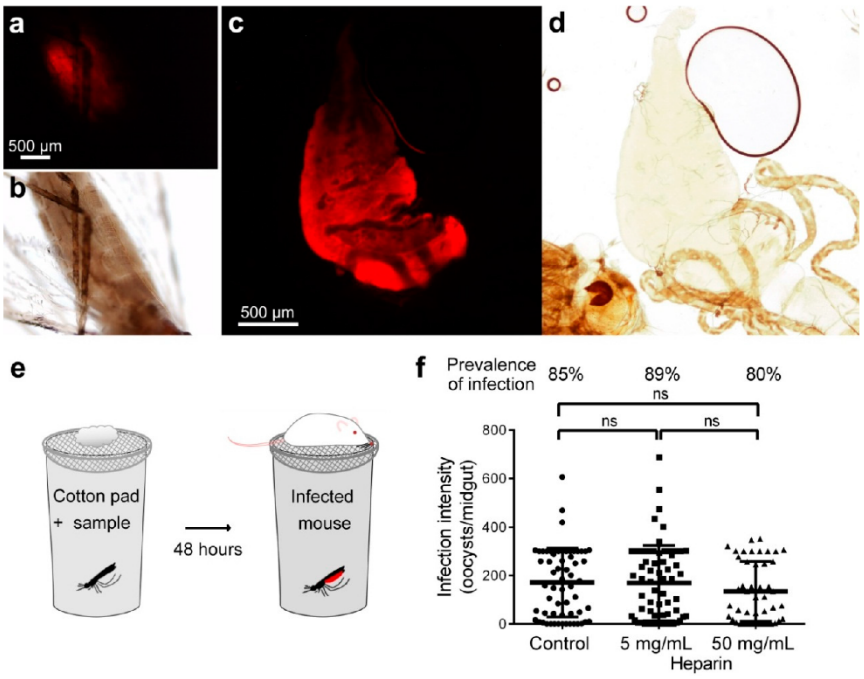

Figure 2. Effect on ookinete development of heparin fed to mosquitoes by sugar meal. (**a**,**c**) Fluorescence detection in (**a**) intact abdomen and (**c**) dissected midgut of heparin-Cy5 fed to *A. stephensi* female mosquitoes in a sugar meal. (**b**,**d**) Bright field images of the microscope fields in panels **a** and **c**, respectively. (**e**) Depiction of the method for sugar feed used in mosquito assays. (**f**) Effect on parasite development of heparin delivered by sugar swaps. ns: not significant.

3.3. Effect on Oocyst Development of Heparin Administered to Mosquitoes by Blood Membrane Feeding

Heparin-Cy5 fed to female *A. stephensi* mosquitoes by whole blood MFAs was detected in the midgut of the insect for at least 24 h after administration (Figure 3a–d and Figure S3). Often, Cy5 fluorescence was only faintly observed in the dissected midgut (Figure 3a,b), but it intensified after having pushed out the blood bolus (Figure 3c,d). This might result from light being absorbed or screened by the compacted blood bolus. Heparin activity on ookinete to oocyst transition was then assessed with this method of administration. Heparin was added to the blood of mice infected with *P. berghei* ANKA-GFP, which was then offered to female *A. stephensi* by MFA (Figure 3e). Unfed mosquitoes were

removed, and eight days later, mosquitoes were dissected, and oocysts were counted. A significant decrease of PI and II was observed in mosquitoes fed with heparin-containing infected blood samples (Figure 3f,h–k). PI was 38% and 23% for respective MFA heparin concentrations of 5 µg/mL and 500 µg/mL, compared to 52% for the heparin-free control, whereas the mean II for the same samples was, respectively, 24.22 ± 65.10, 0.95 ± 4.12, and 36.38 ± 89.57 oocysts per midgut.

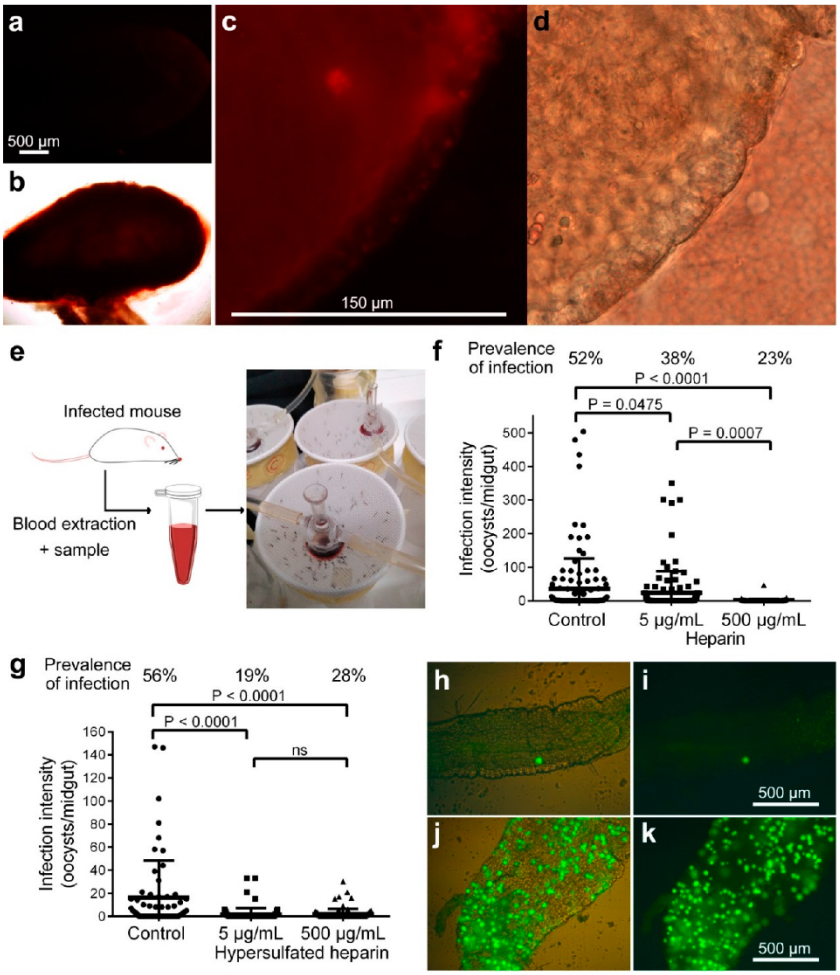

Figure 3. Effect on ookinete development of heparin fed to mosquitoes by membrane feeding assay (MFA). (**a**–**d**) Fluorescence detection of heparin-Cy5 fed to *A. stephensi* female mosquitoes by blood feed. (**a**,**b**) Whole dissected midgut and (**c**,**d**) magnification of the same midgut with the blood bolus pushed away. (**b**,**d**) Bright field images of the microscope fields in panels **a** and **c**, respectively. (**e**) Depiction of the MFA method used in mosquito assays. (**f**) Effect on parasite development of non-modified heparin delivered by MFA. (**g**) Effect on parasite development of hypersulfated heparin delivered by MFA. ns: not significant. (**h**–**k**) Fluorescence images of representative mosquito midguts from the MFA 500 µg/mL non-modified heparin group (**h**,**i**) and from the MFA control group (**j**,**k**); the fluorescence signal is shown alone (**i**,**k**) and merged with bright field images of the midgut contours **h**,**j**).

When a modified heparin with higher proportion of sulfated residues in the polysaccharide chain (hypersulfated heparin) was offered to mosquitoes by MFA, a significant decrease in PI and II

was observed with as little as 5 µg/mL of heparin (Figure 3g). PI was 19% and 28% for respective hypersulfated heparin concentrations of 5 µg/mL and 500 µg/mL compared to 56% for the control, whereas the mean II for the same samples was, respectively, 1.53 ± 5.56, 1.74 ± 4.61, and 16.29 ± 31.94 oocysts per midgut. Although the extensive dialysis performed at the end of the heparin sulfation process should have removed any residual byproduct, future research has to rule out potential interferences of trace chemicals on the mechanism of oocyst formation. No impact on mosquito viability was observed for any of the heparins studied here (data not shown).

The observation that PI in blood feeding assays was significantly lower than in sugar meal experiments might be explained by the presence of sodium citrate, which is a calcium chelator used to prevent blood coagulation. Since the induction of exflagellation in *Plasmodium* requires calcium [17], sodium citrate could have a synergistic effect with heparin potentiating its inhibitory effect on oocyst formation. Heparin is also a potent calcium chelator which binds ca. one Ca^{2+} ion per average disaccharide [18]. At the high 50 mg/mL heparin concentration of sugar meal assays, the calcium binding capacity of heparin was comparable to that of the sodium citrate amount used in MFAs. Although in these experiments no effect of heparin was seen on ookinete development, the suspected immiscibility of sugar feed and blood meal calls for caution before drawing any conclusions regarding the suspected inhibitory effect of calcium chelators on *Plasmodium* development in the mosquito.

3.4. *Effect of Heparin on Fertilization*

When blood from *P. berghei*-infected mice was put into culture to obtain ookinetes and heparin was added to the culture either at the moment of blood extraction (t_0) or 1 h later (t_1), no significant effect was observed in the number of ookinetes produced when compared with untreated control cultures (Figure 4). However, the fold-increase in ookinete numbers when heparin was added at t_0 (ookinetes relative to normalized control: 3.32 ± 2.26 and 2.26 ± 1.18 for 5 µg/mL and 500 µg/mL heparin, respectively), though non-significant due to the high dispersion of the results, could indicate that heparin enhances fertilization. This effect might operate through heparin interactions with coagulation factors, which would facilitate gamete motility. Heparin use in MFAs was previously recommended over other anticoagulants such as EDTA, as better infection rates were obtained [19]. Consistently, no effect on ookinete numbers was observed when heparin was added at t_1, when fertilization has already occurred [20]. These results indicated that the inhibitory activity of heparin on *Plasmodium* mosquito stages is not exerted during fertilization or zygote maturation. Although sodium citrate was not used in ex vivo assays, the presence of 500 µg/mL heparin bound a significant amount of calcium, and yet, exflagellation was not affected. However, the potential role of calcium sequestration on this part of the parasite's development deserves further exploration.

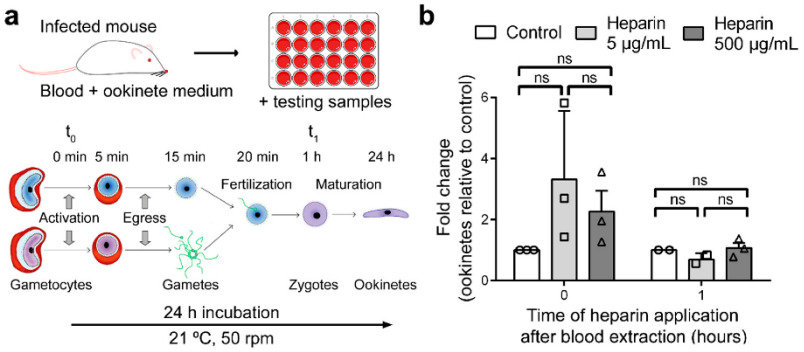

Figure 4. Effect of heparin in the ex vivo development of ookinetes. (**a**) Depiction of the method used for the ex vivo growth of ookinetes. The parasite development scheme has been adapted from Kuehn and Pradel [20]. (**b**) Effect of heparin on ex vivo ookinete maturation analyzed by flow cytometry (see Figure S4 and Table S1). ns: not significant.

4. Discussion

The results presented above validate a potential new antimalarial strategy where heparin binding to ookinetes will prevent the interaction of this *Plasmodium* stage with the mosquito midgut and consequently its development into an oocyst. It has been suggested that chondroitin sulfate is a ligand for the circumsporozoite- and thrombospondin-related anonymous protein-related protein (CTRP) [9], a key molecule for ookinete mobility and parasite development [21]. Characterizing the sGAG ookinete binding domain and sulfation pattern will be important regarding the development of future antimalarials acting on this stage of the parasite's cycle. To start unraveling the relevance of the sulfation pattern in blocking ookinete progression, hypersulfated heparin has been tested here, and has shown interesting potential since the lowest concentration used resulted in a significantly larger inhibition of ookinete development than the same concentration of native heparin. Chemical modifications of heparin or its binding to nanocarriers are strategies that could contribute to increase activity and midgut residence time in view of the potential development of sGAG-based antimalarials as disruptors of the life cycle of *Plasmodium* in the mosquito.

So far, transmission-blocking approaches have focused on the concept of treating humans with vaccines or drugs that will target mosquito stages [22]. A largely unexplored avenue, however, is targeting *Plasmodium* in the insect vector directly [23]. The implementation of antimalarial medicines designed to be delivered directly to mosquitoes might reduce treatment and development costs because the clinical trials otherwise required for therapies to be administered to people could be significantly simplified. Strategies that control malaria using direct action against *Anopheles* are not new but mostly focus on eliminating the vector, either by killing it with pesticides [24] or through the release of sterile males [25]. The administration of drugs to mosquitoes during their blood feed is being used to deliver ivermectin, an endectocide that, at concentrations found in human blood after treatment, is toxic to all *Anopheles* species examined [24]. When *P. falciparum*–infected female *Anopheles gambiae* mosquitoes were exposed to surfaces treated with the antimalarial drug atovaquone, the development of the parasite was completely arrested [26]. Although this strategy is unlikely to work for large hydrophilic molecules like heparin, several other approaches are available for direct drug delivery to mosquitoes, some of which have been used to deliver to dipterans lipid-based [27] and chitosan nanoparticles [28].

The failure of heparin in inhibiting parasite development when delivered in a sugar meal prior to infection of the mosquito indicates that heparin must be present in the midgut simultaneously with ookinetes. This poses a significant obstacle regarding the practical implementation of future antimalarial strategies based on the observations reported here. Heparin is normally present in human plasma in values ranging from 1 mg/L to 2.4 mg/L [29], whereas heparin in the mosquito midgut is active at concentrations >100 times higher. The anticoagulant activity of heparin prevents its administration to people in the amounts required to block ookinete development, although sGAG mimetics [9] or modified heparins having low anticoagulant capacity [30] offer promising perspectives. The use of limited heparin amounts in infected patients for transmission-blocking might actually be beneficial given the described pro-coagulant effects of *Plasmodium*-infected red blood cells [31]. However, to be present in the circulation at the moment of a mosquito bite, the blood residence time of these molecules should be extremely long. An alternative approach could be provided by offering heparin to mosquitoes in an artificial diet simulating vertebrate blood. The available technology is capable of manufacturing artificial blood for mosquito feeding from hemoglobin obtained from citrated rabbit blood [32], outdated bovine blood [33], and other blood-free artificial liquid diets [34–36]. These substitutes mimic in the mosquito the physiological effects of a fresh vertebrate blood meal, supporting ovarian and egg maturation and normal development of offspring into functional adults. Such artificial feedings can substitute direct feeding on mammals and often have prolonged shelf life and do not require refrigeration. For their delivery to mosquitoes, a number of artificial blood feeders are currently under study [37]. This approach would require the presence of attractants in the artificial diet to lure mosquitoes that have already taken a human blood meal and thus potentially carrying ookinetes in their midguts.

The economic landscape of malaria calls for new strategies that take into account the costs of bringing a medicine into the market, which due to expensive clinical trials often prevent promising new drugs from a fast entry into the production pipeline. As a possible approach to solving this problem, the administration of heparin to mosquitoes offers two advantages: first, blocking the life cycle of *Plasmodium* in the mosquito vector through direct drug delivery to the insect, can dramatically shorten product development due to the avoidance of large-scale human tests. Second, applying the three Rs of drug development (rescue, repurpose, reposition) to previously discarded compounds is an interesting strategy to return value to potential treatments in decline or on hold. Heparin is a natural polysaccharide that can be abundantly obtained in large amounts from the intestinal mammalian mucosa and which has a widespread medical use. The results presented here can inspire researchers and entrepreneurs, especially those in malaria endemic regions, to pursue the development of an efficient and economically affordable antimalarial strategy. A chain of heparin production could easily start with the usually discarded mucosae of pigs, goats, sheep, or cows that are consumed for food. In addition, potential strategies to deliver heparin to mosquitoes might involve the use of small containers filled with mosquito attractants, which can boost the economy of many developing regions through either the fabrication of such dispensers made of plastic, glass or aluminum, or the recycling of bottles and cans.

Supplementary Materials: The following are available online at http://www.mdpi.com/2218-273X/10/8/1136/s1, Figure S1. Gating strategy for Figure 1a; Figure S2. Photomicrograph gallery of different time points after heparin-Cy5 administration in sugar feed; Figure S3. Photomicrograph gallery of different time points after heparin-Cy5 administration in MFA; Figure S4. Gating strategy for the data analysis presented in Figure 4b; Table S1. GFP-positive events (n) and corresponding percentages presented in Figure 4b.

Author Contributions: Conceptualization, X.F.-B. and E.L.; methodology, E.L., F.N., H.S., and X.F.-B.; formal analysis, E.L.; investigation, E.L., J.F., J.G., and F.N.; resources, C.R.A.-V., F.N., H.S., and X.F.-B.; writing—original draft preparation, X.F.-B. and E.L.; writing—review and editing, X.F.-B., E.L., H.S., and F.N.; visualization E.L.; supervision, F.N., H.S., and X.F.-B.; project administration, X.F.-B.; funding acquisition, F.N., H.S. and X.F.-B. All authors have read and agreed to the published version of the manuscript.

Funding: X.F.-B. received funding support from (i) Spanish Ministry of Science, Innovation and Universities (http://www.ciencia.gob.es/), grant numbers PCIN-2017-100 and RTI2018-094579-B-I00 (which included FEDER funds), (ii) BIOIBERICA, and (iii) ERA-NET Cofund EURONANOMED (http://euronanomed.net/), grant number 2017-178 (NANOpheles). H.S. and F.N. received funding support from Global Health and Tropical Medicine, Instituto de Higiene e Medicina Tropical, Universidade Nova de Lisboa, GHTM–UID/04413/2020 (https://ghtm.ihmt.unl.pt/).

Acknowledgments: ISGlobal and IBEC are members of the CERCA Programme, *Generalitat de Catalunya*. We acknowledge support from the Spanish Ministry of Science, Innovation and Universities through the *"Centro de Excelencia Severo Ochoa 2019-2023"* Program (CEX2018-000806-S). This research is part of ISGlobal's Program on the Molecular Mechanisms of Malaria, which is partially supported by the *Fundación Ramón Areces*. We are indebted to the Cytometry and Cell Sorting Facility of the *Institut d'Investigacions Biomèdiques August Pi i Sunyer* (IDIBAPS) for technical help. E.L. would like to thank Rafael Oliveira and Helio Rocha for their support and feedback.

Conflicts of Interest: X.F.-B. has received funding from BIOIBERICA and C.R.A.-V. is employed by BIOIBERICA. The funders had no role in the design of the study; in the collection, analyses, or interpretation of data; in the writing of the manuscript, or in the decision to publish the results.

References

1. World Health Organization. *World Malaria Report 2019*; World Health Organization: Geneva, Switzerland, 2019.
2. Sinden, R.; Carter, R.; Drakeley, C.; Leroy, D. The biology of sexual development of *Plasmodium*: The design and implementation of transmission-blocking strategies. *Malar. J.* **2012**, *11*, 70. [CrossRef] [PubMed]
3. Delves, M.; Plouffe, D.; Scheurer, C.; Meister, S.; Wittlin, S.; Winzeler, E.; Sinden, R.E.; Leroy, D. The activities of current antimalarial drugs on the life cycle stages of *Plasmodium*: A comparative study with human and rodent parasites. *PLoS Med.* **2012**, *9*, e1001169. [CrossRef] [PubMed]
4. Kapulu, M.C.; Da, D.F.; Miura, K.; Li, Y.; Blagborough, A.M.; Churcher, T.S.; Nikolaeva, D.; Williams, A.R.; Goodman, A.L.; Sangare, I.; et al. Comparative assessment of transmission-blocking vaccine candidates against *Plasmodium falciparum*. *Sci. Rep.* **2015**, *5*, 11193. [CrossRef]
5. Duffy, P.E.; Kaslow, D.C. A novel malaria protein, Pfs28, and Pfs25 are genetically linked and synergistic as falciparum malaria transmission-blocking vaccines. *Infect. Immun.* **1997**, *65*, 1109–1113. [CrossRef] [PubMed]

6. Kim, T.S.; Kim, H.H.; Moon, S.U.; Lee, S.S.; Shin, E.H.; Oh, C.M.; Kang, Y.J.; Kim, D.K.; Sohn, Y.; Kim, H.; et al. The role of Pvs28 in sporozoite development in *Anopheles sinensis* and its longevity in BALB/c mice. *Exp. Parasitol.* **2011**, *127*, 346–350. [CrossRef]
7. Ancsin, J.B.; Kisilevsky, R. A binding site for highly sulfated heparan sulfate is identified in the N terminus of the circumsporozoite protein: Significance for malarial sporozoite attachment to hepatocytes. *J. Biol. Chem.* **2004**, *279*, 21824–21832. [CrossRef] [PubMed]
8. Boyle, M.J.; Richards, J.S.; Gilson, P.R.; Chai, W.; Beeson, J.G. Interactions with heparin-like molecules during erythrocyte invasion by *Plasmodium falciparum* merozoites. *Blood* **2010**, *115*, 4559–4568. [CrossRef]
9. Mathias, D.K.; Pastrana-Mena, R.; Ranucci, E.; Tao, D.; Ferruti, P.; Ortega, C.; Staples, G.O.; Zaia, J.; Takashima, E.; Tsuboi, T.; et al. A small molecule glycosaminoglycan mimetic blocks *Plasmodium* invasion of the mosquito midgut. *PLoS Pathog.* **2013**, *9*, e1003757. [CrossRef]
10. Dinglasan, R.R.; Alaganan, A.; Ghosh, A.K.; Saito, A.; van Kuppevelt, T.H.; Jacobs-Lorena, M. *Plasmodium falciparum* ookinetes require mosquito midgut chondroitin sulfate proteoglycans for cell invasion. *Proc. Natl. Acad. Sci. USA* **2007**, *104*, 15882–15887. [CrossRef]
11. Marques, J.; Valle-Delgado, J.J.; Urbán, P.; Baró, E.; Prohens, R.; Mayor, A.; Cisteró, P.; Delves, M.; Sinden, R.E.; Grandfils, C.; et al. Adaptation of targeted nanocarriers to changing requirements in antimalarial drug delivery. *Nanomed. NBM* **2017**, *13*, 515–525. [CrossRef]
12. Li, F.; Templeton, T.J.; Popov, V.; Comer, J.E.; Tsuboi, T.; Torii, M.; Vinetz, J.M. *Plasmodium* ookinete-secreted proteins secreted through a common micronemal pathway are targets of blocking malaria transmission. *J. Biol. Chem.* **2004**, *279*, 26635–26644. [CrossRef] [PubMed]
13. Maruyama, T.; Toida, T.; Imanari, T.; Yu, G.; Linhardt, R.J. Conformational changes and anticoagulant activity of chondroitin sulfate following its *O*-sulfonation. *Carbohydr. Res.* **1998**, *306*, 35–43. [CrossRef]
14. Franke-Fayard, B.; Trueman, H.; Ramesar, J.; Mendoza, J.; van der Keur, M.; van der Linden, R.; Sinden, R.E.; Waters, A.P.; Janse, C.J. A *Plasmodium berghei* reference line that constitutively expresses GFP at a high level throughout the complete life cycle. *Mol. Biochem. Parasitol.* **2004**, *137*, 23–33. [CrossRef] [PubMed]
15. Vlachou, D.; Zimmermann, T.; Cantera, R.; Janse, C.J.; Waters, A.P.; Kafatos, F.C. Real-time, in vivo analysis of malaria ookinete locomotion and mosquito midgut invasion. *Cell. Microbiol.* **2004**, *6*, 671–685. [CrossRef] [PubMed]
16. Blagborough, A.M.; Delves, M.J.; Ramakrishnan, C.; Lal, K.; Butcher, G.; Sinden, R.E. Assessing transmission blockade in *Plasmodium* spp. In *Malaria: Methods and Protocols*; Ménard, R., Ed.; Humana Press: Totowa, NJ, USA, 2013; pp. 577–600.
17. Bansal, A.; Molina-Cruz, A.; Brzostowski, J.; Mu, J.; Miller, L.H. *Plasmodium falciparum* calcium-dependent protein kinase 2 is critical for male gametocyte exflagellation but not essential for asexual proliferation. *mBio* **2017**, *8*. [CrossRef]
18. Grant, D.; Moffat, C.F.; Long, W.F.; Williamson, F.B. Ca^{2+}-heparin interaction investigated polarimetrically. *Biochem. Soc. Trans.* **1991**, *19*, 391S. [CrossRef]
19. Solarte, Y.; Manzano, M.R.; Rocha, L.; Castillo, Z.; James, M.A.; Herrera, S.; Arévalo-Herrera, M. Effects of anticoagulants on *Plasmodium vivax* oocyst development in *Anopheles albimanus* mosquitoes. *Am. J. Trop. Med. Hyg.* **2007**, *77*, 242–245. [CrossRef]
20. Kuehn, A.; Pradel, G. The coming-out of malaria gametocytes. *J. Biomed. Biotechnol.* **2010**, *2010*, 976827. [CrossRef]
21. Dessens, J.T.; Beetsma, A.L.; Dimopoulos, G.; Wengelnik, K.; Crisanti, A.; Kafatos, F.C.; Sinden, R.E. CTRP is essential for mosquito infection by malaria ookinetes. *EMBO J.* **1999**, *18*, 6221–6227. [CrossRef]
22. Wells, T.N.C.; van Huijsduijnen, R.H.; Van Voorhis, W.C. Malaria medicines: A glass half full? *Nat. Rev. Drug Discov.* **2015**, *14*, 424–442. [CrossRef]
23. Paaijmans, K.; Fernàndez-Busquets, X. Antimalarial drug delivery to the mosquito: An option worth exploring? *Future Microbiol.* **2014**, *9*, 579–582. [CrossRef] [PubMed]
24. Chaccour, C.; Kobylinski, K.; Bassat, Q.; Bousema, T.; Drakeley, C.; Alonso, P.; Foy, B. Ivermectin to reduce malaria transmission: A research agenda for a promising new tool for elimination. *Malar. J.* **2013**, *12*, 153. [CrossRef] [PubMed]
25. Andreasen, M.H.; Curtis, C.F. Optimal life stage for radiation sterilization of *Anopheles* males and their fitness for release. *Med. Vet. Entomol.* **2005**, *19*, 238–244. [CrossRef] [PubMed]

26. Paton, D.G.; Childs, L.M.; Itoe, M.A.; Holmdahl, I.E.; Buckee, C.O.; Catteruccia, F. Exposing *Anopheles* mosquitoes to antimalarials blocks *Plasmodium* parasite transmission. *Nature* **2019**, *567*, 239–243. [CrossRef] [PubMed]
27. Whyard, S.; Singh, A.D.; Wong, S. Ingested double-stranded RNAs can act as species-specific insecticides. *Insect Biochem. Mol. Biol.* **2009**, *39*, 824–832. [CrossRef]
28. Zhang, X.; Zhang, J.; Zhu, K.Y. Chitosan/double-stranded RNA nanoparticle-mediated RNA interference to silence chitin synthase genes through larval feeding in the African malaria mosquito (*Anopheles gambiae*). *Insect Mol. Biol.* **2010**, *19*, 683–693. [CrossRef]
29. Engelberg, H. Plasma heparin levels in normal man. *Circulation* **1961**, *23*, 578–581. [CrossRef]
30. Boyle, M.J.; Skidmore, M.; Dickerman, B.; Cooper, L.; Devlin, A.; Yates, E.; Horrocks, P.; Freeman, C.; Chai, W.; Beeson, J.G. Identification of heparin modifications and polysaccharide inhibitors of *Plasmodium falciparum* merozoite invasion that have potential for novel drug development. *Antimicrob. Agents Chemother.* **2017**, *61*, e00709–e00717. [CrossRef]
31. Francischetti, I.M.; Seydel, K.B.; Monteiro, R.Q. Blood coagulation, inflammation, and malaria. *Microcirculation* **2008**, *15*, 81–107. [CrossRef]
32. Dias, L.D.S.; Bauzer, L.G.S.D.; Lima, J.B.P. Artificial blood feeding for Culicidae colony maintenance in laboratories: Does the blood source condition matter? *Rev. Inst. Med. Trop. Sao Paulo* **2018**, *60*, e45. [CrossRef]
33. Haldar, R.; Gupta, D.; Chitranshi, S.; Singh, M.K.; Sachan, S. Artificial blood: A futuristic dimension of modern day transfusion sciences. *Cardiovasc. Hematol. Agents Med. Chem.* **2019**, *17*, 11–16. [CrossRef] [PubMed]
34. Marques, J.; Cardoso, J.C.R.; Felix, R.C.; Power, D.M.; Silveira, H. A blood-free diet to rear anopheline mosquitoes. *J. Vis. Exp.* **2020**, *155*, e60144. [CrossRef] [PubMed]
35. Marques, J.; Cardoso, J.C.R.; Felix, R.C.; Santana, R.A.G.; Guerra, M.D.G.B.; Power, D.; Silveira, H. Fresh-blood-free diet for rearing malaria mosquito vectors. *Sci. Rep.* **2018**, *8*, 17807. [CrossRef] [PubMed]
36. Gonzales, K.K.; Hansen, I.A. Artificial diets for mosquitoes. *Int. J. Environ. Res. Public Health* **2016**, *13*, 1267. [CrossRef]
37. Romano, D.; Stefanini, C.; Canale, A.; Benelli, G. Artificial blood feeders for mosquito and ticks-Where from, where to? *Acta Trop.* **2018**, *183*, 43–56. [CrossRef]

Heparin Administered to *Anopheles* in Membrane Feeding Assays Blocks *Plasmodium* Development in the Mosquito

Supplementary Material

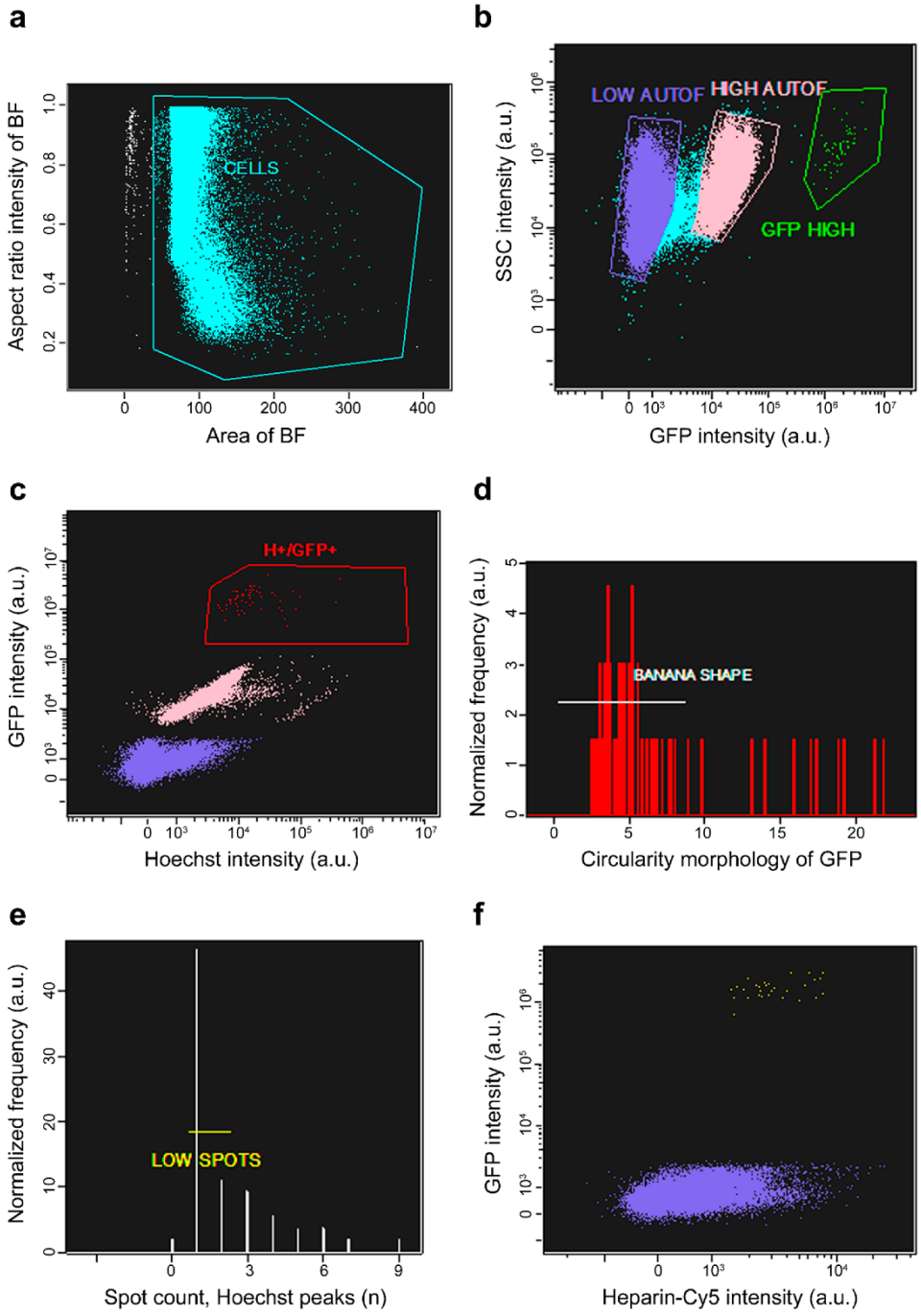

Figure S1. Gating strategy for Figure 1a. (**a**) in a dot plot of Aspect ratio intensity vs. Area of the bright field (BF) images of all events, a cell population was selected (CELLS). (**b**) in a dot plot of side scatter (SSC) intensity against GFP intensity, of the selected CELLS population, three different subgroups were defined: LOW AUTOFLUORESCENCE, HIGH AUTOFLUORESCENCE, and GFP HIGH. (**c**) Again plotting the CELLS population, the HIGH

AUTOFLUORESCENCE subgroup was confirmed to be also autofluorescent in the Hoechst channel. The H+/GFP+ subgroup corresponds to GFP HIGH in panel **b**. (**d**) To select mature ookinetes, the H+/GFP+ subgroup was analysed using a circularity morphology mask from IDEAS® software, selecting elongated, or BANANA SHAPE, cells, indicative of mature ookinetes. (**e**) using the BANANA SHAPE population, the number of Hoechst peaks was analysed with a spot count mask, where the cells with the lowest number of peaks are the LOW SPOTS population. (**f**) LOW SPOTS were mature non-aggregated ookinetes in the sample, plotted together with the LOW AUTOFLUORESCENCE subgroup for comparison. The differences in Cy5 intensity between stained and non-stained samples were then analyzed. The HIGH AUTOFLUORESCENCE subgroup had a similar difference in Cy5 intensity as the LOW AUTOFLUORESCENCE subgroup, but only this one was plotted to facilitate data interpretation. LOW SPOTS subgroup had n of 23, 8 and 6 in the 3 experimental samples, and 5, 3 and 4 in the 3 controls. LOW AUTOFLUORESCENCE subgroup had n of 37258, 47999 and 34332 in the 3 experimental samples and 14819 and 11681 in the controls.

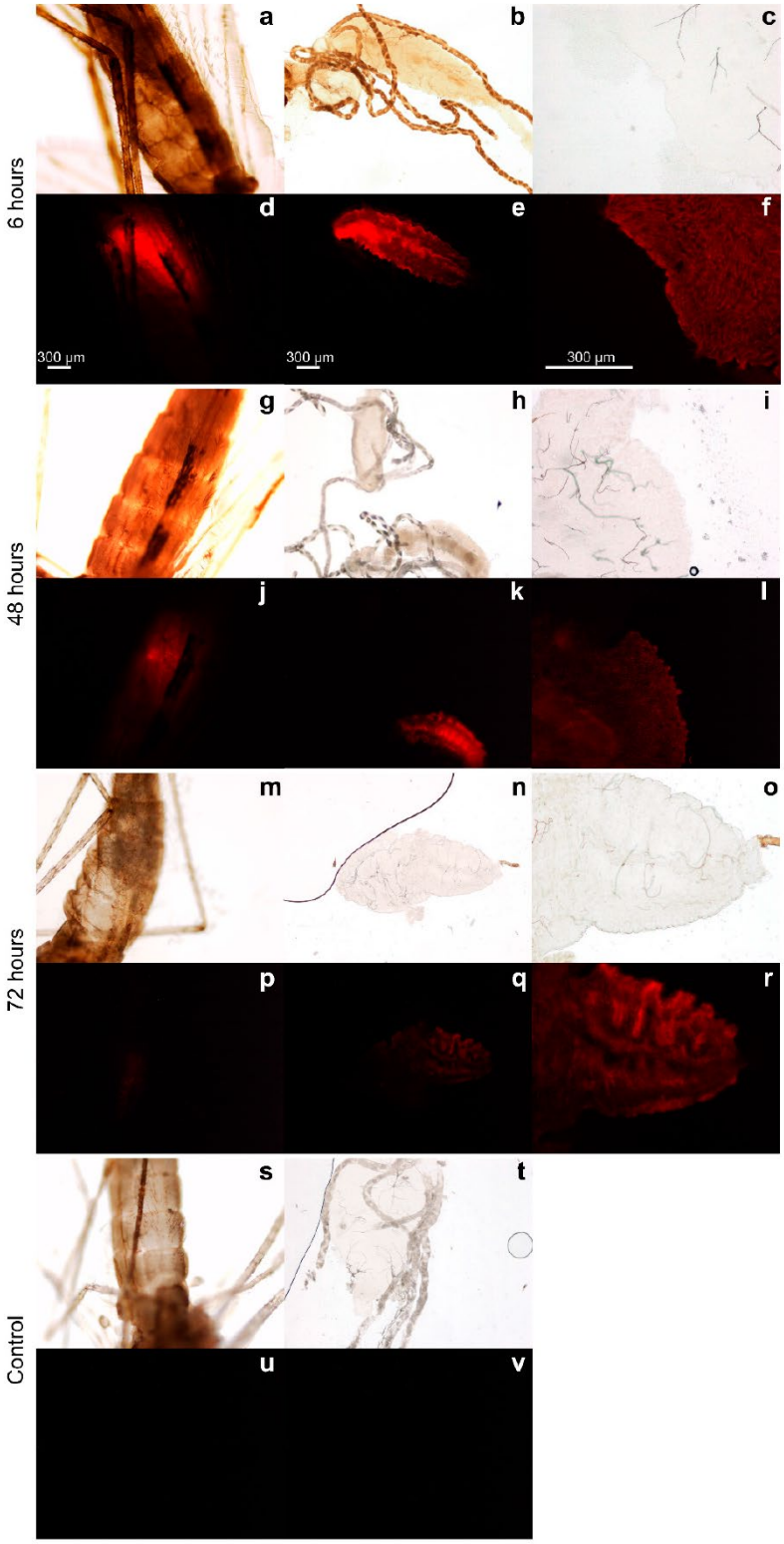
6 hours
48 hours
72 hours
Control
a
b
c
d
e
f
g
h
i
j
k
l
m
n
o
p
q
r
s
t
u
v
300 µm
300 µm
300 µm

4

Figure S2. Photomicrograph gallery of different time points after heparin-Cy5 administration in sugar feed. (**a-c**, **g-i**, **m-o**) Bright field images of mosquito abdomens (**a**,**g**,**m**), dissected midguts (**b**,**h**,**n**) and magnified images of dissected midguts (**c**,**i**,**o**), taken at 6 (**a-c**), 48 (**g-i**), and 72 h after administration (**m-o**). (**d-f**, **j-l**, **p-r**) Below each photomicrograph is the Cy5 fluorescence image of the same region. The non-fluorescent midgut in **h** comes from a non-fed mosquito. (**s-v**) Bright field images of the abdomen (**s**), and dissected midgut (**t**) of a sugar-only-fed control mosquito taken at 6 h after administration, and fluorescence images of the same regions (**u**,**v**, respectively) in the Cy5 emission channel (autofluorescence control).

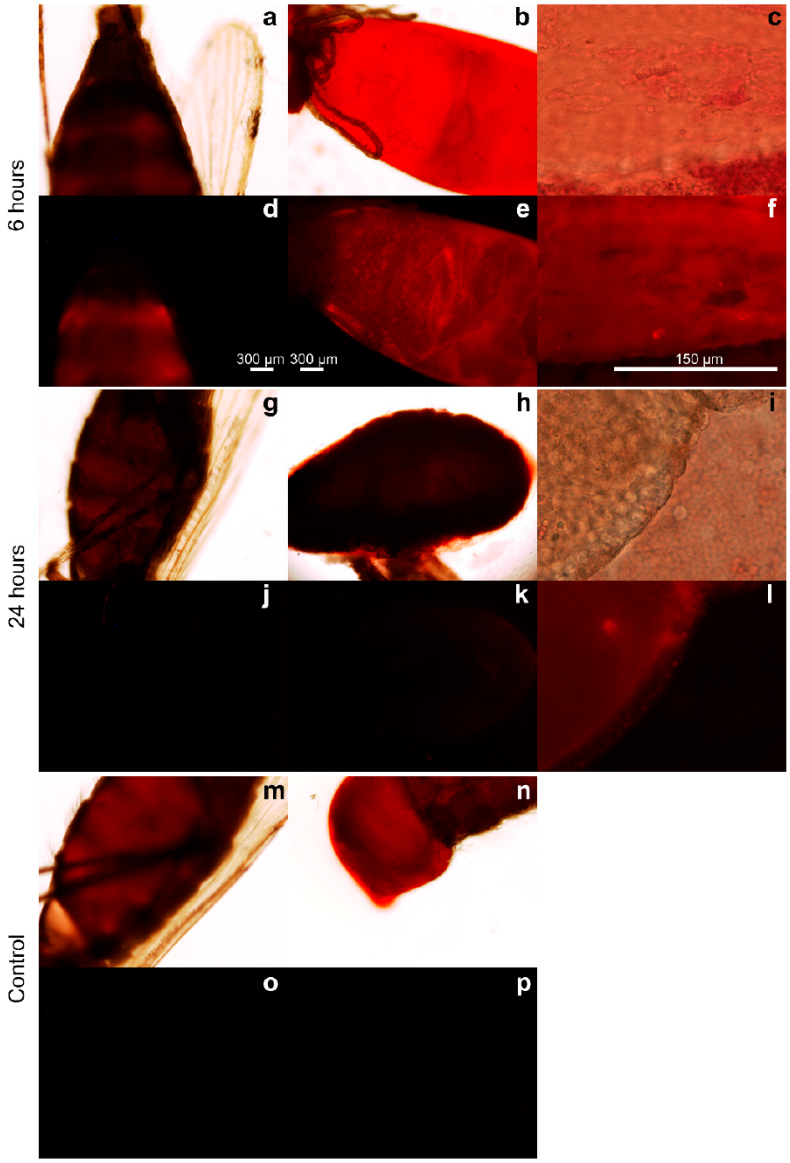

Figure S3. Photomicrograph gallery of different time points after heparin-Cy5 administration in MFA. (**a**-**c**, **g**-**i**) Bright field images of mosquito abdomens (**a**,**g**), dissected midguts (**b**,**h**) and magnified images of dissected midguts after having pushed out the blood bolus (**c**,**i**), taken at 6 (**a**-**c**) and 24 h after administration (**g**-**i**). (**d**-**f**, **j**-**l**) Below each photomicrograph is the Cy5 fluorescence image of the same region. Occasionally, Cy5 fluorescence was not observed in the intact abdomen (**j**), and only faintly in the dissected midgut (**k**), but it intensified after having pushed out the blood bolus (**l**). This might result from light being absorbed or screened by the compacted blood bolus. (**m**,**n**) Bright field images of the abdomen (**m**), and partially dissected midgut (**n**) of a blood-only-fed control mosquito taken at 6 h after administration. (**o**,**p**) Fluorescence images of the same regions in the Cy5 emission channel (autofluorescence control).

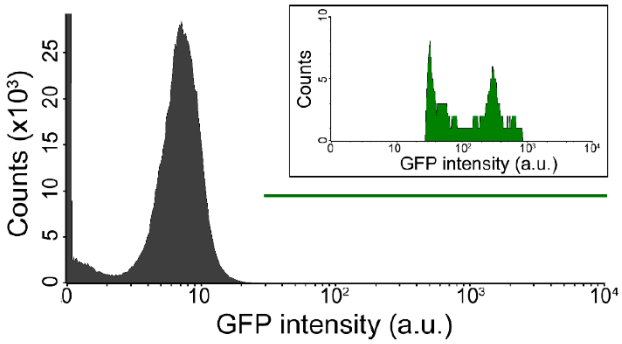

Figure S4. Gating strategy for the data analysis presented in Figure 4b. All the events were analysed in a histogram according to their GFP intensity, and cells were considered GFP-positive when their fluorescence was in the region indicated with a green line. The inset contains a histogram showing an example of GFP-positive events.

Table S1. GFP-positive events (n) and corresponding percentages presented in Figure 4b. Percentages were used for calculating fold change relative to the control in each experiment.

Time (h)	Sample	Replicate	Experiment 1		Experiment 2		Experiment 3	
			GFP-positive events	% of GFP-positive	GFP-positive events	% of GFP-positive	GFP-positive events	% of GFP-positive
0	Heparin 5 µg/mL	1	280	0.0151	462	0.1064	645	0.1381
		2	293	0.0144	458	0.0988	457	0.1142
		3	290	0.0195	465	0.0983	456	0.1114
	Heparin 500 µg/mL	1	262	0.0124	458	0.0753	459	0.0871
		2	278	0.0176	464	0.0789	460	0.0708
		3	283	0.0129	456	0.0659	461	0.0648
	Control	1	193	0.0087	407	0.0240	388	0.0174
		2	212	0.0117	458	0.0420	461	0.0219
		3	303	0.0136	459	0.0468	455	0.0232
1	Heparin 5 µg/mL	1	-	-	357	0.0160	78	0.0035
		2	-	-	290	0.0130	82	0.0041
	Heparin 500 µg/mL	1	268	0.0148	376	0.0169	117	0.0053
		2	277	0.0161	407	0.0198	117	0.0053
		3	275	0.0158	-	-	-	-
	Control	1	-	-	458	0.0215	139	0.0062
		2	-	-	267	0.0133	145	0.0072

Article 3: Development of DNA Aptamers Against *Plasmodium falciparum* Blood Stages Using Cell-Systematic Evolution of Ligands by EXponential Enrichment

Authors: Elena Lantero, Alexandros Belavilas-Trovas, Arnau Biosca, Paula Recolons, Ernest Moles, Elena Sulleiro, Francesc Zarzuela, Yunuen Ávalos-Padilla, Miriam Ramírez, and Xavier Fernàndez-Busquets

Journal: *Journal of Biomedical Nanotechnology*

Volume: 16

Issue: 3

Pages: 315-334

Publication date: 22nd of April 2020

DOI: 10.1166/jbn.2020.2901

Journal Impact Factor: 4.483

Categories: Pharmaceutical Science (Q1), Bioengineering (Q2), Biomedical Engineering (Q2), Materials Science (miscellaneous) (Q2), Medicine (miscellaneous) (Q2), Nanoscience and Nanotechnology (Q2)

Abstract:

New biomarkers have to be developed in order to increase the performance of current antigen-based malaria rapid diagnosis. Antibody production often involves the use of laboratory animals and is time-consuming and costly, especially when the target is Plasmodium, whose variable antigen expression complicates the development of long-lived biomarkers. To circumvent these obstacles, we have applied the Systematic Evolution of Ligands by EXponential enrichment method to the rapid identification of DNA aptamers against Plasmodium falciparum-infected red blood cells (pRBCs). Five 70 b-long ssDNA sequences, and their shorter forms without the flanking PCR primer-binding regions, have been identified having a highly specific binding of pRBCs versus non-infected erythrocytes. Structural analysis revealed G-enriched sequences compatible with the formation of G-quadruplexes. The selected aptamers recognized intracellular epitopes with apparent Kds in the ?M range in both fixed and non-fixed saponin-permeabilized pRBCs, improving >30-fold the pRBC detection in comparison with aptamers raised against Plasmodium lactate dehydrogenase, the gold standard antigen for current malaria diagnostic tests. In thin blood smears of clinical samples the aptamers reported in this work specifically bound all P. falciparum stages versus non-infected erythrocytes, and also detected early and late stages of the human malaria parasites Plasmodium vivax, Plasmodium ovale and Plasmodium malariae. The results are discussed in the context of their potential application in future malaria diagnostic devices.

Article

Journal of
Biomedical Nanotechnology
Vol. 16, 315–334, 2020
www.aspbs.com/jbn

Development of DNA Aptamers Against *Plasmodium falciparum* Blood Stages Using Cell-Systematic Evolution of Ligands by EXponential Enrichment

Elena Lantero[1, 2, 3], Alexandros Belavilas-Trovas[1, 2, 3], Arnau Biosca[1, 2, 3], Paula Recolons[1, 2, 3], Ernest Moles[4, 5, 6], Elena Sulleiro[7], Francesc Zarzuela[7], Yunuen Ávalos-Padilla[1, 2, 3], Miriam Ramírez[2], and Xavier Fernàndez-Busquets[1, 2, 3, *]

[1] *Nanomalaria Group, Institute for Bioengineering of Catalonia (IBEC), The Barcelona Institute of Science and Technology, Baldiri Reixac 10-12, ES-08028 Barcelona, Spain*
[2] *Barcelona Institute for Global Health (ISGlobal, Hospital Clínic-Universitat de Barcelona), Rosselló 149-153, ES-08036 Barcelona, Spain*
[3] *Nanoscience and Nanotechnology Institute (IN2UB), University of Barcelona, Martí i Franquès 1, ES-08028 Barcelona, Spain*
[4] *Children's Cancer Institute, Lowy Cancer Research Centre, UNSW Sydney, 2033 Randwick, NSW, Australia*
[5] *School of Women's and Children's Health, UNSW Sydney, 2052 Sydney, NSW, Australia*
[6] *ARC Centre of Excellence in Convergent Bio-Nano Science and Technology, Australian Centre for NanoMedicine, UNSW Sydney, 2052 Sydney, Australia*
[7] *Microbiology Department, Vall d'Hebron University Hospital (VHUH), Universitat Autònoma de Barcelona, ES-08035 Barcelona, Spain*

New biomarkers have to be developed in order to increase the performance of current antigen-based malaria rapid diagnosis. Antibody production often involves the use of laboratory animals and is time-consuming and costly, especially when the target is *Plasmodium*, whose variable antigen expression complicates the development of long-lived biomarkers. To circumvent these obstacles, we have applied the Systematic Evolution of Ligands by EXponential enrichment method to the rapid identification of DNA aptamers against *Plasmodium falciparum*-infected red blood cells (pRBCs). Five 70 b-long ssDNA sequences, and their shorter forms without the flanking PCR primer-binding regions, have been identified having a highly specific binding of pRBCs versus non-infected erythrocytes. Structural analysis revealed G-enriched sequences compatible with the formation of G-quadruplexes. The selected aptamers recognized intracellular epitopes with apparent K_ds in the μM range in both fixed and non-fixed saponin-permeabilized pRBCs, improving >30-fold the pRBC detection in comparison with aptamers raised against *Plasmodium* lactate dehydrogenase, the gold standard antigen for current malaria diagnostic tests. In thin blood smears of clinical samples the aptamers reported in this work specifically bound all *P. falciparum* stages versus non-infected erythrocytes, and also detected early and late stages of the human malaria parasites *Plasmodium vivax*, *Plasmodium ovale* and *Plasmodium malariae*. The results are discussed in the context of their potential application in future malaria diagnostic devices.

KEYWORDS: *Nanomedicine, Malaria, Plasmodium, Aptamers, Cell-SELEX.*

INTRODUCTION

Malaria, a parasitic disease caused by different species of *Plasmodium*, is one of the main causes of mortality in the tropical and subtropical world population. Although five species cause illness in humans, the most virulent and fatal is *Plasmodium falciparum*, especially when the infection occurs in young children and pregnant women [1]. The World Health Organization (WHO) Global Technical Strategy for Malaria 2016–2030 lists the universal access to malaria diagnosis as an essential part of the strategic framework that should eventually lead to eradicating the disease [2], since knowing parasitemia and parasite species is crucial in order to select the most appropriate drug treatment. Currently, national malaria programs rely on light microscopy and rapid diagnostic tests (RDTs),

*Author to whom correspondence should be addressed.
Email: xfernandez_busquets@ub.edu
Received: 9 March 2020
Accepted: 22 April 2020

which are not sensitive enough to detect low parasite density infections (sub-microscopic malaria in which patients are usually asymptomatic) that are key in the transmission dynamics. On the other hand, molecular techniques can detect sub-microscopic malaria, but are inadequate for massive use because of elevated costs or need for highly trained staff. Therefore, new diagnostic methods are needed if the objective is to advance towards malaria eradication [3, 4].

Although the parasite synthesizes a vast array of molecules to remodel its host red blood cell (RBC), those exported to the cell surface undergo rapid antigenic variation [5, 6]. This fast turnover of exposed antigens counsels a constant search for new therapeutic agents and diagnosis targets. Most current strategies for the identification of specific molecular tags in the malaria parasite or in *Plasmodium*-infected RBCs (pRBCs) rely on a detailed knowledge of the pathogen's physiology and of the pRBC biochemistry or the use of time-consuming and expensive immunological methods such as antibody generation. Alternatively, binding specificities and affinities comparable to those of monoclonal antibodies can be obtained with aptamers, short single-stranded (ss) oligonucleotides capable of specific ligand recognition, much faster and cheaper to produce without having to resort to the use of laboratory animals [7]. They can be either ssDNA or ssRNA, whose three-dimensional structures formed by their self-folding generates topological features that can specifically recognize molecular regions in a similar way as antibodies bind antigenic determinants. Aptamers are able to distinguish different protein isoforms [8], conformational isomers of the same molecule [9], and common structural epitopes in different proteins like those found in amyloid fibrils [10]. In most cases, aptamer binding to its target inhibits biological activity, e.g., due to interference with the catalytic site of an enzyme or with sites involved in ligand-receptor recognition, or to allosteric effects, such as changes in conformational states resulting in loss of function. Aptamers can be identified by *in vitro* selection against almost any target, including antigens which do not induce immune responses in host animals for antibody production, and small molecules like drugs and even metal ions [11]. The versatility of aptamers to recognize nearly any biomolecule in a very specific manner and their higher dry-storage and lyophilisation stability than antibodies makes them effective as diagnostic tools (aptasensors) [12] and attractive as potential therapeutics [13]. Nucleic acid aptamers, which are typically selected from extremely large libraries (containing $\geq 10^{13}$ different oligonucleotide sequences), can modulate the function of virtually any target of biological interest, making them a preferred method of choice for the identification of new bioactive ligands. For *in vivo* applications, aptamers can be chemically modified to confer them resistance against nucleases or tagged with fluorescent reporters and nanoparticles for subcellular localization and pull-down of target proteins [14], respectively.

Aptamers can be developed by Systematic Evolution of Ligands by EXponential enrichment (SELEX) [15–18], which uses iterative *in vitro* selection of combinatorial RNA or DNA pools against a molecular target for the identification of high-affinity oligonucleotide ligands. The method starts by exposing the molecule of interest to a randomly generated ssDNA or RNA library, retrieving the aptamer/target complexes. The binding oligonucleotides are subsequently amplified in a thermal cycler and the resulting PCR products are dissociated in their complementary single strands, which enter again an affinity selection cycle. This process is repeated as many times as it takes to obtain a pool of oligonucleotides specifically binding the selected target. SELEX has been successfully used to obtain aptamers for diagnostic use in infectious diseases [19, 20]. The development of DNA aptamers against *Plasmodium* proteins has been mostly focused on the design of new devices for malaria diagnosis by targeting the parasite's lactate dehydrogenase (LDH) [21–25]. RNA ligands against recombinant *P. falciparum* erythrocyte membrane protein 1 (PfEMP1) have been shown to disrupt aggregates of pRBCs with non-infected erythrocytes (rosettes) that contribute to the pathology of severe malaria by clogging the microvasculature [26]. An attempt to develop therapeutic antimalarial aptamers selected DNA sequences binding the heme group released from hemoglobin as the protein is used as food source by the intraerythrocytic parasite; the resulting suppression of the heme detoxification pathway inhibited *Plasmodium* growth *in vitro* [27].

The variant called cell-SELEX [28–30] uses as targets whole cells or cell membranes [31], and it can be a powerful tool in the discovery of new ligands, as there is no need for prior knowledge of antigenic features. Using whole cells as targets, aptamers can be selected to bind biomarkers differing between two given cell types or between healthy and diseased cells [28, 32]. The capacity of this method for the isolation of high-affinity oligonucleotides against such a complex target as the RBC membrane has been reported [31]. Cell-SELEX offers promising perspectives for the selection of aptamers targeting parasite-derived surface proteins, e.g., in *Trypanosoma* and *Plasmodium* [33, 34]. Its full potential as tool for cell surface target discovery has not been deeply probed yet, but the application of aptamer technology has been proposed for the implementation of new adjunct therapies to be used in current malaria treatments [26, 35]. Presence of surface proteins related to adhesion and sequestration of parasites is widely known [36], although these are easily lost in the cultured lines of *P. falciparum* without any selection pressure. The high variability in these proteins, a mechanism evolved by the pathogen to escape immune system surveillance [37], increases the difficulty of ligand molecule selection.

In this work we present our results on the development of DNA aptamers against pRBCs infected by *P. falciparum*, with the objective of establishing a method for the rapid identification of new markers for malaria diagnosis that could be also of use in future vaccination or targeted therapeutic strategies.

EXPERIMENTAL DETAILS

Preparation of Target Cells

Unless otherwise indicated, oligonucleotides and other reagents were purchased from Sigma–Aldrich. The *P. falciparum* 3D7 strain was grown *in vitro* in group B human erythrocytes using previously described conditions [38]. Parasites (thawed from glycerol stocks) were cultured at 37 °C in T-25 or T-175 flasks (Thermo Fisher Scientific, Rochester, NY, USA) containing human erythrocytes at 3% hematocrit in Roswell Park Memorial Institute (RPMI) complete medium containing Albumax II (Gibco™), supplemented with 2 mM L-glutamine, under a gas mixture of 92.5% N_2, 5.5% CO_2, and 2% O_2. RBCs parasitized with late-form trophozoite and schizont parasite stages corresponding to 24–36 h and 36–48 h post-invasion (hpi), respectively, were purified in 70% Percoll (GE Healthcare, Chicago, USA) [39, 40]. Parasitemia was determined by microscopic counting of blood smears fixed briefly with methanol and stained for 10 min with Giemsa (Merck Chemicals) diluted 1:10 in Sorenson's buffer, pH 7.2. For culture maintenance, parasitemia was kept below 5% late forms and 10% early forms by dilution with freshly washed RBCs and the medium was changed every 1–2 days. Percoll-purified late stages were pelleted (800× g, 6 min) and subjected to fixation in 4% paraformaldehyde followed by cryopreservation at −80 °C in 44% glycerol, 20 g/L sodium lactate, 230 mg/L KCl, and 12 g/L sodium phosphate, pH 6.8. Non-parasitized RBCs from the same blood batch were also cryopreserved and, when required after thawing, fixed as above for their use in counter-SELEX cycles (see below).

SELEX Cycles

For the generation of pRBC-specific DNA aptamers using the SELEX technique (Fig. 1), a single-strand nucleic acid library with invariant PCR primer-binding flanking regions on each end and a randomized central sequence of 40 nucleotides (**ATACCAGCTTATTCA ATT**NNNNNNNNNNNNNNNNNNNNNNNNNNNNNNNNNNNNNNNNNN**AGATAGTAAGTGCAATCT**, 1 μmol) was purchased from DNA Technology A/S (Denmark). 10 nmol of this DNA library was dissolved in 1 mL of RPMI supplemented with 25 mM HEPES, 5 mM $MgCl_2$ and 1 mg/mL BSA, pH 7.4 (binding buffer) and subjected to a first counter-SELEX negative selection process, whereby it was incubated with ca. 10^6 fixed RBCs that had been previously washed three times in washing medium (binding buffer without BSA). Prior to addition to the cells, the library was incubated at 95 °C for 5 min followed by a 10-min incubation in ice. The cells and library mixture was incubated in ice for 1 h under constant stirring (50 rpm), spun down (500× g, 3 min) to remove RBC-binding sequences, and the supernatant containing the free oligonucleotides that did not bind RBCs was added to fixed pRBCs for the next positive selection cycle. This counter-selection step with non-parasitized erythrocytes was repeated again before rounds 4, 7 and 10. After incubation and pull down steps as above, the pelleted cells were rinsed 3 times with washing medium, taken up in 200 μL of double deionized water (ddH_2O; MilliQ system, Millipore) and heated up to 95 °C for 10 min before proceeding to thermal cycler amplification.

pRBC-binding sequences were PCR amplified following the procedures described by Sambrook and Russell [41], using *Taq* DNA polymerase (PCR Master Mix 2×, Thermo Fisher Scientific). As a rule, 20 cycles were programmed in a DNA 2720 Thermal Cycler (Applied Biosystems) 94 °C/56 °C/72 °C, 30 s each, with a 1-min 94 °C extra incubation before the first cycle. The 5′ ends of forward (5′-ATACCAGCTTATTCAATT-3′) and reverse (5′-AGATTGCACTTACTATCT-3′) primers were derivatized with 6-carboxyfluorescein (6-FAM) and tri-biotin, respectively. The PCR mix was distributed in 30 tubes containing 50 μL of reaction each. The resulting amplification products were precipitated by addition of 0.1 vol of 3 M sodium acetate, pH 5, and 2.5 vol of absolute ethanol, thoroughly mixed, and stored overnight at −20 °C. After centrifugation (20,000× g, 45 min, 4 °C), the DNA pellet was washed with 70% ethanol, spun down for 15 min in the same conditions as above, and dried by solvent evaporation for 35 min in a SpeedVac concentrator (SPD 1010, Savant). Finally, the dry pellet was taken up in washing buffer (30 mM HEPES, 500 mM NaCl, 5 mM EDTA, pH 7).

To purify the forward strand, the PCR-amplified DNA (carrying a tri-biotin tag in the reverse strand) was mixed with NeutrAdivin™ High Capacity Agarose Resin (Thermo Fisher Scientific) and loaded in a Micro Bio-Spin chromatography column (Bio-Rad). Columns were washed 16 times with washing buffer before DNA addition, and 10 times afterwards. To elute the forward strand (carrying a 6-FAM tag), 400 μL of 0.1 M NaOH were added to the column, which was subsequently vortexed (30 s) and centrifuged (500× g, 30 s). 3 elutions were performed and immediately neutralized with 0.1 vol of 1 M HCl. The eluted ssDNA was precipitated as above and taken up in binding buffer. This fluorescein-labeled oligonucleotide entered a second identical SELEX cycle and this process was repeated for 10 such rounds of binding and selection, until a set of aptamers was identified that bound pRBCs with the desired specificity and affinity as assessed by fluorescence microscopy and flow cytometry. Finally the selected sequences were subcloned and synthesized in

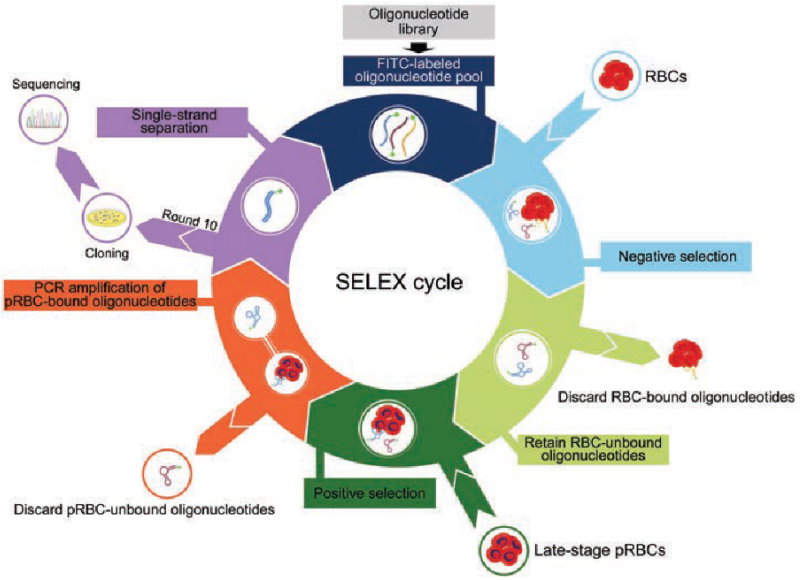

Figure 1. **Scheme of the SELEX process used in this work to obtain DNA aptamers against late-stage pRBCs.**

sufficiently large amounts for the characterization of their binding to pRBCs.

Fluorescence Microscopy and Flow Cytometry Analysis

P. falciparum 3D7 cultures (either fixed, permeabilized non-fixed, or live) and fixed *P. falciparum* NF54 *gexp02-tdTomato* stage IV gametocytes, induced by choline removal [42], and selected by addition of 50 mM *N*-acetyl-D-glucosamine (choline-sensitive transgenic line kindly provided by Portugaliza et al. [43]) were incubated in the presence of 120 pmol of oligonucleotides labeled in their 5′ ends with 6-FAM (λex/em: 488/525 nm) for 60 min in binding buffer at 4 °C with gentle stirring. Aptamers had been previously pretreated by incubating them for 5 min at 95 °C in washing medium at 10× their final concentration, followed by a 10-min incubation on ice. After rinsing with washing medium, cells were stained for 30 min with 4 μg/mL of the DNA dye Hoechst 33342 (λex/em: 350/461 nm), rinsed with washing medium and placed in a 8-well LabTek chamber slide system (Lab-Tek®II, catalog number 155409). For clinical sample testing, blood was obtained by venous puncture with a syringe and was placed in a tube with 6 mM EDTA as anticoagulant. A drop of blood (3 to 5 μL) was deposited on one end of a microscope slide and gently extended with another slide. Informed consent was obtained from all blood donors. The preparations were allowed to dry for at least 3 hours before fixing them in methanol:acetone 1:9 prior to incubating with the aptamers. Fluorescence microscopy analysis was done with an Olympus IX51 fluorescence microscope or with a Leica TCS SP5 laser scanning confocal microscope equipped with a DMI6000 inverted microscope, blue diode (405 nm), Argon (458/476/488/496/514 nm), diode pumped solid state (561 nm) and HeNe (594/633 nm) lasers, and a PLAN APO 63× oil (NA 1.4) immersion objective lens. Non-fixed pRBC cultures were permeabilized with 0.1% w/v saponin in phosphate buffered saline (PBS) for 15 min, rinsed 3 times with washing medium, and treated as above.

For flow cytometry analysis, pRBCs were diluted in PBS to a final concentration of 1–10 × 10^6 cells/mL, and samples were analyzed using a LSRFortessa™ flow cytometer (BD Biosciences) set up with the 5 lasers, 20 parameters standard configuration. The single-cell population was selected on a forward-side scatter scattergram. The fluorochromes Hoechst 33342, 6-FAM, TAMRA or tdTomato, and Alexa Fluor 647 (streptavidin label for detection of biotinylated aptamers) were excited using 350, 488, 561 and 640 nm lasers, and their respective emissions collected with 450/40, 525/40, 582/15 and 730/45 nm filters.

Subcloning and Sequencing of Candidate Oligonucleotides and 2-D Structure Analysis

After 10 rounds of selection, the enriched oligonucleotide pool was PCR-amplified using unlabeled forward and reverse primers and *Pfu* DNA polymerase (Biotools). The resulting products were cloned into the pBluescript SK+ plasmid after its linearization with *Sma*I (New England Biolabs) using T4 DNA Ligase (New England Biolabs) and the ligation product was used for the transformation of heat-shock competent TOP10 *Escherichia coli*

cells (Thermo Fisher Scientific). The transformed cells were grown overnight at 37 °C in Luria Broth agar plates and the recombinant colonies were differentiated with the blue/white screening method after the induction of *lacZ* expression in the presence of X-gal and IPTG. White clones were randomly chosen from the plates and their plasmids were isolated with the GeneJET Plasmid Miniprep Kit (Thermo Fischer Scientific). The successful insertion of sequences from the original library was validated by PCR with the specific forward and reverse primers and by digestion with the restriction enzymes *Not*I and *Sal*I (New England Biolabs); in both approaches DNA bands with the expected lengths were detected in agarose gels. The positive clones were finally sequenced using T7P universal primers (Sanger sequencing service, GENEWIZ GmbH, Leipzig, Germany; https://www.genewiz.com/en-GB/Public/Services/Sanger-Sequencing).

2-D structure analysis was done using the mfold web server (http://unafold.rna.albany.edu/) [44], completing the DNA folding form and selecting ion and temperature conditions present in our incubations (140 mM Na^- and 5.4 mM Mg^{2-}, 4 °C). The potential presence of G-quadruplexes was analyzed using the Quadruplex forming G-Rich Sequences (QGRS) Mapper (http://bioinformatics.ramapo.edu/QGRS/index.php) [45], which was applied for predicting the position and the G-score (likelihood to form a stable G-quadruplex).

Design of a Random Aptamer to be Used as Negative Control

A negative control aptamer (700) was designed by means of an in-house Python script that printed a random 40-base oligonucleotide with the following relative frequencies: A = 17.5%; T = 55%; C = 10% and G = 17.5%. These selected frequencies were obtained by analyzing the relative base frequency of aptamers 19, 24, 30, 77 and 78 (A = 11.2%, T = 17.9%, C = 16.3% and G = 54.6%), and by substituting the frequency of A for C, T for G, G for T and C for A). Frequencies were rounded to obtain an aptamer with a natural number of bases and the unmodified primer-binding sequences were finally added at both ends, obtaining the following oligomer: **ATACCAGCTT ATTCAATT**AGTTGTGGTTGCAACTTTTTATTATTTG TTCGTATCTTTA**AGATAGTAAGTGCAATCT**.

Determination of Apparent K_d and B_{max}

1×10^6 fixed *P. falciparum* 3D7 Percoll-purified trophozoites were incubated in the presence of fluorescein-labeled oligonucleotides (10 different dilutions in triplicates, from 4000 to 7.13 nM, in a final volume of 40 μL) for 60 min in binding buffer at 4 °C. After rinsing twice with washing medium, cells were diluted 1:10 in PBS immediately prior to analysis with a LSRFortessa™ flow cytometer set up with the 4 lasers, 18 parameters standard configuration. The single-cell population was selected on a forward-side scatter scattergram. 6-FAM was excited using a blue laser (488 nm), and its fluorescence collected through a 525/40 nm filter; mean fluorescence intensity was obtained using Flowing Software 2.5.1 (www.btk.fi/cell-imaging; Cell Imaging Core, Turku Centre for Biotechnology, Finland). The equilibrium dissociation constant (K_d) and density of receptors (B_{max}) [46] of the aptamer-cell interaction was obtained by fitting the dependence of intensity of specific binding on the concentration of the aptamers to the equation $Y = B_{max} X/(K_d + X)$ [32]. GraphPad Prism 6 (GraphPad Software, San Diego, USA) was used to plot the saturation curve, selecting analysis of binding by non-linear regression fit, considering one site and comparing total and non-specific (aptamer 700 used as reference) binding data.

Dot Blots and Western Blots

Protein extracts from 8 to 48 hpi parasites were sequentially obtained from a *P. falciparum* 3D7 culture tightly synchronized at ring stages (0 hpi) using a series of sorbitol lysis (7 vol of 5% sorbitol in ddH_2O was added to pelleted cultures and incubated at 37 °C for 7 min, then spun down and washed with washing medium before being placed again in culture conditions) combined with Percoll purification of late stages. Briefly, 2 sorbitol lysis were performed 36 hours apart, followed by a Percoll treatment 36 h after the second sorbitol, and then a final sorbitol was used to select ring stage parasites with a 8-h window after Percoll. Immediately after this last synchronization, cell samples were collected every 8 h, pulled down by centrifugation and washed twice with PBS supplemented with 1× Mini Protease Inhibitor Cocktail (cOmplete™, Roche; one tablet in 10.5 mL for 1× concentration), and then incubated with a 7-fold cell pellet volume of 0.15% saponin in PBS and 1× cOmplete™ at 4 °C for 15 min. Afterwards, samples were centrifuged at 10,000× g for 15 min and the supernatant was recovered (saponin extract fraction). The pellet was further washed 4–5 times, until there was no hemoglobin visible, and then resuspended in 1-fold cell pellet volume of 1% Triton X-100 in PBS supplemented with 1× cOmplete™ and incubated for 30 min at 4 °C. Then samples were centrifuged at 20,000× g for 30 min and the supernatant was recovered (Triton X-100 extract fraction). The remaining pellet was washed 2 times and taken up in 1-fold cell pellet volume of radioimmunoprecipitation assay (RIPA) buffer (150 mM NaCl, 10% glycerol, 2 mM EDTA, 0.5% sodium deoxycholate, 0.2% SDS, 0.1% Triton X-100, 40 mM tris-HCl, pH 7.6) supplemented with 1× cOmplete™. After 15 min incubation, the sample was vortexed for 1 min and sonicated for 30 s, and after a brief incubation (4 °C, 10 min), it was centrifuged (20,000× g, 4 °C, 15 min) and the supernatant was recovered (RIPA buffer extract fraction).

After determining protein concentration using the Pierce™ BCA Protein Assay Kit (Thermo Fisher Scientific) following the manufacturer's indications, cell extracts

were diluted to 0.2 μg protein/μL and 2 μL of them were placed on top of a preactivated polyvinylidene difluoride (PVDF) membrane (BioRad). When the dots dried, the membrane was blocked under orbital stirring (50 rpm) at RT for 1 h with 5% (w/v) skim milk powder in tris-buffered saline (TBS, 150 mM NaCl, 50 mM tris-HCl, pH 7.6) containing 0.05% Tween 20 ($TBSt_{0.05}$), washed again (3×, 5 min) in $TBSt_{0.05}$, and incubated with 600 nM biotin-labeled pretreated aptamer in $TBSt_{0.05}$ containing 0.1% (w/v) skim milk (1 h, RT). After 3 washes with $TBSt_{0.05}$ for 5 min each, the membrane was incubated with 1.5 μg/mL of streptavidin-Alexa Fluor 647 in $TBSt_{0.05}$ containing 0.1% (w/v) skim milk (30 min, RT). After 3 final washes with $TBSt_{0.05}$ for 5 min each, fluorescence images of the membrane strips were obtained with an ImageQuant™ LAS 4000 CCD camera system (GE Healthcare Life Sciences) using red epi-illumination and a R670 Cy5 filter.

For Western blots, 300 μg protein of RIPA fraction extracts from 40 to 48 hpi were loaded into a single-well 12.5% polyacrylamide gel and run for 45 min at 120 V. Then they were transferred overnight to a pre-activated PVDF membrane at 4 °C and 180 V. Membrane strips were washed (2×, 5 min) with TBS and processed as for dot blots but substituting the biotinylated aptamer plus fluorescent streptavidin step by a 1-h incubation with 600 nM 6-FAM-labeled aptamer, and detecting fluorescence with a Y515 filter. As an alternative protocol, electrophoresed extracts were in-gel fixed for 10 min with acetic acid/methanol/H_2O 1:4:5 (v/v/v) and washed (3× H_2O plus 3× washing medium). The gel was then placed in binding buffer to which pretreated fluorescein-labeled aptamers were added at a final concentration of 600 nM, incubated overnight and washed (3×, washing medium) before visualizing the gel in an ImageQuant™ LAS 4000 transilluminator, where the fluorescent bands were excised and processed for liquid chromatography with tandem mass spectrometry (LC-MS/MS) analysis.

Pull Down Assays

0.2 mg of streptavidin-coated magnetic beads (Dynabeads™ MyOne™ Streptavidin C1, Thermo Fisher Scientific) were washed 3 times by magnetic separation with 5 mM tris-HCl, 1 M NaCl, 0.5 mM EDTA, 5 mM $MgCl_2$, pH 7.5. After that, beads were resuspended in 200 μL of the same buffer containing 200 pmol of the biotinylated aptamers, and incubated for 1 h under rotation. Supernatant was removed and unspecific binding sites were blocked by incubation with 0.1% BSA (w/v) in PBS for 1 h. After 5 washes with PBS containing 0.1% Tween 20 (v/v), aptamer-coated beads were incubated overnight in 200 μL PBS with a Triton X-100 protein extract of a *P. falciparum* late stage culture containing 12 μg protein. Then the beads were washed 10 times in PBS supplemented with 145 mM NaCl. To elute bound material, beads were resuspended with Laemmli buffer (60 mM tris-HCl, 2% SDS (w/v), 10% glycerol (v/v), 5% 2-mercaptoethanol (v/v) and 0.002% bromophenol blue (w/v), pH 6.8) and heated up to 95 °C; the supernatants were recovered, loaded into a 12.5% polyacrylamide gel and run for 45 min at 120 V. After silver staining, gel slabs were cut for LC-MS/MS analysis.

In-Gel Tryptic Digestion of Proteins and LC-MS/MS Analysis

After cleaning gel slabs with 50 mM NH_4HCO_3, pH 8.0 (cleaning buffer, CB) and acetonitrile (ACN), the proteins were reduced with 20 mM DTT in CB (60 °C, 60 min) and alkylated in the same buffer supplemented with 50 mM iodoacetamide (RT, 30 min). Gel slices were covered in CB containing 0.1 μg trypsin (sequencing grade modified, Promega), and digested for 16 h at 37 °C. Tryptic peptides were extracted from the gel matrix with 10% formic acid (FA) and ACN washes, and finally dried in a vacuum centrifuge.

The dry peptide mixtures were analyzed by LC-MS/MS in a nanoACQUITY liquid chromatographer (Waters) coupled to a Linear Trap Quadrupole Orbitrap Velos (Thermo Scientific) mass spectrometer. The tryptic digests were resuspended in 1% FA solution, and an aliquot (2 μL) was injected for chromatographic separation. Peptides were trapped in a Symmetry C18TM trap column (5 μm; 180 μm by 20 mm; Waters) and separated using a C18 reverse-phase capillary column (75 μm Øi, 25 cm, nanoACQUITY, 1.7 μm BEH column, Waters). The gradient used for the elution of the peptides was 1 to 40% B in 30 min, followed by a gradient from 40% to 60% B in 5 min ((A) 0.1% FA in water; (B) 0.1% FA in ACN), with a 250 nl/min flow rate. Eluted peptides were subjected to electrospray ionization in an emitter needle (PicoTipTM, New Objective) with an applied voltage of 2000 V. Peptide masses (m/z 300–1600) were analyzed in a data-dependent mode where a full scan MS was acquired in the Orbitrap with a resolution of 60,000 FWHM at 400 m/z. Up to the 15th most abundant peptides (minimum intensity of 500 counts) were selected from each MS scan and then fragmented in the linear ion trap using collisionally induced dissociation (38% normalized collision energy) with helium as the collision gas. The scan time settings were: full MS: 250 ms (1 Microscan) and MSn: 120 ms. Generated ∗.raw data files were collected with Thermo Xcalibur (v. 2.2). A database was created by merging all human protein entries present in the Swiss Prot public database (v. 7/3/2019) with all entries for *P. falciparum* isolate 3D7 present in the public database Uniprot (v. 12/12/19). A small database with common laboratory protein contaminants was also added and ∗.raw

data files obtained in the LC-MS/MS analyses were used to search with the SequestHT search engine using Thermo Proteome Discoverer (v. 1.4.1.14) against the aforementioned database. Both target and a decoy database were searched to obtain a false discovery rate (FDR), and thus estimate the number of incorrect peptide-spectrum matches that exceeded a given threshold, applying preestablished search parameters (enzyme: trypsin; missed cleavage: 2; fixed modifications: carbamidomethyl of cysteine; variable modifications: oxidation of methionine; peptide tolerance: 10 ppm and 0.6 Da for MS and MS/MS spectra, respectively). To improve the sensitivity of the database search, the semi-supervised learning machine Percolator was used to discriminate correct from incorrect peptide spectrum matches. Percolator assigns a q-value to each spectrum, which is defined as the minimal FDR at which the identification is deemed correct (0.01, strict; 0.05, relaxed). These q values are estimated using the distribution of scores from decoy database search. The results were exported as Excel files and only proteins identified with at least two high confidence peptides (FDR $\leq$ 0.01) were considered.

Ethics Statement

The human blood used in this work for *P. falciparum in vitro* cultures was commercially obtained from the *Banc de Sang i Teixits* (www.bancsang.net). Blood was not specifically collected for this research; the purchased units had been discarded for transfusion, usually because of an excess of blood relative to anticoagulant solution. Prior to their use, blood units underwent the analytical checks specified in the current legislation. Blood clinical samples were obtained previous obtainment of the informed consent of the donors. Before being delivered to us, unit data were anonymized and irreversibly dissociated, and any identification tag or label had been removed in order to guarantee the non-identification of the blood donor. No blood data were or will be supplied, and the studies reported here were performed in accordance with the current Spanish *Ley Orgánica de Protección de Datos* and *Ley de Investigación Biomédica* and under protocols reviewed and approved by the Ethical Committee on Clinical Research from the *Hospital Clínic de Barcelona* (Reg. HCB/2018/1223, January 23, 2019) and by the Ethical Committee on Drug Research from the *Hospital Universitari Vall d'Hebron* (Reg. PR(AG)68/2020, February 28, 2020).

RESULTS

Design of a SELEX Protocol for the Identification of *Plasmodium*-Specific Aptamers

During its initial development for the search of pRBC-specific targets, the SELEX process was expected to present itself with a number of problems whose solutions might require the re-examination of standard protocols or

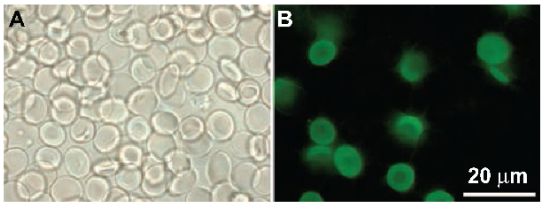

Figure 2. Obtention of cell-specific aptamers by SELEX. (A) Non-infected RBC preparation containing cells from different blood donors treated with a 6-FAM-labeled oligonucleotide pool selected in *P. falciparum* cultures grown using blood from one of the donors. (B) Confocal 6-FAM fluorescence microscopy image of the same microscope field.

the need for controls to be done months after the research started. In this scenario, the intrinsic variant expression of *Plasmodium* antigens [47] presented a significant obstacle if different parasite cultures were to be used throughout the selection, since their changing proteins would be a movable target precluding the enrichment of aptamers recognizing a particular epitope. In addition, if *Plasmodium* cultures had to be prepared weeks apart, different blood batches would need to be used; in preliminary assays where blood from different donors was employed, the SELEX protocol ended up with the unwilling selection of aptamers targeted to blood donor-specific RBC surface antigens (Fig. 2). To minimize these risks, we decided to grow a large pRBC batch cultured with erythrocytes from a single donor, fix it with paraformaldehyde, and store it in frozen aliquots in order to preserve a constant antigen collection throughout the protocol. Because the fixation method used does permeabilize the cells, the potential antigens to be identified could be intracellular pRBC molecules.

Fluorescence microscopy and flow cytometry analysis were used to follow the enrichment in 6-FAM-labeled pRBC-binding aptamers after each SELEX cycle (Fig. 3). Fluorescence microscopy images revealed an increase in the pRBC-associated fluorescein signal with each successive SELEX round, although the intensity of fluorescence in the first cycles was very low and is barely appreciated in Figure 3(A), where the microscope settings applied to all the SELEX rounds were those selected for a correct exposure of round 10. The higher sensitivity of flow cytometry, however, revealed an unexpected finding since even the PCR-amplified original aptamer library exhibited a significant binding to pRBCs relative to uninfected erythrocytes (Fig. 3(B)). With each cycle, the fluorescence signal associated to pRBCs increased whereas non-parasitized RBCs remained aptamer-free. The SELEX cycles were stopped at round 10, when the observed pRBC-associated fluorescence was not significantly different from that detected in round 9. Because the *P. falciparum* culture used in these fluorescence microscopy and flow cytometry analyses was prepared from a new blood batch and parasite stock, we

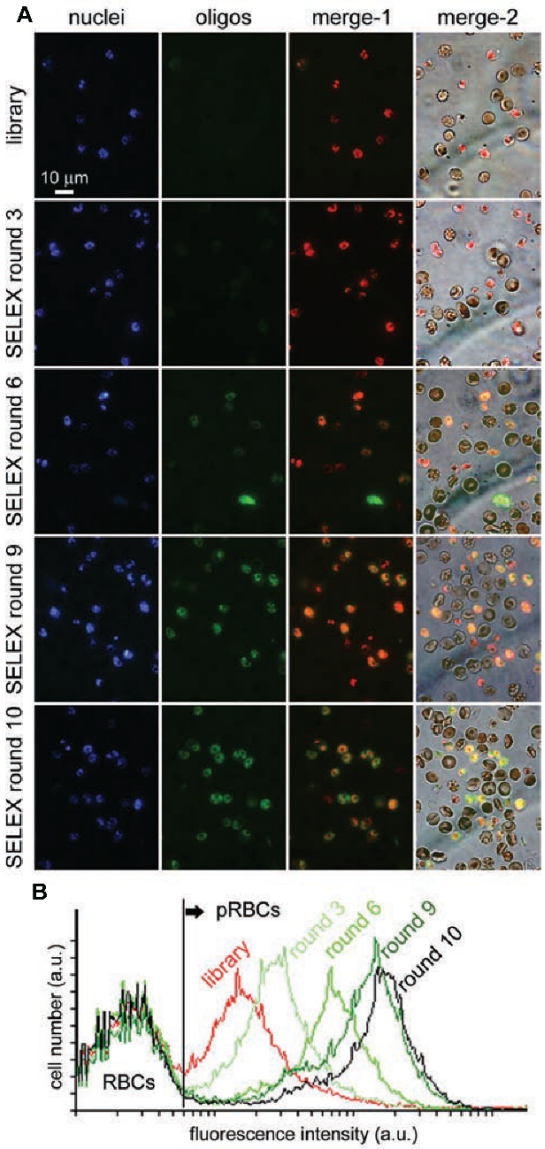

Figure 3. Progressive selection of pRBC-binding aptamers along the SELEX cycles. (A) Fluorescence microscopy of *in vitro P. falciparum* cultures treated with 6-FAM-labeled aptamer pools selected after SELEX rounds 3, 6, 9 and 10. For an easier identification of colocalizing pixels, the blue color has been changed to red in the merge images. Merge-1: Hoechst 33342 (nuclei) and 6-FAM (oligonucleotides) channels; merge-2: Merge-1 superimposed on phase contrast image. The cells used here belonged to a new fixed cell batch different from that used for the SELEX cycles. The microscope settings applied to all the SELEX rounds were those selected for a correct exposure of round 10. (B) Flow cytometry analysis of the same samples from panel A. a.u.: Arbitrary units.

concluded that the aptamers obtained recognized epitopes that are not exclusive of the original pRBC population used for SELEX selection.

Identification of Individual pRBC-Specific Aptamers

The fluorescence microscopy and flow cytometry data presented above suggested that SELEX round 10 was enriched in highly specific pRBC-binding aptamers. In consequence, we proceeded to subclone the round 10 oligonucleotide pool in order to obtain plasmids containing individual aptamers. Five such cloned sequences (aptamers 19, 24, 30, 77 and 78) were PCR-amplified using the fluorescein-labeled forward primer, and when added to fixed pRBC/RBC cocultures they exhibited a complete specificity of binding for pRBCs versus RBCs (Fig. 4).

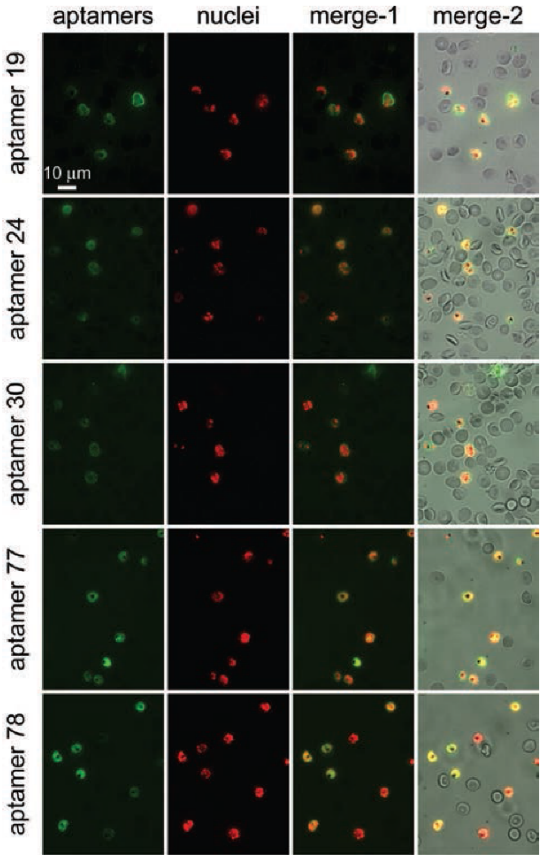

Figure 4. Fluorescence microscopy analysis of the pRBC versus non-infected RBC binding specificity of five selected aptamers PCR-amplified from individual clones using 6-FAM-labeled forward primers. The cells used here belonged to a new fixed cell batch different from that used for the SELEX cycles. For an easier identification of colocalizing pixels, the blue color of Hoechst 33342 has been changed to red.

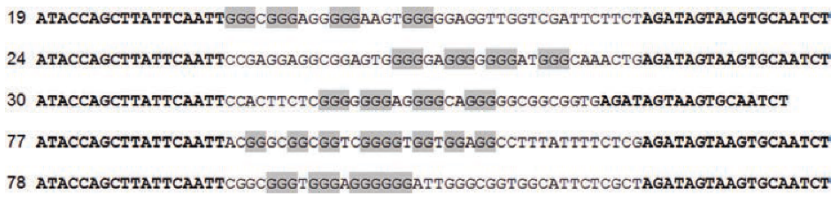

Figure 5. Sequences of the five oligonucleotides whose PCR amplifications using 6-FAM-labeled forward primers showed pRBC binding specificity versus non-infected RBCs. The PCR primer-binding sequences are indicated in bold; non-bold sequences correspond to the aptamers 19s, 24s, 30s, 77s and 78s. Shadowed in grey are the bases predicted to form G-quadruplexes.

After sequencing the five selected oligonucleotides, it was observed that the originally randomized central sequence of 40 nucleotides was in these 5 oligomers largely G-enriched (Fig. 5). Among different architectures, several aptamers have been described to adopt the G-quadruplex structure, which consists of planar arrays of four guanines, each one of them pairing with two neighbors by Hoogsteen bonding [48]. At least four GG pairs in close vicinity on an oligonucleotide sequence are required for G-quadruplex formation, and, according to 2-D structure analysis, this feature is present in all the five pRBC-binding aptamers that had been randomly subcloned from SELEX round 10 (Fig. 5 and Table I).

According to fluorescence microscopy imaging, the chemically synthesized fluorescein-labeled aptamers of these five selected sequences specifically bound pRBCs versus RBCs (Fig. 6(A)) of cell batches different from those used during the SELEX process, indicating that the cellular structures being detected are truly characteristic of *P. falciparum*-infected erythrocytes. The pRBC subcellular distributions of the aptamers were not identical; although cytosolic localization was evident for all of them, the sequences 19, 24 and 30 clearly labeled the host erythrocyte plasma membrane, whereas 77 and 78 colocalized with vesicular structures (Fig. 6(B)). pRBC versus RBC specific binding was quantitatively characterized by flow cytometry (Fig. 6(C)), which confirmed that the five selected aptamers bound ≥84.5% of late-stage pRBCs and ≤0.06% of non-parasitized RBCs (Table II). Aptamer 30 exhibited the most efficient pRBC recognition, binding 95.2% of late stages. A control aptamer (700), which was randomly synthesized but designed to contain a base composition well differentiated from that of the five selected sequences, bound ca. 19.6% of pRBCs. When 6-FAM was substituted by the reporter group TAMRA, binding specificity decreased significantly for aptamer 30 (Table II), suggesting an effect on oligonucleotide folding of the fluorescein group present on the aptamer 5′ end during the SELEX cycles.

Table I. G-scores or likelihood of G-quadruplex presence obtained with the QGRS mapper tool.

Aptamers	G-score
19	39
24	41
30	41
77	20, 21*
78	41

Note: *For aptamer 77, two different G-quadruplexes have been predicted.

Gametocytes, the sole *Plasmodium* stage that can be transmitted from the human to the mosquito vector, were occasionally observed to be also targeted by some aptamers (e.g., aptamer 30 in Fig. 6(A)), which led us to perform a detailed flow cytometry *in vitro* study of *P. falciparum* gametocyte targeting. The results obtained (Table III) indicate that the best performing aptamers bind >60% of gametocytes.

The aptamer 2008s, developed against *P. falciparum* LDH, has been postulated as an ideal biosensor for malaria diagnostic devices [22]. 2008s biotinylated in its 5′ end has been used in targeting analysis assays performed with purified LDH or with cell extracts [49, 50]. We have compared on fixed cells the targeting performance of biotin-2008s with that of the aptamers described here, all of them 5′-biotinylated (Table IV). The flow cytometry results obtained showed a >30 fold improvement in the detection of pRBCs with any of the five aptamers presented in this work relative to 2008s.

Removal of the PCR primer-binding flanking sequences had different effects on the pRBC targeting specificity of the variable 40-base oligonucleotides which were selected (Table II): whereas for aptamers 30 and 78 the change was small, for the other three sequences their shortened forms exhibited a more pronounced reduction in cell target binding, especially evident for oligonucleotide 19, whose late-stage pRBC affinity dropped from 93.0% to 58.5%. Similar variations between long and short forms were observed for gametocyte binding (Table III). According to flow cytometry data of whole cells, and consistently with the use of late-stage pRBCs for the SELEX cycles, early ring stages were not bound by any of the selected sequences. However, RIPA buffer extracts of all stages were positive for all five aptamers (see Fig. 7 for aptamer 19; data not shown for the other aptamers), indicating the presence from early rings to mature schizonts of the targeted epitope(s), whose presence dramatically increased along the intraerythrocytic parasite cycle.

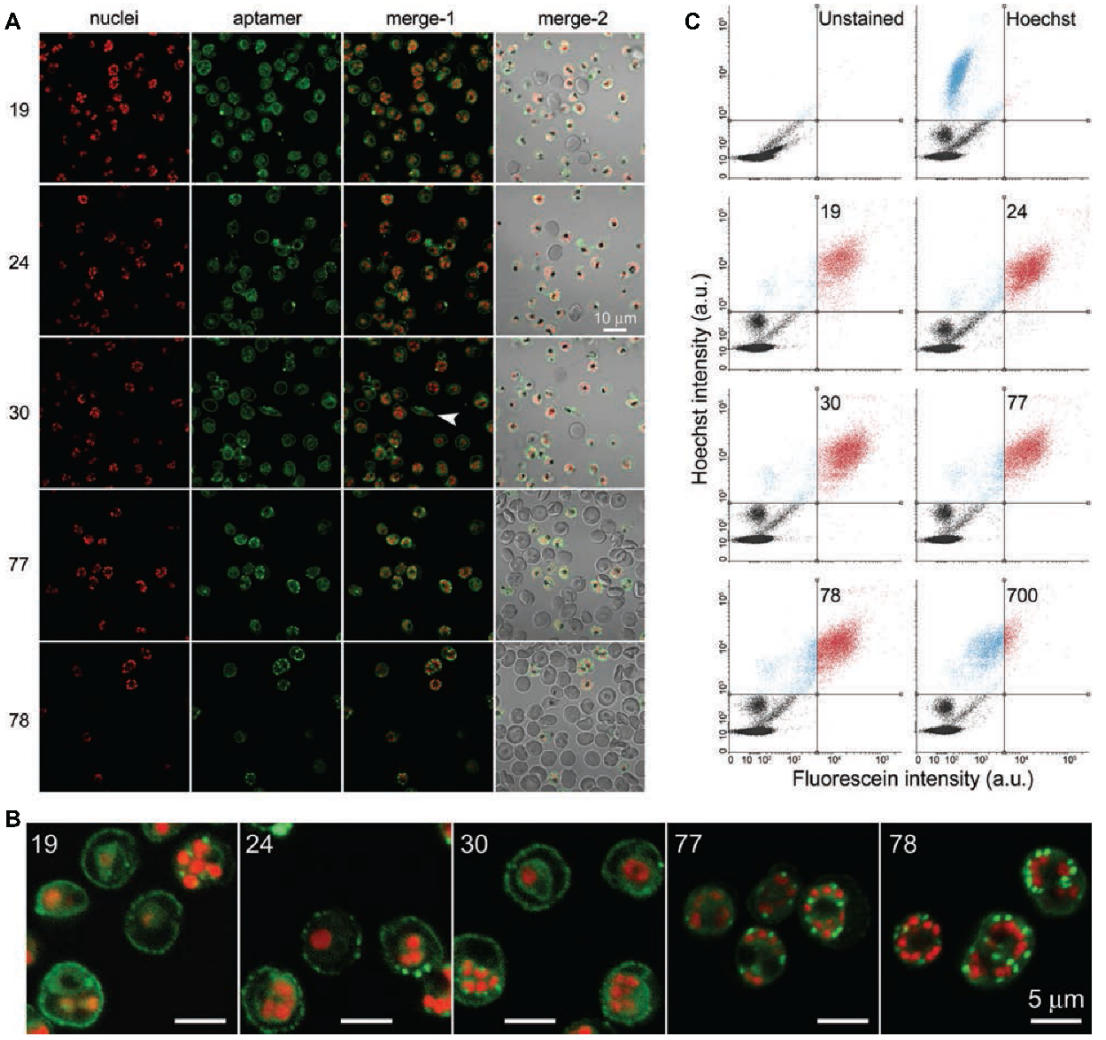

Figure 6. **pRBC versus non-infected RBC binding specificity analysis in fixed *P. falciparum* cultures of the chemically synthesized aptamers labeled with 6-FAM at the 5′ end. (A, B) fluorescence microscopy analysis of (A) cellular and (B) subcellular aptamer targeting. The arrowhead indicates a *P. falciparum* gametocyte. For an easier identification of colocalizing pixels, the blue color of Hoechst 33342 has been changed to red. (C) Quantitative flow cytometry analysis of aptamer targeting. For each panel, late-stage pRBCs are represented in the upper quadrants and 6-FAM-aptamer-bound cells are located in the right-hand quadrants. The cells used here belonged to a new fixed cell batch different from that used during the SELEX cycles. a.u.: Arbitrary units.**

Calculation of Apparent K_d, Apparent B_{max}, and Preliminary Sensitivity Evaluation of *Plasmodium*-Specific Aptamers

The apparent affinity for target cells of the selected fluorescein-labeled aptamers was measured by incubating serial dilutions of them with fixed 3D7 *P. falciparum* trophozoites, using the random sequence of aptamer 700 as nonspecific binding control (Fig. 8 and Table V). Upon removal of the flanking PCR primer-binding sequences (to obtain aptamers 19s, 24s, 30s, 77s and 78s) the new apparent K_d for aptamers 24 and 77 did not change significantly (1.14/1.07 and 1.07/0.90, respectively), whereas for oligonucleotides 19, 30 and 78 the shorter forms had a lower affinity for pRBCs (apparent K_d values: 0.46/1.10, 0.61/1.53, and 0.33/1.77, respectively). Although the differences in apparent K_d between aptamers might be due to the particular concentrations of their respective antigens in the cells if the aptamers are targeting different molecules, the disparities between full-length aptamers and the same sequences after removal of

Table II. Percentage of fixed late stage pRBC/non-parasitized RBC binding of the different aptamers determined from flow cytometry data.

Aptamer	6-FAM-aptamer (%)	6-FAM-aptamer – flanking sequences (%)	TAMRA-aptamer (%)
19	93.04/0.02	58.47/0.01	94.39/0.23
24	94.38/0.06	84.16/0.01	94.10/0.07
30	95.16/0.01	96.45/0.01	6.49/0.00
77	88.27/0.00	77.89/0.00	83.73/0.03
78	84.47/0.00	82.79/0.00	87.24/0.05
700	19.60/0.00	Not determined	Not determined

the primer sequences are expected to be mostly influenced by the change in affinity of the oligonucleotides for their corresponding antigens as the primer-binding regions of their sequences are eliminated.

Four out of the five short aptamers (with exception of 19s) improved in B_{max} relative to the full-length sequences, suggesting that they were able to bind more target sites inside cells, since these shortened sequences likely encounter less steric impediments due to their smaller size. Therefore, a decrease in antigen affinity can be compensated by more available ligands. As a preliminary evaluation of aptamer performance, a ratio can be established between the apparent B_{max} and the apparent K_d (binding potential, $BP = B_{max}/K_d$). The higher this relation, the better cell labeling by the corresponding oligonucleotide, since it will have either a lower K_d (and higher affinity) or a higher B_{max} (and more binding sites), or both. The aptamer ranking according to BP was 30s > 19 > 78 > 24s > 77s > 30 > 78s > 24 > 77 > 19s. No correlation was observed between the efficacy of aptamer target detection and the presence or absence of the PCR primer-binding sequences.

The changes in K_d, B_{max} and BP for each aptamer upon flanking sequence removal (Table VI) showed that whereas K_d decreased or timidly improved (+7% and +19% for 24/24s and 77/77s, respectively), B_{max} increased significantly for the shorter oligonucleotides except for 19/19s, where it fell by 70%. BP values indicated that when the primer-binding flanking sequences were absent, the overall

Table III. Percentage of fixed *P. falciparum* gametocyte/non-nucleated cell binding of the different aptamers determined from flow cytometry data.

Aptamer	6-FAM-aptamer (%)	6-FAM-aptamer – flanking sequences (%)
19	61.06/1.22	36.72/0.71
24	59.94/1.15	57.70/1.01
30	59.49/0.88	64.44/3.44
77	Not determined	43.94/0.58
78	58.42/0.86	49.04/0.61
700	12.17/0.73	Not determined

Table IV. Percentage of fixed late-stage pRBC binding of 5′-biotinylated aptamers determined from flow cytometry data.

	Labeled pRBCs (%)
Free streptavidin control	0.29
Aptamer 19	69.70
Aptamer 24	44.47
Aptamer 30	50.56
Aptamer 77	42.25
Aptamer 78	41.19
Aptamer 2008s (anti-LDH)	1.24

targeting performance ameliorated for 24/24s and, especially, for 30/30s and 77/77s, but it clearly worsened for 78/78s and still more significantly for 19/19s. These results indicated that eliminating the flanking sequences, which were not selected during the SELEX process, can in some cases result in a loss of aptamer binding affinity for the corresponding cell target.

Targeting assays with non-fixed, saponin-permeabilized cells revealed also a pRBC-specific binding of all 5 aptamers (Fig. 9 and Table VII), indicating that the observed specificity was not derived from a fixation artifact. RBCs burst at the saponin concentration used, and most cellular structures remaining in the sample were *P. falciparum* parasites bounded by their parasitophorous vacuole membrane (PVM), exhibiting characteristic rounded shapes slightly smaller than erythrocytes. RBC plasma membrane remains and other erythrocyte debris were still visible around some PVM-enclosed parasites (e.g., see aptamer 19 panel in Fig. 9(B)). Since all aptamers stained both the PVM (Fig. 9) and the pRBC plasma membrane (Fig. 6 and cell debris in Fig. 9), the

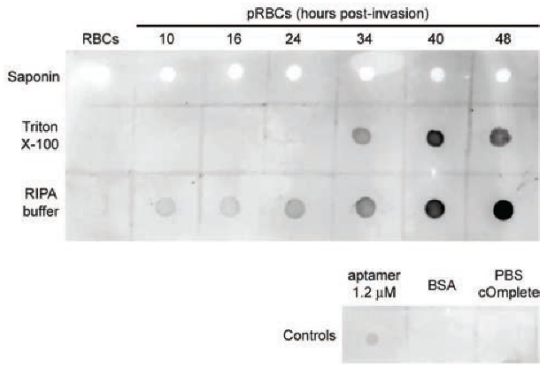

Figure 7. Dot-blot test of the presence in *P. falciparum* extracts of the epitope(s) recognized by 6-FAM-labeled aptamer 19. Saponin, Triton X-100, and RIPA buffer extracts were obtained at different hpi from a *P. falciparum in vitro* culture initially synchronized at ring stages. Each dot contains 0.4 µg of protein in 2 µL of PBS 1× cOmplete™ buffer. The controls include 2.4 pmol of biotin-labeled aptamer 19 and 0.4 µg of BSA, both in 2 µL of PBS 1× cOmplete™, plus the same volume of plain buffer.

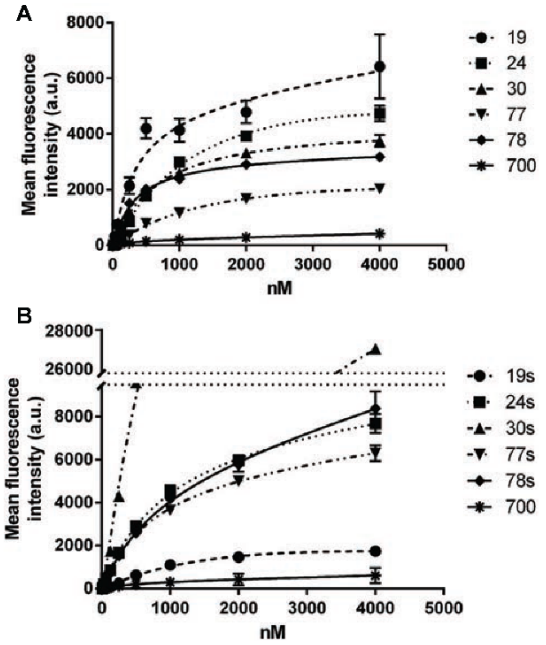

Figure 8. **Analysis of the binding affinity to *P. falciparum* 3D7 Percoll-purified trophozoites of the selected 6-FAM-labeled aptamers. (A) Full-length aptamers. (B) Aptamers lacking the flanking PCR primer-binding regions. a.u.: Arbitrary units.**

targeted epitope(s) likely correspond to parasite molecules that are exported to both cell membranes. This is in agreement with dot blot data (Fig. 7) indicating the presence of the sought-after antigen(s) in Triton X-100 and, especially, in RIPA buffer extracts, which contain cell membrane-bound components. However, targeting assays with live cells did not show binding of the aptamers to pRBCs (data not shown), which clearly suggested that the location of the epitope(s) being detected is intracellular and that the selected oligonucleotides are not able to cross plasma membranes in intact cells.

Table V. **Apparent K_d, B_{max}, and trophozoite binding potential (BP = B_{max}/K_d ratio) for the selected aptamers.**

Aptamer	Apparent K_d (μM)	Apparent B_{max} (a.u.)	BP (a.u.·μM^{-1})
19	0.46±0.08	6.18±0.36	13.4
24	1.14±0.11	5.63±0.23	4.9
30	0.61±0.04	3.91±0.09	6.4
77	1.07±0.12	2.06±0.10	1.9
78	0.33±0.03	3.13±0.07	9.4
19s	1.10±0.15	1.86±0.11	1.7
24s	1.07±0.06	8.50±0.22	8.0
30s	1.53±0.07	36.40±0.81	23.8
77s	0.90±0.06	6.53±0.18	7.3
78s	1.77±0.15	10.48±0.44	5.9

Table VI. **Variation in K_d, B_{max} and BP for full length versus flanking region-lacking aptamers.**

Aptamers	K_d variation	B_{max} variation	BP variation
19/19s	0.42	0.30	0.13
24/24s	1.07	1.51	1.61
30/30s	0.40	9.32	3.70
77/77s	1.19	3.17	3.79
78/78s	0.19	3.35	0.63

Pull-down assays using the aptamers bound to magnetic beads resulted in the detection of several pRBC proteins identified by LC-MS/MS (Table VIII). Western blots of late stage *P. falciparum* cultures probed with the fluorescein-labeled selected aptamers revealed for all of them dominant bands around 15 and 30 kDa (Fig. 10(A)). The aptamer 30s, which had the higher predicted BP (Table V), provided the strongest signal. This aptamer was used to directly probe a SDS-PAGE lane loaded with the same sample extract that had been analyzed in the Western blot. The main fluorescent band cluster at ca. 15-kDa (Fig. 10(B)) could be excised and subjected to LC-MS/MS analysis. Again, several *P. falciparum* proteins were identified (Tables IX–XI), being the putative 60S ribosomal protein L24 the only one that was also detected in pull-down assays with biotinylated aptamer 19. This result is however not conclusive and although, taken together, these data strongly suggest that all the selected aptamers recognize a single epitope that might be present in multiple parasite proteins, the efforts done to identify this antigen have been unsuccessful so far.

To assess the potential use for the future development of diagnostic devices of the selected aptamers, these were tested on clinical samples of malaria-infected blood that had been previously characterized by Giemsa staining (data not shown). Despite having been evolved against *in vitro* cultured trophozoite and schizont stages, all aptamers targeted ring-stage *P. falciparum* parasites (aptamer 24 targeting shown in Fig. 11; data not shown for the rest of aptamers), which are the main form present in thin blood smears of malaria patients. Whenever present, late stages were always efficiently targeted. Targeting of early and late blood stages was also observed for *Plasmodium ovale*, *Plasmodium vivax* and *Plasmodium malariae* clinical samples (Fig. 12).

DISCUSSION

In 2018, around 228 million cases of malaria occurred worldwide, compared with 251 million in 2010 and 231 million in 2017, and the disease caused an estimated 405,000 deaths. In the same year, approximately US$ 2.7 billion was invested globally in malaria control and elimination efforts by governments of malaria endemic countries and international partners—a reduction from the US$ 3.2 billion that was invested in 2017 [1]. Malaria

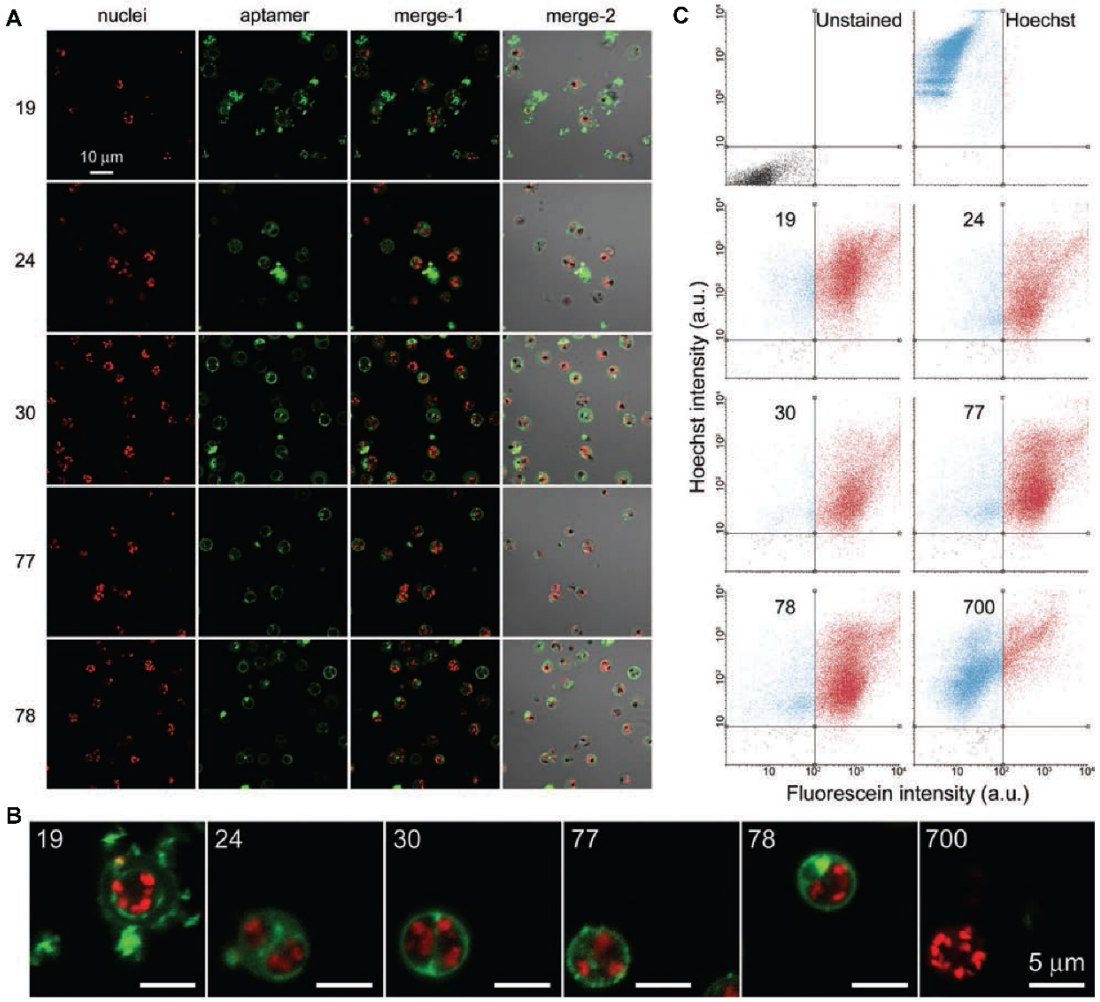

Figure 9. **pRBC versus non-infected RBC binding specificity analysis in non-fixed, saponin-permeabilized *P. falciparum* cultures of the chemically synthesized aptamers labeled with 6-FAM at the 5′ end. (A, B) fluorescence microscopy analysis of (A) cellular and (B) subcellular aptamer targeting. For an easier identification of colocalizing pixels, the blue color of Hoechst 33342 has been changed to red. (C) Quantitative flow cytometry analysis of aptamer targeting. The cells used here belonged to a new fixed cell batch different from that used during the SELEX cycles. a.u.: Arbitrary units.**

has enormous social and economic relevance, including a negative impact on short-term learning function, loss of work/study productivity, and diagnosis/treatment costs. Whereas the global fight against malaria has evolved from a "control" to a still difficult to implement "eradication strategy" [51], elimination, on the other hand, is technically feasible but would need mass population screening.

P. falciparum histidine-rich protein II (PfHRP-II) is widely used as target antigen for specific detection of this species of the parasite, although some reports have claimed variable results obtained with PfHRP-II-based RDTs [52, 53]. In addition, evidences of mutation and deletion of the PfHRP-II gene counsels caution in the use of this biomarker for falciparum malaria [54, 55], which led the WHO to recommend researching alternative targets and methods for detection of *P. falciparum* [56]. In this regard, *Plasmodium* glutamate dehydrogenase (PGDH) and lactate dehydrogenase (PLDH) have received increased attention as specific biomarkers for which aptamers have been developed [49, 50, 57]. Human-infecting plasmodia produce GDH and LDH, whose blood concentration correlates with parasitemia and decreases along patient therapeutic treatment. All *Plasmodium* species infecting humans produce both enzymes, but these are sufficiently variable to allow species-specific recognition [57, 58]. Accordingly, PLDH has been proposed

Table VII. Percentage of saponin-permeabilized, non-fixed pRBC binding of the different 6-FAM-labeled aptamers determined from flow cytometry data. a.u.: Arbitrary units.

Sample	6-FAM-aptamer-labeled pRBCs (%)	6-FAM fluorescence intensity mean (a.u.)	6-FAM fluorescence intensity mean increase relative to aptamer 700
Unstained control	0.0	7.3	–
Hoechst only control	0.5	9.8	–
700	23.4	169.5	1
19	90.6	1191.4	7.0
24	88.4	938.2	5.5
30	93.6	1372.6	8.1
77	78.3	620.7	3.7
78	90.8	893.1	5.3

as a biomarker for parasitemia estimation, species identification, and treatment response monitoring [58, 59], and aptamers raised against falciparum PLDH exhibited a K_d around 40 nM [22]. Recently, DNA aptamers have been generated against a conserved recombinant domain of the high mobility group box 1 protein of *P. falciparum*, to be developed as potential sensing elements of RDTs [60]. These aptamers incur the risk of a loss in antigen binding efficacy if the molecular targets mutate or exhibit variant expression. To overcome this problem, we have explored here the use of a cell-SELEX approach, which, in addition to individual proteins, might also produce aptamers targeting (i) molecular landscapes present in several parasite molecules or (ii) non-proteinaceous antigens, such as lipids, nucleic acids or polysaccharides. Using inertial microfluidic SELEX, RNA aptamers that recognized distinct, surface-displayed epitopes on pRBCs with nanomolar affinity had been developed [61]. Moreover, cell-SELEX has also been successfully used to select aptamers with dissociation constants

Table VIII. *P. falciparum* proteins identified by LC-MS/MS in a pull-down assay performed with biotinylated aptamer 19.

Accession number	Protein
Q76NM3	L-lactate dehydrogenase
Q7KQM0	Triosephosphate isomerase
Q8I0P6	Elongation factor 1-alpha
Q8IL80	Thioredoxin peroxidase 1
Q8IE85	60S ribosomal protein L6, putative
Q8IM10	40S ribosomal protein S8
Q8IDV1	60S ribosomal protein L6-2, putative
Q8IJS2	Cytochrome b-c1 complex subunit 7, putative
O96174	Conserved Plasmodium protein
C6KTB1	Protein DJ-1
O77388	HVA22/TB2/DP1 family protein, putative
C0H516	Ras-related protein RAB7
Q8IJ76	Early transcribed membrane protein 10.2
Q8IEM3	60S ribosomal protein L24, putative
Q8I261	Proteasome subunit beta type

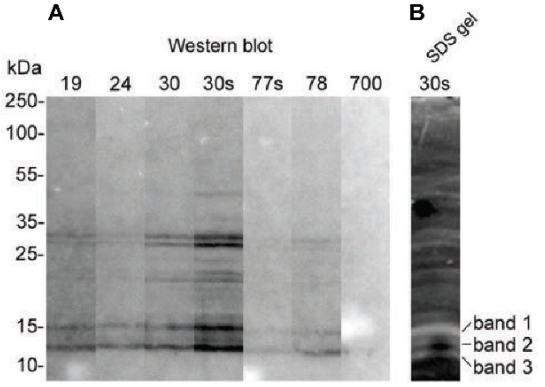

Figure 10. SDS-PAGE and Western blot analysis of aptamer binding. (A) Western blot of late stage *P. falciparum* cultures probed with the selected 6-FAM-labeled aptamers. Since the band pattern was identical for all aptamers, some of them are not shown. (B) 12.5% SDS-PAGE lane where the same late stage extract was loaded but not blotted; instead, it was directly probed with 6-FAM-labeled aptamer 30s. The three bands indicated were separately excised and subjected to LC-MS/MS analysis.

in the nanomolar range against leukemia cells [32, 62], human hepatoma cell line Hep62 [63], and non-small cell lung cancer [64]. In our study, the apparent K_d range from 0.46 ± 0.08 to 1.77 ± 0.15 μM for both full-length and shortened aptamers raised against pRBCs is

Table IX. *P. falciparum* proteins identified by LC-MS/MS in the band 1 of Figure 10.

Accession number	Protein
C6KT18	Histone H2A
C6KSV0	Histone H3
Q8I3U6	40S ribosomal protein S11
Q8I502	40S ribosomal protein S17, putative
Q8IBQ5	40S ribosomal protein S10, putative
O00806	60S acidic ribosomal protein P2
O97320	Histone H2A
Q8IIX0	60S acidic ribosomal protein P1, putative
Q8IAX5	40S ribosomal protein S16, putative
Q8IIA2	40S ribosomal protein S18, putative
Q8I3R6	40S ribosomal protein S24
Q8I3J4	Ubiquitin-conjugating enzyme E2 N, putative
O97241	Ubiquitin-conjugating enzyme E2, putative
Q8IC43	Small exported membrane protein 1
Q8IK02	40S ribosomal protein S20e, putative
Q8I463	60S ribosomal protein L31
Q7K6B1	Protein kinase c inhibitor-like protein, putative
Q8IBJ9	Mago nashi protein homologue, putative
Q8IIC4	Ribonucloprotein
C6KT23	60S ribosomal protein L27a, putative
Q8IBV7	Histone H2B
C0H4F3	Bis(5′-nucleosyl)-tetraphosphatase [asymmetrical]
Q8IDP4	Thioredoxin 2
Q8IIV2	Histone H4

Table IX. Continued.

Accession number	Protein
Q8IIK8	Peptidyl-prolyl cis-trans isomerase
Q6ZMA7	Sexual stage-specific protein
Q8IIJ4	Uncharacterized protein
Q8I3N5	Pre-mRNA-splicing factor BUD31, putative
Q8IKM6	Inner membrane complex sub-compartment protein 3
C6KSR0	Ubiquitin-conjugating enzyme E2, putative
Q8IDB0	40S ribosomal protein S15
C0H4C7	Uncharacterized protein
Q8IIV1	60S ribosomal protein L36
Q8I713	60S ribosomal protein L28
Q8IHU0	60S ribosomal protein L26, putative
O15770	Glutathione reductase
O97231	60S ribosomal protein L44
Q8ILB7	Mitochondrial import inner membrane translocase subunit TIM17, putative
Q8ID43	Nucleoside diphosphate kinase
Q8IIB9	U6 snRNA-associated Sm-like protein LSm1
Q8IKM5	60S ribosomal protein L27
Q8IDE0	Mitochondrial import inner membrane translocase subunit TIM23, putative
Q8IK04	N-terminal acetyltransferase A complex catalytic subunit ARD1, putative
O97248	40S ribosomal protein S23, putative
O97256	Activator of Hsp90 ATPase, putative
Q8I3B0	60S ribosomal protein L32
Q8I607	Ubiquitin-conjugating enzyme E2
O96258	40S ribosomal protein S26
Q8I6T3	Proteasome subunit beta
Q8IDB8	HVA22-like protein, putative
Q8IAW2	Ubiquitin-conjugating enzyme, putative
Q8IEF9	Ring-exported protein 2
Q8I2G0	Aminopeptidase P
A0A144A2H0	Probable cathepsin C
Q8I573	CHCH domain-containing protein
Q76NN7	Peptidyl-prolyl cis-trans isomerase
Q8IIT3	U6 snRNA-associated Sm-like protein LSm4
C0H4C5	Uncharacterized protein
Q8I5C5	Macrophage migration inhibitory factor
O96217	Ribosomal protein L37
C0H4L5	Replication factor A protein 3, putative
C6S3I6	Succinate dehydrogenase subunit 4, putative
Q8IJU2	60S ribosomal protein L35, putative
Q8IIB4	Cofilin/actin-depolymerizing factor homolog 1
Q8II62	60S ribosomal protein L38
Q8II81	Multiprotein bridging factor type 1, putative
Q8I444	Small ubiquitin-related modifier
Q8I3M0	60S ribosomal protein L23, putative
Q8IE09	40S ribosomal protein S15A, putative
Q8I5Q9	Uncharacterized protein
Q8I306	Transcription elongation factor 1 homolog
C0H4V6	14-3-3 protein

comparable to values reported for aptamers generated against *Salmonella typhimurium* using a similar whole-cell SELEX approach like that employed here [65]. These relatively high K_ds are characteristic of glycan-containing aptamer targets [66]. However, since the corresponding molecular antigens have not been identified yet, these K_d

Table X. *P. falciparum* proteins identified by LC-MS/MS in the band 2 of Figure 10.

Accession number	Protein
Q8IIV1	Histone H2B
Q8IBV7	Histone H2B
C6KT18	Histone H2A
O00806	60S acidic ribosomal protein P2
Q8I502	40S ribosomal protein S17, putative
Q8IE09	60S ribosomal protein L23, putative
Q8IJX8	DNA/RNA-binding protein Alba 3
Q8ID43	Nucleoside diphosphate kinase
O77395	40S ribosomal protein S15A, putative
Q8I3U6	40S ribosomal protein S11
Q8IKM6	Inner membrane complex sub-compartment protein 3
Q8IIV2	Histone H4
Q7K6B1	Protein kinase c inhibitor-like protein, putative
Q8I5R8	DNA-directed RNA polymerases I, II, and III subunit RPABC3
Q8IBQ5	40S ribosomal protein S10, putative
Q8I713	60S ribosomal protein L36
Q8IJK8	60S ribosomal protein L30e, putative
Q8I607	Ubiquitin-conjugating enzyme E2
Q8I2G0	Ring-exported protein 2
Q8IAX5	40S ribosomal protein S16, putative
Q8II62	60S ribosomal protein L38
Q8IJ28	Antigen UB05
O97320	Histone H2A
Q8IIT3	U6 snRNA-associated Sm-like protein LSm4
Q8I467	Cofilin/actin-depolymerizing factor homolog 1
Q8I318	EFP domain-containing protein
Q8IK07	Uncharacterized protein
O96265	Small nuclear ribonucleoprotein Sm D2
Q8IC43	Small exported membrane protein 1
O96258	40S ribosomal protein S26
Q8IHU0	60S ribosomal protein L28
O96184	60S ribosomal protein L37a
O97241	Ubiquitin-conjugating enzyme E2, putative
Q8IE05	Trafficking protein particle complex subunit 2, putative
Q8IBD0	Uncharacterized protein
Q8I6T3	Proteasome subunit beta
Q8IM53	Cytochrome c, putative
Q8IIB9	U6 snRNA-associated Sm-like protein LSm1
A0A144A2H0	Aminopeptidase P
Q8IJA5	Transcription elongation factor SPT4, putative
C6KSV0	Histone H3
O97256	Activator of Hsp90 ATPase, putative
Q8I3T9	60S ribosomal protein L2
Q8IKK7	Glyceraldehyde-3-phosphate dehydrogenase
Q8IIJ4	Uncharacterized protein
Q8IBJ9	Mago nashi protein homologue, putative
Q8IJK2	Autophagy-related protein
Q8IIA8	Small nuclear ribonucleoprotein Sm D1
Q8IK02	40S ribosomal protein S20e, putative
Q8IK04	N-terminal acetyltransferase A complex catalytic subunit ARD1, putative
Q8I5C5	Macrophage migration inhibitory factor
Q8IAZ1	Uncharacterized protein
Q8I5V6	U6 snRNA-associated Sm-like protein LSm7, putative
C0H4N9	Uncharacterized protein
Q6ZMA7	Sexual stage-specific protein

Table X. Continued.

Accession number	Protein
P62805	Histone H4
Q8I463	60S ribosomal protein L31
Q8IJT5	Inner membrane complex sub-compartment protein 1
Q8ILB7	Mitochondrial import inner membrane translocase subunit TIM17, putative
C0H4L5	Ribosomal protein L37
Q8IFN5	AP complex subunit sigma
Q8ILN2	Copper transporter, putative
Q8I2N9	CS domain protein, putative
A0A143ZWW5	Ribosome associated membrane protein RAMP4, putative
Q8IDE0	Mitochondrial import inner membrane translocase subunit TIM23, putative
C6KT14	Uncharacterized protein
Q8IFP0	Uncharacterized protein
Q8IER7	Probable DNA-directed RNA polymerase II subunit RPB11
Q8IIX0	60S acidic ribosomal protein P1, putative
Q8IHN5	Uncharacterized protein
Q8I3J4	Ubiquitin-conjugating enzyme E2 N, putative
Q8I3N5	Pre-mRNA-splicing factor BUD31, putative
Q8IIA2	40S ribosomal protein S18, putative
Q8IFN4	BSD-domain protein, putative
Q8IDP4	Thioredoxin 2
C0H574	Uncharacterized protein
Q8IB14	High mobility group protein B2
O97232	1-cys-glutaredoxin-like protein-1
Q8IDB8	HVA22-like protein, putative
Q8IEM3	60S ribosomal protein L24, putative
Q8I4S3	Uncharacterized protein
Q8I488	Parasite-infected erythrocyte surface protein
Q8IM64	Ubiquitin-40S ribosomal protein S27a, putative
C0H4V0	Trafficking protein particle complex subunit 2-like protein, putative
Q8I6V2	Cytochrome c oxidase subunit 2, putative
Q8IJU2	Succinate dehydrogenase subunit 4, putative
O97231	60S ribosomal protein L44
C0H4V6	14-3-3 protein
Q8I3A4	Prefoldin subunit 4
Q8IHP4	Mitochondrial ATP synthase delta subunit, putative
A0A144A372	AP complex subunit sigma
C0H4H3	60S ribosomal protein L39
Q8IKD4	Mitochondrial pyruvate carrier

Table XI. *P. falciparum* proteins identified by LC-MS/MS in the band 3 of Figure 10.

Accession number	Protein
Q8IIV2	Histone H4
Q8I467	Cofilin/actin-depolymerizing factor homolog 1
Q8IIV1	Histone H2B
Q8IE09	60S ribosomal protein L23, putative
O77395	40S ribosomal protein S15A, putative
Q8ILX1	Nuclear transport factor 2, putative
Q8ILN8	40S ribosomal protein S25
Q8IJK8	60S ribosomal protein L30e, putative
Q8IHW4	V-type proton ATPase subunit F
C0H529	Small nuclear ribonucleoprotein Sm D3
Q8I5C5	Macrophage migration inhibitory factor
O96184	60S ribosomal protein L37a
Q8II62	60S ribosomal protein L38
Q9NLB0	Membrane magnesium transporter, putative
Q7KQL8	Thioredoxin
Q8IBD0	Uncharacterized protein
Q8IJX8	DNA/RNA-binding protein Alba 3
O96265	Small nuclear ribonucleoprotein Sm D2
Q8IBV7	Histone H2B
Q8IK07	Uncharacterized protein
Q8IDP4	Thioredoxin 2
Q8II72	Parasitophorous vacuolar protein 1
C0H4A3	Rab5-interacting protein, putative
Q8IHY3	Ubiquitin-related modifier 1 homolog
C6KSV0	Histone H3
Q8I488	Parasite-infected erythrocyte surface protein
O77358	Trafficking protein particle complex subunit 4, putative
Q8IM64	Ubiquitin-40S ribosomal protein S27a, putative
O77367	E3 ubiquitin-protein ligase RBX1, putative
A0A143ZWW5	Ribosome associated membrane protein RAMP4, putative
C0H4H3	60S ribosomal protein L39
Q8I607	Ubiquitin-conjugating enzyme E2
C6S3E6	Pterin-4a-carbinolamine dehydratase
O15770	Glutathione reductase
Q8IE87	Uncharacterized protein
Q8I3X2	Mitochondrial import inner membrane translocase subunit TIM16, putative
Q8IJK2	Autophagy-related protein
C0H4E7	SWIB/MDM2 domain-containing protein, putative
Q8IIA8	Small nuclear ribonucleoprotein Sm D1
Q8IC33	Uncharacterized protein
Q8I4Z4	Translation initiation factor SUI1, putative
O97320	Histone H2A
Q8IDR9	40S ribosomal protein S6
Q8I3L8	Mitochondrial import receptor subunit TOM22, putative
Q8IB14	High mobility group protein B2
C0H574	Uncharacterized protein
O96150	DNA-directed RNA polymerase II 16 kDa subunit, putative
Q8I5A5	Mitosis protein dim1, putative
C6KT18	Histone H2A

values had to be calculated against whole cells. To the best of our knowledge, all available K_d values in the nM range reported for PLDH aptamers were obtained with techniques that used the purified enzyme: isothermal titration calorimetry, electrophoretic mobility shift assay and surface plasmon resonance spectroscopy [22]. When exposed to whole cells *in vitro*, all the aptamers studied here bound *P. falciparum*-infected erythrocytes >30-fold better than the PLDH 2008s aptamer, likely because of a larger number of target epitopes present in each cell.

As opposed to using the purified molecular target, calculation of K_d measuring fluorescence intensity in target cells can be misled as the number of binding sites is unknown. This approach, however, can be adequate in the selection of diagnostic aptamers if these are to be tested with whole cells, where the sensitivity

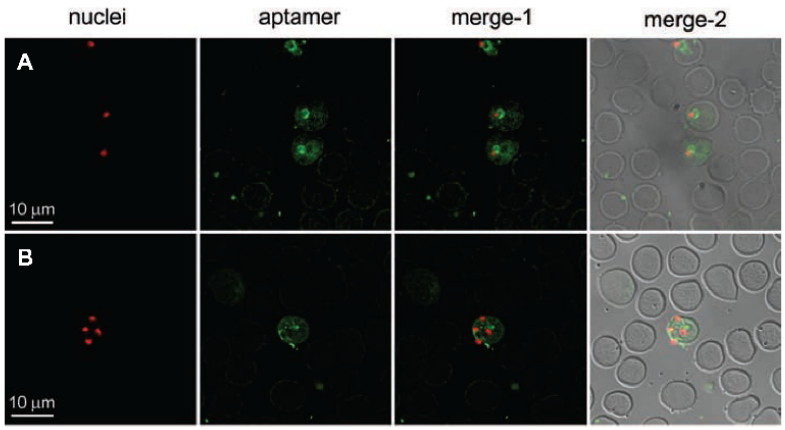

Figure 11. Fluorescence microscopy analysis of falciparum malaria clinical samples. Thin blood smears of a *P. falciparum* infection were probed with 6-FAM-labeled aptamer 24. (A) Ring stages. (B) Late blood stage. For an easier identification of colocalizing pixels, the blue color of Hoechst 33342 has been changed to red.

of detection will depend on the K_d of the aptamer but also on the abundance and availability of the corresponding molecular target within the crowded intracellular environment. Preliminary binding affinity assays of our aptamers evolved by whole-cell SELEX ended up with the identification of multiple proteins being targeted. This result was consistent with the abundance in *Plasmodium* of highly aggregative [67] or adhesive proteins [68], which could be carried together with the aptamer-binding element(s). Alternatively, the binding of DNA oligonucleotides to *Plasmodium* components might be based on some widely represented parasite epitope or on unspecific interactions with protein primary or secondary structures. G-quadruplexes, for instance, have twice the negative charge density per unit length compared to DNA double helices, thus representing an excellent arrangement for interactions with e.g., cationic proteins [48].

In agreement with the experimental design used here, our cell-SELEX proof of concept approach has obtained aptamers against *P. falciparum* late blood stages, mostly trophozoites and schizonts. This might limit diagnostic applications, since a clinical *P. falciparum* infection mainly has early blood stages in the blood circulation. However, according to dot blot assays of *in vitro* cultures and fluorescence microscopy analysis of clinical samples, the selected aptamers target ring stages as well. Late stages can also be found in circulation as result of an apparent reduction or delay in sequestration, usually in high parasitemia *P. falciparum* infections, but occasionally also in asymptomatic cases [69]. These observations encourage the exploration of a potential application of the aptamers developed here as components of future RDT devices, where DNA aptamers could substitute for the antibodies currently used as sensing elements [70]. Among the aptamers developed in this work, 30s would be the most suitable for clinical use given its high BP, although even higher diagnostic specificities could be attained with joint detection strategies where two of the selected aptamers could be used together.

As we are progressing from malaria control to elimination, asymptomatic infections will be increasingly elusive to detect since antibody-based RDTs do not have enough sensitivity [71]. Loop-mediated isothermal amplification assays [72] indicate that it is possible to identify such cases, but it is costly compared to microscopic observation and it is still complicated and challenging to be applied worldwide [73, 74]. A diagnosis alternative could be offered by synthetic bioreceptors like aptamers, which have already been raised against both pan- and species-specific PLDH [21, 49]. The observation that our aptamers bind also erythrocytes infected by *P. malariae*, *P. vivax* and *P. ovale* indicates that their potential applications will be in pan-malaria diagnosis. Several biosensing protocols have been developed employing aptamers against *Plasmodium* LDH, such as colorimetric sensing [24], impedance measurements by electrode functionalization [21] or enzyme capture and colorimetric catalysis [75]. Malaria RDTs based on antibody recognition require a lysis step unless the target antigen is secreted, such as HRP-II, and/or a liquid phase to make the sample move by capillarity [76]. Such platforms providing simple, stable and easy-to-use RDTs can be easily adapted to new *Plasmodium*-specific aptamers like the ones developed here, which would only require a cell permeabilization agent included in the corresponding buffers. This direct detection of parasitized cells is an advantage relative to diagnosis methods relying on antibody detection of parasite antigens, whose decay takes longer than the clearance of parasitemia [77]. The recognition of intracellular epitopes might offer some additional benefits such as less susceptibility to the intense variant

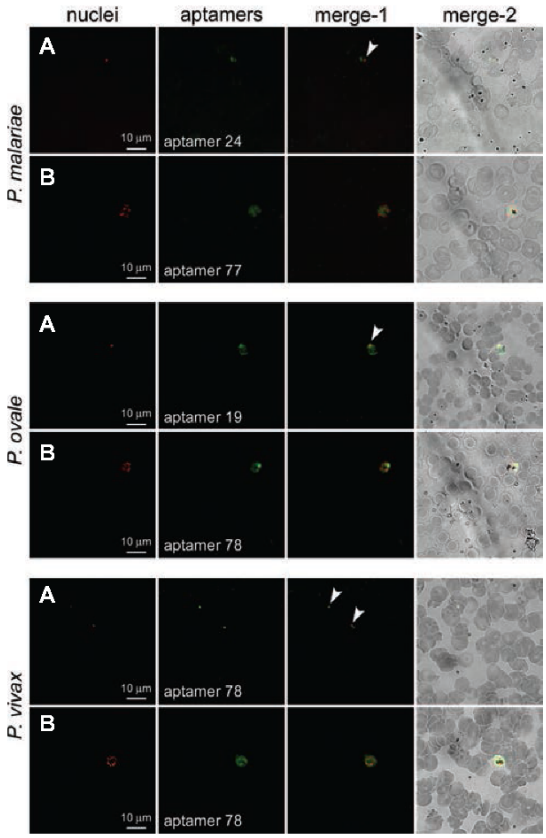

Figure 12. Fluorescence microscopy analysis of malariae, ovale, and vivax malaria clinical samples. Thin blood smears of *P. malariae*, *P. ovale* and *P. vivax* infections were probed with 6-FAM-labeled aptamers. (A) Ring stages. (B) Late blood stages. For an easier identification of colocalizing pixels, the blue color of Hoechst 33342 has been changed to red. Arrowheads indicate the small ring stage nuclei.

expression of *Plasmodium* cell surface-exposed molecular tags [5, 6].

CONCLUSIONS

In this study, several DNA aptamers have been evolved that in *in vitro* studies discriminate with almost complete specificity naïve red blood cells from erythrocytes infected by *P. falciparum* (<0.1% vs. >90% binding to both cell types, respectively). In clinical samples, these aptamers bind all stages of red blood cells infected by *P. falciparum*, *P. vivax*, *P. ovale* and *P. malariae* in fixed thin blood smears. This work provides new synthetic biomarkers that can be easily incorporated in the development of a fast, cost-effective, sensitive and easy to use diagnostic tool, which would be a key asset for future malaria elimination policies.

Disclosure

Patent application: Aptamers for detecting *Plasmodium*-infected red blood cells. Application number: EP20382190.5. Application date: March 13, 2020.

Acknowledgments: This research was funded by grants (i) BIO2014-52872-R and IPANAT, RTI2018-094579-B-I00, *Ministerio de Ciencia, Innovación y Universidades (MICIU), Agencia Estatal de Investigación*, Spain, and *Fondo Europeo de Desarrollo Regional*, and (ii) 2017-SGR-908, *Generalitat de Catalunya*, Spain. ISGlobal and IBEC are members of the CERCA Programme, *Generalitat de Catalunya*. This research is part of ISGlobal's Program on the Molecular Mechanisms of Malaria which is partially supported by the *Fundación Ramón Areces*. Yunuen Ávalos-Padilla acknowledges financial support provided by the European Commission under Horizon 2020's Marie Skłodowska-Curie Actions COFUND scheme (712754) and by the Severo Ochoa programme MICIU [SEV-2014-0425 (2015–2019)], which also supported us through the Centro de Excelencia Severo Ochoa 2019-2023 Program (CEX2018-000806-S). We thank Harvie Portugaliza and Alfred Cortés for the *P. falciparum* NF54 *gexp02-tdTomato* transgenic line. We are indebted to Menelaos Voulgaris for the graphic design of the SELEX cycle scheme.

REFERENCES

1. WHO Global Malaria Programme, **2019**. *World Malaria Report 2019*. Geneva, World Health Organization.
2. World Health Organization, **2015**. *Global Technical Strategy for Malaria 2016–2030*. Geneva, World Health Organization.
3. Kasetsirikul, S., Buranapong, J., Srituravanich, W., Kaewthamasorn, M. and Pimpin, A., **2016**. The development of malaria diagnostic techniques: A review of the approaches with focus on dielectrophoretic and magnetophoretic methods. *Malaria Journal, 15*(1), p.358.
4. Pham, N.M., Karlen, W., Beck, H.P. and Delamarche, E., **2018**. Malaria and the 'last' parasite: How can technology help? *Malaria Journal, 17*(1), p.260.
5. Craig, A. and Scherf, A., **2001**. Molecules on the surface of the *Plasmodium falciparum* infected erythrocyte and their role in malaria pathogenesis and immune evasion. *Molecular and Biochemical Parasitology, 115*(2), pp.129–143.
6. Tilley, L., Dixon, M.W. and Kirk, K., **2011**. The *Plasmodium falciparum*-infected red blood cell. *International Journal of Biochemistry and Cell Biology, 43*(6), pp.839–842.
7. Ruigrok, V.J.B., Levisson, M., Eppink, M.H.M., Smidt, H. and van der Oost, J., **2011**. Alternative affinity tools: More attractive than antibodies? *Biochemical Journal, 436*(1), p.1.
8. Wang, M.S., Black, J.C., Knowles, M.K. and Reed, S.M., **2011**. C-reactive protein (CRP) aptamer binds to monomeric but not pentameric form of CRP. *Analytical and Bioanalytical Chemistry, 401*(4), pp.1309–1318.
9. Thirunavukarasu, D. and Shi, H., **2015**. An RNA aptamer specific to Hsp70-ATP conformation inhibits its ATPase activity independent of Hsp40. *Nucleic Acid Therapeutics, 25*(2), pp.103–112.

10. Mitkevich, O.V., Kochneva-Pervukhova, N.V., Surina, E.R., Benevolensky, S.V., Kushnirov, V.V. and Ter-Avanesyan, M.D., **2012**. DNA aptamers detecting generic amyloid epitopes. *Prion, 6*(4), pp.400–406.

11. Stoltenburg, R., Reinemann, C. and Strehlitz, B., **2007**. SELEX—A (r)evolutionary method to generate high-affinity nucleic acid ligands. *Biomolecular Engineering, 24*, pp.381–403.

12. O'Sullivan, C.K., **2002**. Aptasensors—The future of biosensing? *Analytical and Bioanalytical Chemistry, 372*(1), pp.44–48.

13. Warren, C.L., Mohandas, A., Chaturvedi, I. and Ansari, A.Z., **2009**. Macromolecular interactions: Aptamers. In: *Encyclopedia of Life Sciences*. Chichester, UK, John Wiley & Sons. Vol. 29, pp.582–594.

14. Gao, S., Zheng, X., Jiao, B. and Wang, L., **2016**. Post-SELEX optimization of aptamers. *Analytical and Bioanalytical Chemistry, 408*(17), pp.4567–4573.

15. Ellington, A.D. and Szostak, J.W., **1990**. *In vitro* selection of RNA molecules that bind specific ligands. *Nature, 346*, p.818.

16. Tuerk, C. and Gold, L., **1990**. Systematic evolution of ligands by exponential enrichment: RNA ligands to bacteriophage T4 DNA polymerase. *Science, 249*(4968), p.505.

17. Abelson, J., **1990**. Directed evolution of nucleic acids by independent replication and selection. *Science, 249*(4968), pp.488–489.

18. Robertson, D.L. and Joyce, G.F., **1990**. Selection *in vitro* of an RNA enzyme that specifically cleaves single-stranded DNA. *Nature, 344*, p.467.

19. Zimbres, F.M., Tárnok, A., Ulrich, H. and Wrenger, C., **2013**. Aptamers: Novel molecules as diagnostic markers in bacterial and viral infections? *BioMed Research International, 2013*, p.731516.

20. Ospina-Villa, J.D., López-Camarillo, C., Castañón-Sánchez, C.A., Soto-Sánchez, J., Ramírez-Moreno, E. and Marchat, L.A., **2018**. Advances on aptamers against protozoan parasites. *Genes, 9*(12), p.584.

21. Lee, S., Song, K.M., Jeon, W., Jo, H., Shim, Y.B. and Ban, C., **2012**. A highly sensitive aptasensor towards *Plasmodium* lactate dehydrogenase for the diagnosis of malaria. *Biosensors and Bioelectronics, 35*(1), pp.291–296.

22. Cheung, Y.W., Kwok, J., Law, A.W.L., Watt, R.M., Kotaka, M. and Tanner, J.A., **2013**. Structural basis for discriminatory recognition of *Plasmodium* lactate dehydrogenase by a DNA aptamer. *Proceedings of the National Academy of Sciences of the United States of America, 110*(40), pp.15967–15972.

23. Lee, S., Manjunatha, D.H., Jeon, W. and Ban, C., **2014**. Cationic surfactant-based colorimetric detection of *Plasmodium* lactate dehydrogenase, a biomarker for malaria, using the specific DNA aptamer. *PLOS ONE, 9*(7), p.e100847.

24. Jeon, W., Lee, S., Manjunatha, D.H. and Ban, C., **2013**. A colorimetric aptasensor for the diagnosis of malaria based on cationic polymers and gold nanoparticles. *Analytical Biochemistry, 439*(1), pp.11–16.

25. Godonoga, M., Lin, T.Y., Oshima, A., Sumitomo, K., Tang, M.S.L., Cheung, Y.W., Kinghorn, A.B., Dirkzwager, R.M., Zhou, C., Kuzuya, A., Tanner, J.A. and Heddle, J.G., **2016**. A DNA aptamer recognising a malaria protein biomarker can function as part of a DNA origami assembly. *Scientific Reports, 6*, p.21266.

26. Barfod, A., Persson, T. and Lindh, J., **2009**. *In vitro* selection of RNA aptamers against a conserved region of the *Plasmodium falciparum* erythrocyte membrane protein 1. *Parasitology Research, 105*(6), pp.1557–1566.

27. Niles, J.C., deRisi, J.L. and Marletta, M.A., **2009**. Inhibiting *Plasmodium falciparum* growth and heme detoxification pathway using heme-binding DNA aptamers. *Proceedings of the National Academy of Sciences of the United States of America, 106*(32), pp.13266–13271.

28. Lyu, Y., Chen, G., Shangguan, D., Zhang, L., Wan, S., Wu, Y., Zhang, H., Duan, L., Liu, C., You, M., Wang, J. and Tan, W., **2016**. Generating cell targeting aptamers for nanotheranostics using cell-SELEX. *Theranostics, 6*(9), pp.1440–1452.

29. Berezovski, M.V., Lechmann, M., Musheev, M.U., Mak, T.W. and Krylov, S.N., **2008**. Aptamer-facilitated biomarker discovery (AptaBiD). *Journal of the American Chemical Society, 130*(28), pp.9137–9143.

30. Sefah, K., Shangguan, D., Xiong, X., O'Donoghue, M.B. and Tan, W., **2010**. Development of DNA aptamers using cell-SELEX. *Nature Protocols, 5*, p.1169.

31. Morris, K.N., Jensen, K.B., Julin, C.M., Weil, M. and Gold, L., **1998**. High affinity ligands from *in vitro* selection: Complex targets. *Proceedings of the National Academy of Sciences of the United States of America, 95*(6), pp.2902–2907.

32. Shangguan, D., Li, Y., Tang, Z., Cao, Z.C., Chen, H.W., Mallikaratchy, P., Sefah, K., Yang, C.J. and Tan, W., **2006**. Aptamers evolved from live cells as effective molecular probes for cancer study. *Proceedings of the National Academy of Sciences of the United States of America, 103*(32), pp.11838–11843.

33. Ulrich, H. and Wrenger, C., **2009**. Disease-specific biomarker discovery by aptamers. *Cytometry A, 75A*(9), pp.727–733.

34. Nagarkatti, R., Bist, V., Sun, S., Fortes de Araujo, F., Nakhasi, H.L. and Debrabant, A., **2012**. Development of an aptamer-based concentration method for the detection of *Trypanosoma cruzi* in blood. *PLOS ONE, 7*(8), p.e43533.

35. Nik Kamarudin, N.A.A., Mohammed, N.A. and Mustaffa, K.M.F., **2017**. Aptamer technology: Adjunct therapy for malaria. *Biomedicines, 5*(1), p.1.

36. Albrecht, L., Angeletti, D., Moll, K., Blomqvist, K., Valentini, D., D'Alexandri, F.L., Maurer, M. and Wahlgren, M., **2014**. B-cell epitopes in NTS-DBL1a of PfEMP1 recognized by human antibodies in rosetting *Plasmodium falciparum*. *PLOS ONE, 9*(12), p.e113248.

37. Chan, J.A., Fowkes, F.J.I. and Beeson, J.G., **2014**. Surface antigens of *Plasmodium falciparum*-infected erythrocytes as immune targets and malaria vaccine candidates. *Cellular and Molecular Life Sciences, 71*(19), pp.3633–3657.

38. Cranmer, S.L., Magowan, C., Liang, J., Coppel, R.L. and Cooke, B.M., **1997**. An alternative to serum for cultivation of *Plasmodium falciparum in vitro*. *Transactions of the Royal Society of Tropical Medicine and Hygiene, 91*(3), pp.363–365.

39. Lambros, C. and Vanderberg, J.P., **1979**. Synchronization of *Plasmodium falciparum* erythrocytic stages in culture. *Journal of Parasitology, 65*(3), pp.418–420.

40. Radfar, A., Méndez, D., Moneriz, C., Linares, M., Marín-García, P., Puyet, A., Diez, A. and Bautista, J.M., **2009**. Synchronous culture of *Plasmodium falciparum* at high parasitemia levels. *Nature Protocols, 4*(12), pp.1899–1915.

41. Sambrook, J.F. and Russell, D.W., eds., **2001**. *Molecular Cloning: A Laboratory Manual*, 3rd edn. Cold Spring Harbor, New York, Cold Spring Harbor Laboratory Press.

42. Brancucci, N.M.B., Gerdt, J.P., Wang, C., De Niz M., Philip, N., Adapa, S.R., Zhang, M., Hitz, E., Niederwieser, I., Boltryk, S.D., Laffitte, M.C., Clark, M.A., Grüring, C., Ravel, D., Blancke Soares, A., Demas, A., Bopp, S., Rubio-Ruiz, B., Conejo-Garcia, A., Wirth, D.F., Gendaszewska-Darmach, E., Duraisingh, M.T., Adams, J.H., Voss, T.S., Waters, A.P., Jiang, R.H.Y., Clardy, J. and Marti, M., **2017**. Lysophosphatidylcholine regulates sexual stage differentiation in the human malaria parasite *Plasmodium falciparum*. *Cell, 171*(7), pp.1532–1544.

43. Portugaliza, H.P., Llorà-Batlle, O., Rosanas-Urgell, A. and Cortés, A., **2019**. Reporter lines based on the gexp02 promoter enable early quantification of sexual conversion rates in the malaria parasite *Plasmodium falciparum*. *Scientific Reports, 9*(1), p.14595.

44. Zuker, M., **2003**. Mfold web server for nucleic acid folding and hybridization prediction. *Nucleic Acids Research, 31*(13), pp.3406–3415.

45. Kikin, O., D'Antonio, L. and Bagga, P.S., **2006**. QGRS Mapper: A web-based server for predicting G-quadruplexes in nucleotide sequences. *Nucleic Acids Research, 34*(Web Server issue), pp.W676–W682.

46. Mintun, M.A., Raichle, M.E., Kilbourn, M.R., Wooten, G.F. and Welch, M.J., **1984**. A quantitative model for the *in vivo* assessment of drug binding sites with positron emission tomography. *Annals of Neurology, 15*(3), pp.217–227.

47. Kyes, S., Horrocks, P. and Newbold, C., **2001**. Antigenic variation at the infected red cell surface in malaria. *Annual Review of Microbiology, 55*, pp.673–707.

48. Gatto, B., Palumbo, M. and Sissi, C., **2009**. Nucleic acid aptamers based on the G-quadruplex structure: Therapeutic and diagnostic potential. *Current Medicinal Chemistry, 16*(10), pp.1248–1265.

49. Cheung, Y.W., Dirkzwager, R.M., Wong, W.C., Cardoso, J., D'Arc Neves, C.J. and Tanner, J.A., **2018**. Aptamer-mediated *Plasmodium*-specific diagnosis of malaria. *Biochimie, 145*, pp.131–136.

50. Frith, K.A., Fogel, R., Goldring, J.P.D., Krause, R.G.E., Khati, M., Hoppe, H., Cromhout, M.E., Jiwaji, M. and Limson, J.L., **2018**. Towards development of aptamers that specifically bind to lactate dehydrogenase of *Plasmodium falciparum* through epitopic targeting. *Malaria Journal. 17*(1), p.191.

51. World Health Organization, **2017**. *Integrating Neglected Tropical Diseases into Global Health and Development. 4th WHO Report on Neglected Tropical Diseases*. Geneva, World Health Organization.

52. Mason, D.P., Kawamoto, F., Lin, K., Laoboonchai, A. and Wongsrichanalai, C., **2002**. A comparison of two rapid field immunochromatographic tests to expert microscopy in the diagnosis of malaria. *Acta Tropica, 82*(1), pp.51–59.

53. Rubio, J.M., Buhigas, I., Subirats, M., Baquero, M., Puente, S. and Benito, A., **2001**. Limited level of accuracy provided by available rapid diagnosis tests for malaria enhances the need for PCR-based reference laboratories. *Journal of Clinical Microbiology, 39*(7), pp.2736–2737.

54. Kumar, N., Pande, V., Bhatt, R.M., Shah, N.K., Mishra, N., Srivastava, B., Valecha, N. and Anvikar, A.R., **2013**. Genetic deletion of HRP2 and HRP3 in Indian *Plasmodium falciparum* population and false negative malaria rapid diagnostic test. *Acta Tropica, 125*(1), pp.119–121.

55. Koita, O.A., Doumbo, O.K., Ouattara, A., Tall, L.K., Konaré, A., Diakité, M., Diallo, M., Sagara, I., Masinde, G.L., Doumbo, S.N., Dolo, A., Tounkara, A., Traoré, I. and Krogstad, D.J., **2012**. False-negative rapid diagnostic tests for malaria and deletion of the histidine-rich repeat region of the *hrp2* gene. *American Journal of Tropical Medicine and Hygiene, 86*(2), pp.194–198.

56. World Health Organization, **2017**. *WHO Malaria Policy Advisory Committee Meeting Report*. Geneva, World Health Organization.

57. Singh, N.K., Thungon, P.D., Estrela, P. and Goswami, P., **2019**. Development of an aptamer-based field effect transistor biosensor for quantitative detection of *Plasmodium falciparum* glutamate dehydrogenase in serum samples. *Biosensors and Bioelectronics, 123*, pp.30–35.

58. Piper, R.C., Buchanan, I., Choi, Y.H. and Makler, M.T., **2011**. Opportunities for improving pLDH-based malaria diagnostic tests. *Malaria Journal, 10*, p.213.

59. Atchade, P.S., Doderer-Lang, C., Chabi, N., Perrotey, S., Abdelrahman, T., Akpovi, C.D., Anani, L., Bigot, A., Sanni, A. and Candolfi, E., **2013**. Is a *Plasmodium* lactate dehydrogenase (pLDH) enzyme-linked immunosorbent (ELISA)-based assay a valid tool for detecting risky malaria blood donations in Africa? *Malaria Journal, 12*, p.279.

60. Joseph, D.F., Nakamoto, J.A., Ruiz, O.A.G., Peñaranda, K., Sanchez-Castro, A.E., Castillo, P.S. and Milón, P., **2019**. DNA aptamers for the recognition of HMGB1 from *Plasmodium falciparum*. *PLOS ONE, 14*(4), p.e0211756.

61. Birch, C.M., Hou, H.W., Han, J. and Niles, J.C., **2015**. Identification of malaria parasite-infected red blood cell surface aptamers by inertial microfluidic SELEX (I-SELEX). *Scientific Reports, 5*, p.11347.

62. Sefah, K., Tang, Z.W., Shangguan, D.H., Chen, H., Lopez-Colon, D., Li, Y., Parekh, P., Martin, J., Meng, L., Phillips, J.A., Kim, Y.M. and Tan, W.H., **2009**. Molecular recognition of acute myeloid leukemia using aptamers. *Leukemia, 23*(2), pp.235–244.

63. Xu, J., Teng, I.T., Zhang, L., Delgado, S., Champanhac, C., Cansiz, S., Wu, C., Shan, H. and Tan, W., **2015**. Molecular recognition of human liver cancer cells using DNA aptamers generated via cell-SELEX. *PLOS ONE, 10*(5), p.e0125863.

64. Zhao, Z., Xu, L., Shi, X., Tan, W., Fang, X. and Shangguan, D., **2009**. Recognition of subtype non-small cell lung cancer by DNA aptamers selected from living cells. *Analyst, 134*(9), pp.1808–1814.

65. Dwivedi, H.P., Smiley, R.D. and Jaykus, L.A., **2013**. Selection of DNA aptamers for capture and detection of *Salmonella typhimurium* using a whole-cell SELEX approach in conjunction with cell sorting. *Applied Microbiology and Biotechnology, 97*(8), pp.3677–3686.

66. Masud, M.M., Kuwahara, M., Ozaki, H. and Sawai, H., **2004**. Sialyllactose-binding modified DNA aptamer bearing additional functionality by SELEX. *Bioorganic and Medicinal Chemistry, 12*(5), pp.1111–1120.

67. Pallarès, I., de Groot, N.S., Iglesias, V., Sant'Anna, R., Biosca, A., Fernàndez-Busquets, X. and Ventura, S., **2018**. Discovering putative prion-like proteins in *Plasmodium falciparum*: A computational and experimental analysis. *Frontiers in Microbiology, 9*, p.1737.

68. Coma-Cros, E.M., Biosca, A., Marques, J., Carol, L., Urbán, P., Berenguer, D., Riera, M.C., Delves, M., Sinden, R.E., Valle-Delgado, J.J., Spanos, L., Siden-Kiamos, I., Pérez, P., Paaijmans, K., Rottmann, M., Manfredi, A., Ferruti, P., Ranucci, E. and Fernàndez-Busquets, X., **2018**. Polyamidoamine nanoparticles for the oral administration of antimalarial drugs. *Pharmaceutics, 10*(4), p.225.

69. Lwin, K.M., Ashley, E.A., Proux, S., Silamut, K., Nosten, F. and McGready, R., **2008**. Clinically uncomplicated *Plasmodium falciparum* malaria with high schizontaemia: A case report. *Malaria Journal, 7*, p.57.

70. Ruiz-Vega, G., Arias-Alpízar, K., de la Serna, E., Borgheti-Cardoso, L.N., Sulleiro, E., Molina, I., Fernàndez-Busquets, X., Sánchez-Montalvá, A., Del Campo, F.J. and Baldrich, E., **2019**. Electrochemical POC device for fast malaria quantitative diagnosis in whole blood by using magnetic beads, Poly-HRP and microfluidic paper electrodes. *Biosensors and Bioelectronics, 150*, p.111925.

71. Berzosa, P., de Lucio, A., Romay-Barja, M., Herrador, Z., González, V., García, L., Fernández-Martínez, A., Santana-Morales, M., Ncogo, P., Valladares, B., Riloha, M. and Benito, A., **2018**. Comparison of three diagnostic methods (microscopy, RDT, and PCR) for the detection of malaria parasites in representative samples from Equatorial Guinea. *Malaria Journal, 17*(1), p.333.

72. Oriero, E.C., Okebe, J., Jacobs, J., Van Geertruyden, J.P., Nwakanma, D. and D'Alessandro, U., **2015**. Diagnostic performance of a novel loop-mediated isothermal amplification (LAMP) assay targeting the apicoplast genome for malaria diagnosis in a field setting in sub-Saharan Africa. *Malaria Journal, 14*, p.396.

73. Zelman, B.W., Baral, R., Zarlinda, I., Coutrier, F.N., Sanders, K.C., Cotter, C., Herdiana, H., Greenhouse, B., Shretta, R., Gosling, R.D. and Hsiang, M.S., **2018**. Costs and cost-effectiveness of malaria reactive case detection using loop-mediated isothermal amplification compared to microscopy in the low transmission setting of Aceh Province, Indonesia. *Malaria Journal, 17*(1), p.220.

74. Tangpukdee, N., Duangdee, C., Wilairatana, P. and Krudsood, S., **2009**. Malaria diagnosis: A brief review. *Korean Journal of Parasitology, 47*(2), pp.93–102.

75. Dirkzwager, R.M., Kinghorn, A.B., Richards, J.S. and Tanner, J.A., **2015**. APTEC: Aptamer-tethered enzyme capture as a novel rapid diagnostic test for malaria. *Chemical Communications, 51*(22), pp.4697–4700.

76. World Health Organization, **2018**. *Malaria Rapid Diagnostic Test Performance. Results of WHO Product Testing of Malaria RDTs: Round 8 (2016–2018)*. Geneva, World Health Organization.

77. Mayor, A. and Bassat, Q., **2019**. "Resistance" to diagnostics: A serious biological challenge for malaria control and elimination. *EBioMedicine, 50*, pp.9–10.

Discussion

Along this work, both natural occurring and newly selected targeting molecules against *Plasmodium* parasites have been explored towards two different applications: (1) arrested development in two different parasite stages using natural occuring molecules, and (2) specific targeting that could derive in new diagnostic tools by artificial selection.

In this thesis, the natural occurring targeting molecule selected was heparin and its derivatives. It is known that heparin or compounds from the sGAG family have a direct action in the parasite's development, specifically in two stages: invasion of the RBC by the merozoite [129] and mosquito midgut epithelium invasion by ookinetes [442]. The timeframe between the schizont egress and the merozoite attachment is about 30 seconds [126]. Therefore, heparin has a fast-inhibition activity to RBC invasion. This can be divided into two possible inhibition points: (1) it can block the schizont egress, by entering when the cells starts to burst before full egress [374], and (2) it can attach to the merozoite just before its reorientation on the invasion process. In this sense, heparin is highly effective *in vitro* [129], but *in vivo*, finding the exact timeframe in which heparin can act is far more difficult. This molecule has a circulation time of few hours [527], hence it should be active within the few minutes in which egress and invasion take place. Modifications like depolymerization of heparin can elongate its circulation time (due to less unspecific interactions with plasma molecules or cell surfaces [527]). Alternatively, linking heparin to a nanostructure can elongate its circulation time. This effect could be mediated by size (if the structure is above 20 nm, much less extravasation of the compound is expected), or by limiting its interactions with plasma components [528,529], which could potentially facilitate its availability for interacting with the merozoite.

In the first article here compiled, the experimental strategy started by obtaining heparin derivatives. Five different candidate heparin-derived molecules offered good prospects for their application in blocking the merozoite invasion: their aPTT was equal or lower than 23 IU/mg and they still remained enough active in terms of antimalarial activity, because they had IC_{50}s between 49 and 104 µg/mL. These compounds were proven safe *in vitro* and *in vivo* up to doses of 320 mg/Kg, and thus, high doses of the compound could be safely administered to reach active concentrations. Precisely, the highest concentrations administered were in a range of 8 to 19-fold the IC_{50} and 1.5 to 8-fold the 90% inhibitory concentration of the compounds. However, the compounds did not significantly elongate animal survival or influence

pRBCs percentajes when administered *in vivo*. It was confirmed that their plasma $t_{1/2}$ was rather short (less than 30 min for the compounds tested) and, additionaly, interactions with plasma components might be further limiting their antimalarial activity *in vivo*. After observing this, heparin was covalently linked to the surface of liposomes as a proof of concept design with the purpose of elongating its circulation time. Even though, the future perspective is using polymers or other less expensive formulations, the explored approach was very useful for studying the effect of size and nanostructured stabilization of heparin.

The results showed that the plasma half-live of the heparin-coated liposomes was not longer than that of heparin alone, but the peak concentration was higher for the liposome formulation. These liposomes might limit the extravasation from the beginning as it was observed that heparin concentration and stability in plasma was higher. However, as the clearance dynamics were very similar to that of free heparin, probably the liposomes were not very effective in limiting the interactions with plasma components, which can led to aggregates that are subsequently eliminated by phagocytic cells. In the liposome design explored, we included 2% of 2 KDa PEG to achieve stabilization and a 'limited-interaction' effect. The ratio between PEG-lipid and heparin was approximately 0.3:1. To improve the system, either a composition with longer chains of PEG or a higher PEG:heparin ratio could be explored, but their potential effect in masking the heparin interactions with merozoites should also be ruled out.

Formulations combining heparin with other molecules could provide other characteristics or functionalities. For instance, artesunate linked covalently to heparin has showed to form self-assembled nanostructures that provided longer circulation time for artesunate [454]. This sort of prodrug combination was also explored in this work. We combined heparin with primaquine, and observed that the antimalarial activity was higher for the combination than for the individual compounds. This approach can be further explored with different antimalarials with distinct characteristics, because they may offer other advantages or even synergestic effects. In particular, combining the heparin with other structures targeting either the free merozoite or the schizont egress could increase its activity by synergistic action.

Once the best strategy for enhancing heparin activity *in vivo* is defined, more suitable routes of administration should be explored too. Intravenous administration of antimalarial treatment is only applied for severe cases in which oral administration is not possible [164]. Heparin alone cannot be absorbed orally, but certain formulations containing heparin can

promote its intestinal absorption [530]. The next step in this project aims to test chitosan or cationic polymers for improving the pharmacokinetic profile of sGAGs; these types of molecules could also be platforms for oral delivery because polycationic solutions or nanoparticles promote drug absorption in the digestive tract [356].

Another strategy would be looking for molecules that mimic the sulfate pattern of heparin but already have long circulation times and lack the anticoagulant activity. A list of GAGs and sulfated-polymeric structures have already been assessed *in vitro* [440]. A previous publication pointed out that sulfated cyclodextrins had this inhibiting activity too, and they could even reduce mice parasitemia in a *P. berghei* model [531]. Cyclodextrins are nanostructures that consist in glucose-based rings with the ability of drug encapsulation, thus they could be used in a combination treatment strategy in which both components have an antimalarial effect. Unfortunately, these structures still have problems to solve as they are not orally absorbed and have short circulation times [532]. These drawbacks could be diminished if sulfated cyclodextrins form part of a nanostructure. In this approach, they can interact with polycations thanks to their sulfated groups. This type of combination could enhance the absorption and circulation time of the sulfated sugar-ring, in the same way as for heparin. Their main advantage compared to heparin is that cyclodextrins already lack anticoagulant activity.

Even though it seems that human administration of heparin for malaria treatment still has a long road to go, it may have potential for other applications too. In the second article presented here, heparin was applied to block the parasite's development in the murine model of *P. berghei* during mosquito stages. There is previous evidence of CS proteoglycans involved in the ookinete invasion of the mosquito midgut [442], and heparin interaction with the ookinete surface [447]. Therefore, the next question to solve was whether heparin can block the ookinete invasion of the mosquito midgut and prevent the parasite development. Our results showed that heparin and hypersulfated heparin reduced infection intensity and prevalence when administered together with blood; however, this effect was not that clear when administered in the sugar feed. Despite the intention of this approach was not to deliver sGAGs directly to humans and achieve the transmission blocking effect, other safer compounds could be used with this purpose. For instance, when the sulfated polymer VS1 was administered directly to infected mice and these animals were used to infect mosquitos by direct bite, a reduction in

mosquito infections was achieved [443]. A similar strategy could be developed with nanostructured heparin or derived molecules, with the double advantage of blockthe merozoite invasion and the parasite transmission.

On the other hand, it was worth to explore the direct administration of blocking compounds to mosquitos that will not require long clinical trials. However, heparin alone did not had that transmission blocking effect, probably because the sugar feed in which it is administered was expelled during the blood meal. To obtain longer retention times in the midgut, the best approaches are: (i) to combine heparin with a targeting molecule against the mosquito midgut, or (ii) to test which physicochemical characteristics allow heparin retention and/or higher activity. The next step in this project is testing if hypersulfated heparin has any activity when administered in the sugar feed.

In addition, *Anopheles* species have hemagglutinating activity driven by the interaction with sGAGs [533]. The lectin producing this activity could compete with the sGAGs-binding proteins of the ookinete surface. This might be an added explation of why the heparin did not work in the sugar feed for three reasons: (i) the reduced volume of sugar that mosquitos take compared to blood would already dilute the heparin in the midgut, (ii) expelling liquid while taking the blood meal could also expel most of the heparin taken and (iii) if those mosquitoes lectins are present and blocking the remaining heparin, very few amount would be available for its action. Nevertheless, the last effect does not seem to affect heparin in the blood meal at the same extent, so it would probably be the combination of the 3 suggested points what makes the treatment unsuccessful with the sugar meal. Identifying the specific lectin and investigating its interactions with heparin or other GAGs would be helpful to discard specific molecular arrangements that interact more with the lectin and select others that favors interaction with ookinete surface.

Besides natural occurring ligands as a tool for parasite targeting, the other branch of this work was focused on obtaining new targeting molecules, and explore their potential application. Aptamer development was selected for fulfilling this objective as they can be selected to have the desired level of affinity and specificity, which can compete with the ones of antibodies, but with a less expensive and easier production [458], and they can be easily modified to have a broad range of different applications [496,534]. Cell-SELEX was the selected approach for aptamer identification to obtain new biomarkers for malaria application. Previous trials of selection with fresh parasites from different strains and stages were unsuccessful in

providing aptamers for two main reasons: (1) loss of sequences in the selection (see supplementary information, Figure S.1), and (2) preferential binding to cell-debris that could not be washed away (see supplementary information, Figure S.2). However, the aptamer selection process was successful when the target cells were fixed *P. falciparum* 3D7 trophozoites. In here, the fixation process permeabilized the cells and the aptamers targeted intracellular antigens, which was not the initial objective. Nevertheless, the high specificity obtained and the observation that they could bind different parasite species, opened the possibility for their application as diagnostic tools.

It is likely that the target of our aptamers is a protein, because aptamer-6-FAM signal was observed when incubated with protein extracts. However it is not discarded than such binding site might be a lipid or a saccharide as the signal is present in several bands in the western blot experiments. Therefore, it could correlate with post-translation modification of proteins, perhaps a glycan modification or protein complexes with other biomolecules. We have observed a very similar pattern in western blot staining, which suggest they may bind the same proteins or domains. This may pose some challenges for RDT development based on this aptamers, related to competition for the same target, if those aptamers are used for both capture and detection. The sensitivity of antibody-based RDTs is higher if the capture antibody that retains the protein and the one conjugated to the colloidal gold (used to have a visual result)l do not compete for the same epitopes [535]. This problem can also happen using aptamers. In this regard, different strategies could provide higher sensitivity when using aptamers raised against the same target as: (i) aptamers are smaller than antibodies and will produce less stearic impediments in the binding of another aptamer, therefore, sensibility might be less affected; (ii) when the specific epitope is identified, other aptamers can be selected against other epitopes in the same protein; and (iii) it is possible to combine aptamers with an antibody raised against that protein in the same diagnostic device, substituting just one of the antibodies can already decrease the production costs of the RDTs.

The next steps for RDT development with these aptamers are presumably: (1) modification for nuclease protection, (2) elucidate a sandwich-like strategy, (3) testing strip-like conditions needed for aptamers and (4) increase the number of patient samples to test. Technically, the adaptation of aptamers to RDTs should not imply many difficulties, however problems like cell permeabilization and appropriate buffer selection have to be properly addressed to obtain high specificity and sensibility.

On the other hand, to meet the needs for certain health care settings and/or ease the sample taking in the case of infants, RDT approaches using urine samples instead of blood are being developed, with the same technical approach and antigens (HRP2) as current blood RDTs [536–538]. This technique is less invasive and its specificity is fairly the same than blood RDTs. However the sensitivity is slightly lower and they still have the same antigen-antibody related drawbacks as blood RDTs. As a new strategy, it is possible to identify new biomarkers in urine using SELEX, either proteins or even other types of molecules excreted due to parasite activity.

Additionally, heparin or other sGAGs could also have potential in parasite detection. When merozoite interacts with erythrocytes pursuing invasion, certain proteins are shed in the process. MSP1 and AMA1 are cleaved in the surface of the merozoite [539] and MSP1-33 fragment is released in the plasma, among others. It is precisely the MSP1-33 fragment the one found to interact with heparin [129], however heparin would be limited in its detection, as its specificity will not be as high as an antibody mostly because it interacts with more proteins in the plasma. Other strategies could be applied: a combined retention/detection system of heparin plus a more specific antibody or aptamer could be explored as a cheaper alternative for RDT development.

Any targeting strategy has potential to be applied as useful tool in the malaria field, either coming from the study of molecular interactions between host and parasite or by screening of new biomarkers. The easy modification of GAGs and aptamers and the possibility to combine them with nanostructures, polymers and other materials could provide adaptable tools to meet the needs of the malaria elimination agenda.

Conclusions

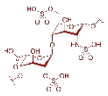

1. The heparin modifications that offered the best balance between reduced anticoagulant activity and maintained antimalarial activity were: medium molecular weight heparin combined with 2-*O*-desulfation, alone or with glycol-splitting; and ultra-low molecular weight heparin, alone or combined with 2-*O*-desulfation and glycol-splitting.

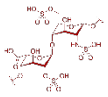

2. The selected heparin-derived molecules did not elicit toxic effects in mice when administered IV up to a concentration of 320 mg/Kg.

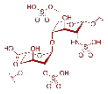

3. The *in vitro* IC_{50}s of the selected compounds were:
    a. 91.95 ± 8.97 µg/mL for 2-*O*-desulfated medium molecular weight heparin,
    b. 79.60 ± 5.38 and 84.20 ± 13.45 µg/mL for the two replicates of 2-*O*-desulfated glycol-split medium molecular weight heparin,
    c. 49.31 ± 5.97 µg/mL for ultra-low molecular weight heparin, and
    d. 104.40 ± 6.03 µg/mL for 2-*O*-desulfated glycol-split ultra-low molecular weight heparin.

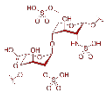

4. *In vivo* activity was assayed with concentrations of 75 or 150 mg/Kg/dose in a 4-day suppressive test. Activity was lower than expected, and their pharmacokinetic profile was a possible cause. Blood circulation times were measured *in vivo*: heparin had a $t_{1/2}$ of 25.74 min and 2-*O*-desulfated glycol-split medium molecular weight heparin had a $t_{1/2}$ of 29.13 min.

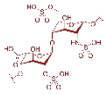

5. Attaching heparin to liposomes did not elongate $t_{1/2}$ (22.40 min), but increased the peak concentration in plasma: from about 18 µg/mL for free heparin, to about 40 µg/mL for the liposomal formulation.

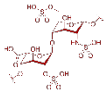

6. Heparin-Cy5 was observed to label *P. berghei* ookinetes in discrete areas of the cell.

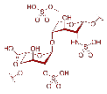

7. Heparin-Cy5 could be administered to *A. stephensi* mosquitoes by sugar feed in cotton swaps and by blood meal in membrane feeding assays. Cy5 signal was observed up to 72 and 24 hours after the administration, respectively.

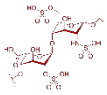

8. Heparin and hypersulfated heparin can block *P. berghei* development in the mosquito when administered together with blood in membrane feeding assays. Heparin could reduce both the prevalence of infection (proportion of mosquitoes infected) and the infection intensity (oocyst/midgut) in a dose-dependent manner for concentrations of 5 and 500 µg/mL. Hypersulfated heparin at 5 µg/mL had similar effect than heparin at 500 µg/mL.

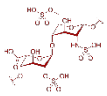

9. Heparin was not effective when administered in sugar feed on cotton swaps before direct mosquito infection using infected mice. Possibly mosquitoes expel the sugar feed to make room for the blood inside the midgut.

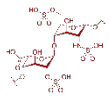

10. The effect of heparin is not exerted during gametocyte egress, gamete fertilization or ookinete maturation. It is likely that it blocks the ookinete interaction with midgut epithelium.

1. Five new aptamers against *Plasmodium falciparum* have been identified. They recognized specifically fixed late stage pRBCs vs. RBCs, by flow cytometry characterization with 6-FAM labeling of the aptamers:
    a. Sequence 19 recognized 93.04% late stage pRBCs / 0.02% RBCs
    b. Sequence 24 recognized 94.38% late stage pRBCs / 0.06% RBCs
    c. Sequence 30 recognized 95.16% late stage pRBCs / 0.01% RBCs
    d. Sequence 77 recognized 88.27% late stage pRBCs / 0.00% RBCs
    e. Sequence 78 recognized 84.47% late stage pRBCs / 0.00% RBCs

2. Selected aptamers could not bind to fresh pRBCs but they bound fixed or permeabilized cells; therefore, their target is intracellular.

3. The characterization of their minimal sequence and the influence of signaling molecule were explored: shorter chains without the primer-binding regions were designed and TAMRA or biotin tags where tested instead of 6-FAM. The following effects were observed:
    a. the shorter version of aptamer 19 (19s) had significant lower binding to pRBCs, the shorter sequences of aptamers 24, 77 and 78 (24s, 77s and 78s) had slightly lower binding than their long versions, while the shorter version of aptamer 30 (30s) had slightly higher binding;
    b. TAMRA tag suppressed aptamer 30 binding to pRBCs, the tag change possibly affects its structure;
    c. and biotin tag was measured by Streptavidin-AlexaFluor 647 recognition, the percentages of pRBCs recognize were lower for all the sequeces. This might be due to steric impediments in the Streptavidin penetration to the cell and binding.

4. Their apparent K_d was calculated using fixed late stage pRBCs and a random sequence (aptamer 700) as control of non-specific binding. Longer and shorter versions of the aptamer sequences had differences in their K_ds but the variation did not correlated with the size, they were specific of sequence. Binding Potential (BP) was defined as B_{max}/K_d ratio, to start exporing which sequences have better singal and binding to late stage pRBCs:
    a. Aptamer 19 had 0.46 ± 0.08 μM of apparent K_d and 19s had 1.10 ± 0.15 μM. Their BP was 13.4 and 1.7 a.u./μM respectively.
    b. Aptamer 24 had 1.14 ± 0.11 μM of apparent K_d and 24s had 1.07 ± 0.06 μM. Their BP was 4.9 and 8.0 a.u./μM respectively.
    c. Aptamer 30 had 0.61 ± 0.04 μM of apparent K_d and 30s had 1.53 ± 0.07 μM. Their BP was 6.4 and 23.8 a.u./μM respectively.
    d. Aptamer 77 had 1.07 ± 0.12 μM of apparent K_d and 77s had 0.90 ± 0.06 μM. Their BP was 1.9 and 7.3 a.u./μM respectively.

e. Aptamer 78 had 0.33 ± 0.03 μM of apparent K_d and 78s had 1.77 ± 0.15 μM. Their BP was 9.4 and 5.9 a.u./μM respectively.

5. The type of protein extracts and stages at which the aptamers' antigen/s can be detected has been identified by dot blot assays, using 6-FAM aptamers for the detection. Then, extracts made with RIPA buffer and parasites between 36 and 48 hours post invasion were used for western blot analysis and direct identification in a SDS-PAGE for gel slicing and mass spectrometry analysis of the bands. Results point to more than one protein being recognized by the aptamers, possibly through a common domain. All aptamers showed the same binding pattern: they were likely binding the same epitope.

6. Comparison by flow cytometry indicated that the 5 sequences here developed could bind pRBCs and provide >30-fold higher signal than that of a pLDH aptamer.

7. They can recognize *P. falciparum*, *P. vivax*, *P. ovale* and *P. malariae* fixed in slides directly from patient blood samples. This is indicative of a possible pan-malaria detection with application in diagnostic purposes.

Supplementary Information

SI.1. Aptamers against gametocytes

Before achieving the selection of the aptamers that was published in Journal of Biomedical Nanotechnology, several attempts with different strategies had been explored. The first approach was to develop aptamers against the surface of the gametocytes, aiming to develop a specific targeting tool against this parasite stage that would allow implementing transmission-blocking strategies.

Gametocytes are known for they sequestration in the bone marrow, however the mechanisms on how they do so are still not known. It has been hypothesized that the stiffness of the gametocyte pRBC prevents that they go into circulation, and it is unlikely that there are surface proteins behind the sequestering, as there are not known adhesive proteins in their surface [135]. In an attempt to identify, at least by gene annotation, possible candidates to be surface antigens in gametocytes, Sutherland searched in PlasmoDB for protein-coding genes that (1) had high mRNA abundance in gametocytes (90–100% of maximum expression), (2) do not had mRNA abundance in late trophozoites (50–100% of maximum expression) and either had a signal peptide or a *Plasmodium* export element motif [540]. By checking again the candidate list that this author proposed, the gene with ID PF14_0753 (currently annotated as Plasmodium exported protein (hyp13), ID PF3D7_1478100), though still with unknown function, it is a exported protein and contains two transmembrane domains, being the best candidate as possible gametocyte surface antigen. Either presence of this protein or other antigens, like sugar modifications or lipid differences in the membrane were expected to be the targets in this aptamer selection.

As the moment for applying counter selection could be decisive driving the selection (if applied before the selection, some potential binding molecules could be accidentally dragged with the counter cells, and if applied after the selection, an enriching the pool of non-target sequences could occur, and maybe the target ones could be less represented in further cycles), two different selection procedures were applied: starting by a counter selection or applying it after the first selection round.

Materials and Methods

The methodology and materials employed were identical to the described in the article presented before, except for the target cells, which were fresh *P. falciparum* E5 gametocytes. Parasite strain was kindly gifted by Dr. Alfred Cortés. 30 mL culture at 5% pRBC and 3% hematocrite was sincronyzed using sorbitol 5% w/v [541], and resuspended in fresh complete medium containing *N*-acetyl-glucosamine at 50 mM, blocked the development of asexual stages. Cultures were maintained changing the medium daily the first 5 days, and each two days until day 8-9. Magnetic Assisted Cell Sorting (MACS®, Miltenyi Biotec) was used for gametocyte concentration, following manufacturer's indications. Counter selections were done before or after the first round of selection, and afterwards every 3 rounds of selection.

Results

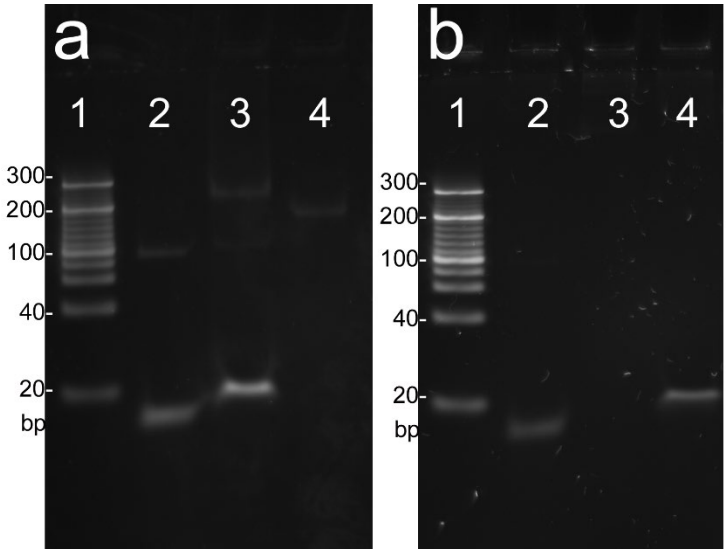

Figure S.1. Images from the electrophoresis gels of DNA samples obtained from the selection with gametocytes. (a) First round of selection, the lanes were: **(a1)** ladder, **(a2)** PCR product after the selection, **(a3)** PCR product after DNA precipitation and **(a4)** ssDNA eluted from the streptavidin column. **(b)** In the fourth round of selection the DNA could not be seen in the electrophoresis gels, the lanes were: **(b1)** ladder, **(b2)** PCR product after the selection, **(b3)** elution from the streptavidin column and **(b4)** flowthrough from the streptavidin column, containing just the primers.

SI.2. Aptamer selection with VAR2CSA expressing line

Another strategy followed for the selection of aptamers was using a parasite line that expresses VAR2CSA variant of PfEMP1: *Plasmodium falciparum* CS2 strain. Selection over immobilized CSA allows to maintain the allele expressed.

Materials and Methods

Materials were purchased in Sigma-Aldrich unless specified. *P. falciparum CS2* line was obtained from Bei Resources (catalogue MRA-96).

The methodology followed was the same as in the third article of this work [542], except for the cell preparation: trophozoite stages of the parasites were selected and purified by 2 different methods: Percoll™ (GE Healthcare) 70% gradient purification (as described in the reference) or gelatin flotation.

For the gelatin flotation [543], parasite culture is concentrated by centrifugation at 500 g for 4 minutes, supernatant discarded and resuspended to make 2.4x pellet volumes with prewarmed washing medium, to which 2.4x pellet volume of Gelofusine® (B. Braun) is added. After homogeneus mixing, the solution is incubated for 30 minutes at 37 ˚C. The upper phase (approximately 1/5 of the volume) is transferred to a new tube, washed with 10 mL washing medium and centrifuged in the same conditions as before, then resuspended in binding buffer.

In these experiments, composition of binding buffer was slightly changed by including 0.1 mg/mL of tRNA from yeast as extra blocking agent. The rest of the components remained the same.

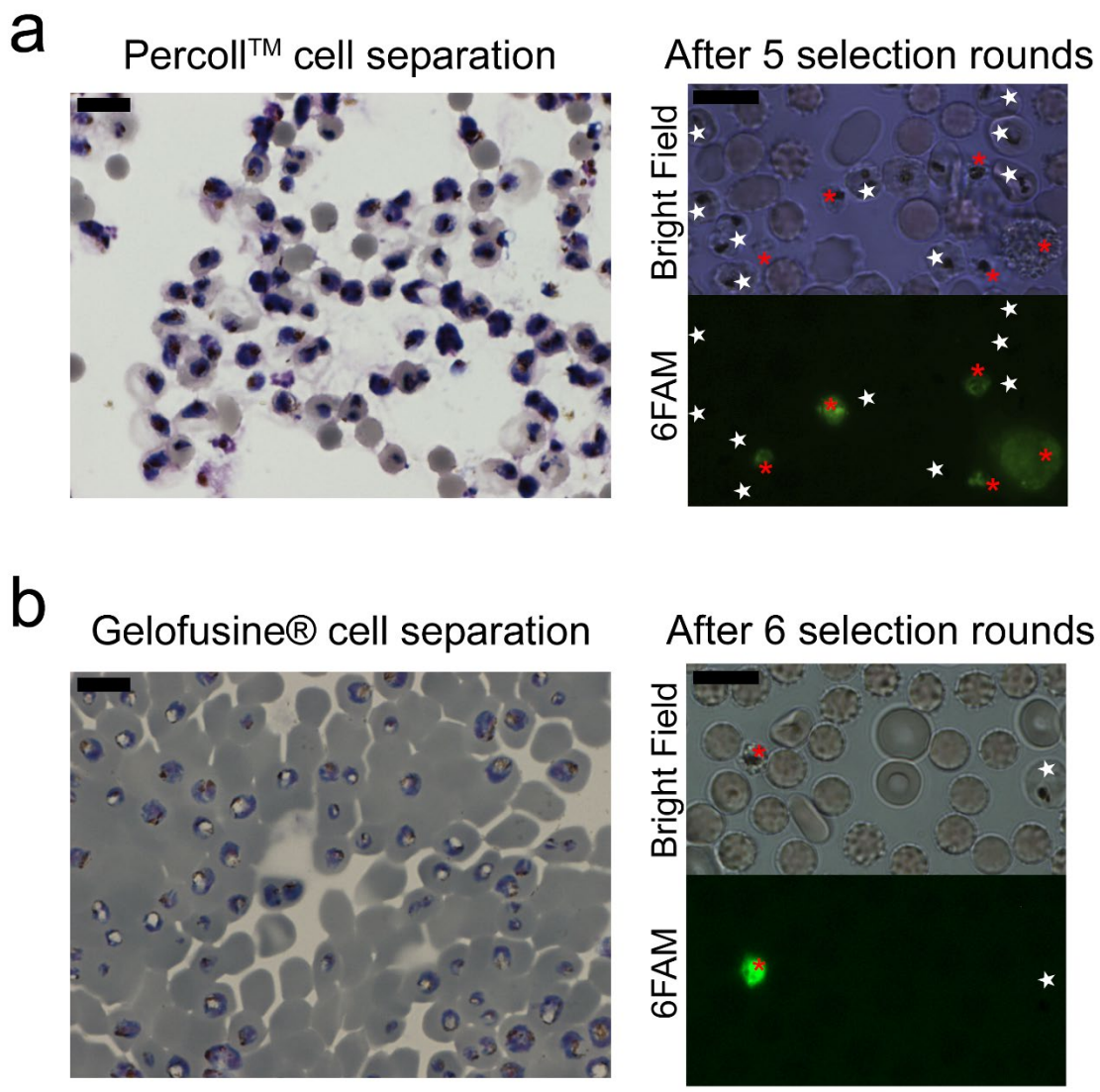

Figure S.2. Results from the two selection processes using *P. falciparum* CS2 parasite cell line. (**a**) The oligonucleotides were incubated with Percoll™ purified late stages of the parasite, in the left image there is a giemsa stain of the purified cells. In this process cell debris from the culture can be taken or the membranes disrupted, and after 5 rounds of selection, 6FAM-labeled oligonucleotides wer mostly binding such structures and not the intact pRBCs. (**b**) In a second selection process, gelatin flotation was used for parasite concentration, and the giemsa stain of the purified cells is shown in the left. On the right, an image of the 6th round oligonucleotide pool incubated with unpurified culture: the oligonucleotides are binding a ruptured cell and not the intact pRBC that appears in the image. In all panels, red asterisks (*) mark the cell debris, ruptured parasites or leukocytes that contain the 6FAM signal from the oligonucleotides, while the white stars (⋆) label the intact pRBCs. The scale bars are 10 μm.

Bibliography

1. WHO Global Malaria Programme. *World Malaria Report 2017*. (2017).
2. WHO Global Malaria Programme. *World Malaria Report 2018*. www.who.int/malaria (2018).
3. WHO Global Malaria Programme. *World Malaria Report 2019*. (2019).
4. Crutcher, J. M. & Hoffman, S. L. Malaria. in *Medical Microbiology. 4th edition.* (ed. Baron, S.) 17 (University of Texas Medical Branch at Galveston, 1996).
5. WHO Global Malaria Programme. *World Malaria Report 2015*. (2015).
6. Bray, R. S. The Malaria Parasites of Anthropoid Apes. *J. Parasitol.* **49**, 888–891 (1963).
7. Liu, W. *et al.* Origin of the human malaria parasite *Plasmodium falciparum* in gorillas. *Nature* **467**, 420–425 (2010).
8. Liu, W. *et al.* Multigenomic Delineation of *Plasmodium* Species of the *Laverania* Subgenus Infecting Wild-Living Chimpanzees and Gorillas. *Genome Biol. Evol* **8**, 1929–1939 (2016).
9. Mita, T. & Jombart, T. Patterns and dynamics of genetic diversity in *Plasmodium falciparum*: What past human migrations tell us about malaria. *Parasitol. Int.* **64**, 238–243 (2015).
10. Cowman, A. F., Healer, J., Marapana, D. & Marsh, K. Malaria: Biology and Disease. *Cell* **167**, 610–624 (2016).
11. Flannery, E. L., Chatterjee, A. K. & Winzeler, E. A. Antimalarial drug discovery-approaches and progress towards new medicines. *Nature Reviews Microbiology* vol. 11 849–862 (2013).
12. Josling, G. A., Williamson, K. C. & Llinás, M. Regulation of Sexual Commitment and Gametocytogenesis in Malaria Parasites. *Annu. Rev. Microbiol* **72**, 501–520 (2018).
13. Joice, R. *et al. Plasmodium falciparum* transmission stages accumulate in the human bone marrow. *Sci. Transl. Med.* **6**, 1–16 (2014).
14. Aguilar, R. *et al.* Molecular evidence for the localization of *Plasmodium falciparum* immature gametocytes in bone marrow. *Blood* **123**, 959–966 (2014).
15. Ramdani, G. *et al.* cAMP-Signalling Regulates Gametocyte-Infected Erythrocyte Deformability Required for Malaria Parasite Transmission. *PLoS Pathog.* **11**, 1–20 (2015).
16. Aly, A. S. I., Vaughan, A. M. & Kappe, S. H. I. Malaria Parasite Development in the Mosquito and Infection of the Mammalian Host. *Annu. Rev. Microbiol.* **63**, 195–221 (2009).
17. Rowe, A., Obeiro, J., Newbold, C. I. & Marsh, K. *Plasmodium falciparum* rosetting is associated with malaria severity in Kenya. *Infect. Immun.* **63**, 2323–2326 (1995).
18. Carlson, J. *et al.* Human cerebral malaria: association with erythrocyte rosetting and lack of anti-rosetting antibodies. *Lancet* **336**, 1457–60 (1990).
19. Hviid, L. The role of *Plasmodium falciparum* variant surface antigens in protective immunity and vaccine development. *Hum. Vaccin.* **6**, 84–89 (2010).
20. Travassos, M. A. *et al.* Children with cerebral malaria or severe malarial anaemia lack immunity to distinct variant surface antigen subsets. *Sci. Rep.* **8**, 1–14 (2018).
21. Salanti, A. *et al.* Evidence for the involvement of VAR2CSA in pregnancy-associated malaria. *J. Exp. Med.* **200**, 1197–1203 (2004).
22. Pasternak, N. D. & Dzikowski, R. PfEMP1: an antigen that plays a key role in the pathogenicity and immune evasion of the malaria parasite *Plasmodium falciparum*. *Int. J. Biochem. Cell Biol.* **41**, 1463–6 (2009).
23. Baum, J., Gilberger, T.-W., Frischknecht, F.

& Meissner, M. Host-cell invasion by malaria parasites: insights from *Plasmodium* and *Toxoplasma*. *Trends Parasitol.* **24**, 557–563 (2008).

24. Singh, S. *et al.* Immunity to recombinant *Plasmodium falciparum* merozoite surface protein 1 (MSP1): Protection in *Aotus nancymai* monkeys strongly correlates with anti-MSP1 antibody titer and in vitro parasite-inhibitory activity. *Infect. Immun.* **74**, 4573–4580 (2006).

25. Pusic, K. M. *et al.* T cell epitope regions of the *P. falciparum* MSP1-33 critically influence immune responses and in vitro efficacy of MSP1-42 vaccines. *PLoS One* **6**, (2011).

26. Malkin, E. *et al.* Phase 1 study of two merozoite surface protein 1 (MSP142) vaccines for *Plasmodium falciparum* malaria. *PLoS Clin. Trials* **2**, (2007).

27. Swearingen, K. E. *et al.* Interrogating the *Plasmodium* Sporozoite Surface: Identification of Surface-Exposed Proteins and Demonstration of Glycosylation on CSP and TRAP by Mass Spectrometry-Based Proteomics. *PLoS Pathog.* **12**, 1–32 (2016).

28. Foth, B. J. & McFadden, G. I. The apicoplast: A plastid in *Plasmodium falciparum* and other apicomplexan parasites. *Int. Rev. Cytol.* **224**, 57–110 (2003).

29. Chakraborty, A. Understanding the biology of the *Plasmodium falciparum* apicoplast; an excellent target for antimalarial drug development. *Life Sci.* **158**, 104–110 (2016).

30. Bannister, L. H., Hopkins, J. M., Fowler, R. E., Krishna, S. & Mitchell, G. H. A brief illustrated guide to the ultrastructure of *Plasmodium falciparum* asexual blood stages. *Parasitology Today* vol. 16 427–433 (2000).

31. Spielmann, T., Montagna, G. N., Hecht, L. & Matuschewski, K. Molecular make-up of the *Plasmodium* parasitophorous vacuolar membrane. *Int. J. Med. Microbiol.* **302**, 179–186 (2012).

32. Maurer, G. Die Malaria perniciosa. *Cent. für Bakteriol. Parasitenkd. und Infekt.* **23**, 695–719 (1902).

33. Mundwiler-Pachlatko, E. & Beck, H.-P. Maurer's clefts, the enigma of *Plasmodium falciparum*. *Proc. Natl. Acad. Sci. U. S. A.* **110**, 19987–19994 (2013).

34. Spielmann, T. & Gilberger, T.-W. Critical Steps in Protein Export of *Plasmodium falciparum* Blood Stages. *Trends Parasitol.* **31**, 514–525 (2015).

35. Langreth, S. G. & Reese, R. T. Antigenicity of the Infected-Erythtocyte and Merozoite surfaces in *Falciparum* Malaria. *J. Exp. Med.* **150**, 1241–1254 (1979).

36. Leech, J. H., Barnwell, J. W., Aikawa, M., Miller, L. H. & Howard, R.]. *Plasmodium falciparum* Malaria: Association of Knobs on the Surface of Infected Erythrocytes with a Histidine-rich Protein and the Erythrocyte Skeleton. *J. Cell Biol.* **98**, 1256–1264 (1984).

37. Rosenthal, P. J. & Meshnick, S. R. Hemoglobin catabolism and iron utilization by malaria parasites. *Mol. Biochem. Parasitol.* **83**, 131–139 (1996).

38. Beaudoin, R. L. & Garnham, P. C. C. Malaria Parasites and Other Haemosporidia. *J. Parasitol.* **54**, 192 (1968).

39. Carbone, T. Sulla nature chimica del pigmento malarico. *G. Accad. Med. Torino.* **39**, 901–905 (1891).

40. Brown, W. H. Malarial Pigment (So-Called Melanin): Its Nature and Mode of Production. *J. Exp. Med.* **13**, 290–299 (1911).

41. Goldie, P., Roth, E. F., Oppenheim, J. & Vanderberg, J. P. Biochemical Characterization of *Plasmodium falciparum* Hemozoin. *Am. J. Trop. Med. Hygene* **43**, 584–596 (1990).

42. Esposito, A. *et al.* FRET Imaging of Hemoglobin Concentration in *Plasmodium falciparum*-Infected Red Cells. *PLoS One* **3**, 10 (2008).

43. McKerrow, J. The Proteases and Pathogenicity of Parasitic Protozoa. *Annu. Rev. Microbiol.* **47**, 821–853 (1993).

44. Milani, K. J., Schneider, T. G. & Taraschi, T. F. Defining the morphology and

mechanism of the hemoglobin transport pathway in *Plasmodium falciparum*-infected erythrocytes. *Eukaryot. Cell* **14**, 415–426 (2015).

45. Fitch, C. D. *et al.* Intracellular Ferriprotoporphyrin IX Is a Lytic Agent. *Blood* **62**, 1165–1168 (1983).

46. Pagola, S., Stephens, P. W., Bohle, D. S., Kosar, A. D. & Madsen, S. K. The structure of malaria pigment β-haematin. *Nature* **404**, 307–310 (2000).

47. Azouzi, S., Kirat, K. El & Morandat, S. Hematin loses its membranotropic activity upon oligomerization into malaria pigment. *Biochim. Biophys. Acta - Biomembr.* **1848**, 2952–2959 (2015).

48. Jani, D. *et al.* HDP - A novel heme detoxification protein from the malaria parasite. *PLoS Pathog.* **4**, 1–15 (2008).

49. Egan, T. J., Mavuso, W. W., Ross, D. C. & Marques, H. M. Thermodynamic factors controlling the interaction of quinoline antimalarial drugs with ferriprotoporphyrin IX. *J. Inorg. Biochem.* **68**, 137–145 (1997).

50. Bachhawat, K., Thomas, C. J., Surolia, N. & Surolia, A. Interaction of chloroquine and its analogues with heme: An isothermal titration calorimetric study. *Biochem. Biophys. Res. Commun.* **276**, 1075–1079 (2000).

51. Kapetanaki, S. & Varotsis, C. Ferryl-oxo heme intermediate in the antimalarial mode of action of artemisinin. *FEBS Lett.* **474**, 238–241 (2000).

52. Reuling, I. J. *et al.* Concentration of *Plasmodium falciparum* gametocytes in whole blood samples by magnetic cell sorting enhances parasite infection rates in mosquito feeding assays. *Malar. J.* **16**, 315 (2017).

53. Rebelo, M. *et al.* Light Depolarization Measurements in Malaria : A New Job for an Old Friend. *Cytom. Part A* **87A**, 437–445 (2015).

54. Nalbandian, R. *et al.* A molecular-based magnet test for malaria. *Am. J. Clin. Pathol.* **103**, 57–64 (1995).

55. Tripathy, U., Giguère-bisson, M., Bohle, D. S., Georges, E. & Wiseman, P. W. Optimization of malaria detection based on third harmonic generation imaging of hemozoin. *Anal. Bioanal. Chem.* **405**, 5431–5440 (2013).

56. Gilson, R. C. *et al.* Growth of *Plasmodium falciparum* in response to a rotating magnetic field. *Malar. J.* **17**, 1–7 (2018).

57. Henry, B. *et al.* The Human Spleen in Malaria: Filter or Shelter? *Trends Parasitol.* **36**, 435–446 (2020).

58. David, P. H., Hommelt, M., Miller, L. H., Udeinya, I. J. & Oliginot, L. D. Parasite sequestration in *Plasmodium falciparum* malaria: Spleen and antibody modulation of cytoadherence of infected erythrocytes. *Med. Sci.* **80**, 5075–5079 (1983).

59. Kyes, S., Horrocks, P. & Newbold, C. Antigenic variation at the infected red blood cell surface in malaria. *Annu. Rev. Microbiol.* **55**, 673–707 (2001).

60. Guizetti, J. & Scherf, A. Silence, activate, poise and switch! Mechanisms of antigenic variation in *Plasmodium falciparum*. *Cell. Microbiol.* **15**, 718–726 (2013).

61. Langhorne, J., Ndungu, F. M., Sponaas, A. M. & Marsh, K. Immunity to malaria: More questions than answers. *Nat. Immunol.* **9**, 725–732 (2008).

62. Tran, T. M. *et al.* An Intensive Longitudinal Cohort Study of Malian Children and Adults Reveals No Evidence of Acquired Immunity to *Plasmodium falciparum* Infection. *Clin. Infect. Dis.* **57**, 40–47 (2013).

63. Pinzon-Charry, A. *et al.* Apoptosis and dysfunction of blood dendritic cells in patients with falciparum and vivax malaria. *J. Exp. Med.* **210**, 1635–1646 (2013).

64. Bañuls, A. L., Thomas, F. & Renaud, F. Of parasites and men. *Infect. Genet. Evol.* **20**, 61–70 (2013).

65. Perry, G. H. Parasites and human evolution. *Evol. Anthropol.* **23**, 218–228 (2014).

66. Lavstsen, T., Salanti, A., Jensen, A. T.,

Arnot, D. E. & Theander, T. G. Sub-grouping of *Plasmodium falciparum* 3D7 *var* genes based on sequence analysis of coding and non-coding regions. *Malar. J.* **2**, 27 (2003).

67. Smith, J. D. The role of PfEMP1 adhesion domain classification in *Plasmodium falciparum* pathogenesis research. *Mol. Biochem. Parasitol.* **195**, 82–87 (2014).

68. Subramani, R. *et al. Plasmodium Falciparum*-infected erythrocyte knob density is linked to the pfemp1 variant expressed. *MBio* **6**, 1–7 (2015).

69. Hviid, L. & Jensen, A. T. R. PfEMP1 - a parasite protein family of key importance in *Plasmodium falciparum* malaria immunity and pathogenesis. in *Advances in Parasitology* (eds. Rollinson, D. & Stothard, J. R.) vol. 88 51–84 (Elsevier Ltd, 2015).

70. Smith, J. D., Rowe, J. A., Higgins, M. K. & Lavstsen, T. Malaria's deadly grip: Cytoadhesion of *Plasmodium falciparum*-infected erythrocytes. *Cell. Microbiol.* **15**, 1976–1983 (2013).

71. Newbold, C. *et al.* Receptor-specific adhesion and clinical disease in *Plasmodium falciparum*. *Am. J. Trop. Med. Hyg.* **57**, 389–398 (1997).

72. Janes, J. H., Wang, C. P., Levin-Edens, E., Vigan-Womas, I. & Guillotte, M. Investigating the Host Binding Signature on the *Plasmodium falciparum* PfEMP1 Protein Family. *PLoS Pathog* **7**, 1002032 (2011).

73. Baruch, D. I. *et al.* Identification of a Region of PfEMP1 That Mediates Adherence of *Plasmodium falciparum* Infected Erythrocyte s to CD36: Conserved Function With Variant Sequence. *Blood* **90**, 3766–3775 (1997).

74. Mustaffa, K. M. F., Storm, J., Whittaker, M., Szestak, T. & Craig, A. G. In vitro inhibition and reversal of *Plasmodium falciparum* cytoadherence to endothelium by monoclonal antibodies to ICAM-1 and CD36. *Malar. J.* **16**, 279 (2017).

75. Mccormick, C. J., Craig, A., Roberts, D., Newbold, C. I. & Berendt, A. R. *Receptor Synergy in Malaria Cytoadherence Intercellular Adhesion Molecule-1 and CD36 Synergize to Mediate Adherence of* Plasmodium falciparum*-infected Erythrocytes to Cultured Human Microvascular Endothelial Cells*. *J. Clin. Invest* vol. 100 http://www.jci.org (1997).

76. Turner, L. *et al.* Severe malaria is associated with parasite binding to endothelial protein C receptor. *Nature* **498**, 502–507 (2013).

77. Petersen, J. E. V. *et al.* Disruption of EPCR-Dependent Functions By Plasmodium *Falciparum Erythrocyte* Membrane Protein 1 (PfEMP1) Can be Rescued By a Soluble EPCR Variant. *Blood* **124**, 577–577 (2014).

78. Lennartz, F. *et al.* Structure-Guided Identification of a Family of Dual Receptor-Binding PfEMP1 that Is Associated with Cerebral Malaria. *Cell Host Microbe* **21**, 403–414 (2017).

79. Vigan-Womas, I. *et al.* Structural Basis for the ABO Blood-Group Dependence of *Plasmodium falciparum* Rosetting. *PLoS Pathog.* **8**, e1002781 (2012).

80. Juillerat, A. *et al.* Biochemical and biophysical characterisation of DBL1α1-varO, the rosetting domain of PfEMP1 from the VarO line of *Plasmodium falciparum*. *Mol. Biochem. Parasitol.* **170**, 84–92 (2010).

81. Juillerat, A. *et al.* Structure of a *Plasmodium falciparum* PfEMP1 rosetting domain reveals a role for the N-terminal segment in heparin-mediated rosette inhibition. *Proc. Natl. Acad. Sci. U. S. A.* **108**, (2011).

82. Angeletti, D., Sandalova, T., Wahlgren, M. & Achour, A. Binding of subdomains 1/2 of PfEMP1-DBL1 α to Heparan sulfate or heparin mediates *Plasmodium falciparum* rosetting. *PLoS One* **10**, 1–15 (2015).

83. Fried, M., Muga, R. O., Misore, A. O. & Duffy, P. E. Malaria Elicits Type 1 Cytokines in the Human Malaria Elicits Type 1 Cytokines in the Human Placenta: IFN-γ and and TNF-α Associated with Pregnancy Outcomes. *J Immunol J. Immunol. by guest Sept.* **160**, 2523–2530 (1998).

84. Umbers, A. J. *et al.* Does Malaria Affect Placental Development? Evidence from *In Vitro* Models. *PLoS One* **8**, (2013).

85. Umbers, A. J., Aitken, E. H. & Rogerson, S. J. Malaria in pregnancy: small babies, big problem. *Trends Parasitol.* **27**, 168–175 (2011).

86. Salanti, A. *et al.* Selective upregulation of a single distinctly structured var gene in chondroitin sulphate A-adhering *Plasmodium falciparum* involved in pregnancy-associated malaria. *Mol. Microbiol.* **49**, 179–191 (2003).

87. Viebig, N. K. *et al.* A single member of the *Plasmodium falciparum* var multigene family determines cytoadhesion to the placental receptor chondroitin sulphate A. *EMBO Rep.* **6**, 775–781 (2005).

88. Beeson, J. G. *et al.* Structural basis for binding of *Plasmodium falciparum* erythrocyte membrane protein 1 to chondroitin sulfate and placental tissue and the influence of protein polymorphisms on binding specificity. *J. Biol. Chem.* **282**, 22426–22436 (2007).

89. Bigey, P. *et al.* The NTS-DBL2X region of VAR2CSA induces cross-reactive antibodies that inhibit adhesion of several *Plasmodium falciparum* isolates to chondroitin sulfate A. *J. Infect. Dis.* **204**, 1125–1133 (2011).

90. Bordbar, B. *et al.* Identification of Id1-DBL2X of VAR2CSA as a key domain inducing highly inhibitory and cross-reactive antibodies. *Vaccine* **30**, 1343–1348 (2012).

91. Singh, K. *et al.* Structure of the DBL3x domain of pregnancy-associated malaria protein VAR2CSA complexed with chondroitin sulfate A. *Nat. Struct. Mol. Biol.* **15**, 932–938 (2008).

92. Srivastava, A. *et al.* Var2CSA Minimal CSA Binding Region Is Located within the N-Terminal Region. *PLoS One* **6**, e20270 (2011).

93. Dahlbäck, M. *et al.* The chondroitin sulfate A-binding site of the VAR2CSA protein involves multiple N-terminal domains. *J. Biol. Chem.* **286**, 15908–15917 (2011).

94. Saveria, T. *et al.* Antibodies to *Escherichia coli*-expressed C-terminal domains of *Plasmodium falciparum* variant surface antigen 2-chondroitin sulfate a (VAR2CSA) inhibit binding of CSA-adherent parasites to placental tissue. *Infect. Immun.* **81**, 1031–1039 (2013).

95. Khunrae, P. *et al.* Full-Length Recombinant *Plasmodium falciparum* VAR2CSA Binds Specifically to CSPG and Induces Potent Parasite Adhesion-Blocking Antibodies. *J. Mol. Biol.* **397**, 826–834 (2010).

96. Srivastava, A. *et al.* Full-length extracellular region of the var2CSA variant of PfEMP1 is required for specific, high-affinity binding to CSA. *Proc. Natl. Acad. Sci.* **107**, 4884–4889 (2010).

97. Rovira-Vallbona, E. *et al.* VAR2CSA Signatures of High *Plasmodium falciparum* Parasitemia in the Placenta. *PLoS One* **8**, (2013).

98. Bachmann, A. *et al.* A comparative study of the localization and membrane topology of members of the RIFIN, STEVOR and PfMC-2TM protein families in *Plasmodium falciparum*-infected erythrocytes. *Malar. J.* **14**, 1–18 (2015).

99. Niang, M. *et al.* STEVOR Is a *Plasmodium falciparum* Erythrocyte Binding Protein that Mediates Merozoite Invasion and Rosetting. *Cell Host Microbe* **16**, 81–93 (2014).

100. Singh, H. *et al.* Expression dynamics and physiologically relevant functional study of STEVOR in asexual stages of *Plasmodium falciparum* infection. *Cell. Microbiol.* **19**, 1–11 (2017).

101. Quintana, M. del P. *et al.* Antibodies in children with malaria to PfEMP1, RIFIN and SURFIN expressed at the *Plasmodium falciparum* parasitized red blood cell surface. *Sci. Rep.* **8**, 3262 (2018).

102. Bouyer, G., Egée, S. & Thomas, S. L. Three types of spontaneously active anionic channels in malaria-infected human red blood cells. *Blood Cells, Mol. Dis.* **36**, 248–254 (2006).

103. Staines, H. M. *et al.* Electrophysiological studies of malaria parasite-infected erythrocytes: Current status. *Int. J.*

Parasitol. **37**, 475–482 (2007).

104. Pillai, A. D. *et al.* Solute Restriction Reveals an Essential Role for clag3-Associated Channels in Malaria Parasite Nutrient Acquisition. *Mol. Pharmacol.* **82**, 1104–1114 (2012).

105. Rovira-Graells, N. *et al.* Deciphering the principles that govern mutually exclusive expression of *Plasmodium falciparum clag3* genes. *Nucleic Acids Res.* **43**, 8243–8257 (2015).

106. Gupta, A. *et al.* CLAG3 Self-Associates in Malaria Parasites and Quantitatively Determines Nutrient Uptake Channels at the Host Membrane. *MBio* **9**, e02293-17 (2018).

107. Pain, M. *et al.* Synergistic Malaria Parasite Killing by Two Types of Plasmodial Surface Anion Channel Inhibitors. *PLoS One* **11**, e0149214 (2016).

108. Mira-Martínez, S. *et al.* Epigenetic switches in clag3 genes mediate blasticidin S resistance in malaria parasites. *Cell. Microbiol.* **15**, 1913–1923 (2013).

109. Pillai, A. D. *et al.* Solute restriction reveals an essential role for clag3-associated channels in malaria parasite nutrient acquisition. *Mol. Pharmacol.* **82**, 1104–1114 (2012).

110. Li HSIAO, L., Howard, R. J., AIKAWAt, M. & Taraschi, T. F. Modification of host cell membrane lipid composition by the intra-erythrocytic human malaria parasite *Plasmodium falciparum*. *Biochem. J* **274**, 121–132 (1991).

111. Tran, P. N. *et al.* Changes in lipid composition during sexual development of the malaria parasite *Plasmodium falciparum*. *Malar. J.* **15**, 73 (2016).

112. Lutz, H. U. & Bogdanova, A. Mechanisms tagging senescent red blood cells for clearance in healthy humans. *Front. Physiol.* **4**, 387 (2013).

113. de Back, D. Z., Kostova, E. B., van Kraaij, M., van den Berg, T. K. & van Bruggen, R. Of macrophages and red blood cells; a complex love story. *Front. Physiol.* **5**, 9 (2014).

114. Sherman, I. W., Prudhomme, J. & Tait, J. F. Altered Membrane Phospholipid Asymmetry in *Plasmodium falciparurn*-infected Erythrocytes. *Parasitol. Today* **13**, 242–243 (1997).

115. Pattanapanyasat, K. *et al.* Febrile temperature but not proinflammatory cytokines promotes phosphatidylserine expression on *Plasmodium falciparum* malaria-infected red blood cells during parasite maturation. *Cytom. Part A* **77**, 515–523 (2010).

116. Totino, P. R. R., Daniel-Ribeiro, C. T. & Ferreira-da-Cruz, M. de F. Evidencing the role of erythrocytic apoptosis in malarial anemia. *Front. Cell. Infect. Microbiol.* **6**, 176 (2016).

117. Facer, C. A. & Agiostratidou, G. High levels of anti-phospholipid antibodies in uncomplicated and severe *Plasmodium falciparum* and in *P. vivax* malaria. *Clin. Exp. Immunol.* **95**, 304–309 (1994).

118. Fernandez-Arias, C. *et al.* Anti-Self Phosphatidylserine Antibodies Recognize Uninfected Erythrocytes Promoting Malarial Anemia Article Anti-Self Phosphatidylserine Antibodies Recognize Uninfected Erythrocytes Promoting Malarial Anemia. *Cell Host Microbe* **19**, 194–203 (2016).

119. Rivera-Correa, J. *et al.* Atypical memory b-cells are associated with *Plasmodium falciparum* anemia through anti-phosphatidylserine antibodies. *Elife* **8**, 1–22 (2019).

120. Manodori, A. B., Barabino, G. A., Lubin, B. H. & Kuypers, F. A. Adherence of phosphatidylserine-exposing erythrocytes to endothelial matrix thrombospondin. *Blood* **95**, 1293–1300 (2000).

121. Eda, S. & Sherman, I. Cytoadherence of Malaria-Infected Red Blood Cells Involves Exposure of Phosphatidylserine. *Cell. Physiol. Biochem.* **12**, 373–384 (2002).

122. Zhang, R., Chandramohanadas, R., Lim, C. T. & Dao, M. Febrile Temperature Elevates the Expression of Phosphatidylserine on *Plasmodium falciparum* (FCR3CSA) Infected Red Blood Cell Surface Leading to Increased

Cytoadhesion. *Sci. Rep.* **8**, 1–10 (2018).

123. Totino, P. R. & Lopes, S. C. Insights into the cytoadherence phenomenon of Plasmodium vivax: The putative role of phosphatidylserine. *Front. Immunol.* **8**, 1148 (2017).

124. Gaur, D., Ghislaine Mayer, D. & Miller, L. H. Parasite ligand–host receptor interactions during invasion of erythrocytes by *Plasmodium merozoites*. *Int. J. Parasitol.* **34**, 1413–1429 (2004).

125. Cowman, A. F. & Crabb, B. S. Invasion of Red Blood Cells by Malaria Parasites. *Cell* **124**, 755–766 (2006).

126. Weiss, G. E., Crabb, B. S. & Gilson, P. R. Overlaying Molecular and Temporal Aspects of Malaria Parasite Invasion. *Trends Parasitol.* **32**, 284–295 (2016).

127. Weiss, G. E. *et al.* Revealing the Sequence and Resulting Cellular Morphology of Receptor-Ligand Interactions during *Plasmodium falciparum* Invasion of Erythrocytes. *PLoS Pathog.* **11**, 1–25 (2015).

128. Boyle, M. J. *et al.* Sequential processing of merozoite surface proteins during and after erythrocyte invasion by *Plasmodium falciparum*. *Infect. Immun.* **82**, 924–936 (2014).

129. Boyle, M. J., Richards, J. S., Gilson, P. R., Chai, W. & Beeson, J. G. Interactions with heparin-like molecules during erythrocyte invasion by *Plasmodium falciparum* merozoites. *Blood* **115**, 4559–4568 (2010).

130. Baldwin, M. R., Li, X., Hanada, T., Liu, S. & Chishti, A. H. Merozoite surface protein 1 recognition of host glycophorin A mediates malaria parasite invasion of red blood cells. *Blood* **125**, 2704–2711 (2015).

131. Kobayashi, K. *et al. Plasmodium falciparum* BAEBL Binds to Heparan Sulfate Proteoglycans on the Human Erythrocyte Surface. *J. Biol. Chem.* **285**, 1716–1725 (2010).

132. Srinivasan, P. *et al.* Disrupting malaria parasite AMA1–RON2 interaction with a small molecule prevents erythrocyte invasion. *Nat. Commun.* **4**, 1–9 (2013).

133. Chiu, C. Y. H. *et al.* Antibodies to the *Plasmodium falciparum* Proteins MSPDBL1 and MSPDBL2 Opsonize Merozoites, Inhibit Parasite Growth, and Predict Protection From Clinical Malaria. *J. Infect. Dis.* **212**, 406–415 (2015).

134. Sinden, R. E. Targeting the Parasite to Suppress Malaria Transmission. *Adv. Parasitol.* **97**, 147–185 (2017).

135. Saeed, M. *et al. Plasmodium falciparum* Antigens on the Surface of the Gametocyte-Infected Erythrocyte. *PLoS One* **3**, e2280 (2008).

136. Peatey, C. L. *et al.* Enhanced gametocyte formation in erythrocyte progenitor cells: A site-specific adaptation by *Plasmodium falciparum*. *J. Infect. Dis.* **208**, 1170–1174 (2013).

137. Nilsson, S. K., Childs, L. M., Buckee, C. & Marti, M. Targeting Human Transmission Biology for Malaria Elimination. *PLoS Pathog.* **11**, 17 (2015).

138. Skinner, J. *et al. Plasmodium falciparum* Gametocyte-Specific Antibody Profiling Reveals Boosting through Natural Infection and Identifies Potential Markers of Gametocyte Exposure. *Infect. Immun.* **83**, 4229–4236 (2015).

139. Van Dijk, M. R. *et al.* A central role for P48/45 in malaria parasite male gamete fertility. *Cell* **104**, 153–164 (2001).

140. Outchkourov, N. S. *et al.* Correctly folded Pfs48/45 protein of *Plasmodium falciparum* elicits malaria transmission-blocking immunity in mice. *Proc. Natl. Acad. Sci. U. S. A.* **105**, 4301–4305 (2008).

141. Quakyi, I. A., Carter, R., Rener, J., Kumar, N. & Good, M. F. The 230-kDa gamete surface protein of *Plasmodium falciparum* is also a target for transmission-blocking antibodies. *J. Immunol.* **139**, 4213–4217 (1987).

142. Macdonald, N. J. *et al.* Structural and Immunological Characterization of Recombinant 6-Cysteine Domains of the *Plasmodium falciparum* Sexual Stage Protein Pfs230. *J. Biol. Chem.* **291**, 19913–19922 (2016).

143. Barr, B. P. J. *et al.* Recombinant Pfs25 Protein of *Plasmodium falciparum* Elicits

Malaria Transmission-blocking Immunity in Experimental Animals. *J. Exp. Med.* **174**, 1203–1208 (1991).

144. Sharma, B. Structure and mechanism of a transmission blocking vaccine candidate protein Pfs25 from *P. falciparum*: A molecular modeling and docking study. *In Silico Biol.* **8**, 193–206 (2008).

145. Simon, N., Kuehn, A., Williamson, K. C. & Pradel, G. Adhesion protein complexes of malaria gametocytes assemble following parasite transmission to the mosquito. *Parasitol. Int.* **65**, 27–30 (2016).

146. Scholz, S. M. *et al. Pf*CCp proteins of *Plasmodium falciparum*: Gametocyte-specific expression and role in complement-mediated inhibition of exflagellation. *Int. J. Parasitol.* **38**, 327–340 (2008).

147. Li, F. *et al. Plasmodium* Ookinete-secreted Proteins Secreted through a Common Micronemal Pathway Are Targets of Blocking Malaria Transmission. *J. Biol. Chem.* **279**, 26635–26644 (2004).

148. Dessens, J. T. *et al.* CTRP is essential for mosquito infection by malaria ookinetes. *EMBO J.* **18**, 6221–6227 (1999).

149. Ramakrishnan, C. *et al.* Vital functions of the malarial ookinete protein, CTRP, reside in the A domains. *Int. J. Parasitol.* **41**, 1029–1039 (2011).

150. Zheng, W. *et al.* Functional characterization of *Plasmodium berghei* PSOP25 during ookinete development and as a malaria transmission-blocking vaccine candidate. *Parasites and Vectors* **10**, 1–11 (2017).

151. Armistead, J. S. *et al. Plasmodium falciparum* subtilisin-like ookinete protein SOPT plays an important and conserved role during ookinete infection of the *Anopheles stephensi* midgut. *Mol. Microbiol.* **109**, 458–473 (2018).

152. Smith, R. C. & Barillas-Mury, C. *Plasmodium* Oocysts: Overlooked Targets of Mosquito Immunity. *Trends Parasitol.* **32**, 979–990 (2016).

153. Ménard, R. The journey of the malaria sporozoite through its hosts: two parasite proteins lead the way. *Microbes Infect.* **2**, 633–642 (2000).

154. Morahan, B. J., Wang, L. & Coppel, R. L. No TRAP, no invasion. *Trends Parasitol.* **25**, 77–84 (2009).

155. Nardin, E. H. *et al.* Circumsporozoite Proteins of Human Malaria Parasites *Plasmodium falciparum* and *Plasmodium vivax*. *J. Exp. Med.* **156**, 20–30 (1982).

156. Zavala, F., Masuda, A., Graves, P. M., Nussenzweig, V. & Nussenzweig, R. S. Ubiquity of the repetitive epitope of the CS protein in different isolates of human malaria parasites. *J. Immunol.* **135**, 2790–2793 (1985).

157. Yang, A. S. P. *et al.* AMA1 and MAEBL are important for *Plasmodium falciparum* sporozoite infection of the liver. *Cell. Microbiol.* **19**, e12745 (2017).

158. Kariu, T., Ishino, T., Yano, K., Chinzei, Y. & Yuda, M. CelTOS, a novel malarial protein that mediates transmission to mosquito and vertebrate hosts. *Mol. Microbiol.* **59**, 1369–1379 (2006).

159. Loutfy, M. R. & Kain, K. C. Drug-Resistant Malaria. in *Reemergence of Established Pathogens in the 21st Century* (eds. Fong, I. W. & Drlica, K.) 335–360 (Kluwer Academic Publishers, 2003).

160. Egan, T. J., Ross, D. C. & Adams, P. A. Quinoline anti-malarial drugs inhibit spontaneous formation of β-haematin (malaria pigment). *FEBS Lett.* **352**, 54–57 (1994).

161. Trape, J.-F. The public health impact of chloroquine resistance in Africa. *Am. J. Trop. Med. Hygene* **64**, 12–17 (2001).

162. Klonis, N. *et al.* Artemisinin activity against *Plasmodium falciparum* requires hemoglobin uptake and digestion. *Proc. Natl. Acad. Sci. U. S. A.* **108**, 11405–11410 (2011).

163. Bridgford, J. L. *et al.* Artemisinin kills malaria parasites by damaging proteins and inhibiting the proteasome. *Nat. Commun.* **9**, 1–9 (2018).

164. World Health Organization. *Guidelines For The Treatment of Malaria - 3rd edition*. *www.who.int/malaria* (2015) doi:10.1016/0035-9203(91)90261-V.

165. Liu, H. *et al.* Metabolism of Piperaquine to Its Antiplasmodial Metabolites and Their Pharmacokinetic Profiles in Healthy Volunteers. *Antimicrob. Agents Chemother.* **62**, e00260-18 (2018).

166. Charmot, G., Amat-Roze, J., Rodhain, F., Le Bras, J. & Coulaud, J. Abord géographique de l'épidémiologie de la chloroquino-résistance de *Plasmodium falciparum* en Afrique tropicale. *Ann. Soc. Belg. Med. Trop. (1920).* **71**, 187–197 (1991).

167. Martin, R. E. *et al.* Chloroquine Transport via the Malaria Parasite's Chloroquine Resistance Transporter. *Science (80-.).* **325**, 1680–1682 (2009).

168. Bachhawat, K., Thomas, C. J., Surolia, N. & Surolia, A. Interaction of chloroquine and its analogues with heme: an isothermal titration calorimetric study. *Biochem. Biophys. Res. Commun.* **276**, 1075–1079 (2000).

169. Henry, M. *et al. Plasmodium falciparum* Na+/H+ exchanger 1 transporter is involved in reduced susceptibility to quinine. *Antimicrob. Agents Chemother.* **53**, 1926–1930 (2009).

170. Price, R. N. *et al.* Mefloquine resistance in *Plasmodium falciparum* and increased *pfmdr1* gene copy number. *Lancet* **364**, 438–337 (2004).

171. Sidhu, A. B. S. *et al.* Decreasing pfmdr1 copy number in Plasmodium falciparum malaria heightens susceptibility to mefloquine, lumefantrine, halofantrine, quinine, and artemisinin. *J. Infect. Dis.* **194**, 528–535 (2006).

172. Dondorp, A. M. *et al.* Artemisinin Resistance in *Plasmodium falciparum* Malaria. *N. Engl. J. Med.* **361**, 455–467 (2009).

173. Ariey, F. *et al.* A molecular marker of artemisinin-resistant *Plasmodium falciparum* malaria. *Nature* **505**, 50–55 (2014).

174. Escobar, C. *et al.* Polymorphisms in *Plasmodium falciparum* K13-Propeller in Angola and Mozambique after the Introduction of the ACTs. *PLoS One* **10**, e0119215 (2015).

175. Li, J. *et al.* Limited artemisinin resistance-associated polymorphisms in *Plasmodium falciparum K13-propeller* and *PfATPase6* gene isolated from Bioko Island, Equatorial Guinea. *Int. J. Parasitol. Drugs Drug Resist.* **6**, 54–59 (2016).

176. Madamet, M. *et al.* Absence of association between polymorphisms in the K13 gene and the presence of *Plasmodium falciparum* parasites at day 3 after treatment with artemisinin derivatives in Senegal. *Int. J. Antimicrob. Agents* **49**, 754–756 (2017).

177. Lin, J. -w. *et al.* Replication of *Plasmodium* in reticulocytes can occur without hemozoin formation, resulting in chloroquine resistance. *J. Exp. Med.* **212**, 893–903 (2015).

178. Lee, R. S., Waters, A. P. & Brewer, J. M. A cryptic cycle in haematopoietic niches promotes initiation of malaria transmission and evasion of chemotherapy. *Nat. Commun.* **9**, 1–9 (2018).

179. Phuc Quang Bui *et al.* Pyronaridine-artesunate Efficacy and Safety in Uncomplicated *Plasmodium falciparum* Malaria in Areas of Artemisinin-resistant Falciparum in Viet Nam (2017–2018). *Clin. Infect. Dis.* **70**, 2187–2195 (2020).

180. van der Pluijm, R. W. *et al.* Triple artemisinin-based combination therapies versus artemisinin-based combination therapies for uncomplicated *Plasmodium falciparum* malaria: a multicentre, open-label, randomised clinical trial. *Lancet* **395**, 1345–1360 (2020).

181. Lobo, L. *et al.* New endoperoxides highly active in vivo and in vitro against artemisinin-resistant *Plasmodium falciparum*. *Malar. J. 2018 171* **17**, 145 (2018).

182. Delves, M. *et al.* The activities of current antimalarial drugs on the life cycle stages of *Plasmodium*: a comparative study with human and rodent parasites. *PLoS Med.* **9**, 1–14 (2012).

183. Kato, N. *et al.* Diversity-oriented synthesis yields novel multistage antimalarial inhibitors. *Nature* **538**, 344–349 (2016).

184. Kerb, R. *et al.* Pharmacogenetics of

antimalarial drugs: effect on metabolism and transport. *Lancet Infect. Dis.* **9**, 760–774 (2009).

185. Walter R J Taylor *et al.* Hemolytic Dynamics of Weekly Primaquine Antirelapse Therapy Among Cambodians With Acute *Plasmodium vivax* Malaria With or Without Glucose-6-Phosphate Dehydrogenase Deficiency. *J. Infect. Dis.* **220**, 1750–1760 (2019).

186. Newton, P. *et al.* Antimalarial Bioavailability and Disposition of Artesunate in Acute Falciparum Malaria. *Antimicrob. Agents Chemother.* **44**, 972–977 (2000).

187. Das, J. L. *et al.* Population Pharmacokinetics of Artemether, Dihydroartemisinin, and Lumefantrine in Rwandese Pregnant Women Treated for Uncomplicated *Plasmodium falciparum* Malaria. *Antimicrob. Agents Chemother.* **62**, e00518-18 (2018).

188. Krishna, S. & White, N. J. Pharmacokinetics of Quinine, Chloroquine and Amodiaquine: Clinical Implications. *Clin. Pharmacokinet.* **30**, 263–299 (1996).

189. Mohamed Ali, A. *et al.* Population Pharmacokinetics of the Antimalarial Amodiaquine: a Pooled Analysis To Optimize Dosing. *Antimicrob. Agents Chemother.* **62**, e2193-17 (2018).

190. Navaratnam, V. *et al.* Pharmacokinetics of Artemisinin-Type Compounds. *Clin. Pharmacokinet.* **39**, 255–270 (2000).

191. De Koning, H. P. *et al.* How do antimalarial drugs reach their intracellular targets? *Front. Pharmacol.* **6**, 1–7 (2015).

192. Alkhalil, A. *et al. Plasmodium falciparum* likely encodes the principal anion channel on infected human erythrocytes. *Blood* **104**, 4279–4286 (2004).

193. Alkhalil, A., Pillai, A. D., Bokhari, A. A. B., Vaidya, A. B. & Desai, S. A. Complex inheritance of the plasmodial surface anion channel in a *Plasmodium falciparum* genetic cross. *Mol. Microbiol.* **72**, 459–469 (2009).

194. Ecker, A., Lehane, A. M., Clain, J. & Fidock, D. A. PfCRT and its role in antimalarial drug resistance. *Trends Parasitol.* **28**, 504–514 (2012).

195. Sidhu, A. B. S. *et al.* Decreasing *pfmdr1* Copy Number in *Plasmodium falciparum* Malaria Heightens Susceptibility to Mefloquine, Lumefantrine, Halofantrine, Quinine, and Artemisinin. *J. Infect. Dis.* **194**, 528–535 (2006).

196. Ngoc Quang, N. *et al.* Comparison of the Pharmacokinetics and Ex Vivo Antimalarial Activities of Artesunate-Amodiaquine and Artemisinin-Piperaquine in Healthy Volunteers for Preselection Malaria Therapy. *Am. J. Trop. Med. Hygene* **99**, 65–72 (2018).

197. Fasinu, P. S. *et al.* Formation primaquine-5,6-orthoquinone, the putative active and toxic metabolite of primaquine via direct oxidation in human erythrocytes. *Malar. J.* **18**, 30 (2019).

198. Kristensen, S., Grinberg, L. & Tønnesen, H. H. *Photoreactivity of biologically active compounds XI. Primaquine and metabolites as radical inducers*. *European Journal of Pharmaceutical Sciences* vol. 5 (1997).

199. Pashynska, V., Stepanian, S., Gömöry, A., Vekey, K. & Adamowicz, L. Competing intermolecular interactions of artemisinin-type agents and aspirin with membrane phospholipids: Combined model mass spectrometry and quantum-chemical study. *Chem. Phys.* **455**, 81–87 (2015).

200. World Health Organization. *WHO Policy recommendation on Intermittent Preventive Treatment during infancy with sulphadoxine-pyrimethamine (SP-IPTi) for* Plasmodium falciparum *malaria control in Africa*. http://malaria.who.int/docs/IPTi/TEGConsultIPTiApr2009Report.pdf (2010).

201. WHO Global Malaria Programme & WHO Department of Reproductive Health and Research WHO Department of Maternal Newborn Child and Adolescent Health. *WHO policy brief for the implementation of intermittent preventive treatment of malaria in pregnancy using sulfadoxine-pyrimethamine (IPTp-SP)*. http://whqlibdoc.who.int/publications/

2010/9789241599412_eng.pdf (2014).

202. World Health Organization. *Policy brief on single-dose primaquine as a gametocytocyde in* Plasmodium falciparum *malaria*. http://www.who.int/malaria/mpac/sep2012/primaquine_single_dose_pf_erg_meeting_report_aug2012.pdf (2015).

203. Centers for Disease Control and Prevention. Malaria - About Malaria - Biology - Anopheles Mosquitoes. https://www.cdc.gov/malaria/about/biology/#tabs-1-5 (2018).

204. Herrera-Varela, M., Orjuela, L. I., Peñalver, C., Conn, J. E. & Quiñones, M. L. *Anopheles* species composition explains differences in *Plasmodium* transmission in La Guajira, northern Colombia. *Mem Inst Oswaldo Cruz, Rio Janeiro* **109**, 952–956 (2014).

205. Bakker, J. W., Loy, D. E., Takken, W., Hahn, B. H. & Verhulst, N. O. Attraction of mosquitoes to primate odours and implications for zoonotic *Plasmodium* transmission. *Med. Vet. Entomol.* **34**, 17–26 (2020).

206. Zohdy, S. *et al.* Small-scale land-use variability affects *Anopheles* spp. distribution and concomitant *Plasmodium* infection in humans and mosquito vectors in southeastern Madagascar. *Malar. J.* **15**, 114 (2016).

207. Manin, B. O. *et al.* Investigating the Contribution of Peri-domestic Transmission to Risk of Zoonotic Malaria Infection in Humans. *PLoS Negl. Trop. Dis.* **10**, e0005064 (2016).

208. Koenker, H. *et al.* Assessing whether universal coverage with insecticide-treated nets has been achieved: is the right indicator being used? *Malar. J.* **17**, 355 (2018).

209. Sinka, M. E. Global Distribution of the Dominant Vector Species of Malaria, *Anopheles* mosquitoes. in *New insights into malaria vectors* (ed. Manguin, S.) (InTech, 2013). doi:10.5772/54163.

210. Govindarajan, M. *et al.* Larvicidal activity of the essential oil from *Amomum subulatum* Roxb. (Zingiberaceae) against *Anopheles subpictus*, *Aedes albopictus* and *Culex tritaeniorhynchus* (Diptera: Culicidae), and non-target impact on four mosquito natural. *Physiol. Mol. Plant Pathol.* **101**, 219–224 (2018).

211. Chaccour, C. J. *et al.* Ivermectin to reduce malaria transmission: a research agenda for a promising new tool for elimination. *Malar. J.* **12**, 153 (2013).

212. Ndo, C. *et al.* X-ray sterilization of the An. arabiensis genetic sexing strain 'ANO IPCL1' at pupal and adult stages. *Acta Trop.* **131**, 124–128 (2014).

213. Mbare, O., Lindsay, S. W. & Fillinger, U. Pyriproxyfen for mosquito control: Female sterilization or horizontal transfer to oviposition substrates by *Anopheles gambiae* sensu stricto and *Culex quinquefasciatus*. *Parasites and Vectors* **7**, 1–12 (2014).

214. Hammond, A. *et al.* A CRISPR-Cas9 gene drive system targeting female reproduction in the malaria mosquito vector *Anopheles gambiae*. *Nat. Biotechnol.* **34**, 78–83 (2016).

215. Kyrou, K. *et al.* A CRISPR–Cas9 gene drive targeting *doublesex* causes complete population suppression in caged *Anopheles gambiae* mosquitoes. *Nat. Biotechnol.* **36**, 1062–1066 (2018).

216. Sumitani, M. *et al.* Reduction of malaria transmission by transgenic mosquitoes expressing an antisporozoite antibody in their salivary glands. *Insect Mol. Biol.* **22**, 41–51 (2013).

217. Dong, Y., Simões, M. L., Marois, E. & Dimopoulos, G. CRISPR/Cas9 -mediated gene knockout of *Anopheles gambiae* FREP1 suppresses malaria parasite infection. *PLoS Pathog.* **14**, e1006898 (2018).

218. Gonzalez-Ceron, L., Santillan, F., Rodriguez, M. H., Mendez, D. & Hernandez-Avila, J. E. Bacteria in Midguts of Field-Collected *Anopheles albimanus* Block *Plasmodium vivax* Sporogonic Development. *J. Med. Entomol.* **40**, 371–374 (2003).

219. Cirimotich, C. M. *et al.* Natural microbe-mediated refractoriness to *Plasmodium* infection in *Anopheles gambiae*. *Science*

(80-.). **332**, 855–858 (2011).

220. Shaw, W. R. *et al. Wolbachia* infections in natural *Anopheles* populations affect egg laying and negatively correlate with *Plasmodium* development. *Nat. Commun.* **7**, 1–7 (2016).

221. Herren, J. K. *et al.* A microsporidian impairs *Plasmodium falciparum* transmission in *Anopheles arabiensis* mosquitoes. *Nat. Commun.* **11**, 2187 (2020).

222. Paton, D. G. *et al.* Exposing Anopheles mosquitoes to antimalarials blocks *Plasmodium* parasite transmission. *Nature* **567**, 239–243 (2019).

223. World Health Organization. Malaria vaccine: WHO position paper – January 2016. *Wkly. Epidemiol. Rec.* **91**, 33–52 (2016).

224. The RTSS Clinical Trials Partnership. First Results of Phase 3 Trial of RTS,S/AS01 Malaria Vaccine in African Children. *N. Engl. J. Med.* **365**, 1863–1875 (2011).

225. Agnandji, S. T. *et al.* Efficacy and Safety of the RTS,S/AS01 Malaria Vaccine during 18 Months after Vaccination: A Phase 3 Randomized, Controlled Trial in Children and Young Infants at 11 African Sites. *PLoS Med.* **11**, e1001685 (2014).

226. European Medicines Agency. *Committee for medicinal products for human use (CHMP) - Minutes of the meeting on 20-23 July 2015*. www.ema.europa.eu/contact (2015).

227. Shiratsuchi, T. *et al.* A potent malaria vaccine based on adenovirus with dual modifications at Hexon and pVII. *Vaccine* **35**, 6990–7000 (2017).

228. Collins, K. A., Snaith, R., Cottingham, M. G., Gilbert, S. C. & Hill, A. V. S. Enhancing protective immunity to malaria with a highly immunogenic virus-like particle vaccine. *Sci. Rep.* **7**, 1–15 (2017).

229. Cawlfield, A. *et al.* Safety, toxicity and immunogenicity of a malaria vaccine based on the circumsporozoite protein (FMP013) with the adjuvant army liposome formulation containing QS21 (ALFQ). *Vaccine* **37**, 3793–3803 (2019).

230. Oneko, M. *et al.* Feasibility of direct venous inoculation of the radiation-attenuated *Plasmodium falciparum* whole sporozoite vaccine in children and infants in Siaya, western Kenya. *Vaccine* **38**, 4592–4600 (2020).

231. Belnoue, E. *et al.* Protective T Cell Immunity against Malaria Liver Stage after Vaccination with Live Sporozoites under Chloroquine Treatment. *J. Immunol.* **172**, 2487–2495 (2004).

232. Wijayalath, W. *et al.* Strain-Specific Protective Effect of the Immunity Induced by Live Malarial Sporozoites under Chloroquine Cover. *PLoS One* **7**, e45861 (2012).

233. Reuling, I. J. *et al.* An open-label phase 1/2a trial of a genetically modified rodent malaria parasite for immunization against *Plasmodium falciparum* malaria. *Sci. Transl. Med.* **12**, eaay2578 (2020).

234. Versiani, F. G., Almeida, M. E., Mariuba, L. A., Orlandi, P. P. & Nogueira, P. A. N-terminal *Plasmodium vivax* merozoite surface protein-1, a potential subunit for malaria vivax vaccine. *Clin. Dev. Immunol.* **2013**, (2013).

235. Jessica Longley, R. *et al.* A Multi-Stage *Plasmodium vivax* Malaria Vaccine Candidate Able to Induce Long-Lived Antibody Responses Against Blood Stage Parasites and Robust Transmission-Blocking Activity. *Front. Cell. Infect. Microbiol.* **9**, 135 (2019).

236. Douglas, A. D. *et al.* A PfRH5-based vaccine is efficacious against heterologous strain blood-stage *Plasmodium falciparum* infection in *Aotus* monkeys. *Cell Host Microbe* **17**, 130–139 (2015).

237. Younis, S., Faber, B. W., Kocken, C. H. M. & Remarque, E. J. Identification of adjuvants for clinical trials performed with *Plasmodium falciparum* AMA1 in rabbits. *BMC Immunol.* **20**, 25 (2019).

238. Raj, D. K. *et al.* Antibodies to PfSEA-1 block parasite egress from RBCs and protect against malaria infection. *Science (80-.).* **344**, 871–877 (2014).

239. Raj, D. K. *et al.* Anti-PfGARP activates

programmed cell death of parasites and reduces severe malaria. *Nature* **582**, 104–108 (2020).

240. Jepsen, M. P. G. *et al.* The malaria vaccine candidate GMZ2 elicits functional antibodies in individuals from malaria endemic and non-endemic areas. *J. Infect. Dis.* **208**, 479–488 (2013).

241. Fried, M., Nosten, F., Brockman, A., Brabin, B. J. & Duffy, P. E. Maternal antibodies block malaria. *Nature* **395**, 851–852 (1998).

242. Fried, M. & Duffy, P. E. Designing a VAR2CSA-based vaccine to prevent placental malaria. *Vaccine* **33**, 7483–7488 (2015).

243. Gbédandé, K. *et al.* Clinical development of a VAR2CSA-based placental malaria vaccine PAMVAC: Quantifying vaccine antigen-specific memory B & T cell activity in Beninese primigravidae. *Vaccine* **35**, 3474–3481 (2017).

244. Sirima, S. B. *et al.* PRIMVAC vaccine adjuvanted with Alhydrogel or GLA-SE to prevent placental malaria: a first-in-human, randomised, double-blind, placebo-controlled study. *Lancet Infect. Dis.* **20**, 585–597 (2020).

245. Salinas, N. D., Tang, W. K. & Tolia, N. H. Blood-Stage Malaria Parasite Antigens: Structure, Function, and Vaccine Potential. *J. Mol. Biol.* **431**, 4259–4280 (2019).

246. Chichester, J. A. *et al.* Safety and immunogenicity of a plant-produced Pfs25 virus-like particle as a transmission blocking vaccine against malaria: A Phase 1 dose-escalation study in healthy adults. *Vaccine* **36**, 5865–5871 (2018).

247. Singh, S. K. *et al.* Improving the malaria transmission-blocking activity of a *Plasmodium falciparum* 48/45 based vaccine antigen by SpyTag/SpyCatcher mediated virus-like display. *Vaccine* **35**, 3726–3732 (2017).

248. Coelho, C. H. *et al.* Chronic helminth infection does not impair immune response to malaria transmission blocking vaccine Pfs230D1-EPA/Alhydrogel® in mice. *Vaccine* **37**, 1038–1045 (2019).

249. Datta, D. *et al.* Comparative functional potency of DNA vaccines encoding *Plasmodium falciparum* transmission blocking target antigens Pfs48/45 and Pfs25 administered alone or in combination by *in vivo* electroporation in rhesus macaques. *Vaccine* **35**, 7049–7056 (2017).

250. Alves, E. *et al.* Evaluation of *Plasmodium vivax* Cell-Traversal Protein for Ookinetes and Sporozoites as a Preerythrocytic *P. vivax* Vaccine. *Clin. Vaccine Immunol.* **24**, e00501-16 (2017).

251. Cunha, J. A. *et al.* Increased *Plasmodium falciparum* Parasitemia in Non-splenectomized *Saimiri sciureus* Monkeys Treated with Clodronate Liposomes. *Front. Cell. Infect. Microbiol.* **7**, 408 (2017).

252. Payne, D. *Use and limitations of light microscopy for diagnosing malaria at the primary health care level*. *Bulletin of the World Health Organization* vol. 66 (1988).

253. Chotivanich, K., Silamut, K. & Day, N. P. J. Laboratory diagnosis of malaria infection – A short review of methods. *Aust. J. Med. Sci.* **27**, 11–15 (2006).

254. Snounou, G. *et al.* High sensitivity of detection of human malaria parasites by the use of nested polymerase chain reaction. *Mol. Biochem. Parasitol.* **61**, 315–320 (1993).

255. Snounou, G., Viriyakosol, S., Jarra, W., Thaithong, S. & Brown, K. N. Identification of the four human malaria parasite species in field samples by the polymerase chain reaction and detection of a high prevalence of mixed infections. *Mol. Biochem. Parasitol.* **58**, 283–292 (1993).

256. Rana, R. *et al.* Sequence Analysis of the K13 -Propeller Gene in Artemisinin Challenging *Plasmodium falciparum* Isolates from Malaria Endemic Areas of Odisha, India: A Molecular Surveillance Study. *Biomed Res. Int.* **2020**, 8475246 (2020).

257. Kevin Baird, J., Purnomo, T. R. & Jones, T. R. Diagnosis of malaria in the field by

fluorescence microscopy of QBC® capillary tubes. *Trans. R. Soc. Trop. Med. Hyg.* **86**, 3–5 (1992).

258. Cho, S. J. *et al.* A Novel Malaria Pf/Pv Ab Rapid Diagnostic Test Using a Differential Diagnostic Marker Identified by Network Biology. *Int. J. Biol. Sci* **12**, 824–835 (2016).

259. Greenhouse, B. *et al.* Priority use cases for antibody-detecting assays of recent malaria exposure as tools to achieve and sustain malaria elimination. *Gates Open Res.* **3**, 17 (2019).

260. World Health Organization. *Malaria Rapid Diagnostic Test Performance*. (2015).

261. Notomi, T. *et al.* Loop-mediated isothermal amplification of DNA. *Nucleic Acids Res.* **28**, 1–7 (2000).

262. Zelman, B. W. *et al.* Costs and cost-effectiveness of malaria reactive case detection using loop-mediated isothermal amplification compared to microscopy in the low transmission setting of Aceh Province, Indonesia. *Malar. J.* **17**, 12 (2018).

263. World Health Organization. *Malaria rapid diagnostic test performance: results of WHO product testing of malaria RDTs: round 8 (2016–2018)*. (2018).

264. Donald, W. *et al.* The Utility of Malaria Rapid Diagnostic Tests as a Tool in Enhanced Surveillance for Malaria Elimination in Vanuatu. *PLoS One* **11**, e0167136 (2016).

265. Stuck, L. *et al.* Malaria infection prevalence and sensitivity of reactive case detection in Zanzibar. *Int. J. Infect. Dis.* **97**, 337–346 (2020).

266. Aung, P. P. *et al.* Challenges in early phase of implementing the 1-3-7 surveillance and response approach in malaria elimination setting: A field study from Myanmar. *Infect. Dis. Poverty* **9**, 18 (2020).

267. Wongsrichanalai, C., Barcus, M. J., Muth, S., Sutamihardja, A. & Wernsdorfer, W. H. A Review of Malaria Diagnostic Tools: Microscopy and Rapid Diagnostic Test (RDT). **77**, 119–127 (2007).

268. Jimenez, A. *et al.* Analytical sensitivity of current best-in-class malaria rapid diagnostic tests. *Malar. J.* **16**, 128 (2017).

269. Miller, R. S., McDaniel, P. & Wongsrichanalai, C. Following the course of malaria treatment by detecting parasite lactate dehydrogenase enzyme. *Br. J. Haematol.* **113**, 558–562 (2001).

270. Poti, K. E., Sullivan, D. J., Dondorp, A. M. & Woodrow, C. J. HRP2: Transforming Malaria Diagnosis, but with Caveats. *Trends Parasitol.* **36**, 112–127 (2020).

271. Dalrymple, U., Arambepola, R., Gething, P. W. & Cameron, E. How long do rapid diagnostic tests remain positive after anti-malarial treatment? *Malar. J.* **17**, 228 (2018).

272. Koita, O. A. *et al.* False-Negative Rapid Diagnostic Tests for Malaria and Deletion of the Histidine-Rich Repeat Region of the *hrp2* Gene. *Am. J. Trop. Med. Hyg* **86**, 194–198 (2012).

273. Kozycki, C. T. *et al.* False-negative malaria rapid diagnostic tests in Rwanda: impact of *Plasmodium falciparum* isolates lacking hrp2 and declining malaria transmission. *Malar. J.* **16**, 123 (2017).

274. Gillet, P. *et al.* Prozone in malaria rapid diagnostics tests: how many cases are missed? *Malar. J.* **10**, 166 (2011).

275. Ho, M. F. *et al.* Circulating antibodies against *Plasmodium falciparum* histidine-rich proteins 2 interfere with antigen detection by rapid diagnostic tests. *Malar. J.* **13**, 480 (2014).

276. Tambo, M., Mwinga, M. & Mumbengegwi, D. R. Loop-mediated isothermal amplification (LAMP) and Polymerase Chain Reaction (PCR) as quality assurance tools for Rapid Diagnostic Test (RDT) malaria diagnosis in Northern Namibia. *PLoS One* **13**, e0206848 (2018).

277. Chiodini, P. L. *et al.* The heat stability of *Plasmodium* lactate dehydrogenase-based and histidine-rich protein 2-based malaria rapid diagnostic tests. *Trans. R. Soc. Trop. Med. Hyg.* **101**, 331–337 (2007).

278. Global Malaria Programme. *Recommended selection criteria for*

procurement of malaria rapid diagnostic tests. https://www.who.int/malaria/publications/atoz/9789241514965/en/ (2018).

279. Ling, X.-X. *et al.* Cost-effectiveness analysis of malaria rapid diagnostic tests: a systematic review. *Infect. Dis. Poverty* **8**, 104 (2019).

280. Xiao, L., Takada, H., Maeda, K., Haramoto, M. & Miwa, N. Antioxidant effects of water-soluble fullerene derivatives against ultraviolet ray or peroxylipid through their action of scavenging the reactive oxygen species in human skin keratinocytes. *Biomed. Pharmacother.* **59**, 351–358 (2005).

281. Monteiro-Riviere, N. A. *et al.* Safety Evaluation of Sunscreen Formulations Containing Titanium Dioxide and Zinc Oxide Nanoparticles in UVB Sunburned Skin: An *In Vitro* and *In Vivo Study*. *Toxicol. Sci.* **123**, 264–280 (2011).

282. Vance, M. E. *et al.* Nanotechnology in the real world: Redeveloping the nanomaterial consumer products inventory. *Beilstein J. Nanotechnol* **6**, 1769–1780 (2015).

283. European Commission. European Commission. Enviroment. Deffinition of a Nanomaterial. *Enviroment* 1 http://ec.europa.eu/environment/chemicals/nanotech/faq/definition_en.htm (2014).

284. Mafune, F., Kohno, J., Takeda, Y. & Kondow, T. Formation of Gold Nanoparticles by Laser Ablation in Aqueous Solution of Surfactant. *J. Phys. Chem. B* **105**, 5114–5120 (2001).

285. Hyeon, T. Chemical synthesis of magnetic nanoparticles. *Chem. Commun.* **3**, 927–934 (2003).

286. Mohanpuria, P., Rana, N. K. & Yadav, S. K. Biosynthesis of nanoparticles: Technological concepts and future applications. *Journal of Nanoparticle Research* vol. 10 507–517 (2008).

287. Jeevanandam, J., Barhoum, A., Chan, Y. S., Dufresne, A. & Danquah, M. K. Review on nanoparticles and nanostructured materials: History, sources, toxicity and regulations. *Beilstein Journal of Nanotechnology* vol. 9 1050–1074 (2018).

288. Skandrani, N. *et al.* Lipid nanocapsules functionalized with polyethyleneimine for plasmid DNA and drug co-delivery and cell imaging. *Nanoscale* **6**, 7379–7390 (2014).

289. Tan, A., Rajadas, J. & Seifalian, A. M. Exosomes as nano-theranostic delivery platforms for gene therapy. *Adv. Drug Deliv. Rev.* **65**, 357–67 (2013).

290. Panyam, J. & Labhasetwar, V. Biodegradable nanoparticles for drug and gene delivery to cells and tissue. *Adv. Drug Deliv. Rev.* **64**, 61–71 (2012).

291. Conde, J. *et al.* Design of Multifunctional Gold Nanoparticles for *In Vitro* and *In Vivo* Gene Silencing. *ACS Nano* **6**, 8316–8324 (2012).

292. Tan, W. B., Huang, N. & Zhang, Y. Ultrafine biocompatible chitosan nanoparticles encapsulating multi-coloured quantum dots for bioapplications. *J. Colloid Interface Sci.* **310**, 464–470 (2007).

293. Wang, S.-H., Lee, C.-W., Chiou, A. & Wei, P.-K. Size-dependent endocytosis of gold nanoparticles studied by three-dimensional mapping of plasmonic scattering images. *J. Nanobiotechnology* **8**, 33 (2010).

294. Yang, B., Liu, Z., Liu, H. & Nash, M. A. Next Generation Methods for Single-Molecule Force Spectroscopy on Polyproteins and Receptor-Ligand Complexes. *Frontiers in Molecular Biosciences* vol. 7 85 (2020).

295. Olofsson, L., Rindzevicius, T., Pfeiffer, I. & Ka, M. Surface-Based Gold-Nanoparticle Sensor for Specific and Quantitative DNA Hybridization Detection. *Langmuir* **19**, 10414–10419 (2003).

296. Conde, J. *et al.* In vivo tumor targeting via nanoparticle-mediated therapeutic siRNA coupled to inflammatory response in lung cancer mouse models. *Biomaterials* **34**, 7744–53 (2013).

297. Barkalina, N., Charalambous, C., Jones, C. & Coward, K. Nanotechnology in reproductive medicine: Emerging applications of nanomaterials.

Nanomedicine **10**, 921–938 (2014).

298. Zazo, H., Colino, C. I. & Lanao, J. M. Current applications of nanoparticles in infectious diseases. *J. Control. Release* **224**, 86–102 (2016).

299. McNeil, S. E. *Characterization of Nanoparticles Intended for Drug Delivery*. *Methods in Molecular Biology* vol. 1682 (Humana Press, 2018).

300. Vijayakumar, S. & Ganesan, S. In Vitro Cytotoxicity Assay on Gold Nanoparticles with Different Stabilizing Agents. *J. Nanomater.* **2012**, 1–9 (2012).

301. Huang, H. & Yang, X. Synthesis of Chitosan-Stabilized Gold Nanoparticles in the Absence/Presence of Tripolyphosphate. *Biomacromolecules* **5**, 2340–2346 (2004).

302. Shen, H., Jawaid, A. M. & Snee, P. T. Poly(ethylene glycol) Carbodiimide Coupling Reagents for the Biological and Chemical Functionalization of Water-Soluble Nanoparticles. *ACS Nano* **3**, 915–923 (2009).

303. Brennan, J. L. *et al.* Bionanoconjugation via Click Chemistry : The Creation of Functional Hybrids of Lipases and Gold Nanoparticles. *Bioconjug. Chem.* **17**, 1373–1375 (2006).

304. Peng, L.-H. *et al.* TAT conjugated cationic noble metal nanoparticles for gene delivery to epidermal stem cells. *Biomaterials* **35**, 5605–5618 (2014).

305. Rojo, J. *et al.* Gold glyconanoparticles as new tools in antiadhesive therapy. *Chembiochem* **5**, 291–7 (2004).

306. Della Pepa, M. E. *et al.* Role of nanoparticles in treatment of human parasites. in *Nanotechnology Applied To Pharmaceutical Technology* (eds. Rai, M. & Santos, C. A. dos) 307–333 (Springer, 2017). doi:10.1007/978-3-319-70299-5_13.

307. Joshi, M., Pathak, S., Sharma, S. & Patravale, V. Design and *in vivo* pharmacodynamic evaluation of nanostructured lipid carriers for parenteral delivery of artemether: Nanoject. *Int. J. Pharm.* **364**, 119–126 (2008).

308. Mühlebach, S. Regulatory challenges of nanomedicines and their follow-on versions: A generic or similar approach? *Adv. Drug Deliv. Rev.* **131**, 122–131 (2018).

309. Gregoriadis, G. Drug entrapment in liposomes. *FEBS Lett.* **36**, 292–296 (1973).

310. Nisini, R., Poerio, N., Mariotti, S., De Santis, F. & Fraziano, M. The multirole of liposomes in therapy and prevention of infectious diseases. *Front. Immunol.* **9**, (2018).

311. Barenholz, Y. (Chezy). Doxil ®-The first FDA-approved nano-drug: Lessons learned. *J. Control. Release* **160**, 117–134 (2012).

312. Isacchi, B. *et al.* Artemisinin and artemisinin plus curcumin liposomal formulations: enhanced antimalarial efficacy against *Plasmodium berghei*-infected mice. *Eur. J. Pharm. Biopharm.* **80**, 528–34 (2012).

313. Rajendran, V., Singh, C. & Ghosh, P. C. Improved efficacy of doxycycline in liposomes against *Plasmodium falciparum* in culture and *Plasmodium berghei* infection in mice. *Can. J. Physiol. Pharmacol.* **96**, 1145–1152 (2018).

314. Ismail, M., Ling, L., Du, Y., Yao, C. & Li, X. Liposomes of dimeric artesunate phospholipid: A combination of dimerization and self-assembly to combat malaria. *Biomaterials* **163**, 76–87 (2018).

315. Raza, M., Bharti, H., Singal, A., Nag, A. & Ghosh, P. C. Long circulatory liposomal maduramicin inhibits the growth of *Plasmodium falciparum* blood stages in culture and cures murine models of experimental malaria. *Nanoscale* **10**, 13773–13791 (2018).

316. Duan, S. *et al. In vivo* antimalarial activity and pharmacokinetics of artelinic acid-choline derivative liposomes in rodents. *Parasitology* **147**, 58–64 (2020).

317. Rajendran, V. *et al.* Stearylamine liposomal delivery of monensin in combination with free artemisinin eliminates blood stages of *Plasmodium falciparum* in culture and *P. berghei*

infection in murine malaria. *Antimicrob. Agents Chemother.* **60**, 1304–1318 (2016).

318. Roces, C. B. *et al.* Rapid scale-up and production of active-loaded PEGylated liposomes. *Int. J. Pharm.* **586**, 119566 (2020).

319. Baruah, U. K. *et al.* Design, characterization and antimalarial efficacy of PEGylated galactosylated nano lipid carriers of primaquine phosphate. *Artif. Cells, Nanomedicine, Biotechnol.* **46**, 1809–1829 (2018).

320. Ben Mamoun, C. *et al. Transfer of genes into* Plasmodium falciparum *by polyamidoamine dendrimers*. *Molecular and Biochemical Parasitology* vol. 103 www.elsevier.com/locate/parasitology (1999).

321. Urbán, P. *et al.* Use of poly(amidoamine) drug conjugates for the delivery of antimalarials to *Plasmodium*. *J. Control. Release* **177**, 84–95 (2014).

322. Mukaya, E. H., Van Zyl, R., Van Vuuren, N. J. & Yangkou Mbianda, X. Polymeric prodrugs containing neridronate and ferrocene: Synthesis, characterization, and antimalarial activity. *Int. J. Polym. Mater. Polym. Biomater.* **67**, 401–409 (2018).

323. Mukaya, H. E., Van Zyl, R. L., Jansen van Vuuren, N. C., Chen, C. T. & Mbianda, X. Y. Synthesis, characterization, biological evaluation, and drug release study of polyamidoamine-containing neridronate. *Int. J. Polym. Mater. Polym. Biomater.* **68**, 489–498 (2019).

324. Agrawal, P., Gupta, U. & Jain, N. K. Glycoconjugated peptide dendrimers-based nanoparticulate system for the delivery of chloroquine phosphate. *Biomaterials* **28**, 3349–3359 (2007).

325. Bhadra, D., Bhadra, S. & Jain, N. K. PEGylated Peptide Dendrimeric Carriers for the Delivery of Antimalarial Drug Chloroquine Phosphate. *Pharm. Res.* **23**, 623–633 (2006).

326. Movellan, J. *et al.* Amphiphilic dendritic derivatives as nanocarriers for the targeted delivery of antimalarial drugs. *Biomaterials* **35**, 7940–7950 (2014).

327. Martí Coma-Cros, E. *et al.* Micelle carriers based on dendritic macromolecules containing bis-MPA and glycine for antimalarial drug delivery. *Biomater. Sci.* **7**, 1661–1674 (2019).

328. Bhadra, D., Bhadra, S. & Jain, N. K. Pegylated lysine based copolymeric dendritic micelles for solubilization and delivery of artemether. *J. Pharm. Pharm. Sci.* **8**, 467–482 (2005).

329. Ramazani, A., Keramati, M., Malvandi, H., Danafar, H. & Kheiri Manjili, H. Preparation and *in vivo* evaluation of anti-plasmodial properties of artemisinin-loaded PCL–PEG–PCL nanoparticles. *Pharm. Dev. Technol.* **23**, 911–920 (2018).

330. Liu, T. & Thierry, B. A Solution to the PEG Dilemma: Efficient Bioconjugation of Large Gold Nanoparticles for Biodiagnostic Applications using Mixed Layers. *Langmuir* **28**, 15634–15642 (2012).

331. Isacchi, B. *et al.* Conventional and long-circulating liposomes of artemisinin: preparation, characterization, and pharmacokinetic profile in mice. *J. Liposome Res.* **21**, 237–244 (2011).

332. Malhotra, M. *et al.* Ultrafine chitosan nanoparticles as an efficient nucleic acid delivery system targeting neuronal cells. *Drug Dev. Ind. Pharm.* **35**, 719–726 (2009).

333. Wang, B. & Lu, T. Novel stable cytokine delivery system in physiological pH solution: chitosan oligosaccharide/heparin nanoparticles. *Int. J. Nanomedicine* **10**, 3417–3427 (2015).

334. Tripathy, S. *et al.* Synthesis, characterization of chitosan–tripolyphosphate conjugated chloroquine nanoparticle and its in vivo anti-malarial efficacy against rodent parasite: A dose and duration dependent approach. *Int. J. Pharm.* **434**, 292–305 (2012).

335. Yaméogo, J. B. G. *et al.* Self-assembled biotransesterified cyclodextrins as Artemisinin nanocarriers – I: Formulation, lyoavailability and *in vitro*

antimalarial activity assessment. *Eur. J. Pharm. Biopharm.* **80**, 508–517 (2012).

336. Kashyap, A. *et al.* Chloroquine diphosphate bearing dextran nanoparticles augmented drug delivery and overwhelmed drug resistance in Plasmodium falciparum parasites. *Int. J. Biol. Macromol.* **114**, 161–168 (2018).

337. Meyer, C. T. *et al.* Quantifying Drug Combination Synergy along Potency and Efficacy Axes Article Quantifying Drug Combination Synergy along Potency and Efficacy Axes. *Cell Syst.* **8**, 97–108 (2019).

338. Rajendran, V., Pachauri, M. & Ghosh, P. C. Combinatorial Effects of Monensin in Liposome Formulations with Antimalarial Drugs Against Blood Stages of *Plasmodium falciparum* in Culture and *P. berghei* Infection. *Curr. Drug ther.* **13**, 74–82 (2017).

339. Biosca, A., Dirscherl, L., Moles, E., Imperial, S. & Fernàndez-Busquets, X. An ImmunoPEGliposome for Targeted Antimalarial Combination Therapy at the Nanoscale. *Pharmaceutics* **11**, 341 (2019).

340. Jain, S. A. *et al.* Parasite impairment by targeting *Plasmodium*-infected RBCs using glyceryl-dilaurate nanostructured lipid carriers. *Biomaterials* **35**, 6636–6645 (2014).

341. Prabhu, P. *et al.* Nanostructured lipid carriers of artemether-lumefantrine combination for intravenous therapy of cerebral malaria. *Int. J. Pharm.* **513**, 504–517 (2016).

342. Kumar, S., Singh, R. K., Sharma, R., Murthy, R. S. R. & Bhardwaj, T. R. Design, synthesis and evaluation of antimalarial potential of polyphosphazene linked combination therapy of primaquine and dihydroartemisinin. *Eur. J. Pharm. Sci.* **66**, 123–137 (2015).

343. Kumar, S., Singh, R. K., Murthy, R. S. R. & Bhardwaj, T. R. Synthesis and evaluation of substituted poly(Organophosphazenes) as a novel nanocarrier system for combined antimalarial therapy of primaquine and dihydroartemisinin. *Pharm. Res.* **32**, 2736–2752 (2015).

344. Tang, W. L. *et al.* Development of a Rapidly Dissolvable Oral Pediatric Formulation for Mefloquine Using Liposomes. *Mol. Pharm.* **14**, 1969–1979 (2017).

345. Tahara, K., Nishio, M. & Takeuchi, H. Evaluation of liposomal behavior in the gastrointestinal tract after oral administration using real-time *in vivo* imaging. *Drug Dev. Ind. Pharm.* **44**, 608–614 (2017).

346. Karn, P. R. *et al.* Mucoadhesive liposomal delivery systems: the choice of coating material. *Drug Dev. Ind. Pharm.* **37**, 482–488 (2011).

347. Martinez-Correa, H. A. *et al.* Composition and antimalarial activity of extracts of *Curcuma longa* L. obtained by a combination of extraction processes using supercritical CO2 , ethanol and water as solvents. *J. Supercrit. Fluids* **119**, 122–129 (2017).

348. Coma-Cros, E. M. *et al.* Antimalarial activity of orally administered curcumin incorporated in eudragit®-containing liposomes. *Int. J. Mol. Sci.* **19**, 1–11 (2018).

349. Manconi, M. *et al.* Nanoformulation of curcumin-loaded eudragit-nutriosomes to counteract malaria infection by a dual strategy: Improving antioxidant intestinal activity and systemic efficacy. *Int. J. Pharm.* **556**, 82–88 (2019).

350. Kim, J. Y. *et al.* 2D Inorganic-Antimalarial Drug-Polymer Hybrid with pH-Responsive Solubility. *Chem. - An Asian J.* **10**, 2264–2271 (2015).

351. Patil, S., Suryavanshi, S., Pathak, S. & Sharma, S. Evaluation of novel lipid based formulation of β-Artemether and Lumefantrine in murine malaria model. *Int. J. Pharm.* **455**, 229–234 (2013).

352. Dwivedi, P. *et al.* Arteether nanoemulsion for enhanced efficacy against *Plasmodium yoelii* nigeriensis malaria: An approach by enhanced bioavailability. *Colloids Surfaces B Biointerfaces* **126**, 467–475 (2015).

353. Memvanga, P. B., Coco, R. & Préat, V. An oral malaria therapy: Curcumin-loaded lipid-based drug delivery systems

combined with β-arteether. *J. Control. Release* **172**, 904–913 (2013).

354. Omwoyo, W. N. *et al.* Development, characterization and antimalarial efficacy of dihydroartemisinin loaded solid lipid nanoparticles. *Nanomedicine Nanotechnology, Biol. Med.* **12**, 801–809 (2016).

355. Prabhu, P., Suryavanshi, S., Pathak, S., Sharma, S. & Patravale, V. Artemether-lumefantrine nanostructured lipid carriers for oral malaria therapy: Enhanced efficacy at reduced dose and dosing frequency. *Int. J. Pharm.* **511**, 473–487 (2016).

356. Schulz, J. D., Gauthier, M. A. & Leroux, J. Improving oral drug bioavailability with polycations? *Eur. J. Pharm. Biopharm.* **97**, 427–37 (2015).

357. Martí Coma-Cros, E. *et al.* Polyamidoamine Nanoparticles for the Oral Administration of Antimalarial Drugs. *Pharmaceutics* **10**, 225 (2018).

358. Anand, P. *et al.* Design of curcumin-loaded PLGA nanoparticles formulation with enhanced cellular uptake, and increased bioactivity in vitro and superior bioavailability in vivo. *Biochem. Pharmacol.* **79**, 330–8 (2010).

359. Oyeyemi, O. *et al.* Curcumin-Artesunate Based Polymeric Nanoparticle; Antiplasmodial and Toxicological Evaluation in Murine Model. *Front. Pharmacol.* **9**, 562 (2018).

360. Akhtar, F., Rizvi, M. M. A. & Kar, S. K. Oral delivery of curcumin bound to chitosan nanoparticles cured *Plasmodium yoelii* infected mice. *Biotechnol. Adv.* **30**, 310–320 (2012).

361. Shaikh, J., Ankola, D. D., Beniwal, V., Singh, D. & Kumar, M. N. V. R. Nanoparticle encapsulation improves oral bioavailability of curcumin by at least 9-fold when compared to curcumin administered with piperine as absorption enhancer. *Eur. J. Pharm. Sci.* **37**, 223–230 (2009).

362. Mishra, A., Kaushik, N. K., Sardar, M. & Sahal, D. Evaluation of antiplasmodial activity of green synthesized silver nanoparticles. *Colloids Surfaces B Biointerfaces* **111**, 713–718 (2013).

363. Gandhi, P. R., Jayaseelan, C., Kamaraj, C., Rajasree, S. R. R. & Regina Mary, R. *In vitro* antimalarial activity of synthesized TiO2 nanoparticles using Momordica charantia leaf extract against *Plasmodium falciparum*. *J. Appl. Biomed.* **16**, 378–386 (2018).

364. Murugan, K. *et al.* Magnetic nanoparticles are highly toxic to chloroquine-resistant *Plasmodium falciparum*, dengue virus (DEN-2), and their mosquito vectors. *Parasitol. Res.* **116**, 495–502 (2017).

365. Wang, K.-K. *et al.* Eradication of Plasmodium falciparum from Erythrocytes by Controlled Reactive Oxygen Species via Photodynamic Inactivation Coupled with Photofunctional Nanoparticles. *ACS Appl. Mater. Interfaces* **9**, 12975–12981 (2017).

366. Bhadra, D., Yadav, A. K., Bhadra, S. & Jain, N. K. Glycodendrimeric nanoparticulate carriers of primaquine phosphate for liver targeting. *Int. J. Pharm.* **295**, 221–233 (2005).

367. Joshi, V. M. & Devarajan, P. V. Receptor-mediated hepatocyte-targeted delivery of primaquine phosphate nanocarboplex using a carbohydrate ligand. *Drug Deliv. Transl. Res.* **4**, 353–364 (2014).

368. Tomiya, N. *et al.* Liver-targeting of primaquine-(poly-γ-glutamic acid) and its degradation in rat hepatocytes. *Bioorganic Med. Chem.* **21**, 5275–5281 (2013).

369. Longmuir, K. J., Robertson, R. T., Haynes, S. M., Baratta, J. L. & Waring, A. J. Effective Targeting of Liposomes to Liver and Hepatocytes *In Vivo* by Incorporation of a *Plasmodium* Amino Acid Sequence. *Pharm. Res.* **23**, 756–769 (2006).

370. Robertson, R. T., Baratta, J. L., Haynes, S. M. & Longmuir, K. J. Liposomes Incorporating a *Plasmodium* Amino Acid Sequence Target Heparan Sulfate Binding Sites in Liver. *J. Pharm. Sci.* **97**, 3257–3273 (2007).

371. Haynes, S. M., Longmuir, K. J., Robertson, R. T., Baratta, J. L. & Waring, A. J.

Liposomal Polyethyleneglycol and Polyethyleneglycol-Peptide Combinations for Active Targeting to Liver *In Vivo*. *Drug Deliv.* **15**, 207–217 (2008).

372. Longmuir, K. J., Haynes, S. M., Baratta, J. L., Kasabwalla, N. & Robertson, R. T. Liposomal delivery of doxorubicin to hepatocytes in vivo by targeting heparan sulfate. *Int. J. Pharm.* **382**, 222–233 (2009).

373. Gupta, Y., Jain, A. & Jain, S. K. Transferrin-conjugated solid lipid nanoparticles for enhanced delivery of quinine dihydrochloride to the brain. *J. Pharm. Pharmacol.* **59**, 935–940 (2007).

374. Glushakova, S. *et al.* Exploitation of a newly-identified entry pathway into the malaria parasite-infected erythrocyte to inhibit parasite egress. *Sci. Rep.* **7**, 12250 (2017).

375. Urbán, P., Estelrich, J., Cortés, A. & Fernàndez-Busquets, X. A nanovector with complete discrimination for targeted delivery to *Plasmodium falciparum*-infected versus non-infected red blood cells *in vitro*. *J. Control. Release* **151**, 202–211 (2011).

376. Moles, E., Moll, K., Ch'ng, J.-H., Parini, P. & Fernàndez-Busquets, X. Development of drug-loaded immunoliposomes for the selective targeting and elimination of rosetting *Plasmodium falciparum*-infected red blood cells. *J. Control. Release* **241**, 57–67 (2016).

377. Moles, E. *et al.* Immunoliposome-mediated drug delivery to *Plasmodium*-infected and non-infected red blood cells as a dual therapeutic/prophylactic antimalarial strategy. *J. Control. Release* **210**, 217–229 (2015).

378. Moles, E. *et al.* ImmunoPEGliposomes for the targeted delivery of novel lipophilic drugs to red blood cells in a falciparum malaria murine model. *Biomaterials* **145**, 178–191 (2017).

379. Heikham, K. D. *et al.* Preferential targeting of human erythrocytes infected with the malaria parasite *Plasmodium falciparum* via hexose transporter surface proteins. *Int. J. Pharm.* **483**, 57–62 (2015).

380. Marques, J. *et al.* Application of heparin as a dual agent with antimalarial and liposome targeting activities toward *Plasmodium*-infected red blood cells. *Nanomedicine* **10**, 1719–1728 (2014).

381. Ssemaganda, A. *et al.* Induction of *Plasmodium*-Specific Immune Responses Using Liposome-Based Vaccines. *Frontiers in Immunology* vol. 10 135 (2019).

382. Beck, Z., Matyas, G. R. & Alving, C. R. Detection of liposomal cholesterol and monophosphoryl lipid A by QS-21 saponin and Limulus polyphemus amebocyte lysate. *Biochim. Biophys. Acta - Biomembr.* **1848**, 775–780 (2015).

383. Ssemaganda, A. *et al.* Mannosylated liposomes formulated with whole parasite *P. falciparum* blood-stage antigens are highly immunogenic in mice. *Vaccine* **38**, 1494–1504 (2020).

384. Huang, W.-C. *et al.* A malaria vaccine adjuvant based on recombinant antigen binding to liposomes. *Nat. Nanotechnol.* **13**, 1174–1181 (2018).

385. Kumar, R. *et al.* Nanovaccines for malaria using *Plasmodium falciparum* antigen Pfs25 attached gold nanoparticles. *Vaccine* **33**, 5064–5071 (2015).

386. Seth, L. *et al.* Development of a self-assembling protein nanoparticle vaccine targeting *Plasmodium falciparum* Circumsporozoite Protein delivered in three Army Liposome Formulation adjuvants. *Vaccine* **35**, 5448–5454 (2017).

387. Santhosh, S. B., Ragavendran, C. & Natarajan, D. Spectral and HRTEM analyses of *Annona muricata* leaf extract mediated silver nanoparticles and its Larvicidal efficacy against three mosquito vectors *Anopheles stephensi, Culex quinquefasciatus,* and *Aedes aegypti*. *J. Photochem. Photobiol. B Biol.* **153**, 184–190 (2015).

388. Murugan, K. *et al. Datura metel*-synthesized silver nanoparticles magnify predation of dragonfly nymphs against the malaria vector *Anopheles stephensi*. *Parasitol. Res.* **114**, 4645–4654 (2015).

389. Kumar, D., Kumar, G., Das, R. & Agrawal, V. Strong larvicidal potential of silver nanoparticles (AgNPs) synthesized using *Holarrhena antidysenterica* (L.) Wall. bark extract against malarial vector, *Anopheles stephensi* Liston. *Process Saf. Environ. Prot.* **116**, 137–148 (2018).

390. Rajput, S., Dinesh Kumar, · & Agrawal, V. Green synthesis of silver nanoparticles using Indian Belladonna extract and their potential antioxidant, anti-inflammatory, anticancer and larvicidal activities. *Plant Cell Rep.* **39**, 921–939 (2020).

391. Murugan, K. *et al. Sargassum wightii*-synthesized ZnO nanoparticles reduce the fitness and reproduction of the malaria vector *Anopheles stephensi* and cotton bollworm *Helicoverpa armigera*. *Physiol. Mol. Plant Pathol.* **101**, 202–213 (2018).

392. Dhanesh Gandhi, A. *et al.* Lichen *Parmelia sulcata* mediated synthesis of gold nanoparticles: an eco-friendly tool against *Anopheles stephensi* and *Aedes aegypti*. *Environ. Sci. Pollut. Res.* **26**, 23886–23898 (2019).

393. Maltha, J., Gillet, P. & Jacobs, J. Malaria rapid diagnostic tests in travel medicine. *Clinical Microbiology and Infection* vol. 19 408–415 (2013).

394. Alnasser, Y. *et al.* Colorimetric Detection of *Plasmodium vivax* in Urine Using MSP10 Oligonucleotides and Gold Nanoparticles. *PLoS Negl. Trop. Dis.* **10**, e0005029 (2016).

395. Tangchaikeeree, T. *et al.* Combination of PCR and dual nanoparticles for detection of *Plasmodium falciparum*. *Colloids Surfaces B Biointerfaces* **159**, 888–897 (2017).

396. DiscoGnosis - disc-shaped point-of-care platform for infectious disease diagnosis. http://www.discognosis.eu/.

397. DiscoGnosis: Diagnosing infectious diseases at the point-of-care | Shaping Europe's digital future. https://ec.europa.eu/digital-single-market/en/news/discognosis-diagnosing-infectious-diseases-point-care .

398. Lindahl, U., Couchman, J., Kimata, K. & Esko, J. D. Proteoglycans and sulfated glycosaminoglycans. in *Essentials of Glycobiology* (eds. Varki, A., Cummings, R. D., Esko, J. D. & Al., E.) (Cold Spring Harbor Laboratory Press, 2017). doi:10.1101/glycobiology.3e.017.

399. Boulanger, M. J., Tonkin, M. L. & Crawford, J. Apicomplexan parasite adhesins: novel strategies for targeting host cell carbohydrates. *Curr. Opin. Struct. Biol.* **20**, 551–559 (2010).

400. Almer, J., Gesslbauer, B. & Kungl, A. J. Therapeutic strategies to target microbial protein–glycosaminoglycan interactions. *Biochem. Soc. Trans.* **46**, 1505–1515 (2018).

401. Mulloy, B., Hogwood, J., Gray, E., Lever, R. & Page, C. P. Pharmacology of Heparin and Related Drugs. *Pharmacol. Rev. Pharmacol Rev* **68**, 76–141 (2016).

402. Xu, D. & Esko, J. D. Demystifying Heparan Sulfate–Protein Interactions. *Annu. Rev. Biochem.* **83**, 129–157 (2014).

403. Lever, R., Mulloy, B. & Page, C. P. *Heparin - A Century of Progress*. *Handbook of Experimental Pharmacology* vol. 207 (2012).

404. Pancake, S. J., Holt, G. D., Mellouk, S. & Hoffman, S. L. Malaria Sporozoites and C ircumsporozoite Proteins Bind Specifically to Sulfated Glycoconjugates. *J. Cell Biol.* **117**, 1351–1357 (1992).

405. Pradel, G., Garapaty, S. & Frevert, U. Proteoglycans mediate malaria sporozoite targeting to the liver. *Mol. Microbiol.* **45**, 637–651 (2002).

406. Holt, G. D., Krivan, H. C., Gasic, G. J. & Ginsburg, V. Antistasin, an Inhibitor of Coagulation and Metastasis, Binds to Sulfatide (Gal(3-SO4)B1-1Cer) and Has a Sequence Homology with Other Proteins That Bind Sulfated Glycoconjugates. *J. Biol. Chem.* **264**, 12138–12140 (1989).

407. Holt, G. D., Pangburn, M. K. & Ginsburg, V. Properdin Binds to Sulfatide [Gal(3-SO4)B1-1Cer] and Has a Sequence Homology with Other Proteins That Bind Sulfated Glycoconjugates. *J. Biol. Chem.* **265**, 2852–2855 (1990).

408. Ying, P. *et al.* The Malaria Circumsporozoite Protein: Interaction of the Conserved Regions I and II-Plus with Heparin-like Oligosaccharides in Heparan Sulfate. *Exp. Parasitol.* **85**, 168–182 (1997).

409. Rathore, D. *et al.* Direct Measurement of the Interactions of Glycosaminoglycans and a Heparin Decasaccharide with the Malaria Circumsporozoite Protein. *Biochemistry* **40**, 11518–11524 (2001).

410. Ancsin, J. B. & Kisilevsky, R. A Binding Site for Highly Sulfated Heparan Sulfate Is Identified in the N Terminus of the Circumsporozoite Protein. *J. Biol. Chem.* **279**, 21824–21832 (2004).

411. Barragan, A., Spillmann, D., Kremsner, P. G., Wahlgren, M. & Carlson, J. *Plasmodium falciparum*: Molecular Background to Strain-Specific Rosette Disruption by Glycosaminoglycans and Sulfated Glycoconjugates. *Exp. Parasitol.* **91**, 133–143 (1999).

412. Vogt, A. M., Winter, G., Wahlgren, M. & Spillmann, D. Heparan sulphate identified on human erythrocytes: a *Plasmodium falciparum* receptor. *Biochem. J.* **381**, 593–597 (2004).

413. Vogt, A. M. *et al.* Heparan sulfate on endothelial cells mediates the binding of *Plasmodium falciparum* – infected erythrocytes via the DBL1α domain of PfEMP1. **101**, 2405–2411 (2003).

414. Vogt, A. M. *et al.* Release of Sequestered Malaria Parasites upon Injection of a Glycosaminoglycan. *PLoS Pathog.* **2**, 853–863 (2006).

415. Kyriacou, H. M. *et al.* In Vitro Inhibition of *Plasmodium falciparum* Rosette Formation by Curdlan Sulfate. *Antimicrob. Agents Chemother.* **51**, 1321–1326 (2007).

416. Leitgeb, A. M. *et al.* Low Anticoagulant Heparin Disrupts *Plasmodium falciparum* Rosettes in Fresh Clinical Isolates. *Am. J. Trop. Med. Hygene* **84**, 390–396 (2011).

417. Leitgeb, A. M. *et al.* Inhibition of merozoite invasion and transient de-sequestration by sevuparin in humans with *Plasmodium falciparum* malaria. *PLoS One* **12**, e0188754 (2017).

418. Saiwaew, S. *et al.* Effects of sevuparin on rosette formation and cytoadherence of *Plasmodium falciparum* infected erythrocytes. *PLoS One* **12**, e0172718 (2017).

419. Xiao, L. *et al.* Sulfated Polyanions Inhibit Invasion of Erythrocytes by Plasmodial Merozoites and Cytoadherence of Endothelial Cells to Parasitized Erythrocytes. *Infect. Immun.* **64**, 1373–1378 (1996).

420. Adams, Y. *et al.* Inhibition of *Plasmodium falciparum* Growth In Vitro and Adhesion to Chondroitin-4-Sulfate by the Heparan Sulfate Mimetic PI-88 and Other Sulfated Oligosaccharides. *Antimicrob. Agents Chemother.* **50**, 2850–2852 (2006).

421. Bastos, M. F. *et al.* Fucosylated Chondroitin Sulfate Inhibits *Plasmodium falciparum* Cytoadhesion and Merozoite Invasion. *Antimicrob. Agents Chemother.* **58**, 1862–1871 (2014).

422. Skidmore, M. A. *et al.* A semi-synthetic glycosaminoglycan analogue inhibits and reverses *Plasmodium falciparum* cytoadherence. *PLoS One* **12**, e0186276 (2017).

423. Lucchi, N. W., Koopman, R., Peterson, D. S. & Moore, J. M. *Plasmodium falciparum*-infected red blood cells selected for binding to cultured syncytiotrophoblast bind to chondroitin sulfate A and induce tyrosine phosphorylation in the syncytiotrophoblast. *Placenta* **27**, 384–394 (2006).

424. Hviid, L. The case for PfEMP1-based vaccines to protect pregnant women against *Plasmodium falciparum* malaria. *Expert Rev. Vaccines* **10**, 1405–1414 (2011).

425. Achur, R. N., Valiyaveettil, M., Alkhalil, A., Ockenhouse, C. F. & Gowda, D. C. Characterization of proteoglycans of human placenta and identification of unique chondroitin sulfate proteoglycans of the intervillous spaces that mediate the adherence of *Plasmodium falciparum*-infected erythrocytes to the placenta. *J. Biol. Chem.* **275**, 40344–40356 (2000).

426. Achur, R. N., Valiyaveettil, M. & Gowda, D. C. The low sulfated chondroitin sulfate proteoglycans of human placenta have sulfate group-clustered domains that can efficiently bind *Plasmodium falciparum*-infected erythrocytes. *J. Biol. Chem.* **278**, 11705–11713 (2003).

427. Alkhalil, A., Achur, R. N., Valiyaveettil, M., Ockenhouse, C. F. & Gowda, D. C. Structural requirements for the adherence of *Plasmodium falciparum*-infected erythrocytes to chondroitin sulfate proteoglycans of human placenta. *J. Biol. Chem.* **275**, 40357–64 (2000).

428. Muthusamy, A. *et al.* Chondroitin sulfate proteoglycan but not hyaluronic acid is the receptor for the adherence of *Plasmodium falciparum*-infected erythrocytes in human placenta, and infected red blood cell adherence up-regulates the receptor expression. *Am. J. Pathol.* **170**, 1989–2000 (2007).

429. Chotivanich, K. *et al. Plasmodium vivax* Adherence to Placental Glycosaminoglycans. *PLoS One* **7**, 1–7 (2012).

430. Muthusamy, A. *et al. Plasmodium falciparum*-infected erythrocytes adhere both in the intervillous space and on the villous surface of human placenta by binding to the low-sulfated chondroitin sulfate proteoglycan receptor. *Am. J. Pathol.* **164**, 2013–2025 (2004).

431. Agbor-Enoh, S. T. *et al.* Chondroitin sulfate proteoglycan expression and binding of *Plasmodium falciparum*-infected erythrocytes in the human placenta during pregnancy. *Infect. Immun.* **71**, 2455–2461 (2003).

432. Rieger, H. *et al.* Cytoadhesion of *Plasmodium falciparum* - Infected erythrocytes to chondroitin-4-sulfate is cooperative and shear enhanced. *Blood* **125**, 383–391 (2015).

433. Clausen, T. M. *et al.* Structural and functional insight into how the *Plasmodium falciparum* VAR2CSA protein mediates binding to chondroitin sulfate A in placental malaria. *J. Biol. Chem.* **287**, 23332–23345 (2012).

434. Clark, D., Su, S. & Davidson, E. Saccharide anions as inhibitors of the malaria parasite. *Glycoconjugates J.* **14**, 473–479 (1997).

435. Kobayashi, K. *et al.* Analyses of Interactions Between Heparin and the Apical Surface Proteins of *Plasmodium falciparum*. *Sci. Rep.* **3**, 10 (2013).

436. Esko, J. D., Prestegard, J. H. & Linhardt, R. J. Proteins that Bind Sulfated Glycosaminoglycans. in *Essentials of Glycobiology* (eds. Varki, A., Cummings, R. D., Esko, J. D. & Al., E.) (Cold Spring Harbor Laboratory Press, 2017). doi:10.1101/glycobiology.3e.038.

437. Zhang, Y. *et al.* Proteomic analysis of *Plasmodium falciparum* schizonts reveals heparin-binding merozoite proteins. *J. Proteome Res.* **12**, 2185–2193 (2013).

438. Kulane, A. *et al.* Effect of different fractions of heparin on *Plasmodium falciparum* merozoite invasion of red blood cells in vitro. *Am. J. Trop. Med. Hyg.* **46**, 589–594 (1992).

439. Marques, J., Vilanova, E., Mourão, P. A. S. & Fernàndez-Busquets, X. Marine Organism Sulfated Polysaccharides Exhibiting Significant Antimalarial Activity and Inhibition of Red Blood Cell Invasion by *Plasmodium*. *Sci. Rep.* **6**, 14 (2015).

440. Boyle, M. J. *et al.* Identification of Heparin Modifications and Polysaccharide Inhibitors of *Plasmodium falciparum* Merozoite Invasion That Have a Potential for Novel Drug Development. *Antimicrob. Agents Chemother.* **61**, 1–17 (2017).

441. Tiemeyer, M., Nakato, H. & Esko, J. D. Arthropoda. in *Essentials of Glycobiology* (eds. Varki, A., Cummings, R. D., Esko, J. D. & Al., E.) (Cold Spring Harbor Laboratory Press, 2017). doi:10.1101/glycobiology.3e.026.

442. Dinglasan, R. R. *et al. Plasmodium falciparum* ookinetes require mosquito midgut chondroitin sulfate proteoglycans for cell invasion. *PNAS* **104**, 15882–15887 (2007).

443. Mathias, D. K. *et al.* A Small Molecule Glycosaminoglycan Mimetic Blocks *Plasmodium* Invasion of the Mosquito Midgut. *PLoS Pathog.* **9**, e1003757

(2013).

444. Basseri, H. R., Javazm, M. S., Farivar, L. & Abai, M. R. Lectin-carbohydrate recognition mechanism of *Plasmodium berghei* in the midgut of malaria vector *Anopheles stephensi* using quantum dot as a new approach. *Acta Trop.* **156**, 37–42 (2016).

445. Baia-da-silva, D. C. *et al.* Microanatomy of the American Malaria Vector Anopheles aquasalis (Diptera: Culicidae: Anophelinae) Midgut: Ultrastructural and Histochemical Observations. *J. Med. Entomol.* **56**, 1636–1649 (2019).

446. Mccormick, C. J., Tuckwell, D. S., Crisanti, A., Humphries, M. J. & Hollingdale, M. R. Identification of heparin as a ligand for the A-domain of *Plasmodium falciparum* thrombospondin-related adhesion protein. *Mol. Biochem. Parasitol.* **100**, 111–124 (1999).

447. Marques, J. *et al.* Adaptation of targeted nanocarriers to changing requirements in antimalarial drug delivery. *Nanomedicine Nanotechnology, Biol. Med.* **13**, 515–525 (2017).

448. Monteiro De Castro Côrtes, L. *et al.* Participation of heparin binding proteins from the surface of *Leishmania (Viannia) braziliensis* promastigotes in the adhesion of parasites to *Lutzomyia longipalpis* cells (Lulo) *in vitro*. *Parasites and Vectors* **5**, 10 (2012).

449. Gonzalez, M. S. *et al.* Involvement of sulfated glycosaminoglycans on the development and attachment of *Trypanosoma cruzi* to the luminal midgut surface in the vector, *Rhodnius prolixus*. *Parasitology* **138**, 1870–1877 (2011).

450. Gonzalez, M. S. & Silva, L. F. Involvement of sulfated glycosaminoglycans on the development and attachment of *Trypanosoma cruzi* to the luminal midgut surface in the vector, *Rhodnius prolixus*. *Parasitology* **138**, 1870–1877 (2011).

451. Sinnis, P. *et al.* Mosquito Heparan Sulfate and Its Potential Role in Malaria Infection and Transmission. *J. Biol. Chem.* **282**, 25376–25384 (2007).

452. Armistead, J. S., Wilson, I. B. H., van Kuppevelt, T. H. & Dinglasan, R. R. A role for heparan sulfate proteoglycans in *Plasmodium falciparum* sporozoite invasion of anopheline mosquito salivary glands. *Biochem. J.* **438**, 475–483 (2011).

453. Muga, J. O., Gathirwa, J. W., Tukulula, M. & Jura, W. G. Z. O. In vitro evaluation of chloroquine-loaded and heparin surface-functionalized solid lipid nanoparticles. *Malar. J.* **17**, 133 (2018).

454. Ismail, M., Du, Y., Ling, L. & Li, X. Artesunate-heparin conjugate based nanocapsules with improved pharmacokinetics to combat malaria. *Int. J. Pharm.* **562**, 162–171 (2019).

455. Najer, A. *et al.* Nanomimics of Host Cell Membranes Block Invasion and Expose Invasive Malaria Parasites. *ACS Nano* **8**, 12560–12571 (2014).

456. Najer, A., Thamboo, S., Palivan, C. G., Beck, H.-P. & Meier, W. Giant Host Red Blood Cell Membrane Mimicking Polymersomes Bind Parasite Proteins and Malaria Parasites. *Chim. Int. J. Chem.* **70**, 288–291 (2016).

457. Najer, A. *et al.* Analysis of Molecular Parameters Determining the Antimalarial Activity of Polymer-Based Nanomimics. *Macromol. Rapid Commun.* **36**, 1923–1928 (2015).

458. Jayasena, S. D. *Aptamers: An Emerging Class of Molecules That Rival Antibodies in Diagnostics*. https://academic.oup.com/clinchem/article-abstract/45/9/1628/5643446 (1999).

459. Ozer, A., Pagano, J. M. & Lis, J. T. New Technologies Provide Quantum Changes in the Scale, Speed, and Success of SELEX Methods and Aptamer Characterization. *Mol. Ther. Nucleic Acids* **3**, e183 (2014).

460. Ashrafuzzaman, M., Tseng, C.-Y., Kapty, J., Mercer, J. R. & Tuszynski, J. A. A Computationally Designed DNA Aptamer Template with Specific Binding to Phosphatidylserine. *Nucleic Acid Ther.* **23**, 418–426 (2013).

461. Ellington, A. D. & Szostak, J. W. In vitro selection of RNA molecules that bind specific ligands. *Nature* **346**, 818–822

(1990).

462. Tuerk, C. & Gold, L. Systematic evolution of ligands by exponential enrichment: RNA ligands to bacteriophage T4 DNA polymerase. *Science (80-.).* **249**, 505–510 (1990).

463. Stoltenburg, R., Reinemann, C. & Strehlitz, B. SELEX-A (r)evolutionary method to generate high-affinity nucleic acid ligands. *Biomol. Eng.* **24**, 381–403 (2007).

464. Warren, C. L., Mohandas, A., Chaturvedi, I. & Ansari, A. Z. Macromolecular Interactions: Aptamers. in *Encyclopedia of Life Sciences* (ed. John Wiley & Sons, I.) vol. 29 582–594 (John Wiley & Sons, Ltd, 2009).

465. Frith, K. A. *et al.* Towards development of aptamers that specifically bind to lactate dehydrogenase of Plasmodium falciparum through epitopic targeting. *Malar. J.* **17**, 191 (2018).

466. Stoltenburg, R., Reinemann, C. & Strehlitz, B. FluMag-SELEX as an advantageous method for DNA aptamer selection. *Anal. Bioanal. Chem.* **383**, 83–91 (2005).

467. Wang, J. *et al.* Particle Display: A Quantitative Screening Method for Generating High-Affinity Aptamers. *Angew. Chemie Int. Ed.* **53**, 4796–4801 (2014).

468. Oh, S. S. *et al.* Improving Aptamer Selection Efficiency through Volume Dilution, Magnetic Concentration, and Continuous Washing in Microfluidic Channels. *Anal. Chem.* **83**, 6883–6889 (2011).

469. Hicke, B. J. *et al.* Tenascin-C Aptamers Are Generated Using Tumor Cells and Purified Protein. *J. Biol. Chem.* **276**, 48644–48654 (2001).

470. Mendonsa, S. D. & Bowser, M. T. In Vitro Evolution of Functional DNA Using Capillary Electrophoresis. *J. Am. Chem. Soc.* **126**, 20–21 (2004).

471. Jing, M. & Bowser, M. T. Isolation of DNA aptamers using micro free flow electrophoresis. *Lab Chip* **11**, 3703–3709 (2011).

472. Yang, J. & Bowser, M. T. Capillary electrophoresis-SELEX selection of catalytic DNA aptamers for a small-molecule porphyrin target. *Anal. Chem.* **85**, 1525–1530 (2013).

473. Stoltenburg, R., Nikolaus, N. & Strehlitz, B. Capture-SELEX: Selection of DNA Aptamers for Aminoglycoside Antibiotics. *J. Anal. Methods Chem.* **2012**, 415697 (2012).

474. Birch, C. M., Hou, H. W., Han, J. & Niles, J. C. Identification of malaria parasite-infected red blood cell surface aptamers by inertial microfluidic SELEX (I-SELEX). *Sci. Rep.* **5**, 1–16 (2015).

475. Sefah, K., Shangguan, D., Xiong, X., O'Donoghue, M. B. & Tan, W. Development of DNA aptamers using Cell-SELEX. *Nat. Protoc.* **5**, 1169–1185 (2010).

476. Lyu, Y. *et al.* Generating cell targeting aptamers for nanotheranostics using cell-SELEX. *Theranostics* **6**, 1440–1452 (2016).

477. Tolle, F., Wilke, J., Wengel, J. & Mayer, G. By-product formation in repetitive PCR amplification of DNA libraries during SELEX. *PLoS One* **9**, 1–12 (2014).

478. Thiel, W. H. *et al.* Nucleotide Bias Observed with a Short SELEX RNA. *Nucleic Acid Ther.* **21**, 253–263 (2011).

479. Svobodová, M., Pinto, A., Nadal, P. & Sullivan, C. K. O. Comparison of different methods for generation of single-stranded DNA for SELEX processes. *Anal. Bioanal. Chem.* **404**, 835–842 (2012).

480. Green, L. S. *et al.* Nuclease-resistant nucleic acid ligands to vascular permeability factor/vascular endothelial growth factor. *Chem. Biol.* **2**, 683–695 (1995).

481. Jellinek, D. *et al.* Potent 2'-Amino-2/-deoxypyrimidine RNA Inhibitors of Basic Fibroblast Growth Factor. *Biochemistry* **34**, 11363–11372 (1995).

482. Ruckman, J. *et al.* 2'-fluoropyrimidine RNA-based aptamers to the 165-amino acid form of vascular endothelial growth factor (VEGF165): Inhibition of receptor binding and VEGF-induced vascular permeability through interactions requiring the exon 7-encoded domain. *J.*

Biol. Chem. **273**, 20556–20567 (1998).

483. Elmén, J. *et al.* LNA-mediated microRNA silencing in non-human primates. *Nature* **452**, 896–899 (2008).

484. Pieken, W., Tasset, D., Janjic, N., Gold, L. & Kirschenheuter, G. P. High affinity nucleic acid ligand containing modified nucleotides. *United States Patent* vol. 270 938 (1997).

485. Lee, K. Y. *et al.* Bioimaging of Nucleolin Aptamer-Containing 5-(N-benzylcarboxyamide)-2-deoxyuridine More Capable of Specific Binding to Targets in Cancer Cells. *J. Biomed. Biotechnol.* **2010**, 168306 (2010).

486. Fan, X., Sun, L., Wu, Y., Zhang, L. & Yang, Z. Bioactivity of 2′-deoxyinosine-incorporated aptamer AS1411. *Sci. Rep.* **6**, 12 (2016).

487. Kasahara, Y. *et al.* Effect of 3'-end capping of aptamer with various 2',4'-bridged nucleotides: Enzymatic post-modification toward a practical use of polyclonal aptamers. *Bioorg. Med. Chem. Lett.* **20**, 1626–1629 (2010).

488. Dougan, H. *et al.* Extending the Lifetime of Anticoagulant Oligodeoxynucleotide Aptamers in Blood. *Nucl. Med. Biol.* **27**, 289–297 (2000).

489. Healy, J. M. *et al.* Pharmacokinetics and Biodistribution of Novel Aptamer Compositions. *Pharm. Res.* **21**, 2234–2246 (2004).

490. Majumder, P., Gomes, K. N. & Ulrich, H. Aptamers: from bench side research towards patented molecules with therapeutic applications. *Expert Opin. Ther. Pat.* **19**, 1603–1613 (2009).

491. VEGF Inhibition Study in Ocular Neovascularization (V.I.S.I.O.N.) Clinical Trial Group. Year 2 Efficacy Results of 2 Randomized Controlled Clinical Trials of Pegaptanib for Neovascular Age-Related Macular Degeneration. *Ophthalmology* **113**, 1508.e1-1508.e25 (2006).

492. Lee, H. *et al.* Enhanced Human Epidermal Growth Factor Receptor 2 Degradation in Breast Cancer Cells by Lysosome-Targeting Gold Nanoconstructs. *ACS Nano* **9**, 9859–9867 (2015).

493. Mehlhorn, A. *et al.* Aptamer-Based Biosensors for Antibiotic Detection: A Review. *Biosensors* **8**, 54 (2018).

494. Wang, M. S., Black, J. C., Knowles, M. K. & Reed, S. M. C-reactive protein (CRP) aptamer binds to monomeric but not pentameric form of CRP. *Anal. Bioanal. Chem.* **401**, 1309–1318 (2011).

495. Guo, K.-T. *et al.* A new technique for the isolation and surface immobilization of mesenchymal stem cells from whole bone marrow using high-specific DNA aptamers. *Stem Cells* **24**, 2220–2231 (2006).

496. Kruspe, S., Mittelberger, F., Szameit, K. & Hahn, U. Aptamers as Drug Delivery Vehicles. *ChemMedChem* **9**, 1998–2011 (2014).

497. Ogawa, A., Murashige, Y. & Takahashi, H. Canonical translation-modulating OFF-riboswitches with a single aptamer binding to a small molecule that function in a higher eukaryotic cell-free expression system. *Bioorg. Med. Chem. Lett.* **28**, 2353–2357 (2018).

498. Wang, J. *et al.* A novel RNA aptamer-modified riboswitch as chemical sensor. *Anal. Chim. Acta* **1100**, 240–249 (2020).

499. Mustafina, K., Fukunaga, K. & Yokobayashi, Y. Design of Mammalian ON-Riboswitches Based on Tandemly Fused Aptamer and Ribozyme. *ACS Synth. Biol.* **9**, 19–25 (2020).

500. Tang, D. J. *et al.* A SAM-I riboswitch with the ability to sense and respond to uncharged initiator tRNA. *Nat. Commun.* **11**, 1–11 (2020).

501. Velasques, J. E., Trejo, A. V., Marsh, J. M. & Penner, G. A. Aptamers for Hair Care Applications. 93 (2020).

502. Velasques, J. E. *et al.* Aptamers for Personal Care Applications. 71 (2020).

503. Lee, S. *et al.* A highly sensitive aptasensor towards *Plasmodium* lactate dehydrogenase for the diagnosis of malaria. *Biosens. Bioelectron.* **35**, 291–6 (2012).

504. Jeon, W., Lee, S., Manjunatha, D. H. & Ban, C. A colorimetric aptasensor for the

diagnosis of malaria based on cationic polymers and gold nanoparticles. *Anal. Biochem.* **439**, 11–6 (2013).

505. Lee, S., Manjunatha, D. H., Jeon, W. & Ban, C. Cationic surfactant-based colorimetric detection of *Plasmodium* lactate dehydrogenase, a biomarker for malaria, using the specific DNA aptamer. *PLoS One* **9**, e100847 (2014).

506. Cheung, Y.-W. *et al.* Structural basis for discriminatory recognition of *Plasmodium* lactate dehydrogenase by a DNA aptamer. *Proc. Natl. Acad. Sci. U. S. A.* **110**, 15967–72 (2013).

507. Dirkzwager, R. M., Kinghorn, A. B., Richards, J. S. & Tanner, J. A. APTEC: aptamer-tethered enzyme capture as a novel rapid diagnostic test for malaria. *Chem. Commun. (Camb).* **51**, 4697–700 (2015).

508. Cheung, Y.-W. *et al.* Aptamer-mediated *Plasmodium* -specific diagnosis of malaria. *Biochimie* **145**, 131–136 (2018).

509. Fraser, L. A. *et al.* A portable microfluidic Aptamer-Tethered Enzyme Capture (APTEC) biosensor for malaria diagnosis. *Biosens. Bioelectron.* **100**, 591–596 (2018).

510. Wang, W.-X. *et al.* Specific and sensitive detection of *Plasmodium falciparum* lactate dehydrogenase by DNA-scaffolded silver nanoclusters combined with an aptamer. *Analyst* **142**, 800–807 (2017).

511. Godonoga, M. *et al.* A DNA aptamer recognising a malaria protein biomarker can function as part of a DNA origami assembly. *Sci. Rep.* **6**, 1–12 (2016).

512. Tang, M. S. *et al.* An aptamer-enabled DNA nanobox for protein sensing. *Nanomedicine Nanotechnology, Biol. Med.* **14**, 1161–1168 (2018).

513. Shiu, S., Fraser, L., Ding, Y. & Tanner, J. Aptamer Display on Diverse DNA Polyhedron Supports. *Molecules* **23**, 1695 (2018).

514. Jain, P., Chakma, B., Singh, N. K., Patra, S. & Goswami, P. Aromatic Surfactant as Aggregating Agent for Aptamer-Gold Nanoparticle-Based Detection of *Plasmodium* Lactate Dehydrogenase. *Mol. Biotechnol.* **58**, 497–508 (2016).

515. Jain, P., Das, S., Chakma, B. & Goswami, P. Aptamer-graphene oxide for highly sensitive dual electrochemical detection of *Plasmodium* lactate dehydrogenase. *Anal. Biochem.* **514**, 32–37 (2016).

516. Liu, D.-X. *et al.* A Novel Peptide Aptamer to Detect *Plasmodium falciparum* Lactate Dehydrogenase. *J. Biomed. Nanotechnol.* **15**, 204–211 (2019).

517. Singh, N. K., Arya, S. K., Estrela, P. & Goswami, P. Capacitive malaria aptasensor using *Plasmodium falciparum* glutamate dehydrogenase as target antigen in undiluted human serum. *Biosens. Bioelectron.* **117**, 246–252 (2018).

518. Singh, N. K., Dema Thungon, P., Estrela, P. & Goswami, P. Development of an aptamer-based field effect transistor biosensor for quantitative detection of *Plasmodium falciparum* glutamate dehydrogenase in serum samples. *Biosens. Bioelectron.* **123**, 30–35 (2018).

519. Josephid, D. F. *et al.* DNA aptamers for the recognition of HMGB1 from *Plasmodium falciparum*. *PLoS One* **14**, 20 (2019).

520. Thirunavukarasu, D. & Shi, H. An RNA Aptamer Specific to Hsp70-ATP Conformation Inhibits its ATPase Activity Independent of Hsp40. *Nucleic Acid Ther.* **25**, 103–112 (2015).

521. Niles, J. C., Derisi, J. L. & Marletta, M. A. Inhibiting *Plasmodium falciparum* growth and heme detoxification pathway using heme-binding DNA aptamers. *Proc. Natl. Acad. Sci. U. S. A.* **106**, 13266–71 (2009).

522. Nik Kamarudin, N., Mohammed, N. & Mustaffa, K. Aptamer Technology: Adjunct Therapy for Malaria. *Biomedicines* **5**, 1 (2017).

523. Barfod, A., Persson, T. & Lindh, J. In vitro selection of RNA aptamers against a conserved region of the *Plasmodium falciparum* erythrocyte membrane protein 1. *Parasitol. Res.* **105**, 1557–1566 (2009).

524. Kamarudin, N. A. A. N., Sat, J. N. A., Zaidi, N. F. M. & Mustaffa, K. M. F. Evolution of specific RNA aptamers via SELEX

targeting recombinant human CD36 protein: A candidate therapeutic target in severe malaria. *Asian Pac. J. Trop. Biomed.* **10**, 23–32 (2020).

525. Albrecht, L. *et al.* B-cell epitopes in NTS-DBL1α of PfEMP1 recognized by human antibodies in Rosetting *Plasmodium falciparum*. *PLoS One* **9**, e113248 (2014).

526. Duffy, S. & Avery, V. M. Routine In Vitro Culture of *Plasmodium falciparum*: Experimental Consequences? *Trends Parasitol.* **34**, (2018).

527. Hirsh, J., Anand, S. S., Halperin, J. L. & Fuster, V. Guide to Anticoagulant Therapy : Heparin. *Circulation* **103**, 2994–3018 (2001).

528. Miura, Y., Aoyagi, S., Kusada, Y. & Miyamoto, K. The characteristics of anticoagulation by covalently immobilized heparin. *J. Biomed. Mater. Res.* **14**, 619–630 (1980).

529. Duan, X. & Li, Y. Physicochemical characteristics of nanoparticles affect circulation, biodistribution, cellular internalization, and trafficking. *Small* vol. 9 1521–1532 (2013).

530. Mousa, S. A. *et al.* Pharmacokinetics and pharmacodynamics of oral heparin solid dosage form in healthy human subjects. *J. Clin. Pharmacol.* **47**, 1508–1520 (2007).

531. Crandall, I. E. *et al.* Sulfated cyclodextrins inhibit the entry of *Plasmodium* into red blood cells. Implications for malarial therapy. *Biochem. Pharmacol.* **73**, 632–642 (2007).

532. Gidwani, B. & Vyas, A. A Comprehensive Review on Cyclodextrin-Based Carriers for Delivery of Chemotherapeutic Cytotoxic Anticancer Drugs. *Biomed Res. Int.* **2015**, 198268 (2015).

533. Francischetti, I. M. B., Ma, D. & Andersen, J. F. Evidence for a Lectin Specific for Sulfated Glycans in the Salivary Gland of the Malaria Vector, *Anopheles gambiae*. *PLoS One* **9**, e107295 (2014).

534. Mairal, T. *et al.* Aptamers: molecular tools for analytical applications. *Anal. Bioanal. Chem.* **390**, 989–1007 (2008).

535. Piper, R. C., Buchanan, I., Choi, Y. H. & Makler, M. T. Opportunities for improving pLDH-based malaria diagnostic tests. *Malar. J.* **10**, 213 (2011).

536. Oguonu, T. *et al.* The performance evaluation of a urine malaria test (UMT) kit for the diagnosis of malaria in individuals with fever in south-east Nigeria: Cross-sectional analytical study. *Malar. J.* **13**, 403 (2014).

537. Samal, A. G. *et al.* Pathogens and Global Health The sensitivity and specificity of a urine based Rapid Diagnostic Test for the diagnosis of *Plasmodium falciparum* in a malaria endemic area in Odisha, India. *Pathog. Glob. Health* **111**, 383–387 (2017).

538. Oyibo, W. A. *et al.* Multicenter pivotal clinical trial of urine malaria test for rapid diagnosis of *Plasmodium falciparum* malaria. *J. Clin. Microbiol.* **55**, 253–263 (2017).

539. Harris, P. K. *et al.* Molecular identification of a malaria merozoite surface sheddase. *PLoS Pathog.* **1**, 0241–0251 (2005).

540. Sutherland, C. J. Surface antigens of *Plasmodium falciparum* gametocytes-A new class of transmission-blocking vaccine targets? *Mol. Biochem. Parasitol.* **166**, 93–98 (2009).

541. Lambros, C. & Vanderberg, J. P. Synchronization of *Plasmodium falciparum* Erythrocytic Stages in Culture. *J. Parasitol.* **65**, 420 (1979).

542. Lantero, E. *et al.* Development of DNA Aptamers Against *Plasmodium falciparum* Blood Stages Using Cell-Systematic Evolution of Ligands by EXponential Enrichment. *J. Biomed. Nanotechnol.* **16**, 315–334 (2020).

543. Jensen, J. B. Concentration from continuous culture of erythrocytes infected with trophozoites and schizonts of *Plasmodium falciparum*. *Am. J. Trop. Med. Hyg.* **27**, 1274–1276 (1978).

544. Krause, R. G. E. *et al.* Plasmodium glyceraldehyde-3-phosphate dehydrogenase: A potential malaria diagnostic target. *Exp. Parasitol.* **179**, 7–19 (2017).